On the interaction between model membrane systems mimicking eukaryotic membranes and the antimicrobial peptide indolicidin

The effect of cholesterol content and lipid rafts

Kari Kristine Almåsvold Borgos

Thesis submitted for the degree of
Master in biomolecules and biomaterials
60 credits

Department of Chemistry
Faculty of Mathematics and Natural Sciences

UNIVERSITY OF OSLO

Spring 2022

On the interaction between model membrane systems mimicking eukaryotic membranes and the antimicrobial peptide indolicidin

The effect of cholesterol content and lipid rafts

Kari Kristine Almåsvold Borgos

© 2022 Kari Kristine Almåsvold Borgos

On the interaction between model membrane systems mimicking eukaryotic membranes and the antimicrobial peptide indolicidin

http://www.duo.uio.no/

Printed: Reprosentralen, University of Oslo

Abstract

Due to the pressing matter of rising pathogen resistance to antibiotics and the slow development of new drugs, it is of great interest to research alternative therapeutics. Antimicrobial peptides (AMPs) are thought to be promising candidates because of their wide range of action, their selectivity towards pathogens, and a mode of action which mainly targets the membrane structure. By disrupting the membrane and not attacking specific chemical targets, the bacteria would have to completely reorganise the membrane structure to gain resistance against AMPs. However, AMP drug design is challenging because the exact mode of action of many peptides is still unknown. It has long been thought that the high cholesterol content in eukaryotic cells is essential in the selectivity of AMPs, protecting the host cells. In later years, the theory of lipid rafts (phase-separated domains) in eukaryotic membranes has received significant attention. Reports on the impact of cholesterol and phase separation on peptide interactions have differed. Some studies report a protecting effect of cholesterol in live cells and model membranes, while others report no such effect, especially for phase-separated systems. To gain insight into the role of cholesterol and lipid rafts, we systematically studied the impact of the peptide indolicidin on the structure and order of model membranes. To mimic the sterol content and raft presence of eukaryotic cell membranes, we used liposomal vesicles with varying cholesterol content and different zwitterionic lipid compositions, giving homogeneous and phase-separated membranes.

Model membrane structure was examined using small-angle scattering methods with X-rays (SAXS) and neutrons (SANS). Scattering experiments have the advantage of being essentially probe free and observing structures in the relevant size range. By comparing analytical scattering models to the scattering curves obtained by SAXS, relevant bilayer structural information could be obtained. SANS was used to confirm the presence of rafts/domains and observe how the lateral order changed upon the addition of indolicidin. Calorimetric experiments were used to probe the lipid order in the membranes.

The results showed that higher concentrations of indolicidin could solubilise the membranes, forming micelles and bicelles. A trend seemed to emerge of the homogeneous membranes being more protected the more liquid they were. Thus, more cholesterol is protective for lipids in the gel phase, while less cholesterol is protective for lipids in the liquid disordered phase. Raft presence and phase segregation had significant implications on the peptide-membrane interactions. No solubilisation occurred in the samples with medium- and large-sized rafts. The SANS results showed that indolicidin acted as a so-called lineactant, reducing the line tension between domains, causing the domains to become more disordered and merge. We hypothesise that indolicidin has a mode of action where it inserts itself in the liquid disordered phase, introducing defects that may cause solubilisation unless the membrane fluidity is high enough to reorganise the membrane to distribute the defects efficiently.

The findings are important as they provide new insight that helps piece together several pieces of a larger picture: the interactions between AMPs and biological membranes. The complexity of the model systems of this thesis surpasses those commonly applied in literature. So, even though model membranes have a far simpler composition than biological membranes, the observed behaviour of indolicidin in our model systems gives us important indications of its mode of action and how it is affected by different factors in the membrane.

Sammendrag

På grunn av økt antibiotikaresistens blant bakterier og et lavt antall nye antibiotika-kurer er det enorm interesse for nye alternativer til antibiotika. En lovende gruppe kandidater er antimikrobielle peptider (AMP). De er effektive mot et bredt spekter av patogener, utviser stor grad av selektivitet, og antas å først og fremst angripe membranens struktur. Det er foreløpig vanskelig å utvikle medisiner med AMP-er da det fortsatt ikke er kjent nøyaktig hvordan de fleste peptidene interagerer med membraner. Det har lenge vært antatt at effekten av høy konsentrasjon av kolesterol i eukariotiske celler har en beskyttende effekt mot peptider. De siste årene har interessen for faseseparerte domener i membranen, såkalte "lipid rafts", vært stor. Likevel er det splittede meninger om hvordan domener og mengde kolesterol i membranen påvirker interaksjonen med peptider. For å få mer innsikt i rollene til kolesterol og domener ønsket vi å systematisk studere interaksjoner mellom peptidet indolicidin og ulike modellmembraner. For å etterligne sterol konsentrasjonen og domenene som dannes i eukariotiske celler brukte vi liposomer med ulike kolesterol-konsentrasjoner og ulike sammensetninger av zwitterioniske lipider som gav homogene eller fase-separerte membraner.

Strukturen til modell-membranene ble undersøkt ved bruk av lav-vinkel spredningsteknikker. Lav-vinkel røntgen (SAXS) eller nøytron spredning (SANS) gir strukturell informasjon om prøven. Fordeler ved bruk av spredningsteknikker er at systemet kan studeres uten bruk av kjemiske markører som kan påvirke systemets egenskaper, og at man observerer strukturer i relevante størrelsesordener. Ved å sammenlikne analytiske sprednings-modeller og SAXS-data kan man få verdifull informasjon om strukturen til bilaget. SANS ble brukt til å bekrefte domenedannelse i systemene, og for å studere hvordan indolicidin påvirket lipidenes laterale orden. Lipidenes generelle orden ble studert med bruk av "Differential Scanning Calorimetry" (DSC), en kalorimetrisk metode som måler prøvens varmekapasitet.

Resultatene viste at høyere konsentrasjoner av indolicidin kan løse opp membraner, og at det da dannes miceller og biceller. Resultatene viste en trend hvor mer flytende membraner var mer beskyttet mot solubilisering. Det kan virke som om kolesterol kun har en beskyttende effekt i de tilfellene hvor det ikke bidro til høyere orden og stivhet i membranen. Det ble også observert stor forskjell i solubilisieringen av membraner med faseseparerte domener. Domener med større membraner virket å være mer beskyttet enn membraner med små, eller ingen domener. SANS-resultatene viste at indolicidin sannsynligvis kan fungere som en "lineactant", hvor det reduserer linjespenningen mellom domener og den kontinuerlige fasen. Resultatet er uordnede domener som flyter sammen. Vi fremmer en hypotese hvor indolicidin interagerer med membraner ved å sette seg inn i de mer flytende fasene og introdusere defeter som kan føre til solubilisering, med mindre lipidene er flytende nok til å raskt omorganisere seg og fordele stresset fra defektene.

Funnene i oppgaven er et viktig ledd i å pusle sammen deler av et større bilde, nemlig interaksjonene mellom AMP-er og biologiske mebraner. Selv om modell-membraner er svært forenklede systemer når det kommer til sammensetning, så vil en forståelse av hvordan interaksjoner med indolicidin, og AMP-er generelt, påvirkes av ulike faktorer i membranen være svært nyttig for å forstå hvordan AMP-er virker.

Acknowledgements

The research presented in this thesis was carried out from August 2020 to May 2022 at the Department of Chemistry, the University of Oslo, under the supervision of Professor Reidar Lund. All scattering data presented were collected at the European Synchrotron Radiation Facility in Grenoble, France and the Paul Scherrer Institut in Villigen, Switzerland.

First and foremost, I would like to thank my supervisor Professor Reidar Lund for the opportunity to work on such an exciting project. At all stages of the project, you provided excellent guidance, scientific input and support. I am very grateful to have had such an engaged supervisor as you are.

Secondly, I want to thank my co-supervisors, Victoria A. Bjørnestad and Vladimir R. Koynarev, for their invaluable support. The visit to PSI would never have been possible without you. I especially want to thank Victoria for answering all my experimental and theoretical questions. Not to mention the great help you have been in my understanding of scattering theory and with modifying the analytical scattering models. Your feedback during the writing process lifted the quality of this thesis. Vladimir, I am truly happy and thankful that you were chosen for the PhD project that allowed us to cooperate this last semester and a half. Your understanding of the project led to highly constructive discussions, and together with your feedback on previous drafts, you helped gather all the loose ends and make sense of it all. I would never have gotten this far without the both of you, and I wish you both all the best of luck with the rest of your PhD projects. I can't wait to see what you will discover in the future.

I also wish to thank my co-supervisor, Dr Josefine Eilsøe Nielsen, for the best possible introduction to the project and the great advice that helped me get started on this thesis, and for helping me revise the final draft. All analytical scattering models were modified with assistance from Prof. Reidar Lund, Dr Josefine E. Nielsen and Victoria A. Bjørnestad, and developed by them and so many more, with a special thanks to Dr Vitaliy Pipich for assistance with the models in QtiKWS-QtiSAS. Other people I want to acknowledge are my fellow master's students Marlene Andersen Nham, Ola Krogseth and Hannah Anor for great experimental help, fun discussions and moral support when needed; the rest of the Bio^3 Sof-Matter group for a great social and learning environment, and for running samples at the ESRF on my behalf; the staff at the ESRF for kindly running samples on our behalf when covid-restrictions prevented us from visiting their facilities; Head Engineer Bente A. Breiby at the Department of Pharmacy for running our DSC samples; and Dr Joachim Kohlbrecher for his help with the experiments at PSI.

I would like to thank my partner, Erik Alsgaard, for his invaluable love and support. Finally, I want to thank my sister for the great feedback on my writing and figures, my lovely niece for always cheering me up and telling me I'm the best, and the rest of my family for your unlimited support.

Contents

List of Figures

List of Tables

Abbreviations

Table 1: Abbreviations used in the thesis.

AMP	Anti microbial peptide
SAS	Small-Angle Scattering
SANS	Small-Angle Neutron Scattering
SAXS	Small-Angle X-ray Scattering
PC	Phosphatidylcholine
PE	Phosphoethanolamine
PG	Phoshatidylglycerine
DOPC	1,2-dioleoyl-sn-glycero-3-phosphocholine
DPPC	1,2-dipalmitoyl-sn-glycero-3-phosphocholine
Chol	Cholesterol
l_d	Liquid disordered
l_o	Liquid ordered
T_m	Melting temperature
PS	Phosphatidylserine
AFM	Atomic force microscopy
DMPC	Dimyristoylphosphocholine
CMC	Critical micellar concentration
MLVs	Multi-lamellar vesicles
ULVs	Unilamellar vesicles
SLD	Scattering-length density
POPC	1-palmitoyl-2-oleoyl-sn-glycero-3-phosphocholine
DSPC	1,2-distearoyl-sn-glycero-3-phosphocholine
DSC	Differential Scanning Calorimetry
PEG	Polyehtylene-glycol
DMPE	1,2-dimyristoyl-sn-glycero-3-phosphoethanolamine

Chapter 1

Introduction

The story of Alexander Fleming and his discovery of penicillin in 1928 is well known to most of us, and since 1945 penicillin and other antibiotics have been an essential part of the fight against infections [1]. Antibiotics are used to treat and prevent bacterial infections. When bacteria adapt in response to these drugs, they can become antibiotic-resistant. In the same year that penicillin became publicly available (1945), Fleming famously warned about the danger of over-reliance on antibiotics and the threat of bacteria evolving resistance [2].

The World Health Organisation (WHO) stated, "antibiotic resistance is one of the biggest threats to global health, food security and development today" [3]. It is estimated that in 2019 4.95 million deaths were associated with antimicrobial resistance [4]. As bacterial infections develop resistance to more of the available antibiotics, they become harder to treat. In addition to measures applied to minimise the use of antibiotics and the spread of infections, research on new antibiotics is a significant focus in the health industry. Still, the number of new antibiotics entering the market has decreased in recent decades [5].

One of the alternatives to existing antibiotics currently being researched is antimicrobial peptides (AMPs). These peptides are part of the innate immune system of virtually all organisms and cause mainly lysis of bacterial cells, while some may also attack intracellular targets [6]. Although the exact mode of action of many AMPs is still unknown, several different mechanisms of action have been proposed. The main reason why AMPs are considered to be so promising is the non-specificity of membrane interactions where the AMPs attack the life-essential membrane itself instead of specific biochemical pathways [7, 8]. Therefore, the advantages of peptides over conventional antibiotics include a slower emergence of resistance, broad-spectrum activity, and the ability of some peptides to modulate the host immune response [7, 9, 10]. Even though the properties mentioned earlier make AMPs obvious candidates for future drug development, there are some drawbacks. Additionally to being quite costly to produce, AMPs have short amino acid sequences that are easily degraded in the bloodstream, and since they have non-specific modes of action they also show some degree of toxicity toward human cells. It is essential to know the exact mode of action in the membrane to solve these problems [6].

Indolicidin is a small AMP that has shown antimicrobial action against bacteria, fungi, as well as parasitic eukaryotes [11]. There are several reasons why indolicidin is one of the most studied AMPs for pharmacological use. First, the short amino acid sequence makes indolicidin

relatively easy to synthesise. Second, in addition to showing antibacterial activity against multi-drug-resistant *Escherichia coli* bacteria, it has been shown to exhibit marginal hemolysis in red blood cells from sheep [12]. Studies on the interaction between indolicidin and *E. coli* cells suggest that indolicidin may act through inhibition of DNA synthesis, acceleration of phospholipid dynamics, or induction of membrane thinning, promoting cell leakage [11, 13, 14]. Thus, although it has been studied for many years, the mode of action of indolicidin on bacterial and eukaryotic cells is not yet fully understood.

Precisely what causes the selectivity of specific peptides is not yet fully understood, and this is where this project aims to contribute. A hypothesis suggests that cholesterol acts as a protecting agent in eukaryotic cells, based on the lack of sterols in the bacterial membrane compared to the high concentration in eukaryotic membranes. Therefore, part of the main focus of this thesis will be to study the effect of cholesterol content on the interaction between lipid bilayers and the AMP indolicidin.

Another important property of biological eukaryotic membranes is the proposed existence of rafts or domains that house different integral proteins essential for processes such as intercellular signalling. However, their exact physical properties, and even their existence, remain somewhat controversial. Several studies have been conducted on the action of indolicidin on bacterial membranes, homogeneous model membranes, and model membranes mimicking bacterial cells. They have generally found that at low or physiologically relevant concentrations of indolicidin, it inserts itself in the outer part of the membrane without altering the membrane structure to a large degree [13, 15–18]. Some also report the formation of small irregular pores and disruption of intracellular targets [19]. Regardless of the exact bactericidal action, membrane interactions will be present. It is therefore essential to understand how indolicidin interacts with the membrane in order to fully comprehend its mode of action. Our group has done extensive research on the interactions between indolicidin and model systems mimicking bacterial membranes, making indolicidin an obvious candidate for this thesis [13, 20–23]. To complement the knowledge obtained on indolicidin's interaction with bacterial membranes, this thesis aims to study the effect of indolicidin on model membranes that mimic eukaryotic cells, in an effort to gain insight into its toxicity.

Since biological plasma membranes are incredibly complicated structures with hundreds of different lipids and membrane proteins, it would be difficult to identify the specific interactions with the peptide. This raises the need for a model membrane system that keeps the relevant elements from the biological membranes while at the same time being simple enough to accurately observe and describe the effects of the interaction with the peptide. Liposomes are good candidates for simple model systems seeing as they have a closed phospholipid bilayer (the main component of biological membranes). Different properties and membranes may be mimicked by varying the composition of lipids in the system. One of the main differences between the lipid composition of eukaryotic and bacterial membranes is the comparatively high amount of negatively charged lipids in the outer leaflet of the bacterial membrane. Multicellular eukaryotic membranes mainly contain zwitterionic lipids and cholesterol [24]. By varying the zwitterionic lipid composition of saturated and unsaturated lipids, we expect the emergence of lipid domains with tunable sizes in the model membranes. In this way, we can study how phase separation and raft size affect the interaction between indolicidin and model eukaryotic

membranes and hopefully shed light on the origin of toxicity of indolicidin.

Small-angle scattering (SAS) with X-rays and neutrons is a non-invasive technique used to study nanoscale structures, often in solution. Since it probes the right size domain under physiologically relevant conditions, the method is optimal for investigating the structure of the model membranes and how they change upon interactions with AMPs. Using neutrons makes it possible to obtain resolution in the bilayer plane and observe lateral phase separation. To obtain relevant structural information from the scattering data, analytical models that describe the structure of the liposomal bilayer and how it changes upon the addition of peptides are needed.

In summary, the main aim of this thesis is to understand better what protects eukaryotic membranes from AMPs by investigating the interaction between the AMP indolicidin and:

1. homogeneous model membrane systems with increasing cholesterol content in an effort to understand the proposed protective properties of cholesterol.

2. heterogeneous model membrane systems to look at the effect of raft size on the interactions.

Chapter 2

Background

2.1 Biological cell membranes

Cell membranes are phospholipid bilayers that regulate the flow of molecules between the extracellular and cytoplasmic environment [7]. The physical organisation of lipids and other membrane components allows the membrane to function as a permeability barrier, protecting the internal environment in the cell. All living organisms can be grouped into two families: *prokaryotes* and *eukaryotes*. Prokaryotes are cells without a nucleus and are almost exclusively single-cell organisms like bacteria. Eukaryotes are nucleated cells, and most are oxygen-dependent organisms, including plants, fungi, and animals. A common feature is that the membranes are composed of lipid bilayers, integral membrane proteins, and glycolipids. Biological membranes consist of hundreds of lipid species with varying head groups and chain compositions. Heterogeneity does not only affect proteins embedded in the membrane because certain lipid species can form clusters or domains in the membrane. Recent efforts in understanding eukaryote membranes have centred mainly around the existence of lipid rafts; the clustering of cholesterol with specific lipids [25–27].

2.1.1 Bacterial membranes

Bacterial membranes are divided into two categories: *Gram-positive* and *Gram-negative*. *Peptidoglycans*, sugar and amino acid polymers are essential components of bacterial membranes. The main differences between Gram-positive and Gram-negative membranes are the thickness of the peptidoglycan layer and the presence or absence of an outer lipid layer [28]. Gram-positive bacteria have a thick peptidoglycan layer outside the cytoplasmic membrane but do not have an outer lipid membrane nor lipopolysaccharides (lipids bound to chains of sugar molecules). The cell wall of Gram-negative bacteria has an inner and an outer lipid membrane, where the outer membrane contains integral membrane proteins and lipopolysaccharides. The outer and inner membranes are separated by a peptidoglycan layer [28, 29]. All bacteria have at least 15% anionic lipids, which may contribute to the selectivity of positive antimicrobial peptides. The negative charge and lack of rigidifying sterols in the bacterial membrane seem to be determinants of the selectivity of AMPs towards these pathogens [30, 31]. Figure 2.1 presents

an overview of the most relevant differences between eukaryotic and bacterial cell membranes.

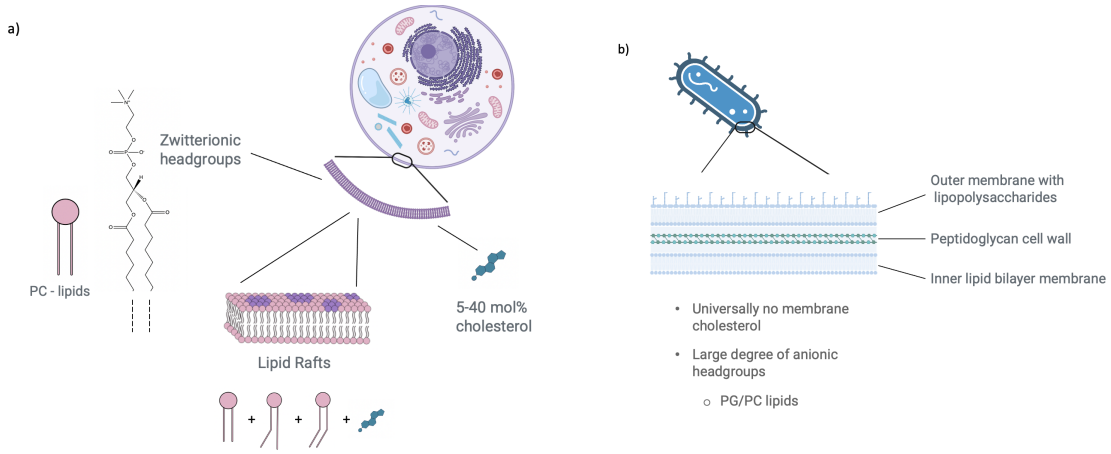

Figure 2.1: The main differences between (a) a eukaryotic membrane, with lipid rafts, cholestrol and mostly zwitterionic headgroups (for example phosphocholine (PC)) and (b) a Gram-negative bacterial membrane with a large degree of anionic headgroups (for example phosphoglycerol (PG)) in addition to zwitterionic headgroups. The gram negative bacterial membrane consists of a peptidoglycan cell wall surrounded by an outer lipid membrane containing lipopolysaccharides. Created with BioRender.com

2.1.2 Phospholipid bilayers

Most biological membranes are phospholipid bilayers. As seen in Figure 2.2, phospholipid bilayers consist of double layers of lipids. The polar head groups face the aqueous environment, and the non-polar fatty acid chains face each other, forming a hydrophobic core. Membranes are essential for the life and functions of cells. They regulate the transport of molecules in and out of cells and compartmentalise processes within the cell.

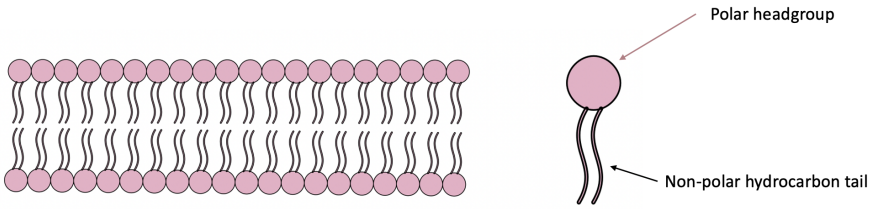

Figure 2.2: Sketch of a phospholipid bilayer (left) and a single phospholipid (right) with a polar head group and two non-polar acyl chains colloquially called a lipid tail.

Most lipids in biological membranes are composed of a head group connected to non-polar fatty acid chains, colloquially called *tails* [32]. The head group of phospholipids consists of a glycerol-3-phosphate group connected to another, usually polar group. The tails

may be saturated or unsaturated. Saturated tails have only single bonds between the carbon atoms, making them highly flexible because of their relatively free rotation. Unsaturated tails contain one or more double bonds where the pi-bond restricts free rotation. Figure 2.3 shows a general drawing of the chemical structure, where x denotes the headgroup substituent. Some common head groups are phosphatidylcholine (PC), phosphoethanolamine (PE), and phosphatidylglycerol (PG); their structure is shown in figure 2.3. Phosphatidylcholine has a choline headgroup substituent, while PE has an ethanolamine group, and both are neutral at physiological pH. PG has a glycerol group and is negatively charged at physiological pH [32].

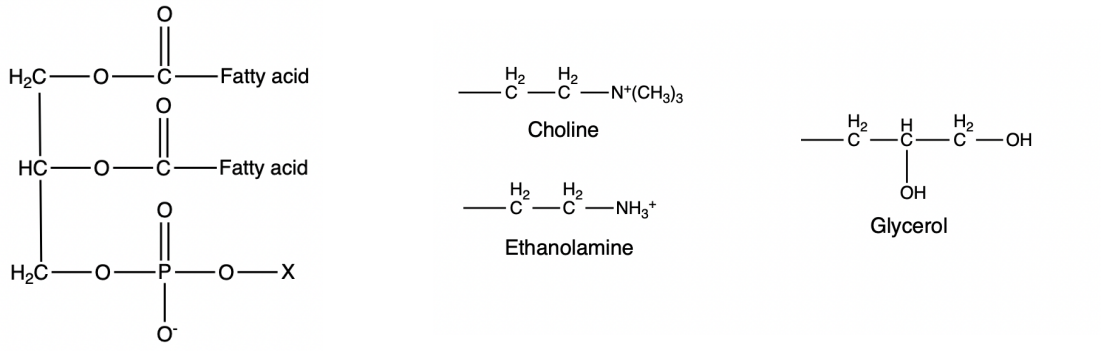

Figure 2.3: General structure of glycerophospholipids and common headgroup substituents; choline, ethanolamine, and glycerol. X denotes the headgroup substituent. Figure made using Chemdraw.

The lipids used in this thesis are all PC and PE lipids with different degrees of saturation.

2.1.3 Eukaryotic membranes

Two fundamental properties distinguish eukaryotic from prokaryotic lipid membranes: the high cholesterol content and the lack of lipids with negatively charged headgroups in eukaryotic membranes. Sterols are a class of lipids with a steroid nucleus (a fused system of four rings), a hydroxyl group, and a hydrocarbon chain [33]. Very few bacteria produce sterols, and those that do produce only small amounts [34]. In contrast to prokaryote cell membranes, eukaryotic cells have between 5 and 40 mol% cholesterol in the membrane. Sterols are one of the most abundant components in biological eukaryotic membranes and are known to affect short and long-range order, protein function, and cell growth [35]. As will be seen in the following subsections, high sterol content facilitates the lateral phase separation that creates what is commonly known as *lipid rafts*.

Cholesterol

Cholesterol consists of four fused, non-planar rings, an OH group, and a small hydrocarbon tail, as can be seen from the structure in figure 2.4. The $-OH$ group gives cholesterol a weak amphiphilic character, and the fused-ring system provides greater rigidity than other membrane lipids. Cholesterol is, therefore, an essential molecule in the regulation of membrane fluidity.

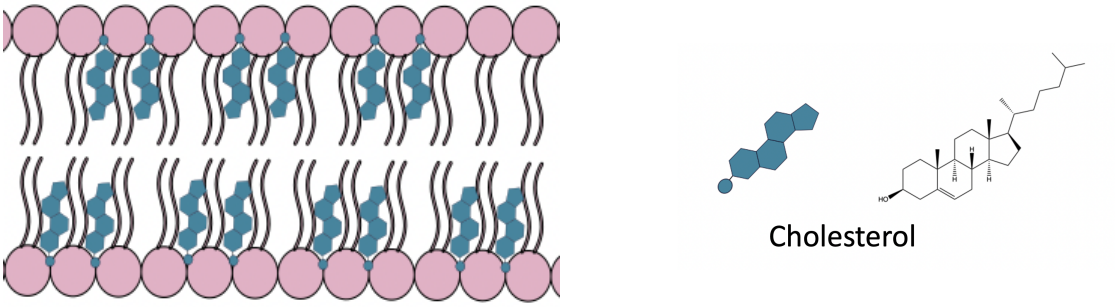

Figure 2.4: A sketch of cholesterol in the membrane. The OH-group is depicted to be residing in the headgroup region of the lipid bilayer.

Because cholesterol is an amphiphilic molecule, it incorporates easily into the lipid membrane. The polar $-OH$ group is positioned in the bilayer-water interface and the ring system with the hydrocarbon tail in the hydrophobic core [36]. The position of cholesterol in the bilayer depends on the degree of saturation of the lipids [37]. The most common position assumed in saturated and mono-/di-unsaturated lipids is the "canonical upright position", where the hydroxyl group is located near the lipid/water interface, and the hydrocarbon tail extends into the bilayer hydrophobic core [38]. In this position, the hydrophobic parts of two cholesterol molecules are shielded from unfavourable interactions with water by the neighbouring lipid head group.

The topic of cholesterol in membranes remains controversial. Several models have been proposed, describing the location of cholesterol. The *umbrella model* first proposed by Feigenson and Huang [39] in 1999 is based on the canonical upright position and suggests that one phospholipid headgroup may shield two cholesterol molecules from unfavourable interactions between the solvent and the hydrophobic residues. The work of Rheinstadter and Mouritsen [40] supports the umbrella model, as the distribution of cholesterol in DPPC bilayers appeared to be homogeneous. A problem with this model is that it requires extensive unfavourable pairwise interactions, as seen in subsection 3.1.2 on thermodynamics of domain formation. It also requires the translational diffusion of cholesterol to be very slow compared to the lipids, in order to maintain a regular arrangement, but their diffusion coefficients are comparable in binary mixtures [41]. Another model is the *statistical-mechanical model* based on the microscopic interactions between cholesterol and various states of the PC lipids (liquid ordered, liquid disordered, solid). This model can explain the high temperature and broad transition obtained for PC lipids and cholesterol binary mixtures, supporting the liquid ordered (l_o) - liquid disordered (l_d) phase coexistence model [41]. Yet another model proposes the formation of *condensed complexes* of cholesterol and lipids in exact stoichiometric ratios [41].

The field also seems to be split concerning the preferential partitioning of cholesterol into saturated lipid domains. Mouritsen [36] argues that cholesterol has a higher affinity for saturated lipids because their conformationally ordered tails provide tight interactions with the

hydrophobic surface of cholesterol. Kučerka and Marquardt [37, 38] found that increasing unsaturation increases the tilt of the cholesterol molecule away from the bilayer normal, thereby supporting cholesterol's preference for saturated lipids. In bilayers composed of polyunsaturated lipids, cholesterol resides in the middle of the bilayer, oriented along the bilayer axis. Due to the high disorder of unsaturated acyl chains, incorporating cholesterol would imply a large entropy-penalty in ordering these lipids, supporting a higher affinity for saturated lipids [41]. Fritsching *et al.* [42], on the other hand, reported no preferential interaction of cholesterol with the saturated lipid in a ternary mixture of unsaturated dioleoylglycerophosphocholine (DOPC), saturated dipalmitoylphosphatidylcholine (DPPC), and cholesterol.

Cholesterol thickens the bilayer through the condensation effect [43, 44]. The addition of cholesterol causes the area per lipid to decrease more than expected from ideal mixing. Since the membrane's hydrocarbon region volume is approximately conserved, a decrease in the surface area leads to increased membrane thickness. Cholesterol's condensing and acyl chain ordering effects on phospholipids in their liquid disordered (l_d) state are well established and assigned to the sterol's rigid ring structure limiting trans $\rightarrow$ gauche isomerisation of neighbouring phospholipid acyl chains [43].

Given the assumed preference of cholesterol for ordered chains, one would think it preferred the solid ordered phase. However, the rigid ring structure has a peculiar shape and size, which does not fit well with the packing of the lipids in the gel phase and may decrease the order of the gel phase lipids. Due to the preference for conformationally ordered chains and its size/shape restrictions, cholesterol is proposed to introduce a new liquid phase: the liquid ordered phase. In this phase, the lipids have a substantial positional disorder and lateral mobility, while the chains have significant conformational order [35, 36]. Cholesterol therefore shows a dual effect on membranes, rigidifying them while at the same time maintaining fluidity essential for membrane function. By inhibiting the ordering of the fatty acid chains, cholesterol also broadens the temperature range of the phase transition [32]. The formation of the new l_o phase coexisting with the l_d phase has led to the observation of nano- and microdomains, often referred to as *lipid rafts*.

2.1.4 Lipid rafts

The complex composition of biological membranes with many different proteins and lipid species gives a non-uniform membrane at a molecular level. Besides compositional variation, differences in the physical state of the lipids may lead to lateral lipid domain formation [45]. Domain formation can be described as a phase separation into liquid ordered l_o and liquid disordered l_d phases facilitated by the presence of sterols (see figure 2.5). Lipid rafts are domains of lateral organisation of lipids and proteins in biological membranes. They are generally small, dynamic, enriched in sterols and sphingolipids, and compartmentalise cellular processes [27]. The existence of lipid rafts and their application to biological membranes has long been, and to some degree still is, controversial. There is also an issue in extrapolating observations from a simplified model system to a complex living cell. Model systems do not accurately describe the proportion of the two phases in biological membranes, and there is currently no clear explanation for how lipid rafts in the outer leaflet could organise signal-transducing molecules in the inner leaflet of the plasma membrane [25]. On the other hand, several studies [46, 47] support the

use of model systems to study rafts as they may reproduce many of the properties expected in vivo, including the coexistence of l_o and l_d phases and the ability to concentrate saturated lipids, cholesterol and integral proteins that bind to specific antibodies. The physicochemical forces driving the formation of the domains are pretty well understood, but the biological existence and relevance remain elusive [25].

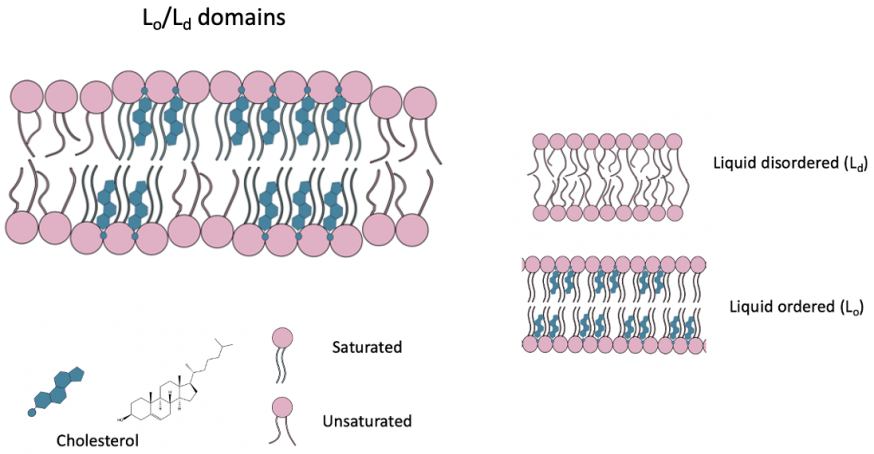

Figure 2.5: Sketch of cholesterol ordering of unsaturated lipids and liquefying lipids in the gel phase, causing domain formation. Cholesterol affects the physical properties of the lipids, creating a new phase: the liquid ordered, l_o, phase.

For binary mixtures of PC lipids and cholesterol, there have been several reports on phase separation in mixtures with saturated lipids. In the mixtures reported, the condensation effect increased the thickness of the bilayer where cholesterol is incorporated, proposing that phase separation occurs to minimise regions of hydrophobic mismatch at interfaces between areas of different heights [41, 48]. Given the small size of the observed separations, there are still discussions about whether the heterogeneities can be described as a l_o/l_d phase separation [41]. In contrast to binary mixtures, there is broad consensus that phase separation occurs in some ternary mixtures of cholesterol with two phospholipids where one has a low T_m and is typically unsaturated, and the other has a high T_m, often saturated [41].

For model membranes composed of lipids with different head groups, the structure of the head groups will also affect domain formation. The thermal stability of ordered domains has been found to decrease with the structure of the polar headgroup for 1-palmitoyl, 2-oleoyl (PO) lipids in the order PE > PS (phosphatidylserine) > PC. It has also been shown for other acyl chain lipids that the headgroup structure affects the ability to pack the lipids tightly and hence affects the stability of domains [49]. According to Bakht *et al.* [49], lipids with a low transition temperature (unsaturated lipids) can stabilise ordered domain formation by saturated lipids and cholesterol by 1) having structures resulting in immiscibility of the low- and high melting lipids

and 2) having structures that allow for tight packing within ordered domains.

2.2 Antimicrobial Peptides (AMPs)

Antimicrobial peptides (AMPs) are essential molecules in the innate immune system of virtually all organisms [7]. In general, they are peptides with about 15-40 amino acid residues, a molecular mass less than 10 kDa (approximately $1.6 \cdot 10^{-20}$g, or the weight of $\frac{1}{3.9 \cdot 10^{16}}$ hair strand), and a net positive charge. Small as they are, they prove a mighty weapon in the fight against pathogens. They have a broad range of activity and act on bacteria, fungi, parasites, viruses and even cancer cells. The pathogen membrane seems to be the key target of the AMPs with which it interacts in a non-specific manner. Bacteria would therefore require a profound redesign of their membrane for it to develop resistance, which is why they are so promising as future antibiotics [7, 21, 50].

Despite the general physical properties being similar for most peptides, they exist in a wide range of secondary structures and have limited sequence homology. The most common secondary structures are amphipathic α-helices, peptides with two to four β-strands and random loop structures. Linear α-helical peptides are, so far, the largest group of known AMPs, [7] with examples like Magainin (found in the African clawed frog) and Melittin (from bee venom). Indolicidin is a bovine peptide with a primarily random coil structure [20].

Several factors modulate the activity of the peptides. The most important factors are thought to be the membrane electric potential (which depends on the interaction between lipid head groups and the cationic peptide) and the membrane curvature/packing of lipids. Hydrophobic and van der Waals interactions between the peptide and the hydrocarbon chain of the lipids may also disrupt the lipid packing and have a significant impact on the membrane structure [7]. Several modes of action have been proposed. Among the most common are membrane permeabilisation through the formation of pores and solubilisation in a detergent-like way [7].

2.2.1 Modes of action

AMPs that target bacteria work primarily by permeabilising their cell membranes but do not lyse erythrocytes [51]. According to Epand and Epand [50], there are at last three major types of antimicrobial action:

1. Membrane interactions: can include permeabilising the membrane or affecting specific membrane functions [50].

2. Interactions with an intracellular target: given the positive charge of the peptides, they can interact with the negatively charged DNA, leading to a cytotoxic action [50, 52]. Since the DNA in bacterial cells is not enveloped, AMPs can form complexes with the DNA and thus inhibit transcription and synthesis, and rigidify the cytoplasm through crosslinked networks [53].

3. Stimulation of the innate immune system by promoting the release of natural defence peptides as well as stimulating phagocytic cells [50].

Following is a description of the most common models used to describe membrane disruption by pore formation and micellisation, followed by other models of membrane interaction. Figure 2.6 shows a sketch of the membrane disrupting and thinning/thickening actions.

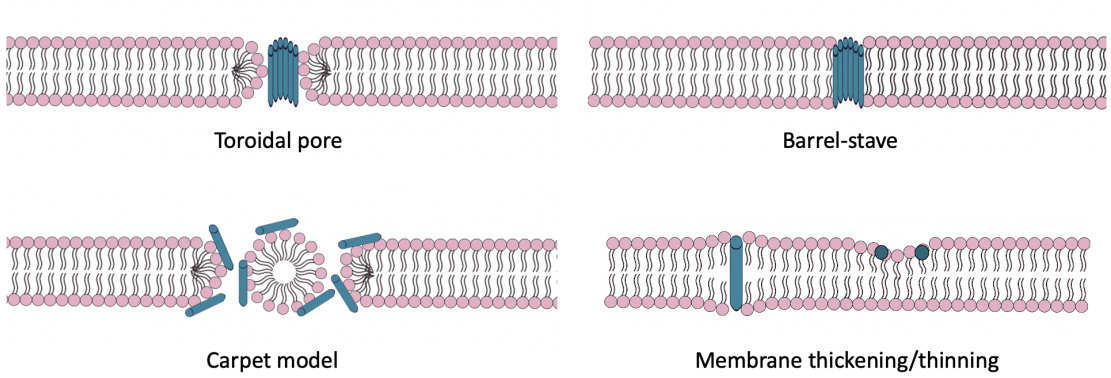

Figure 2.6: Some of the proposed modes of action for AMPs: the toroidal pore formation where peptides bend the membrane into leaflets; the barrel-stave model, where the peptides form a barrel-like pore; the carpet model the peptides are absorbed on the membrane surface, and might form pores above a threshold concentration; peptide caused membrane thickening or thinning.

Toroidal pore model

In the toroidal pore model, the peptides are partitioned into the membrane, disrupting it by inducing a bend in the membrane leaflets. The bending of the membrane creates membrane tension which may lead to disintegration of the membrane, creating pores lined with both peptides and the lipid head groups [7].

Barrel-stave model

In the barrel-stave model, peptides bundle up in a barrel-shaped central tunnel, giving the model its name. This mechanism is usually induced by peptides with a significant degree of hydrophobicity [7]. The hydrophobic domains of the peptide face the hydrophobic chains in the membrane bilayer, while the hydrophilic domains line the pore.

Carpet model

In the carpet model, peptides are adsorbed on the bilayer surface like a carpet [7]. This mode of action is especially prominent when the membrane has a large degree of anionic headgroups to which cationic AMPs can bind. Above a threshold concentration, the peptides might form pores, allowing additional AMPs to access the membrane. The membrane may disintegrate and form micelles or other smaller structures.

Several non-membranolytic mechanisms have also been reported. These include membrane thinning or thickening, electroporation, lipid segregation, and the formation of non-lamellar phases [7]:

Membrane thickening and thinning

Membrane thickening may occur when there is a mismatch between the length of the acyl chains and the inserted peptide, leading to membrane deformation to accommodate for the peptide [54]. Local membrane thinning is observed by, for example, Melittin before pore formation. It is caused by hydrophobic interactions between the bound peptide and the lipid tails, resulting in lipid packing frustration, forcing the polar lipid head groups aside, and hence membrane thinning [7].

Electroporation

Electroporation occurs when the interaction of the cationic peptide with the membrane promotes an electric potential difference across the membrane. When the potential reaches approximately 0.2V, a pore is believed to be created [7].

Lipid segregation

Peptide induced lipid segregation separates anionic and zwitterionic lipids by clustering the anionic lipids with the cationic peptides. The occurrence of lipid segregation might introduce line defects that increase the membrane's permeability [7]. Indolicidin is a small cationic peptide. Since bacterial membranes have a high amount of lipids with negatively charged headgroups, one proposed mode of action has been lipid segregation of anionic lipids around indolicidin. However, Nielsen *et al.* [20] have shown that in model membranes that mimic bacterial membranes, indolicidin does not promote any lateral segregation. Another possibility is that the peptide interacts preferentially with different lipid tails or phases, thus promoting a lateral phase separation.

Non-lamellar phase formation

A more recent discovery [7] has been the ability of some AMPs to produce membrane perturbations by the formation of non-lamellar phases. Lipids may self-assemble into structures like micelles, tubes, and lamellar structures (for example, bilayers). Under specific conditions, they may also form hexagonal or cubic phases. For biological membranes, the phase behaviour is obviously far more complex than for pure lipid systems [7].

2.2.2 Indolicidin

Indolicidin is a small peptide with only 13 amino acid residues and is extracted from bovine neutrophils (a type of white blood cells). As seen in Figure 2.7, showing its structure and sequence, it is rich in the aromatic amino acids tryptophan and proline and has a net positive

charge of +4. Contrary to many of the most studied AMPs, which are alpha-helical, indolicidin is known to be largely unstructured in solution [18, 20, 21].

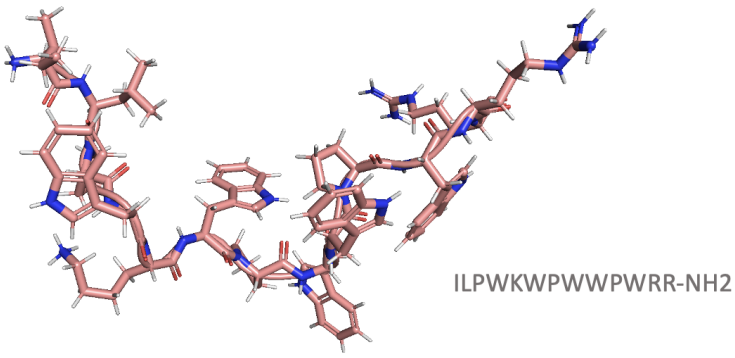

Figure 2.7: Structure and amino acid sequence of indolicidin (figure made using PyMOL). I = isoleucine, L = leucine, P = proline, W = tryptophan, K = lysine, R = arginine.

By performing model analysis on pure indolicidin scattering, Nielsen *et al.* [20] showed that indolicidin in solution exists mainly as random coil structures but with some (about 1%) peptide-sheet formation (Figure 2.8). The amphipathic nature of the peptide, together with the disordered shape, makes it reasonable to assume that it will interact mainly with the interface between the hydrophobic tail region and the hydrophilic head group regions, as supported by observations by Nielsen *et al.* [20].

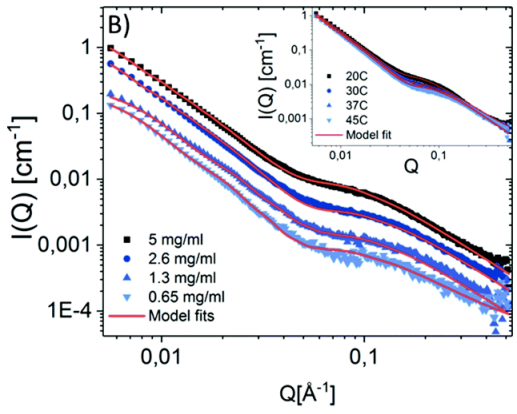

Figure 2.8: Scattering curve of free indolicidin with the model fit. The inset graph shows that increased temperature cannot break up the enlarged structures (the concentration shown is 5 mg/mL). Reused with permission from [20].

Indolicidin is known to interact with both Gram positive and Gram negative bacteria [11, 18]. The large amount of tryptophan is thought to function as an anchor between the peptide and the head group region of the membrane, playing an important role in preferential partition of peptides (in addition to charge). As mentioned in the introduction, the exact mode of action is still unknown, as indolicidin has been reported to both interact with the membrane, and attack internal targets such as bacterial DNA. In addition to antibacterial activity, indolicidin has also been shown to be reasonably potent against fungi as well as protozoa [11].

Previous studies have suggested different interactions between indolicidin and model membranes, depending on the concentration and the method of investigation. At physiologically relevant concentrations indolicidin has been reported to insert itself in the outer region of bacterial mimicking membranes with anionic and zwitterionic headgroups, without significantly altering the thickness or overall structure of the membranes [13, 55]. At higher concentrations, partial insertion into the bilayer and lipid removal in a disordered fashion have been observed using SAXS, Quartz crystal microbalance with dissipation monitoring, neutron reflectometry and atomic force microscopy (AFM) [20–22, 56]. Others suggest that indolicidin acts through an irregular barrel-stave or toroidal pore model [15, 57, 58]. Falla *et al.* (1996) [18] showed that permeabilisation of the E-coli membrane does not lead to lysis, suggesting that the mode of action is composed of different actions, supported by Hsu *et al.* (2005) [19], who suggested that indolicidin may pass through the membrane by a self-promoted uptake pathway ad bind to DNA, inhibiting DNA synthesis. Recent studies indicate that indolicidin is less protected and thus less incorporated in membranes with zwitterionic head groups than anionic head groups [16]. As a consequence, it should be less incorporated into eukaryotic membranes than prokaryotic membranes.

A suggested mode of action of indolicidin in zwitterionic membranes is as an organic anionic carrier. Disturbing the regulation of osmotic balance can lead to rupture of the erythrocyte membrane, which may explain its haemolytic activity [59]. A study by Shaw *et al.* [57] performed on binary PC membranes using AFM (atomic force microscopy) suggests local membrane thinning and solubilisation upon addition of indolicidin. The same study suggests that indolicidin preferentially inserts itself into the fluid phase domains and that the indolicidin-membrane association is greatly influenced by specific electrostatic interactions, lipid fluidity, and peptide concentration [57]. At sufficiently high concentrations, other studies support the idea that indolicidin may form pores in PC-membranes, for example, according to the toroidal pore model [60]. A study using supported DMPC bilayers saw the formation of worm-like micelles at high concentrations of indolicidin, proposing an AMP mode of action driven by the reduction of line tension [17].

2.2.3 The effect of cholesterol and lipid rafts on the interaction between antimicrobial peptides and membranes

Because of the inherent lack of sterols in bacterial membranes, cholesterol has long been hypothesised to play an important role in the selectivity of antimicrobial peptides. One way cholesterol is believed to prevent the action of AMPs is by counteracting the membrane thinning effect of some peptides. Because of the condensation effect provided by cholesterol, fewer

peptides are expected to bind to the membrane, reducing the membrane thinning effect, which leads to a decrease in their potency. This aspect is of major importance for the pharmacological use of AMPs since it is believed that the toxicity to host cells is partially inhibited by the presence of cholesterol, as demonstrated in several studies[7]. For the peptide magainin 2, it has been shown that sterols, like cholesterol, reduced the erythrocyte membrane susceptibility to the peptide [51]. On the other hand, a study done by McHenry *et al.* [61] showed that cholesterol only inhibits membrane disruption to a significant degree in homogeneous model membranes but not in mixed lipid systems (DOPC/DPPC) upon interaction with Magainin analogues. However, few studies have looked at both the effect of cholesterol and presence of domains.

The effect of the presence of lipid rafts or l_o/l_d domains on peptide interactions has been studied to a larger degree. Oreopoulos *et al.* [56] and Shaw *et al.* [57] both used ternary systems of one saturated lipid (DPPC and DSPC respectively), unsaturated DOPC, and cholesterol to study interactions with indolicidin. Both studies suggested a preference of indolicidin for the l_d phase, and that indolicidin may alter the membrane thickness. Shaw *et al.* observed a disordering of the rafts as a consequence of peptide insertion, suggesting that disruption of rafts might be an important part of the mechanism of indolicidin. A study by Pokorny *et al.* [62] looked at the role of lipid rafts in the mechanism of the AMP δ-lysin, which is known to lyse eukaryotic cells. They found that δ-lysin preferntially partitions into the l_d phase in model membranes of POPC/cholesterol/sphingomyelin, and that the increased concentration in the l_d phase facilitates lysis [62].

Many studies point towards a preference of a wide range of AMPs to the l_d phase [56, 57, 62, 63]. Su *et al.* [63] used coarse-grained simulations to study the preference of four different alpha-helical peptides for the l_o and l_d phase, and found that all studied peptides showed a clear preference for the l_d phase. At the highest peptide concentration the l_d phase seemed to become saturated, and some AMPs were driven into the l_o domains [63]. Interestingly, preferential insertion in the domain interface regions was seen for all four peptides. The preference of lipids for the l_d phase may be explained enthalpically [63]. For lipids in both phases the presence of peptides led to favourable peptide-lipid interactions, above all in the l_o phase where the density of peptide-lipid interactions is higher [63]. However, peptide adsorption always comes with a cost in weakened lipid-lipid interactions, especially between lipids in the more compact and ordered l_o phase [63]. By concentrating the peptide in the l_d phase, more favourable lipid-lipid interactions in the l_o phase compensates energetically for the weakened lipid-lipid and peptide-lipid interactions in the l_d phase, and for the entropic tendency to distribute homogeneously in the membrane [63]. The interface is so energetically favourable because peptides may interact with l_o lipids to some extent, and thus lower their interaction energy, while at the same time not interfere with the lipid-lipid interactions in the l_o phase [63].

In summary, there seems to be a consensus that lipid rafts affects the interactions of peptides, and that most peptides seem to preferentially partition into the l_d domains and interface regions. Studies by Shaw *et al.* and Su *et al.* points to peptides having a possible mechanism including the decrease of line tension and subsequent disruption of domains. However, there are still many unanswered questions regarding the mechanisms of AMPs in membranes containing rafts, and how cholesterol affects said interactions.

Chapter 3

Theory

3.1 Thermodynamics of self-assembly

The ability of molecules to self-assemble and form larger structures is essential for life; cellular membrane formation, stabilisation and interactions with proteins and DNA are all based on said process. *Why* specific molecules aggregate in solution can be understood by looking at the thermodynamics of the system, which is the systematic discussion of the transfer of energy [64, p. 14, 15]. In simpler terms, thermodynamics deals with how the internal energy of the system and the entropy work together to create the most energetically favourable systems. The equilibrium state is often defined as the state where the system's free energy is minimised. At constant pressure and temperature, the Gibbs free energy is defined as

$$G = H - TS, \tag{3.1}$$

where the enthalpy, H, measures the internal energy arising from, for example, chemical bonds, and hydrophobic and electrostatic interactions. Entropy, S, is often described as a measure of disorder. More accurately, it is a measure of the distribution of energy. The entropy is high if the energy is distributed over many different modes of motion (rotational, vibrational and translocational). According to the Second Law of Thermodynamics, all spontaneous processes are accompanied by increased entropy. Looking at larger systems with n moles, we often look at the chemical potential, which is the molar free energy:

$$\Delta\mu = \frac{\Delta G}{n}. \tag{3.2}$$

When a large number of particles are present in a solution, the intermolecular interactions relating to the thermodynamic relations in the system become more complicated as the interactions with the solvent have to be taken into consideration. Larger particles will also exhibit long-range order in addition to molecular binding forces. Consequently, geometric conditions and steric effects must be considered together with intermolecular forces to understand systems of macromolecules like lipids.

Lipids and their aggregates are soft materials, meaning that they and their systems are soft, flexible, and fluid-like. This is because the lipids in the structures are not held together by

strong covalent or ionic bonds but by weaker van der Waals, hydrophobic, hydrogen-binding and screened electrostatic interactions [65]. The hydrophobic effect is the predominant driving force of self-assembly. When the hydrophobic parts of the molecules are exposed to the solvent, water molecules tend to organise themselves so that the least number of charges face the hydrophobic species. Because the water molecules surrounding the hydrophobic molecules are more ordered than in bulk, there is a loss of entropy associated with the ordering. When hydrophobic molecules group together, the non-polar surface exposed to the solvent is reduced, thereby reducing the number of water molecules that have to order around the structure. There is also an entropy loss when ordering the lipids into micelles, so micellisation occurs when the energy loss from ordering the lipids is smaller than the energy gain by shielding the hydrophobic tails. The hydrophobic effect is illustrated in figure 3.1 (molecules not to scale).

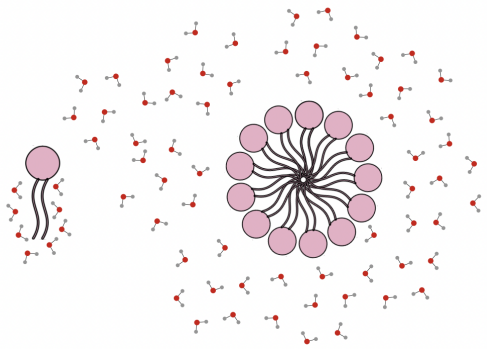

Figure 3.1: The hydrophobic effect. The water molecules form an ordered structure around the hydrophobic tails. Shielding the tails from the solvent decreases the entropy of the water molecules.

The association of lipid "monomers" into aggregated systems like micelles can be thought of as a reaction where N monomers m form aggregates (micelles) of P lipids a_P:

$$P \cdot m \xrightarrow{k} a_P, \tag{3.3}$$

where k denotes the equilibrium constant [66]. Assuming that all micelles contain exactly P lipids, the equilibrium constant can be written as

$$k = \frac{[a_P]}{[m]^P}, \tag{3.4}$$

following the law of mass action. $[a_P]$ and $[m]$ denote the concentrations of aggregates and lipids, respectively. The parameter ν describes the number of molecules per object (that is, monomers plus micelles), and is given by

$$\nu = \frac{[m] + P[a_P]}{[m] + [a_P]}. \tag{3.5}$$

Combining the equations (3.4) and (3.5), gives ν as

$$\nu([m]) = \frac{1 + Pk[m]^{P-1}}{1 + k[m]^{P-1}}. \tag{3.6}$$

Micellisation is a cooperative process, meaning that the system changes its state rapidly once the process has begun. The model described above predicts a sharp transition at the critical micelle concentration (CMC), the concentration at which monomers start to form aggregates. Figure 3.2 shows a plot of ν as a function of $[m]$, and the sharp transition is observed at a point corresponding to $\frac{1}{k} = [m]^{P-1}$. This monomer concentration is CMC.

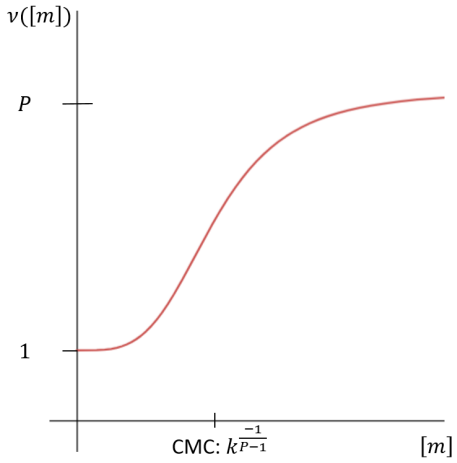

Figure 3.2: Illustration of the model describing CMC and micelle formation. Below the CMC, most molecules exist as monomers in solution. Above the CMC, most molecules are in micelles of P monomers.

Below the CMC, $[m]$ is large, and P small, so ν will approach 1, and the solution will predominantly contain lipid monomers. Above the CMC ν approaches the micelle aggregation number (the number of lipid molecules in a micelle), so the solution will mostly contain aggregates [66]. Above the CMC, the concentration of monomers will remain constant while the concentration of aggregates increases linearly. From the perspective of thermodynamic interactions, the CMC can be expressed using interaction free energy. Identical molecules in a stable system of aggregated structures in solution are required by equilibrium thermodynamics to have the same chemical potential. The equilibrium constant, as seen in Equation (3.4), can be expressed in terms of the free energy of a molecule in solution (monomer) μ_1^0, and in the aggregate μ_P^0 as

$$k = \exp\left(P(\mu_P^0 - \mu_1^0)k_B T\right), \tag{3.7}$$

where k_B is the Boltzmann constant and T is the temperature [65].

Rewriting the law of mass action with expression (3.7) gives the concentration of aggregates as

$$[a_P] = P(x_1 \exp(\frac{\mu_1^0 - \mu_N^0}{k_B T}))^P. \tag{3.8}$$

Since the total concentration of lipids has to be equal to $\Sigma_P[a_P]$, the concentration of monomers cannot exceed $[m] = \exp(-\frac{\mu_1^0 - \mu_P^0}{k_B T})$, which defines the critical micelle concentration as:

$$cmc = \exp(-\frac{\mu_1^0 - \mu_P^0}{k_B T}). \tag{3.9}$$

As seen in Equation (3.9), the concentration of aggregates depends on the interaction free energy and the temperature. To form large, stable aggregates, the interactions between the molecules and the solvent cannot be the same for the aggregated and dispersed states. The chemical potential of the lipids in the aggregated state must be less than the chemical potential of the monomers: $\mu_P^0 < \mu_1^0$. The interaction energy has, as will be explained, several contributing factors. The dependency on temperature seems to be quite simple in this expression, but the complicated effect of temperature on the fatty acid chains will also affect the hydrophobic parameters.

Micelles and liposomes, as depicted in figure 3.3, are common self-assembly structures for lipids. The structures are formed and maintained due to a balance of two effects: (1) the hydrophobic free energy, which increases with the surface area, and (2) the electrostatic repulsion between headgroups.

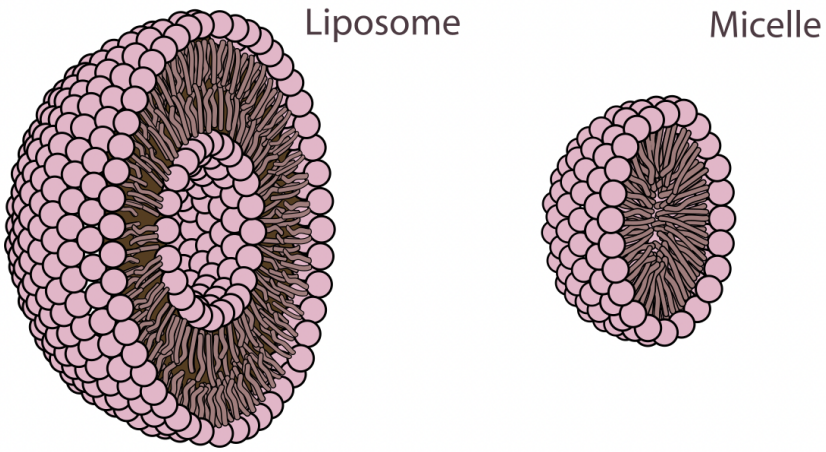

Figure 3.3: Illustration of the cross-section of two common self-assembled structures; the liposome to the left and the micelle to the right. Adapted from reference [67]

Tanford and Israelachvili [65, 68] described the preferential partitioning free energy of a micelle of surface area a as

$$\Delta\mu^0(a) = \gamma a + \frac{c}{a}, \tag{3.10}$$

where γ is the interfacial tension between the micelle and the solvent, and c is a constant. The first part, γa, describes the hydrophobic effect. Because the hydrophobic free energy increases with increased surface area (per headgroup), smaller surface areas are favoured. The second part of Equation (3.10), c/a, describes the electrostatic repulsion between head groups. Increasing the surface area decreases the free energy and is therefore favourable. The size of the micelle is a balance between these opposing forces. A micelle should be large enough to have a shielded hydrophobic core but small enough to allow for well-separated headgroups by sufficient surface curvature. As seen in figure 3.4 the opposing forces act in all directions in the micelles. For simplicity, it is often assumed that the forces studied act in the same plane.

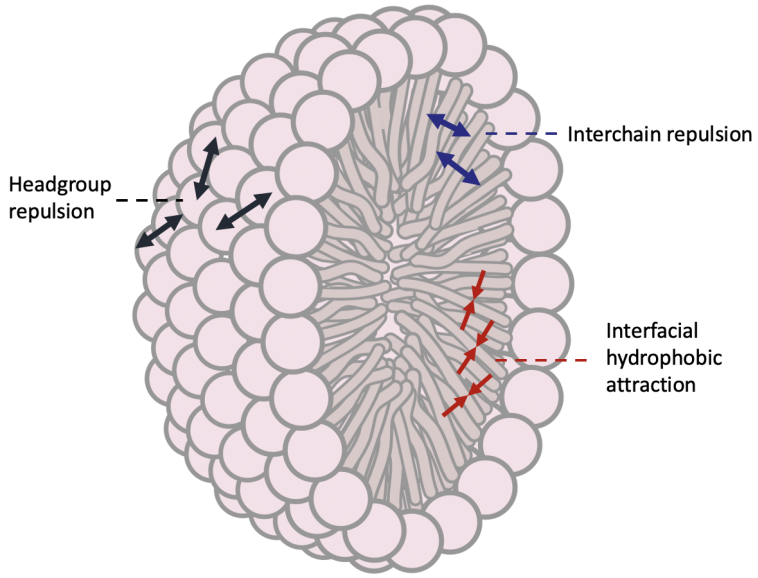

Figure 3.4: Opposing forces in micelle formation: headgroup and interchain repulsions favours larger volume, while the hydrophobic attraction between chains tend to minimise the volume.

The equilibrium area of the head group is found by minimisation of the free energy function. Assuming that both forces act in the same plane, the equilibrium area is:

$$a_0 = \sqrt{\frac{c}{\gamma}}. \tag{3.11}$$

Rearranging Equation (3.8) and inserting the expression obtained for the constant into Equation (3.7) gives the free energy as a function of the equilibrium area and the surface tension, two measurable quantities [65, 68]:

$$\Delta\mu^0(a) = 2\gamma a_0 + \frac{\gamma}{a}(a - a_0)^2. \tag{3.12}$$

As can be seen from Equation (3.12), any deviation from the equilibrium surface area is energetically unfavourable. Since the area of the head group, and hence μ_N^0, depends on the shape of the molecules, geometrical packing restrictions must be evaluated to determine

which structures are the most favourable. This is where the packing parameter enters. The packing parameter p gives a numeric estimate of what structure is the most stable based on the geometrical considerations:

$$p = \frac{v}{a_0 l_c}, \tag{3.13}$$

where v is the volume of the hydrophobic chain and l_c is the maximum effective length the hydrophobic chains may assume [65]. The geometry with the lowest possible surface for a given volume is a sphere. For spheres, the radius R, hydrocarbon volume v, and surface area a per lipid at the water-lipid interface are related by

$$R = \frac{3v}{a}. \tag{3.14}$$

Since the radius of a spherical micelle cannot exceed l_c, the critical condition for the formation of spheres is

$$\frac{1}{3} = \frac{v}{a_0 l_c}. \tag{3.15}$$

Suppose the critical condition for spheres is exceeded. In that case, other structures will form, as seen in figure 3.5: if the packing parameter is $\frac{1}{3} < p < \frac{1}{2}$, worm-like micelles are formed; if $\frac{1}{2} < p < 1$, cylindrical micelles are formed; and planar bilayers like in liposomes are formed for $p \geq 1$.

Regardless of the structure, there are two criteria aggregated structures must satisfy: (1) no point in the structure can be further away from the lipid-water interface than the critical length l_c, and (2) the total volume of the hydrocarbon core V and the total surface area A must approximately satisfy the relation $V/v = A/a_0 = P$.

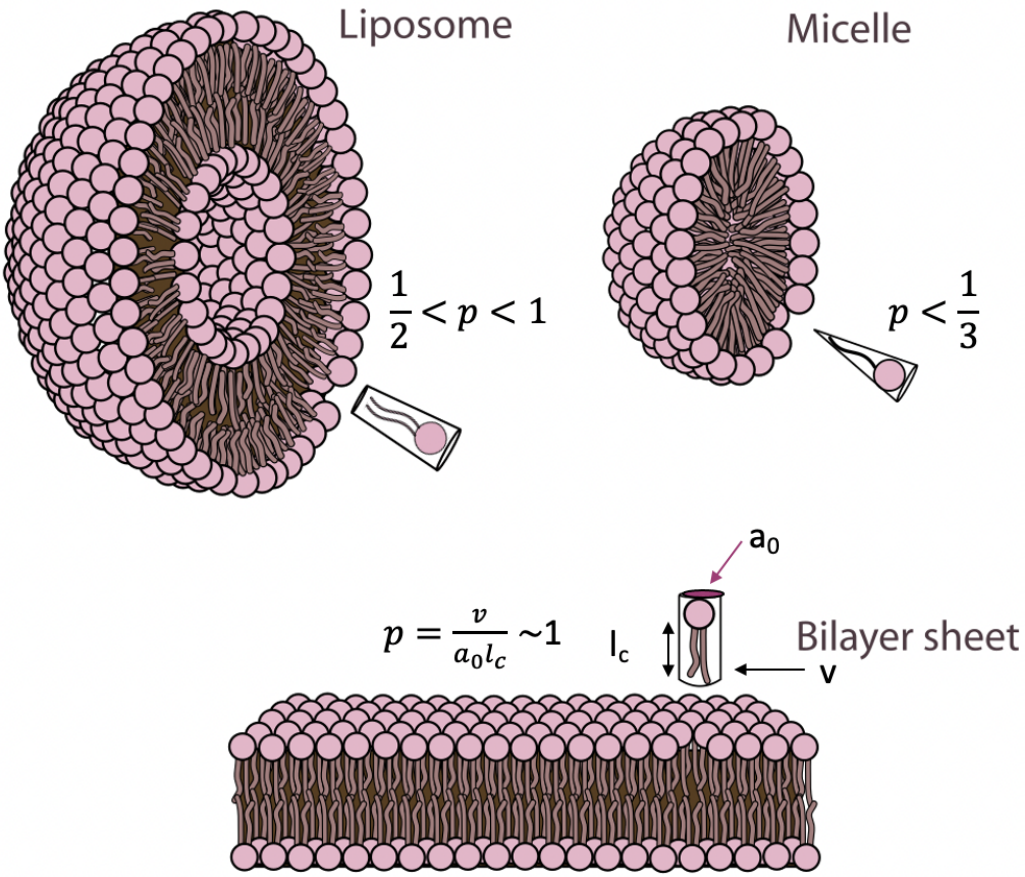

Figure 3.5: Different lipid geometries will prefer to pack differently, giving differently shaped aggregates. The packing parameter, p, is used to predict what aggregates different monomers prefer. Figure inspired by [65].

3.1.1 Liposomes and planar bilayers

Liposomes are closed, solvent-filled vesicles bounded by a bilayer. The diameter is usually several hundred angstroms ($1\text{Å} = 10^{-10}m$), and they are generally quite uniform in size. The thickness of the bilayer can be estimated from the maximum length of a lipid in [Å] given by [68]:

$$l_{max}(n) = 1.5 + 1.265n, \tag{3.16}$$

where n is the number of carbon atoms in the tail. For tails with 16-20 carbon atoms the expected maximum thickness of the bilayers are 21.74 - 26.8 Å. Typically, the thickness of the tail group region is $20 - 30$Å, and the thickness of the head groups is approximately $7 - 10$Å

[68].

Because lipids with two acyl chains have a more rectangular shape, they often prefer to pack in bilayer structures. The tail volume is relatively large compared to the headgroup volume, giving a packing parameter of around 1. Additionally, doubling the number of hydrophobic chains gives a larger hydrophobic interaction potential, so the CMC will, according to Equation 3.9, have a very low value [65]. This predicts that phospholipids will form thermodynamically stable bilayer structures even at low lipid concentrations.

The reasons why spherical vesicles are formed, rather than infinitely large bilayer sheets, are mainly entropic and hydrophobic. Following the hydrophobic effect discussed above, fewer hydrophobic chains will be exposed to the solvent if the vesicle is closed. A smaller aggregation number will also always be entropically favoured. As long as the structures can maintain a surface area close to the optimal area a_0, closed vesicles are the preferred structures. For planar bilayers, the packing parameter has to be approximately 1. The lipids have to have a more cone-shaped structure to pack in the outer leaflet for the curved bilayer in vesicles, which demands $p < 1$ [65]. These packing restrictions will not apply to the inner leaflet, as it has a negative curvature, as seen in figure 3.5.

Up until now, all forces have been assumed to act in the same plane. Curvature effects must be considered when the curved interface affects the interaction energy μ_P^0 [65]. When taking into account the repulsive forces between adjacent head groups at a distance $+D$ above the hydrocarbon-water interface and between chains at a distance $-D$ below the interface, the mean energy of a molecule in a bilayer vesicle is

$$\mu_N^0 = 2\gamma a_0(1 - \frac{Dt}{4R^2}) = \mu_\infty^0 - \frac{\gamma a_0 Dt}{2R^2}, \tag{3.17}$$

where t is the bilayer thickness. D is the distance at which the repulsive forces can be modelled to be laterally acting. For phospholipids, the inter-chain repulsion dominates due to the high hydrophobic potential, so D will be negative, increasing the mean energy [65]. If the liposome radius $R \to \infty$, the energy approaches that of an infinite planar bilayer, μ_∞^0, and the contributions from curvature effects vanish. Since larger radii will decrease the mean energy, larger vesicles are energetically more favourable than smaller ones. Circular bilayer discs close up to form liposomes when the line tension energy (favours curling) exceeds the bending energy (opposes curling). It can be shown that a bilayer will form a vesicle if $R > 4k_b/\lambda$ [65]. k_b is the bending modulus, and λ is the line tension. Typical obtained values for liposome radii are between 10 and 100 nm.

Even though the CMC for lipid bilayers is very low, liposomes do not form spontaneously. A conventional route for preparing liposomes is through the hydration of films of stacked planar bilayers followed by sonication and extrusion. Lipids are dissolved in organic solvents like methanol and chloroform and then dried to form a stacked bilayer film. Upon rehydration, the water molecules penetrate the film, separating the bilayers. The bilayer edges merge to form multi-lamellar vesicles (MLVs), which are several bilayer vesicles surrounding each other. Upon sonication of MLVs, ultrasonic waves disrupt the vesicles, and smaller, unilamellar vesicles (ULVs) are formed. To get a smaller size distribution, it is common to extrude the lipid solution, pressing it through a membrane with uniform cylindrical pores [69]. A sketch of the mechanism is shown in figure 3.6.

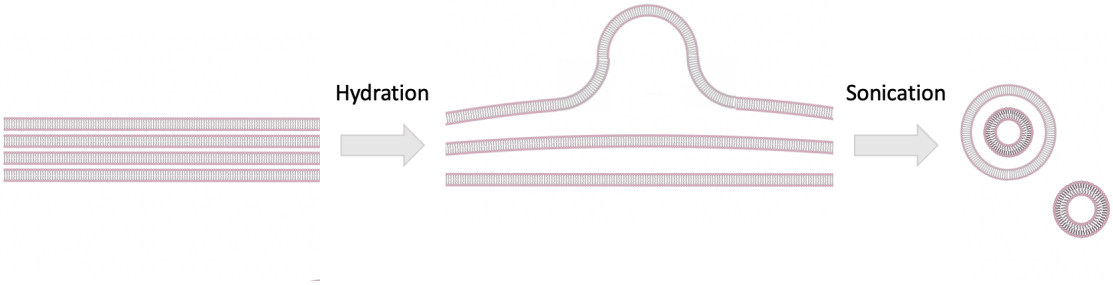

Figure 3.6: Preparation of multi-lamellar vesicles. Dry lipid bilayer stacks are hydrated and then sonicated.

It is possible for the equilibrium distribution of soft amphiphilic molecules, like lipids, to peak at several aggregation numbers. This means that, in the same system, smaller aggregates, like micelles, can exist in equilibrium with larger vesicles like liposomes [65].

3.1.2 Thermodynamics of domain formation

Following the thermodynamic description of lipid aggregation, the same principles may be applied to describe the formation and stabilisation of rafts. In a lipid monolayer, rafts may be considered as 2D micelles at the surface, with their formation driven by line-tension reduction [70]. Across a bilayer, domains can be coupled (phase-separated in both leaflets) or isolated. The shape and size of domains are the results of line tension and repulsive lipid interactions. Line tension arises from mismatching properties at the domain interfaces, such as differing lipid tail lengths. A larger mismatch of bilayer thickness between the l_o and l_d domains increases the line tension and results in larger domains. An increased domain area gives a smaller interface perimeter and minimises the boundary energy [71].

As mentioned in Section 3.1.2 on the thermodynamics of self-assembly, the interactions between lipids are generally weak: as a consequence, massive phase separations are generally not expected. Small, dynamic lipid domains, probably stabilised by membrane proteins, are more probable [45]. If the magnitude of the lipid-lipid interaction energies were large, phase separation would be irreversible, giving static structures. In model membranes, lipids typically have differences in chemical potential between -1.255 and $+1.255$ kJ/mol, while complete phase separation usually requires about 1.674 kJ/mol [45]. Almeida *et al.* [41, 45] explain the thermodynamic process of raft formation as follows. Since a large number of molecules are involved, the interactions are amplified and domains formed, but the processes are reversible and non-static. When considering the self-assembly thermodynamics, it was assumed that the aggregates were in equilibrium. Since biological membranes are not in equilibrium, domain formation is dynamic. In order to persist for long enough to be structurally relevant in the membrane, the domains would have to be thermodynamically stabilised. In a model system in

equilibrium domains are formed as a consequence of differential interactions between membrane components. Consider a bilayer leaflet seen from above as in Figure 3.7. Each lipid is approximately surrounded by six nearest-neighbour lipids, and as a simplification, the lipids are considered to occupy positions in a tetragonal lattice.

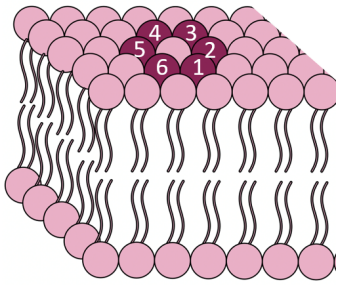

Figure 3.7: Each lipid in the membrane has approximately six neighbours.

If there are two different lipid species in the membrane, for example, PC and PE, and both are in the fluid state, there are three lipid-lipid interactions involved: PC-PC, PE-PE and PC-PE. To describe the chemical potential change for a "reaction" where two PC lipids and two PE lipids mix, as seen in figure 3.8, we only need one parameter; the difference between the PC-PE interaction and the average of the PC-PC and PE-PE interactions [41]:

$$\omega_{PE,PC} = g_{PE,PC} - \frac{1}{2}(g_{PE,PE} + g_{PC,PC}), \tag{3.18}$$

where $g_{PE,PE}$ and $g_{PC,PC}$ are the Gibbs free energies of interaction between two PE or two PC lipids, and $g_{PE,PC}$ is the Gibbs free energy of interaction between one PE and one PC lipid. The interaction energy, ω, represents half of the Gibbs reaction energy of the mixing reaction. The more positive and large $\omega_{PE,PC}$ is, the less the different species prefer to mix, and the more domains are stabilised. Random mixing occurs if $\omega_{PE,PC} = 0$. Moreover, if $\omega_{PE,PC} < 0$, they will mix even more randomly. At large negative values, a checkerboard pattern will theoretically form [41]. This fundamental principle remains the same, even when more species are included in the membrane and the interactions become more complicated. The values of $\omega_{PE,PC}$ indicates whether or not domains will form, but not where these interactions originate. They may, for example, include the conformational entropy of the acyl chains, hydrogen bonds and hydrophobic interactions [41].

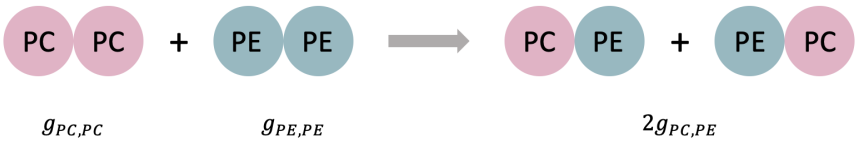

Figure 3.8: Visualisation of an exchange reaction between two pairs of like lipids to produce two pairs of unlike lipids. $g_{PC,PC/PE,PE/PC,PE}$ is the Gibbs free energy of interaction between two lipids. Figure inspired by [41].

Experimental determinations of ω_{AB} have found that most unlike lipid-lipid interactions are repulsive ($\omega_{AB>0}$), and the lipids prefer to interact with like neighbours. However, for the interaction between cholesterol and saturated PC-lipids the interaction is often negative, indicating a preference for mixing ($\omega_{AB} < 0$). The hydrophobic mismatch is an essential part of the interactions (although not the only contribution). A proposed explanation for the phase separation in cholesterol/PC mixtures is that cholesterol is positioned in the l_o phase as a lipid but may partially enter the bilayer midplane in the l_d phase to minimise the hydrophobic thickness mismatch at the phase interface [41].

The temperature dependence of lipid-lipid interactions is practically none in the l_d phase of low cholesterol content and unsaturated lipids. At the same time, ω_{AB} varies significantly in the l_o phase. At increasing temperatures, the values of ω_{AB} increases, becoming less and less favourable for mixing [41]. Almeida *et al.* [41] conclude that the phase separation observed in many mixed systems is a result of simple lipid-lipid interactions, where all that is needed to form domains is that the interactions of two lipids coupled through a favourable thermodynamic interaction with another lipid species with which they interact unfavourably lead to an enhancement of the repulsive interaction and therefore to clustering into domains.

3.2 Physical properties of lipid bilayers

Biological membranes are soft materials. In day-to-day life, we know soft matter as, for example, mayonnaise, milk, glue, and toothpaste. Lipid membranes are structured liquids where the molecules have substantial conformational freedom and complexity. However, since they are self-assembled structures held together by the forces described in the previous section, they can be described as a two-dimensional liquid with restricted motion [72]. The lipids have relatively rapid lateral movement, but the transmembrane movement is restricted. One of the most well-known models describing membrane behaviour is the *fluid mosaic model*. In the early 1970s, Singer and Nicolson proposed a model that incorporated several of the commonly observed properties of membranes: The fluid mosaic model, based on thermodynamic principles of organisation of proteins and lipids, bilayer asymmetry and lateral mobility. In short, the model describes cell membranes as a matrix of fluid phospholipids with fast lateral motion and integral globular proteins inserted in the matrix. Although the model works quite well in describing the general membrane properties, it fails to describe the existence of membrane domains or rafts

[73, 74].

Lipids are dynamic molecules that move in many different manners. They constantly change conformation, wobbling, protruding out of the bilayer and moving around. Different processes occur over several time spans. The movement of a lipid from one leaflet to the other is extremely slow and can take up to several hours and possibly days [32]. Because of the amphiphilic nature of the lipids, it is energetically unfavourable for the large, polar head group to pass through the hydrophobic core. The fastest motions are conformational changes caused by rotations around $C-C$ bonds, followed by a rotation of the entire molecule and in-plane lateral movements. These processes have a time span of picoseconds to tens of nanoseconds [32]. The lateral mobility of the lipids in bilayers means that they can be considered two-dimensional fluids. Due to the rotations around $C-C$ bonds in the lipid tails, the interior core of bilayers is in constant motion. The polarity of the head groups extends to the ester and amide bonds linking them to the tails. This means that water molecules might penetrate the membrane to a depth of about 15Å. Because of the repulsive interactions between head groups, the motion becomes more restricted, and the bilayer's viscosity increases dramatically closer to the head groups. The tails will also bend and interdigitate, trying to fill gaps in the bilayer caused by different chain lengths or kinks in the tails caused by double bonds [75].

Like water existing in different physical states at different temperatures (vapour, liquid water and ice), lipids may exist in different phases with different properties depending on the temperature/environment. Different phases represent different degrees of order and are connected through phase transitions. At the main phase transition for lipids (often also called the melting transition), the lipids undergo a phase change from disordered chains with rapid lateral diffusion to a liquid crystal with more ordered acyl chains and decreased fluidity. Below the phase transition occurring at lower temperatures, the lipids are a semi-crystalline gel-like solid [36]. To completely describe the different phases, different labels are needed for the conformational and the translational degrees of freedom. When referring to the conformational, internal motions of the fatty acid chains, the labels *disordered* and *ordered* are used. *Liquid* and *solid* are used to describe the translational degrees of freedom. The phase below the main phase transition is the solid-disordered phase (often just called the gel phase) s, while above the phase transition, the lipids are in the liquid-disordered phase l_d [36]. As discussed in Section 2.1.3, the presence of cholesterol with an ordering effect may introduce a third phase; the liquid-ordered phase l_o. The transition temperature depends on the length and saturation of the fatty acid chains. Increasing chain length increases the attractive van der Waals interactions, and more energy is required to disrupt the ordered packing. In unsaturated lipids, cis double bonds introduce kinks in the chains, decreasing their order. The melting temperature therefore decreases with the degree of unsaturation [76]. For most biological membranes, the transition temperature ranges between 10 and $40^{\circ}C$.

When a bilayer is composed of several different lipid species, there is no longer a single phase transition but a transition that expands over a larger temperature range. For cholesterol-containing membranes, the formation of cholesterol-depleted domains will cause this phase transition to sharpen and have a measurably larger enthalpy, since cholesterol causes a broadening of the transition and lowering of the enthalpy [77].

3.3 Small-angle scattering theory

Scattering techniques are some of the most powerful non-invasive methods used for structural characterisation of materials whose size is between 10 and 10.000 Å [78]. Because of the non-invasive nature of scattering techniques and the liposome diameter being $\sim$ 1000Å, scattering techniques are a natural choice for studying the structure of liposomes. Other techniques commonly applied to studying lipid system structures are X-ray diffraction (XRD), Atomic force microscopy (AFM), neutron reflectometry and single-crystal microbalance.

This section will briefly discuss general scattering theory before taking a closer look at small-angle scattering with X-rays and neutrons. The general theory applies to scattering from different sources, but the scattering processes are not the same. Light scatters as a result of differences in the polarizability in the sample. X-rays are scattered when interacting with the electrons, whereas neutrons interact with the nuclei in the sample. Moving forward, the focus will be on SAXS, small-angle scattering with X-rays.

The general setup is shown in figure 3.9 and consists of an incident monochromatic beam (i.e. neutrons or X-rays) with a wavevector k_0 that is scattered by the sample. The scattered intensity is recorded by a detector at a given scattering angle θ with respect to the incident radiation resulting in a scattering pattern on the detector. The scattering pattern consists of the registered intensity at different wavevectors, $\vec{Q}$. Braggs law famously gives the scattering angles from coherent scattering of waves and is valid for periodic crystal lattices. Using the Bragg equation, it can be shown that the wavevector has an inverse proportionality to the real length-scales (d), $d = \frac{2\pi}{\vec{Q}}$. Smaller wavevectors will hence correspond to larger structures. Even though the Bragg Equation is strictly valid only for periodic crystals, the inverse proportionality is still valid for more disordered systems. After radially averaging the scattering pattern to obtain a 1D pattern, the scattering of the buffer is subtracted from the sample scattering. This leaves only the scattering pattern of the structure one wants to study. By comparing this pattern to the theoretical scattering from analytical models, valuable structural information is obtained.

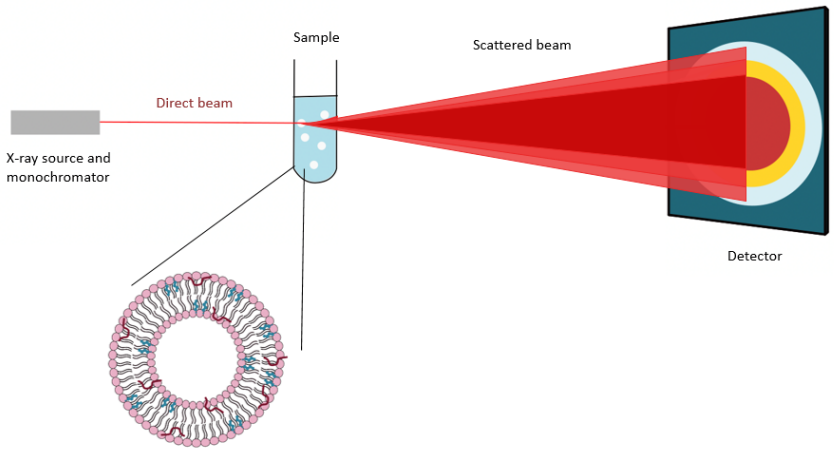

Figure 3.9: SAXS setup: an x-ray source and monochromator gives a direct beam that scatters in a sample, resulting in a scattering pattern on the detector.

3.3.1 Elastic small-angle scattering

Scattering is either inelastic or elastic. In inelastic scattering, some of the kinetic energy is not conserved but, for example, converted into sound waves or dissipated heat. Elastic scattering occurs when the energy of the scattered waves and the incident beam is equal, $E_0 = E_s$. For X-rays, the electric field generated by the incident beam interacts with the samples' electrons causing them to oscillate and emit photons. The emitted photons have a spherical electric field with the same energy as the incoming radiation. Therefore, only elastic scattering is considered in SAXS.

The electric field of a plane-wave of monochromatic light is given by

$$E_I(\vec{r},t) = E_0 \exp[i(\vec{k_0}\vec{r} - \omega t)], \tag{3.19}$$

where the incident wave E_0 is polarized perpendicular to the scattering plane, $\vec{k_0}$ is the propagation vector, also called the wave vector, and ω is the angular frequency in the medium [79].

A sketch of the scattering event is shown in figure 3.10. Since it is more practical to consider waves, and not particles, we can say that the incoming and scattered beam waves have the same energy. The corresponding wavefunction to Equation (3.19) is defined using the maximum amplitude A as [80]

$$\Psi(\vec{r},t) = A \exp(i(\vec{k_0}\vec{r} - \omega t)). \tag{3.20}$$

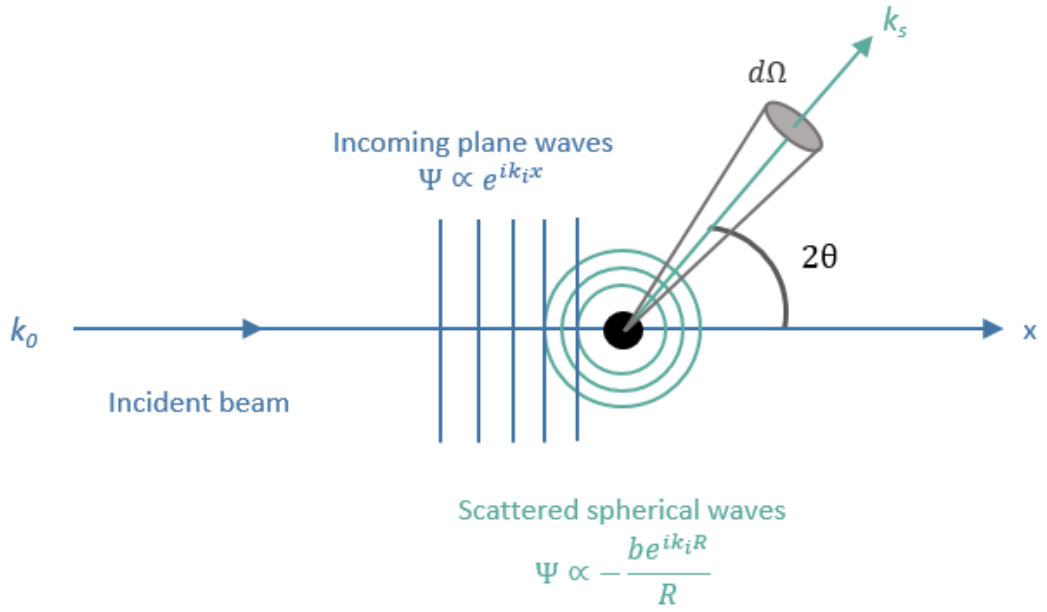

Figure 3.10: Illustration of the basic scattering event principle, figure inspired by [81]. Incoming plane waves are scattered as spherical waves.

In figure 3.10, $d\Omega$ is the solid angle, which is the infinitesimal angle in which incoming particles with a cross-sectional area of $d\sigma$ are scattered into. The scattering vector expresses the momentum transfer and is defined as the difference between the scattered wavevector (k_s) and the incident wavevector (k_0) [79]:

$$|\vec{Q}| \equiv |\vec{k_s} - \vec{k_0}|. \tag{3.21}$$

each of the wavevectors is defined as

$$k_i \equiv |\vec{k_i}| = \frac{2\pi}{\lambda}, \tag{3.22}$$

where λ is the wavelength of the radiation [79]. Inserting for the wavevectors and following geometrical considerations the scattering vector can be written as

$$|\vec{Q}| = \frac{4\pi}{\lambda} \sin(\frac{\theta}{2}). \tag{3.23}$$

A figure of a simple scattering event and the corresponding scattering vector is shown in figure 3.11.

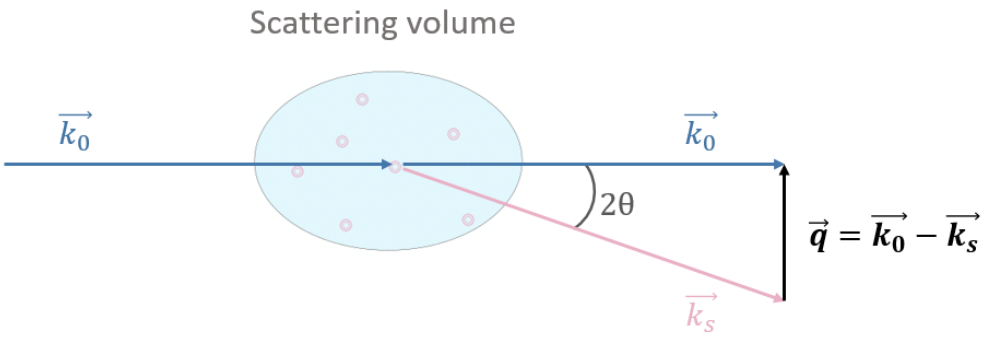

Figure 3.11: A basic scattering event in a sample scattering volume, the part of the sample both illuminated by the incoming radiation and seen by the detector. The scattering vector q is the momentum transfer between the incident wave k_0 and the scattered wave k_s.

Treating the incoming radiation as plane waves the amplitudes at position $\vec{R}$ are expressed as [80]:

$$A_i(\vec{R}) = A_0 \exp(i\vec{k_s}\vec{R}). \tag{3.24}$$

Here A_0 is the amplitude of the incidental wave. The scattered waves are spherical waves, but because the detector is so far away from the sample, the detected waves are considered to be planar [79]. The amplitude of scattered waves is given by Equation (3.25) [80], where b is the scattering length, a measure of the interaction strength that describes how well a given material scatters the probing waves

$$A_s(\vec{R}) = A_0 \exp(i\vec{k_s}\vec{R}) \cdot \frac{b}{\vec{R}}. \tag{3.25}$$

Unlike the collimated incident beam, the scattered beam will have a number of particles per unit area that decreases with distance R, hence the $1/R$ dependency. The scattering length b depends on the type of radiation source and the electron density or nuclei of the sample. Generally, it is defined as

$$b_j(\vec{q},t) = \int_{V_j} \Delta(r_j,t) \exp(-i\vec{q}\vec{R}_j) d^3\vec{r}_j \tag{3.26}$$

where the integration runs over the entire sample volume containing all scattering particles j [79]. $\rho(r_j,t)$ can be thought of as the local density of scattering material. If there is no change in dielectric constant or no difference in how the electrons/nuclei in the sample and solvent scatter the radiation, $\Delta\rho(r_j,t)$ and hence b will be zero, and no scattering event occurs. Assuming that all scattering processes are single scattering processes (Born approximation) and that the sample does not perturb the probing field, the total scattering event can be described as a superposition of each scattered amplitude [82]. This can be written as

$$A(\vec{Q}) = \sum_i b_i \exp(-i\vec{Q}r_i) \tag{3.27}$$

where r_i is the position of each scattering particle.

The detector measures scattered intensity, not amplitude, and the relation between these parameters is

$$I(\vec{Q},t) = |A(\vec{Q},t)|^2. \tag{3.28}$$

So the instantaneous scattered intensity is [79, 80]:

$$I_s(\vec{Q},t) = \frac{A_0^2}{r^2} \sum_{j=1}^{N} \sum_{k=1}^{N} b_j(\vec{Q},t) b_k^*(\vec{Q},t) \exp\left[-i\vec{Q}[\vec{r_j}(t) -]\vec{r_k}(t)\right]. \tag{3.29}$$

In dilute systems, the behaviour of scattering particles is uncorrelated, so by omitting prefactors and taking the ensemble average, the intensity can be written as [79]:

$$\langle I_s(\vec{Q},t)\rangle = \sum_{j=1}^{N} \langle |b_j(\vec{Q})|^2 \rangle \tag{3.30}$$

For identical particles, the scattering length and form factor is the same for all scatterers [79], so the intensity is

$$\langle I_s(\vec{Q},t)\rangle = N\langle |b_j(\vec{Q})|^2 \rangle = N\langle |b(0)|^2 \rangle P(Q) \tag{3.31}$$

where $P(Q)$ is the form factor defined so that $P(Q) \to 1$ as $Q \to 0$ [79]. The form factor depends on the distribution of scattering material and is defined as

$$P(Q) = \frac{\langle |b_j(Q)|^2 \rangle}{\langle |b_j(0)|^2 \rangle}. \tag{3.32}$$

Since the density of scatterers depends on the sample's morphology, the form factor is used to determine the structural information of the sample. Not all particles will have the exact same size but a range of different sizes. This causes a smearing of the oscillations in the form factor as seen in 3.12, because the form factor at each Q-value will be an average of the form factor of differently sized particles [83]. Polydispersity in the particles is accounted for in the form factor by integration over a normalised size distribution, $D(N)$ [83]:

$$\overline{P(Q)} = \int D(N) P(Q,N) dN. \tag{3.33}$$

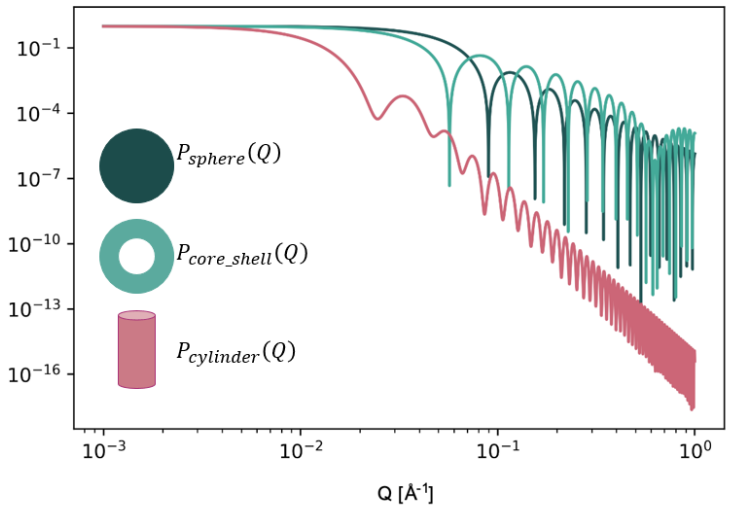

Figure 3.12: Form factors (P(Q)) of a sphere, core-shell system and a cylinder. The radius of the sphere is set to 50 Å. The core-shell has an inner radius of 50 Å and an outer radius of 60 Å. The cylinder has a radius of 50 Å and a length of 150 Å.

The detector measures the intensity by counting the flux of photons or neutrons hitting the detector. The total scattering cross-section $\sigma = 4\pi b^2$ is a measure of the probability that the sample scatters an incoming X-ray photon or neutron [82]. It is independent of the angle and shows that the ratio between scattered and incident radiation is proportional to the scattering length squared. The *differential scattering cross-section* is given by Equation (3.34) and describes the probability of a photon/neutron being scattered into the given unit solid angle, $d\Omega$.

$$D(\theta) = \frac{d\sigma(Q)}{d\Omega} \tag{3.34}$$

The intensity obtained is connected to the differential scattering cross-section per unit of volume V of the illuminated sample [78], as can be seen in Equation (3.35). To directly evaluate and compare scattering data from different sources, the number of photons scattered in the solid angle $\Delta\Omega$ in the direction 2θ has to be normalised with respect to the number of transmitted photons since some of the incident beam will be absorbed in the material. The scaled absolute intensity is

$$I_{abs} = \frac{1}{V}\frac{d\sigma(Q)}{d\Omega} = \frac{C}{C_0 \Delta\Omega T e_S}. \tag{3.35}$$

Here C and C_0 represent the flux collected at the detector and of the incident beam. T is the sample transmission, and e_S is the sample thickness. $d\Omega$ is the area of the solid angle the wave is scattered into. Higher electron density will give stronger scattering, meaning that heavier atoms have larger scattering lengths. Neutrons, on the other hand, are scattered by nuclear magnetic

interactions. The strength of neutron scattering is described by the total neutron scattering cross-section, a measure of the effective surface of the neutron-nucleus interaction potential [78]. The scattering lengths of neutrons do not increase linearly with atom size, but may vary significantly between different isotopes. The dependency of the scattering length on atomic number is shown in figure 3.13.

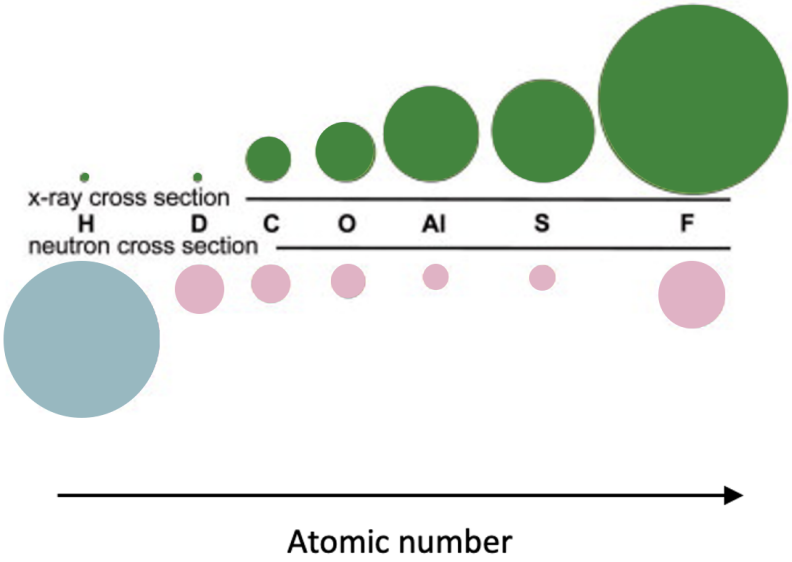

Figure 3.13: Scattering lengths of neutrons and x-rays. X-ray scattering lengths increases systematically with atomic number. Neutron scattering lengths, however, do not have a systematic dependence. The neutron scattering length of hydrogen has a different color, as it also has a large incoherent scattering (in addition to the coherent scattering which dominates for the other depicted atoms). Figure modified from [84] reprinted with permission.

According to the static approximation, the scattering cross-section per particle at small angles can be expressed using

$$\frac{d\sigma}{d\Omega}(Q) = \frac{1}{N}[\sum_i b_i \exp(iQR)]^2, \tag{3.36}$$

where b_i is the scattering length of the particle at position R in the sample and N is the number of particles [78]. Another option is to use the scattering length density (SLD) $\rho(r) = \sum \rho(r)_i b_i$ to express Equation 3.36 as

$$\frac{d\sigma}{d\Omega} = \frac{1}{N}[\int_V \rho_i(r) \exp(iQR) d^3r]^2. \tag{3.37}$$

For X-ray scattering the scattering length density is defined as $\rho(r) = (e^2/mc^2)n_{el}(r)$ where (e^2/mc^2) is the Thompson scattering length of an electron and n_{el} is the electron number density in the sample which for SAXS is the number of electrons divided by the volume of a scatterer; $n_{el} = \frac{Z}{V}$ [79]. The neutron scattering length density depends on the coherent scattering length

of the elements constituting the scatterer, which is then divided by the volume of the scatterer, $\rho = \frac{b}{V}$. For isotropic systems, the scattering will have a circular symmetry around $Q = 0$, so the scattering cross-section equations depend only on the magnitude of the scattering vector, $|\vec{Q}| = Q$.

For SANS (primarily), the measured scattering data consists of a Q-dependent, coherent term and a Q-independent, incoherent background [82]. The incoherent scattering occurs when incident neutron waves interact independently with each nucleus in the sample. The scattered waves have random or intermediate relative phases and do not interfere with each other. The incoherent scattering is especially strong from samples containing ^1H hydrogen as this isotope has a strong incoherent scattering. In figure 3.13 the neutron SLD of hydrogen has a different colour as the coherent scattering has an opposite sign compared to deuterium [84]. After the data has been reduced to account for details of the experimental instrumentation, the measured scattering intensities can be expressed as

$$I(\theta, \lambda) \rightarrow I(Q) = \frac{d\Sigma_{coh}(Q)}{d\Omega} + \frac{d\Sigma_{incoh}}{d\Omega}. \tag{3.38}$$

3.3.2 Contrast

Contrast is defined as the difference in scattering length density of the sample and the solvent, $\Delta\rho = (\rho - \rho_0)$ [79]. This excess scattering gives scattering intensities sensitive to the sample studied. For a binary system (i.e. solvent and liposomes only), the scattering intensity is a function that depends on Q, the number density of scatterers (n_z), the contrast, the volume of a single particle of component 1 (V_1), the inter-particle structure factor $S(Q)$, the form factor $P(Q)$, and a constant background (B) originating from solvent and incoherent scattering [85]:

$$I(Q) = n_z \Delta\rho^2 V_1^2 P_1(Q) S_1(Q) + B. \tag{3.39}$$

The form factor $P(Q)$ can be expressed in terms of the form factors $P_i(Q)$ and form factor amplitudes $A_i(Q)$ of the different components in the sample.

The intensity of the measured radiation depends on whether the scattering process is constructive or destructive. The interference, in turn, depends on the phase difference between incoming and scattered radiation. By superposition of the scattering from each nucleus, the average effect of the phase difference is given in the form factor amplitude [79]:

$$A(Q) = \frac{1}{N} \sum_{j=1}^{N} \langle \exp(-iQ \cdot r_j) \rangle \tag{3.40}$$

Where $Q \cdot r_j$ is the length of the path of the scattered radiation compared to the incoming radiation, and $\langle \dots \rangle$ denotes the average over multiple configurations of the particle. The amplitude cannot be measured independently. Instead, the form factor $P(Q) = A(Q)A^*(Q)$, where $A^*(Q)$ is the complex conjugate of $A(Q)$, is measured. The form factor can now be written as

$$P(Q) = \frac{1}{N^2} \sum_{j=1}^{N} \sum_{k=1}^{N} \langle \exp[-iQ \cdot (r_j - r_k)] \rangle \tag{3.41}$$

For non-uniform objects with multiple possible configurations a probability distribution must be applied to describe the density distribution.

$S_1(q)$ is the inter-particle structure factor that includes the correlations between the positions of the scattering particles in the sample. If the sample is sufficiently diluted, the structure factor approaches 1, $S_1(q) \approx 1$.

The scattering data analysis can be done both by using models and by model-independent analysis. In this thesis, the analyses were performed using analytical models. The analytical model used will be presented in the next section, and the idea is to fit the analytical function to the obtained data to find structural information.

Contrast variation in SANS

In SANS, the scattering can arise from three components: SLD contrast between the average bilayer composition and the solvent, a variation in SLD in the direction normal to the bilayer (between the head- and tail-group shells), and a lateral variation in SLD in the plane of the bilayer [71]. When preparing the samples for neutron scattering, one must first decide what structures one wants to study and tune the contrast accordingly. To observe lateral phase segregation, the SLD from the solvent and the average SLD of the tails were matched to the headgroup SLD, as illustrated in figure 3.14. To adjust the SLD of the solvent, the ratio of D_2O/H_2O in the buffer is tuned. For the acyl chain groups, the SLD can be varied by adjusting the ratio of deuterated/protiated chains in the bilayer. In order to see the rafts, the SLDs were matched using a solvent with 34.6% D_2O and $\sim$ 67% tail deuterated DSPC-d_70 (as a percentage of the total amount of DSPC) [71]. When the lipids are randomly distributed in the membrane, no excess scattering should, in theory, be observed. When phase separation and raft formation occur, the lateral segregation of saturated and unsaturated lipids creates contrast in the acyl chain region, resulting in a scattering intensity depending on the size of the rafts [71].

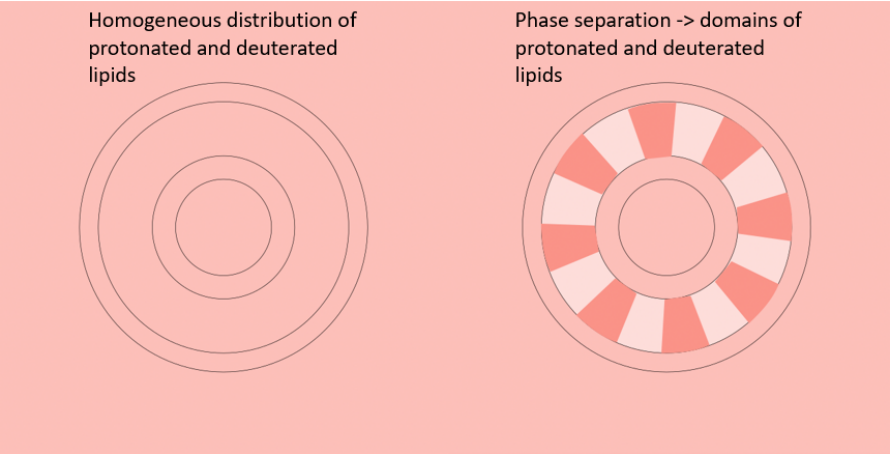

Figure 3.14: SANS contrast variation. The SLDs of the head groups and the solvent are matched to the average SLD of the tails so that when the tails are mixed randomly (left), the excess scattering is zero. When the lipids phase separate, areas with increased contrast become detectable (right).

3.4 Instrumentation and data processing

3.4.1 SAXS

The primary data obtained from a scattering experiment is the 2D detector image. When treating the data, each pixel must first be scaled according to the transmitted intensity and data collection time. The beamstop, intermodulus gaps, and hot pixels are removed by applying a mask, leaving only the scattered beam. This is usually done by calibrating with a reference sample that scatters homogeneously, giving a flat field that can also correct for the sample being 2-dimensional while the scattered waves are spherical.

The next step is the azimuthal integration (radial averaging) of every frame. At a given radius on the detector $r_{det} = d_{detector} \cdot \tan\theta$, where $d_{detector}$ is the detector distance and θ the scattering angle, the average of every pixel in that area is taken. Measurements of the direct beam give the centre of the radius. For each radius, the average scattering vector $\langle Q \rangle$ is calculated as [86]

$$\langle Q \rangle = \frac{4\pi \sin\langle\theta\rangle}{\langle\lambda\rangle}. \tag{3.42}$$

As seen from equation (3.42), one needs the calibrated values for the wavelength, sample to detector distance and beam position in order to get a correct intensity distribution. The radial averaging converts the two-dimensional data frames into one-dimensional scattering curves of I vs Q [87, 88].

After the radial averaging, the data must be background corrected by subtracting the background and normalising the data. The background scattering stems from the buffer, capillary and other sources. After subtraction, the only scattering left is from the particles of interest alone and the excluded volume [88]. Normalisation of the flux and instrumental setup is done by monitoring the transmitted beam intensity at the beam stop with an internal standard and the

intensity measured during data acquisition [87]. At BM29, the internal standard used is water at $20°C$, which has a known scattering cross-section of

$$\frac{d\Sigma}{d\Omega}_{st}(Q=0) = 1.632 \cdot 10^{-1}. \tag{3.43}$$

The standard intensity I_{st} is given by subtracting the empty cell measurement from the water intensity. Absolute calibration relates the measured intensity I to the differential scattering cross-section per unit volume, given by [89]

$$\frac{d\Sigma}{d\Omega}(Q) = \left[\frac{d\Sigma}{d\Omega}_{st}(Q=0) / \left(\frac{I_{st}(Q)-I_b}{d_{st}T_{st+cell}}\right)\right] \cdot \frac{I_s(Q)-I_b}{d_s T_{s+cell}}, \tag{3.44}$$

where I_s and I_b are the intensities of the sample and background scattering respectively, d_s and d_{st} are the thicknesses of the sample and standard, and T_{s+cell} and $T_{st+cell}$ are the transmissions through the sample and standard in the container (cell) respectively. The first part of equation (3.44) is a scaling factor that provides the data on an absolute scale and ensures that data from different sources may be analysed and compared directly [89].

When the data have been correctly normalised, the sample and buffer frames are averaged. Since the samples are measured over several frames, radiation damage may occur, giving altered scattering, especially at low q-values. The software at BM29 may detect radiation damage and exclude frames that vary with more than a certain amount from the average. This software reduction was applied for the samples of DMPC/Chol and their indolicidin interactions, while the rest were subtracted using the BioXTAS RAW software developed by Soren Skou [90].

The final step is to analyse the data qualitatively and quantitatively. The analytical models used for the quantitative analysis are described in Section 3.5. They were programmed in C++ in the Qti-software developed by Vitaliy Pipich [91]. The program uses different function minimisation methods to optimise structural parameters. The Nelder-Mead simplex algorithm is effective but sensitive to local minima, so it was supplemented with the Levenberg-Marquardt method. The size-polydispersity was calculated with a built-in option that utilises a Gaussian distribution of the radii.

3.4.2 Data processing in SANS

The first step in the data treatment process is the an-isotropic reduction of the raw data. Here, the data are corrected for scattering from the sample holder, general background, and incoherent scattering using water as a calibration scatterer. Additionally, the data are corrected for the transmission of each sample and the absolute scaling factors. In the second step, the obtained two-dimensional data is converted to one-dimensional data as described in section 4.2. The last step of the data treatment before analysis is merging data obtained at different Q-ranges [92].

3.4.3 Differential Scanning Calorimetry

Differential Scanning Calorimetry (DSC) is a thermal analysis technique based on the measurement of the heat required to increase the temperature of the sample and a reference. It is especially useful in qualitative and quantitative studies for determining heat capacities and

exothermic and endothermic phase transitions. There are two types of DSC instruments: heat flux DSC and power compensated DSC. In heat-flux DSC, the temperature of the sample and the reference is changed in a specific program, and the temperature difference is measured as a function of heat. Power compensated DSC directly measures a sample's enthalpy change during a thermal event (like a phase transition). In power compensated DSC, there are two separate chambers, and the instrument always maintains the same temperature. When a thermal event occurs, the heat power has to change in order to maintain a constant temperature [93]. A DSC curve is usually a graph of heat capacity, or heat flux, plotted against temperature or time, as shown in figure 3.15. The rate of heat flow has a unit of energy per unit time per unit mass, usually in units of Wg^{-1}, and heat flow into the sample is typically indicated by a positive peak [93]. This is the endothermic convention. In the exothermic convention, positive peaks indicate exothermic events [94]. The transition enthalpy is found from DSC curves by integrating the corresponding peak.

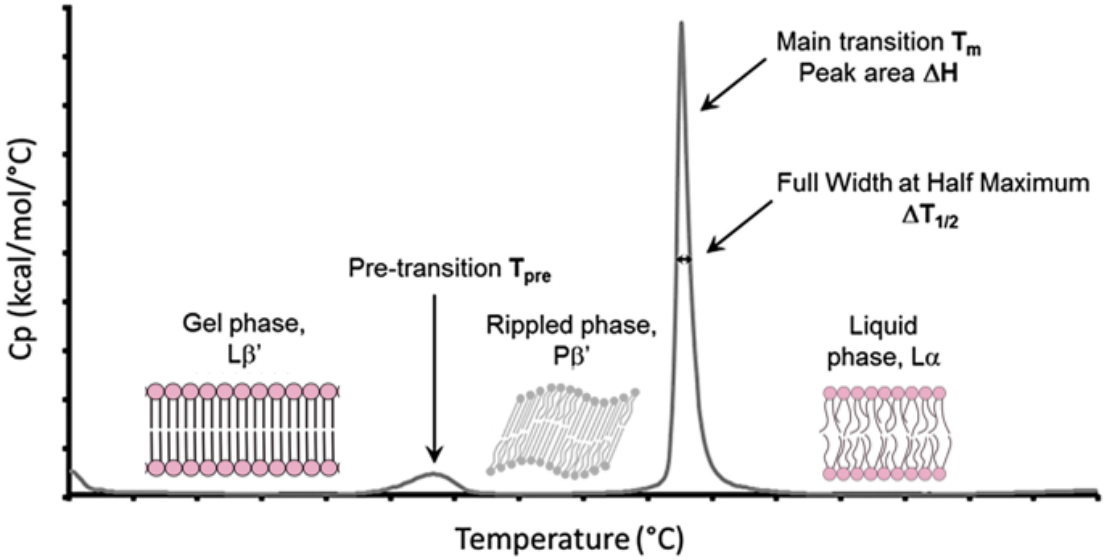

Figure 3.15: Sketch of a typical DSC curve for lipid bilayers. To the left of the main transition one finds the gel phase and rippled phase, while the liquid phase is to the right of the main transition peak. Adapted from Jobin and Alves [95] with permission from Springer eBook. Copyright Springer Nature 2019.

3.5 Analytical scattering models

3.5.1 What is a model?

To understand the world, we need the appropriate tools to describe it. A model should be detailed enough to satisfactory represent the real-world behaviour we are studying but not too complicated so that it becomes difficult to interpret the results. Let us say you want to describe

a plane to different people. A simple drawing of the shape of the aircraft flying in the sky may suffice to explain the concept to a child. However, if you were going to commission an actual plane, the contractors would need very detailed and highly accurate blueprints.

The choice of model membrane systems and how we describe them using analytical models is a careful balance between representing the relevant properties of the biological membrane and the actual scattering data and not obscuring the results by including too many parameters. In this section, the form factors used in the different models are described before gradually building up the analytical model from the simple core-shell model. As mentioned in Section 3.3.2, the scattering intensity for a dilute sample ($S(Q) \sim 1$) is given by

$$I(Q) = n_z \Delta\rho^2 V_1^2 P_1(Q) + B. \tag{3.45}$$

To describe the samples' scattering behaviour, analytical models must be able to quite accurately describe the number densities and the SLDs, and they must have the correct form factor.

3.5.2 Form factors

Since scattering is caused by variations in electron density, different refractive indices, or nucleic properties, the distribution of scatterers determines the form of the scattered waves. As mentioned in Section 3.3.2 form factors, $P(Q)$, describe the form of the scattered waves, which again are dependent on the structure of the scatterers. The form factor is the squared form factor amplitude: $P(Q) = A(Q)^2$. In this section, the relevant basic form factor amplitudes will be described, followed by the gradual modification of the analytical model with the simple core-shell model as a starting point.

Sphere

For a sphere with a uniform distribution of scattering material, the form factor amplitude is expressed as [85]

$$A_{sphere}(Q) = \frac{3(\sin(Qr) - Qr\cos(Qr))}{(Qr)^3}. \tag{3.46}$$

Shell

A shell is a sphere of scattering material with an aqueous core. The form factor is simply obtained by subtracting the scattering from the aqueous core from the shell scattering, weighted with the appropriate volumes. Generally, the form factor amplitude is written as [85]:

$$A_{shell} = \frac{V(R_1)A_{sphere}(Q,R_1) - V(R_2)A_{sphere}(Q,R_2)}{V(R_1) - V(R_2)}. \tag{3.47}$$

where R_1 is the outer radius of the shell and R_2 is the inner radius of the shell. The volumes are given by the volume of spheres

$$V(R) = \frac{4\pi R^3}{3}. \tag{3.48}$$

Cylinder

The scattering amplitude expression for a cylinder was first given by Fournet in 1949 and is expressed as [85]:

$$A_{cyl}(Q) = \int_0^{\pi/2} \left[\frac{2J_1(QR\sin\alpha)}{QR\sin\alpha} \frac{\sin(QL\cos\alpha/2)}{QL\cos\alpha/2} \right]^2 \sin\alpha d\alpha \tag{3.49}$$

Here R is the radius of the cylinder, and L is its length. The first-order Bessel function J_1 describes waves in cylindrical coordinates.

Gaussian chains

Random coils, also called Gaussian chains, that do not have a self-avoiding behaviour have a form factor amplitude defined as

$$A(Q)_{chain} = 2\frac{\exp(-u)+u-1}{u^2}, \tag{3.50}$$

where $u = \langle R_g^2 \rangle Q^2$, and $\langle ... \rangle$ denotes the ensemble average [85]. The radius of gyration is the average distance form the centre of gravity of a polymer chain to the chain end [96].

3.5.3 Gaussian chain model

Free peptide in solution scatters like a Gaussian chain. The scattering intensity is hence given by

$$I_{free} = n_{p,free} \cdot (\rho_P - \rho_{solvent})^2 \cdot P_{chain}(Q, R_{g,p}), \tag{3.51}$$

where the number of free peptide scatterers in solution is

$$n_{p,free} = c_{peptide} \cdot f_{free} \cdot V_p. \tag{3.52}$$

$P_{chain}(Q, Rg_p) = A_{chain}(Q, Rg_p)^2$ is the scattering form factor of a Gaussian chain with a radius of gyration Rg_p, as discussed in the previous section.

3.5.4 Pure peptide scattering

Since indolicidin has been shown to have a disordered, random coil structure in solution, its scattering may be modelled analytically using the form factor of a Gaussian chain together with some peptide sheet formation [22, 97]. The intensity is defined as

$$I(Q) = \Phi \cdot V_p \cdot \Delta\rho^2 \cdot (P_{chain}(Q, R_{g,p}) \cdot f_{chain} + N_p \cdot P_{sheet}(Q) \cdot (1 - f_{chain})) \tag{3.53}$$

The first term in the intensity equation, Φ, is the volume fraction of the polymer. The volume of the polymer is V_p and $\Delta\rho$ is the contrast between the SLD of the polymer and the solvent, and f_{chain} is the fraction of free chains. The form factor for the Gaussian chain is described in Section 3.5.2.

The second part of the intensity comes from scattering from peptoid sheets. N_p is the average number of peptides in each sheet, and is defined as $N_p = \frac{abc}{V_p}$, where a, b and c are the dimensions of the rectangular fibers (sheets). c is the length of the fibres, while a and b are the height and width of the fibres. The form factor for sheets, assuming that the length c is much larger than the width and height, is [22]

$$P_{sheet}(Q) = F_c(Q) \cdot \frac{1}{2\pi} \int_0^{2\pi} A_{sheet}(Q,\alpha)^2 d\alpha, \tag{3.54}$$

where the scattering amplitude is given by

$$A_{sheet}(Q,\alpha) = \frac{\sin(Qb \cdot \cos(\alpha)/2)}{Qb \cdot \cos(\alpha)/2} \cdot \frac{\sin(Qa \cdot \cos(\alpha)/2)}{Qa \cdot \cos(\alpha)/2} \tag{3.55}$$

The $F_c(Q)$ is

$$F_c(Q) = \left(\frac{2 \cdot Si(Qc)}{Qc} - \frac{4\sin^2 Qc/2}{Qc} \right)^2. \tag{3.56}$$

Here $Si(Qc) = \int_0^x t^{-1} \sin t dt$.

3.5.5 A simple shell model

The simplest possible model for the scattering of liposomes is a shell model, as seen in figure 3.16. The total intensity is a superposition of the intensity from a solvent filled core, calculated using the form factor of a sphere shown in Equation (3.46), and a shell containing the lipid bilayer. To calculate the intensity of the shell, a first approximation is to use the average scattering length density of the head group scattering and the tail scattering and apply the form factor of a shell as described in Equation (3.47).

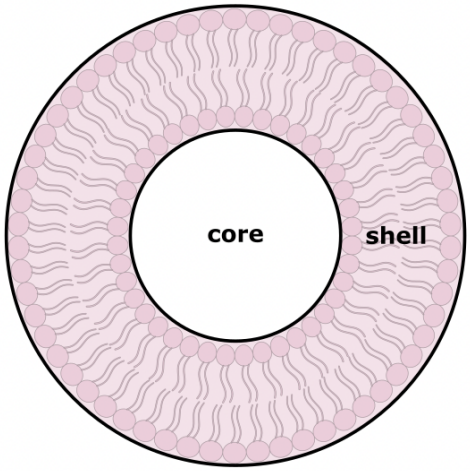

Figure 3.16: Sketch of the simple core-shell model describing the structure of a liposome as one shell surrounding an inner solvent-filled core (inner *i*, core *c*, outer *o*.

Since the scattering from the head groups differs substantially from the tail scattering, a more accurate model is required to give a satisfying reproduction of the scattering data.

3.5.6 Three-shell model

To describe the scattering from the vesicles analytically, a three-shell model was used as a starting point. The model describes vesicles using concentric shells of finite thicknesses, as shown in figure 3.17.

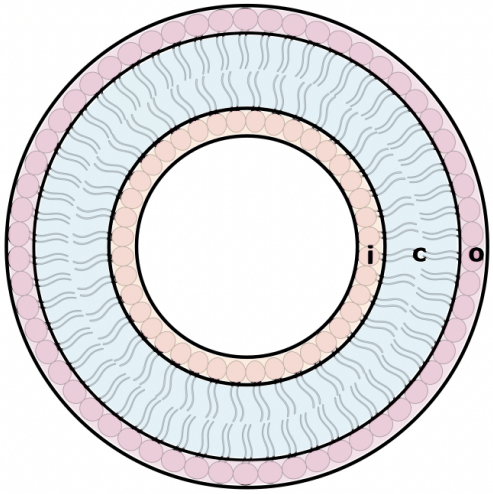

Figure 3.17: Sketch of the three shell model describing the structure of a liposome as three consecutive shells (inner i, core c, outer o).

The inner solvated shell consists of headgroups and water, scattering with the amplitude $A(q)_i$. The middle shell, also called the core, contains the tail groups with scattering amplitude $A(q)_c$. The outer shell contains the outer headgroups and water with amplitude $A(q)_o$. The liposome scattering intensity is defined as

$$I_{lip}(Q) = n_z \cdot A_{lip}(Q)^2 \tag{3.57}$$

where n_z is the number density of particles found from the concentration and aggregation number P_{agg}

$$n_z = \frac{n_{mol}}{P_{agg}} = \frac{c_{mol} \cdot N_A}{P_{agg}}. \tag{3.58}$$

$A_{lip}(Q)$ is the form factor amplitude scaled by each shells contrast and volume, and is defined as

$$A_{lip}(Q) = \Delta\rho_i A_i(Q) V_i + \Delta\rho_c A_c(Q) V_c + \Delta\rho_o A_o(Q) V_o. \tag{3.59}$$

V_i, V_c and V_o are the volumes of the inner head group, the tail (core) group and the outer head group shells, respectively. The volume of the inner core is

$$V_1 = 4\pi \frac{R_i^3}{3}, \tag{3.60}$$

and the volumes of the spheres confined by each shell are defined as

$$V_i = 4\pi \frac{(R_i + t_i)^3}{3}, \tag{3.61}$$

$$V_c = 4\pi \frac{(R_i + t_i + D_c)^3}{3}, \tag{3.62}$$

$$V_o = 4\pi \frac{(R_i + t_i + D_c + t_o)^3}{3}. \tag{3.63}$$

R_i is the inner radius of the vesicle, D_c is the thickness of the hydrocarbon region and $t_{i/o}$ is the thickness of the inner and outer head group shells. As described for the basic form factor amplitude of shells in Equation (3.47), the amplitude contributions from each shell can be written as

$$A_{h,i}(Q) = \frac{V_i A(Q, R_i + t_i) - V_1 A(Q, R_i)}{V_i - V_1}, \tag{3.64}$$

$$A_c(Q) = \frac{V_c A(Q, R_i + t_i + D_c) - V_i A(Q, R_i + t_i)}{V_c - V_i}, \tag{3.65}$$

$$A_{h,i}(Q) = \frac{V_o A(Q, R_i + t_i + D_c + t_o) - V_c A(Q, R_i + t_i + D_c)}{V_o - V_c}. \tag{3.66}$$

Using the spherical form factor amplitude, $A(Q,R)_{sphere}$, as described in Section 3.5.2 gives the scattering amplitudes of the shells as

$$A(Q)_{shell} = \frac{V(R_i)A(Q,R_i)_{sphere} - V(R_{i-1})A(Q,R_{i-1})_{sphere}}{V(R_i) - V(R_{i-1})}, \tag{3.67}$$

where R_i and R_{i-1} is the outer and inner radii of the given shell. Since lipids are dynamic molecules a smearing factor $\exp(-\frac{Q^2\sigma_{i/i-1}^2}{2})$ is multiplied with the scattering amplitudes [98]. Here σ_i and σ_{i-1} are the disorder parameters for the inner and outer boundaries of the shell implying how much the given radii may vary from the set value.

The contrast of a shell $\Delta\rho_i$ is defined as the scattering length density of the given shell minus that of the solvent (ρ_0), $\Delta\rho = \rho_{i/c/o} - \rho_0$. For the hydrocarbon region, the scattering length density is calculated as the number of electrons in the shell, Z_{tail}, times the Thompson scattering length, r_0, divided by the volume of the tail region:

$$\rho_c = \frac{Z_{tail}}{V_{tail}} r_0. \tag{3.68}$$

For the head group regions, one must also consider the hydration. Which is, the amount of water penetrating the shells. For the head group shells, the scattering length density is calculated as

$$\rho_{outer} = (1 - f_{w,o}) \cdot \rho_{head} + f_{w,o} \cdot \rho_0, \tag{3.69}$$

$$\rho_{inner} = (1 - f_{w,i}) \cdot \rho_{head} + f_{w,i} \cdot \rho_0, \tag{3.70}$$

where $f_{w,o/i}$ is the fraction of water that is contained in the outer and inner shell calculated as the fraction not occupied by lipids in the shell. The fraction occupied by lipids is given by the volume of a headgroup multiplied by the number of lipids in the inner/outer head group shell, divided by the volume of the shell.

$$f_{w,o/i} = 1 - \frac{V_{head} \cdot P_{agg} \cdot 0.5}{V_{o/i}} \tag{3.71}$$

The scattering length density of the head group, ρ_{head} is calculated in the same way as for the hydrocarbon region

$$\rho_{head} = \frac{Z_{head}}{V_{head}} \cdot r_0. \tag{3.72}$$

3.5.7 Contribution of Polyethyleneglycol chains

The polymer Polyethyleneglycol (PEG) connected to lipids is often included in liposomes and drug delivery systems using lipid aggregates to enhance stability and circulation time. The liposomes used in this thesis contain a small amount of PEG-ylated DMPE lipids to increase stability and decrease multilamellarity, the structure of which is shown in figure 3.18. Therefore, it is necessary to account for the scattering of PEG in the analytical model.

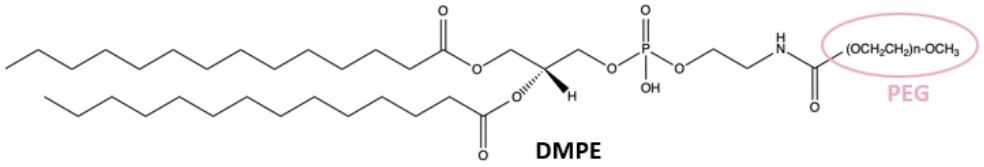

Figure 3.18: Chemical structure of PEGylated DMPE (1,2-Dimyristoyl-sn-glycero-3-phosphoethanolamine). Figure made using Chemdraw.

The PEG chains on the inner and outer leaflet of the lipid bilayer have a Gaussian random coil conformation. They can therefore be described using the analytical model developed by Arleth *et al.* [20, 99]:

The scattering intensity from PEGylated liposomes is described as

$$I_{PEG-liposomes}(Q) = I_{lip}(Q) + I_{chain}(Q) + I_{c_ic_i}(Q) + I_{c_ic_o}(Q) + I_{c_oc_o}(Q) + I_{sc_o}(Q) + I_{sc_i}(Q) \tag{3.73}$$

where I_{lip} is the scattering intensity from the liposomes and $I_{chain}(Q)$ is the scattering from the PEG-chains alone with the scattering

$$I_{chain}(Q) = n\Delta\rho_{PEG}^2 V_{PEG}^2 N_{PEG} \cdot A_{Gauss}(Q), \tag{3.74}$$

where n is the number of scatterers, $\Delta\rho$ is the contrast, V_{PEG} is the partial specific molecular volume of a single PEG chain, A_{Gauss} the form factor amplitude of a Gaussian chain as described in Section 3.5.2 and N_{PEG} is the number of PEG chains per liposomes and is defined as

$$N_{PEG} = f_{PEG} \cdot P_{agg}, \tag{3.75}$$

where f_{PEG} is the fraction of PEG-modified lipids in the liposomes.

The subsequent terms are interference terms. They describe how scattered waves from different PEG-chains interfere with each other. $I_{c_ic_i}(Q)$ and $I_{c_oc_o}(Q)$ are the interference terms between chains attached to the inner surface of the vesicles and between the PEG chains on the outer surface, respectively. $I_{c_ic_o}(Q)$ is the inter-interference between the inner and outer PEG chains. The interference terms are defined as follows using the form factor amplitude for

Gaussian chains, having the centre of mass of the PEG chains at a distance Rg away from the liposome surface:

$$I_{c_ic_i}(Q) = \Delta\rho_{PEG}^2 V_{PEG}^2 N_{PEG} f_{inner} \cdot (N_{PEG} f_{inner} - 1) \cdot \left[\frac{1-\exp[-(QR_g)^2]}{(QR_g)^2}\right]^2 \cdot \left[\frac{\sin(Q(R_{inner}-R_g))}{Q(R_{inner}-R_g)}\right]^2 \tag{3.76}$$

the $\frac{\sin Qr}{Qr}$ term averages the form factor intensity over all directions. In case the distribution of PEGylated lipids is not uniform in each leaflet, the fraction f_{inner} of PEG in the inner leaflet is used.

$$I_{c_oc_o}(Q) = \Delta\rho_{PEG}^2 V_{PEG}^2 N_{PEG}(1-f_{inner}) \cdot (N_{PEG}(1-f_{inner}) - 1) \cdot \left[\frac{1-\exp[-(QR_g)^2]}{(QR_g)^2}\right]^2 \cdot \left[\frac{\sin(Q(R_{outer}-R_g))}{Q(R_{outer}-R_g)}\right]^2 \tag{3.77}$$

$$I_{c_ic_o}(Q) = \Delta\rho_{PEG}^2 V_{PEG}^2 N_{PEG}^2 f_{inner} \cdot (1-f_{inner}) \cdot \left[\frac{1-\exp[-(QR_g)^2]}{(QR_g)^2}\right]^2 \cdot \left[\frac{\sin(Q(R_{inner}-R_g))}{Q(R_{inner}R_g)}\right] \cdot \left[\frac{\sin(Q(R_{outer}-R_g))}{Q(R_{outer}R_g)}\right] \tag{3.78}$$

where R_{inner} and R_{outer} are the inner and outer radii of the liposomes and are defined as

$$R_{inner} = R_i - R_g - d_{corr} \tag{3.79}$$

$$R_{outer} = R_{tot} + R_g + d_{corr} \tag{3.80}$$

The displacement factor d_{corr} describes how compressible the PEG-chains are. The last two terms are interference cross-terms of the outer and inner chains with the bilayer:

$$I_{sc_i} = A(Q,R)_{lip} \cdot \Delta\rho_{PEG} V_{PEG} 2N_{PEG}(1-f_{inner}) \cdot (N_{PEG}(1-f_{inner}) - 1) \cdot \left[\frac{1-\exp[-(QR_g)^2]}{(QR_g)^2}\right] \cdot \left[\frac{\sin(Q(R_{inner}-R_g))}{Q(R_{inner}-R_g)}\right] \tag{3.81}$$

$$I_{sc_o} = A(Q,R)_{lip} \cdot \Delta\rho_{PEG} V_{PEG} 2N_{PEG} f_{inner} \cdot (N_{PEG} f_{inner} - 1) \cdot \left[\frac{1-\exp[-(QR_g)^2]}{(QR_g)^2}\right] \cdot \left[\frac{\sin(Q(R_{outer}-R_g))}{Q(R_{outer}-R_g)}\right] \tag{3.82}$$

3.5.8 Cholesterol

Since the lipids used in this thesis are saturated or mono- or di-unsaturated, several findings support the assumption that the cholesterol most likely will be in its canonical upright position [37, 100]. Therefore, the model includes cholesterol in the scattering from the lipid tails by modifying the tail volume. The exception is the polar OH group which is assumed to reside in

the polar head group region. To account for the hydroxyl-groups placement in the head group region, the volume and electrons of the *OH* group were added in the inner and outer head group shells, assuming the "pseudo-molecule" approximation:

$$V_{tail,modified} = (f_{chol} \cdot \frac{M_{chol}}{d_{chol}} + (1 - f_{chol}) \cdot \frac{M_{tail}}{d_{tail}}) \cdot \frac{1}{N_A}, \tag{3.83}$$

where f_{chol} is the fraction of cholesterol in the liposomes, M_{chol} is the molecular weight of cholesterol and d_{chol} is the density of cholesterol in the liposomes. When including cholesterol the hydration factor must be modified as

$$f_{w,i} = 1 - \frac{V_{head} \cdot P_{agg} \cdot (1 - f_{chol})}{V_i} \tag{3.84}$$

and the scattering from the hydrocarbon region is described as the sum of scattering from lipids and cholesterol. First, the scattering length density of the tail region is modified:

$$\rho_{chol} = \frac{Z_{chol}}{V_{chol}} \cdot r_0 \tag{3.85}$$

$$\rho_{tail,modified} = \frac{(Z_{chol} - Z_{OH}) \cdot r_0}{(V_{chol} - V_{OH})} \cdot f_{chol} + \frac{Z_{tail}}{V_{tail}} \cdot r_0 \cdot (1 - f_{chol}) \tag{3.86}$$

The scattering from the head region includes the scattering from the *OH* group:

$$\rho_{OH} = \frac{Z_{OH} \cdot r_0}{V_{OH}} \tag{3.87}$$

$$\rho_{head,modified} = \rho_{OH} \cdot f_{chol} + \frac{Z_{head} \cdot r_0}{V_{head}} \cdot (1 - f_{chol}) \tag{3.88}$$

This modified scattering length density is used to calculate the total scattering intensity.

3.5.9 Inclusion of peptide

To account for peptide insertion in the liposomes, the scattering length densities of each shell are modified using fractions of peptide located in each shell. The contrasts of the shells with peptide included are

$$\Delta\rho_i = (1 - fp_{IS} \cdot rPL - fwi) \cdot \rho_{head,modified} + fwi \cdot \rho_{solvent} + fp_{IS} \cdot rPL \cdot \rho_{peptide} - \rho_{solvent}, \tag{3.89}$$

$$\Delta\rho_c = (1 - fp_{HC} \cdot rPL) \cdot \rho_{tail,modified} + fp_{HC} \cdot rPL \cdot \rho_{peptide} - \rho_{solvent}, \tag{3.90}$$

$$\Delta\rho_o = (1 - fp_{OS} \cdot rPL - fwo) \cdot \rho_{head,modified} + fwo \cdot \rho_{solvent} + fp_{OS} \cdot rPL \cdot \rho_{peptide} - \rho_{solvent}. \tag{3.91}$$

Where fp_{IS}, fp_{HC} and fp_{OS} are the fractions of peptides in the inner head group shell, the hydrocarbon region and the outer head group shell respectively. *rPL* is the molar fraction of peptide:lipid in the liposomes:

$$rPL = \frac{c_p}{c_l + c_p} \cdot (1 - f_{free}). \tag{3.92}$$

Here $c_{p/l}$ is the molar concentration of peptide and lipid in the vesicles, and f_{free} is the fraction of free peptide in solution.

The amplitude of the liposome scattering can now be written as

$$A(Q) = V_i \cdot \Delta\rho_i \cdot A_{h,i}(Q) + \Delta\rho_c \cdot V_c \cdot A_c Q + \Delta\rho_o \cdot V_o \cdot A_{h,o}(Q). \tag{3.93}$$

And the number density of liposome scatterers is updated to include the peptide as well as the lipids:

$$nz = \frac{n_{mol,lip} + n_{mol,pep} \cdot (1 - f_{free})}{P_{agg}}, \tag{3.94}$$

where the aggregation number P_{agg} is calculated from the ratio *rPL*.

3.5.10 Thickness polydispersity

The size distribution that the form factors are integrated over in the three-shell model includes the polydispersity in the radii of the micelle (see equation (3.33)). In addition to the liposome size distribution there may be a distribution of bilayer thickness, especially when considering rafts. In order to include this polydispersity the parameters depending on the bilayer thickness were integrated between a set Dc_{min} and Dc_{max} of $Dc \pm \sigma_c \cdot Dc$. Where Dc is the thickness of the hydrocarbon region and σ_c is the variance in the Gaussian distribution:

$$f(x_c, \overline{Dc}) = \frac{1}{\sigma_c \cdot Dc \cdot \sqrt{2\pi}} \cdot \exp\left(\frac{-(x_c - Dc)^2}{2 \cdot \sigma_c^2 \cdot Dc^2}\right), \tag{3.95}$$

x_c is the value of the bilayer thickness at each step in the integral.

The average intensity with the thickness polydispersity accounted for then becomes:

$$I_{tot}(Q) = \int_{Dc_{min}}^{Dc_{max}} f(x_c, \overline{Dc}) \cdot I(Q, x_c) dx_c, \tag{3.96}$$

where $I(Q, x_c) = A_{lip}(Q, x_c)^2$ is the average intensity without accounting for polydispersity, and $A_{lip}(Q, x_c)^2$ is the amplitude of scattering from the liposomes, as iven in Equation (3.93).

3.5.11 Multi-lamellar structures

Some of the samples showed small degrees of multilamellarity. Due to the presence of multiple layers close to each other, the system has quasi long-range order, and Bragg-peak scattering can be observed. In the scattering curve, multilamellarity is seen as emerging peaks/flattening in the curve at low Q-values.

To account for the multilamellarity, a structure factor was added. The factor accounts for variations in the bilayer separations using a stacking disorder. Paracrystalline theory describes the disorder in the stacking, that is, the presence of small variations in the separation of the bilayers [101, pp. 650–653]. The structure factor given by paracrystalline theory is

$$S_{PT}(Q,N,d,\Delta,N_{diff}+) = N_{diff} + \sum_{N_k=N-2\sigma}^{N+2\sigma} x_k S_{k,PT}, \tag{3.97}$$

where N is the average number of stacked bilayers, d the distance between the bilayers, Δ is the stacking disorder parameter and N_{diff} accounts for a diffuse background due to uncorrelated scattering bilayers. The last term is given by

$$S_{k,PT} = N_k + 2\sum_{m=1}^{N_k-1}(N_k - m)\cos(mQd)\exp(-\frac{m^2Q^2\Delta^2}{2}), \tag{3.98}$$

and is a structure factor for low and fixed stacking numbers N.

3.5.12 Micelle and bicelle scattering

In the cases where the addition of peptides disrupted the vesicle structure, likely structures formed by the self-assembling lipids are micelles or bicelles. The model was modified to include the formation of mixed peptide-lipid micelles.

Micelle scattering

Micelles are spherical aggregates of lipids and peptides, as seen in figure 3.19.

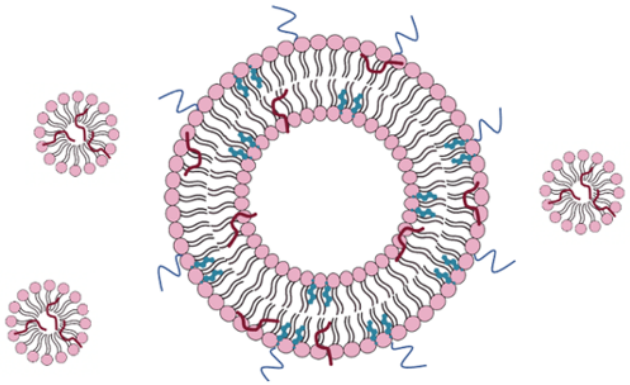

Figure 3.19: A liposome and micelles with incorporated peptides

The intensity of the micelle scattering is given by [22]:

$$I_{micelle}(Q) = n_z \cdot P_{micelle}(Q), \tag{3.99}$$

where the number of scattering micelles is defined as

$$n_z = \frac{n_{micelle}}{P_{agg}} = \frac{c_{micelle} \cdot \frac{N_A}{1000}}{P_{agg}}. \tag{3.100}$$

The concentration of micelles, $c_{micelle}$, is calculated by the molar concentration of lipids times the fraction of lipids in micelles (and not in the liposomes), f_{LinM}, plus the molar concentration of peptides times the fraction of peptides that are in the micelles, f_{PinM}, $f_{L,micelle}$ and $f_{p,micelle}$ respectively

$$c_{micelle} = Mconc_{lipid} \cdot f_{L,micelle} + Mconc_{peptide} \cdot f_{p,micelle}. \tag{3.101}$$

Where $Mconc_{lipid}$ and $Mconc_{peptide}$ are the total molar concentrations of lipids and peptides, respectively, and the fractions of lipids and peptides incorporated in the micelles are $f_{L/p,micelle}$.

The aggregation number of the micelle, $P_{agg,micelle}$ is defined as

$$P_{agg,micelle} = \frac{V_{micelle}}{(VtotL + ratioPLmic \cdot Vp)}, \tag{3.102}$$

where $VtotL$ is the volume of lipid molecules, including the fraction of cholesterol (as described above), $ratioPLmic$ is the ratio between peptides and lipids in the micelles, and Vp is the peptide volume. The volume of the micelles with radius $r_{micelle}$ is given by

$$V_{micelle} = \frac{4\pi}{3}(r_{micelle})^3. \tag{3.103}$$

The last term in the intensity expression is the modified form factor of a homogeneous sphere, and it is defined as

$$P_{micelle}(Q) = \left[V_{micelle} \cdot \Delta\rho_{micelle} \cdot A_{micelle}(Q)\right]^2, \tag{3.104}$$

where the scattering amplitude, $A_{micelle}(Q)$, is the spherical form factor amplitude described in Section 3.5.2.

The scattering contrast is the difference between the scattering length density of the micelle and the solvent. Since we assumed that the micelles are homogeneous spheres the scattering length density of the micelles are calculated as an average of the lipids (with cholesterol) and peptide scattering:

$$\rho_{micelle} = \frac{\rho_{head,L} \cdot V_{head,L} + \rho_{tail,L} \cdot V_{tail,L} + \rho_p \cdot V_p \cdot ratioPL_{mic}}{V_{head,L} + V_{tail,L} + V_p \cdot ratioPL_{mic}}, \tag{3.105}$$

$$\Delta\rho_{micelle} = \rho_{micelle} - \rho_{solvent}. \tag{3.106}$$

The total scattering intensity with the micelle scattering is:

$$I(Q) = n_z \cdot P_{lip}(Q) + I_{mic} + bcg + I_{free}, \tag{3.107}$$

where the number density of scatterers n_z in the lipid vesicles is defined as

$$nz = \frac{((1 - f_{linM}) \cdot n_{lip} \cdot N_A + n_{pep} \cdot N_A \cdot (1 - f_{free} - f_{pinM}))}{P_{agg}}. \tag{3.108}$$

Bicelle scattering

Bicelles discs that can be modelled like short cylinders with an extra layer around the edge, not only at the top and bottom. This rim contains mainly head groups and peptides. Figure 3.20 shows the 3D structure and a cross-section of a bicelle with its structural parameters.

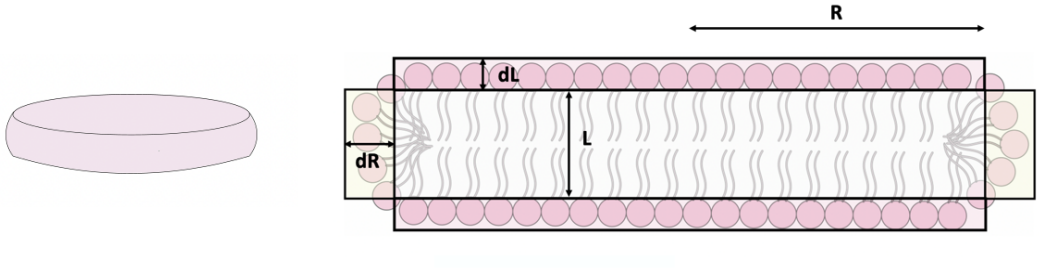

Figure 3.20: Bicelle 3D structure (left) and cross-section (right). R is the radius of the bicelle, L the length of the hydrocarbon core, dL and dR are the respective thicknesses of the headgroups outside the length and width.

The bicelle can be modelled as a core-shell cylinder with radius R where the core is the hydrocarbon bilayer part of the bicelle. The shell is divided into two different sections; the one above and below the bilayer plane, which has a thickness of dL, and the shell surrounding the cylinder parallel to the bilayer normal, with a thickness of dR.

The intensity is again defined by the scattering form factor and the number of scatterers:

$$I_{bicelle}(Q) = n_z \cdot P_{bicelle} + bcg \tag{3.109}$$

where $n_z = \frac{n_{lip}+r_{PL}\cdot n_{pep}}{P_{agg,b}}$ is the number of scatterers in the bicelle defined by the number of lipids and peptides, the peptide:lipid ratio (r_{PL}) and the aggregation number. $P_{agg,b}$ is the aggregation number, $P_{bicelle}(Q)$ the form factor of a cylinder as described in Section 3.5.2 and bcg is the incoherent background.

The aggregation number of a bicelle is defined as the volume of the core cylinder divided by the volume of a lipid tail

$$P_{agg,b} = \frac{\pi \cdot R^2 \cdot L}{V_{tail}}, \tag{3.110}$$

$$P_{agg,b} = \frac{V_{core}}{V_{lipid} + rPL \cdot V_{pep}}, \tag{3.111}$$

The form factor of a cylinder weighted with the volume and contrast is defined as

$$F_{cyl}(Q) = [\Delta\rho \cdot V_{tot} \cdot A_{cyl}(Q)]^2 \cdot \sin\alpha \tag{3.112}$$

The bicelle and its core and rim can be thought of as stacked cylinders. The core cylinder of the hydrocarbon bilayer has a scattering amplitude defined by

$$A_{core}(Q) = \frac{2 \cdot \sin(Q \cdot H \cdot \cos\alpha)}{(Q \cdot H \cdot \cos\alpha)} \cdot \frac{J1(Q \cdot R \cdot \sin\alpha)}{Q \cdot R \cdot \sin\alpha} \cdot \exp(-\sigma_{core} \cdot \sigma_{core} \cdot Q^2), \tag{3.113}$$

in which $H = L/2$ and J_1 is the Bessel function of first order. The next cylinder we consider is the cylinder including the rim parallel to the bilayer plane, which has a thickness of dL. The scattering amplitude is defined as

$$A_{core+dL}(Q) = \frac{2 \cdot \sin((Q \cdot H + Q \cdot dL) \cdot \cos\alpha)}{((Q \cdot H + Q \cdot dL) \cdot \cos\alpha)} \cdot \frac{J1(Q \cdot R \cdot \sin\alpha)}{Q \cdot R \cdot \sin\alpha} \cdot \exp(-\sigma_{shell} \cdot \sigma_{shell} \cdot Q^2). \tag{3.114}$$

The final scattering amplitude needed is the one for the entire bicelle, that is, the core and the rim:

$$\begin{aligned} A_{core+dL+dR}(Q) = & \frac{2 \cdot \sin((Q \cdot H + Q \cdot dL) \cdot \cos\alpha)}{((Q \cdot H + Q \cdot dL) \cdot \cos\alpha)} \\ & \cdot \frac{J1((Q \cdot R + Q \cdot dR) \cdot \sin\alpha)}{(Q \cdot R + Q \cdot dR) \cdot \sin\alpha} \cdot \exp(-\sigma_{shell} \cdot \sigma_{shell} \cdot Q^2), \end{aligned} \tag{3.115}$$

where dR is the thickness of the rim parallel to the bilayer normal. This thickness is added to the core radius in the cylinder. The interfacial smearing factors, $\sigma_{core/shell}$ were explicitly added to each scattering amplitude to have better control over where the uncertainties were.

The volumes of the cylinders are defined as:

$$V_{core} = \pi \cdot R^2 \cdot L, \tag{3.116}$$

$$V_{core+dL} = \pi \cdot (R^2 \cdot (L + 2 \cdot dL)), \tag{3.117}$$

$$V_{core+dL+dR} = \pi \cdot ((R + dR)^2 \cdot (L + 2 \cdot dL)). \tag{3.118}$$

The contrasts multiplied with the corresponding volumes and form factor amplitudes of each shell are added together and squared to define the form factor:

$$F_{core+dL+dR}(Q) = (\rho_{head,dR} - \rho_{sol}) \cdot (V_{core+dL+dR} \cdot A_{core+dL+dR}(Q) - V_{core+dL} \cdot A_{core+dL}(Q)), \tag{3.119}$$

$$F_{core+dL}(Q) = (\rho_{head,dL} - \rho_{sol}) \cdot (V_{core+dL} \cdot A_{core+dL} - V_{core} \cdot A_{core}(Q)), \tag{3.120}$$

$$F_{core}(Q) = (\rho_{tail} - \rho_{sol}) \cdot (v_{core} \cdot A_{core}(Q)), \tag{3.121}$$

$$P_{bicelle}(Q) = \int_0^{\pi/2} (F_{core}(Q) + F_{core+dL}(Q) + F_{core+dL+dR}(Q))^2 \cdot \sin\alpha d\alpha. \tag{3.122}$$

The scattering length densities of the three different regions are

$$\rho_{tail} = \frac{Z_{tail}}{V_{tail}} \cdot r_0, \tag{3.123}$$

$$\rho_{head,dR} = \frac{Z_{head,dR}}{V_{head,dR}} \cdot r_0, \tag{3.124}$$

$$\rho_{head,dL} = \frac{Z_{head,dR}}{V_{head,dL}} \cdot r_0, \tag{3.125}$$

Where Z_i is the average number of electrons in the tail and different head-group regions, and they are given by

$$Z_{tail} = Z_{tail,l} + r_{p,l} \cdot Z_{tail,p}. \tag{3.126}$$

Here $Z_{tail,l}$ is the number of electrons in the lipid tails, $r_{p,l}$ is the ratio of peptides to lipids and $Z_{tail,p} = f_{p,tail} \cdot Z_p$ is the number of electrons from the peptide located in the tail region. The number of electrons in the rim regions is calculated in the same way, having, in addition, the fraction of lipid/peptide located in the different rim regions $f_{l/p,dR/dL}$, assuming that the head-groups not located in the dR region must be in the dL region.

$$Z_{head,dR} = f_{l,dR} \cdot Z_{head,l} + r_{p,l} \cdot f_{p,dR} \cdot (Z_p - Z_{tail,p}), \tag{3.127}$$

$$Z_{head,dL} = (1 - f_{l,dR}) \cdot Z_{head,l} + r_{p,l} \cdot (1 - f_{p,dR}) \cdot (Z_p - Z_{tail,p}). \tag{3.128}$$

If the peptide and lipids are equally distributed, the fraction of each in the dR rim are

$$f_{l,dR} = f_{p,dR} = \frac{V_{core,dR}}{V_{core,dR} + V_{core,dL}}. \tag{3.129}$$

Else, the fraction of peptide and lipid in the rim are

$$f_{l,dR} = \frac{P_{agg,b} \cdot V_{head,dL}}{V_{core+dL} - V_{core}}, \tag{3.130}$$

$$f_{p,dR} = \frac{P_{agg,b} \cdot V_{head,dR}}{V_{core+dL+dR} - V_{core+dL}}. \tag{3.131}$$

Using the fractions of lipid and peptide in the rims and ratios of lipid to peptide, modified lipid volumes are calculated as

$$V_{tail} = V_{tail,l} + r_{p,l} \cdot V_p \cdot f_{p,tail}, \tag{3.132}$$

$$V_{head,dR} = f_{l,dR} \cdot V_{head,l} + r_{p,l} \cdot f_{p,dR} \cdot V_p \cdot (1 - f_{p,tail}), \tag{3.133}$$

$$V_{head,dL} = (1 - f_{l,dR} \cdot V_{head,l} + r_{p,l} \cdot (1 - f_{p,dR}) \cdot V_p \cdot (1 - f_{p,tail}). \tag{3.134}$$

Taking the hydration of the headgroup shells into account, the fraction of solvent in the rim is given by

$$f_{w,dR} = 1 - \frac{P \cdot V_{head,dR}}{V_{core,dR}}, \tag{3.135}$$

$$f_{w,dL} = 1 - \frac{P \cdot V_{head,dL}}{V_{core,dL}}, \tag{3.136}$$

where the volumes of the rims are $V_{head,dR} = V_{core+dR} - V_{core}$ and $V_{head,dL} = V_{core+dL} - V_{core}$. with the modified aggregation number $P = \frac{V_{core}}{V_{tail}}$.

3.5.13 Recap of the analytical models

To find the perfect fit to sample scattering data, the analytical model(s) have to be chosen carefully. Figure 3.21 gives an overview over the analytical three-shell model and the applied modifications. Starting from the simplest approximation of the liposomes as layered shells, more detail and precision is obtained by including the scattering from cholesterol as an own component, then adding the peptide scattering and polydispersity in thickness not only size. For some samples, a degree of multilammelarity had to be considered, and for others scattering from bicelles and micelles were essential components.

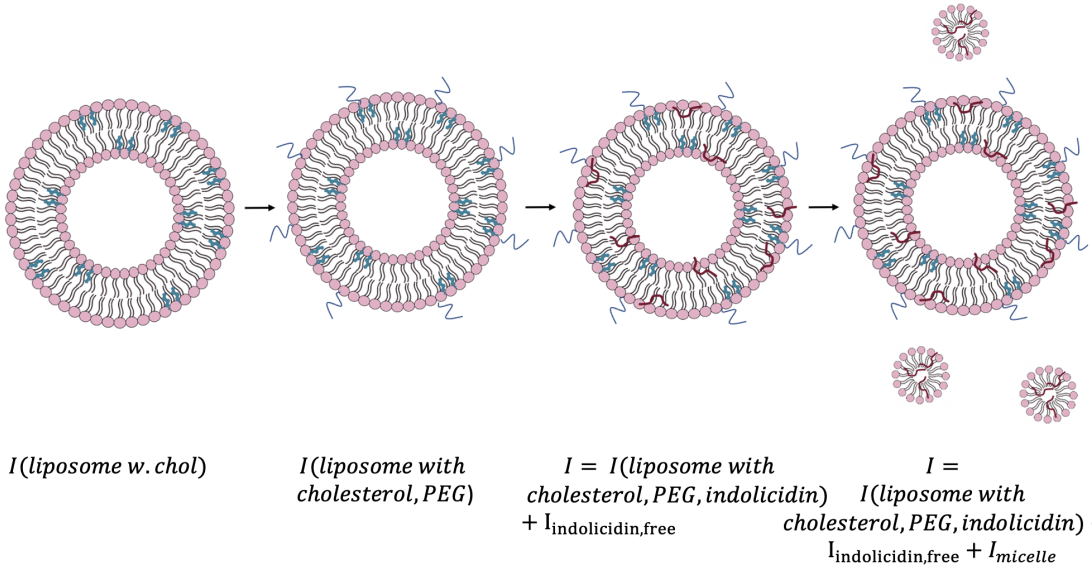

Figure 3.21: Gradual modification of the analytical model from a three-shell model with incorporated cholesterol to a model including scattering from PEGylated lipids and indolicidin, and finally micelle scattering.

Chapter 4

Experimental methods

4.1 Sample preparation

The samples were prepared following a standard liposome preparation protocol [102]. The lipids were purchased from Avanti Polar Lipids and used without further purification. The lipids were first weighed using a VWR analytical balance and added to a round bottom flask. Then they were dissolved in a one to three mixture of methanol and chloroform. The added volume of organic solvent was the same as the final volume after hydration. The organic solvent mixture was evaporated using a rotary evaporator under a vacuum down to 40 mbar in a heat bath at or above the melting temperature of the highest melting lipid. The samples composed of lipids with different degree of saturation were dried under a nitrogen gas flow, and then dried using the rotary evaporator under vacuum to ensure complete evaporation of the solvent.

When the solvent had evaporated, the dry lipid film was rehydrated by adding Tris-buffer (pH = 7.4) to the desired concentrations and dissolving the film using a waterbath at the same temperature as in the dehydration step. The sample was transferred to a sonicator after approximately an hour (depending on how easily the film dissolved). Sonication waves disrupt the suspension of large multilamellar liposomes, forming small unilamellar liposomes. The liposomes were extruded through a 100 nm polycarbonate membrane filter to give monodisperse, passing the sample through the filter a minimum of 21 times. The extruder was also heated to ensure that the mixture was above the lipids' transition temperature.

4.1.1 Lipid composition

The chemical structures of the lipids used in this thesis are illustrated in figure 4.1. For the first model system, the homogeneous membrane, the lipid 1,2-dimyristoyl-sn-glycero-3-phosphocholine (DMPC) was used together with 0, 20 and 40 mol% cholesterol. DMPC, with its zwitterionic head group, is commonly used in model membrane systems for eukaryotic membranes. As mentioned in section 2.1.3, eukaryote membranes contain mainly zwitterionic lipids and up to 40-50 *mol%* cholesterol [103]. Other binary systems were prepared by cholesterol and 1,2-dioleoyl-sn-glycero-3-phosphocholine (DOPC), and cholesterol and 1,2-distearoyl-sn-glycero-3-phosphocholine (DSPC).

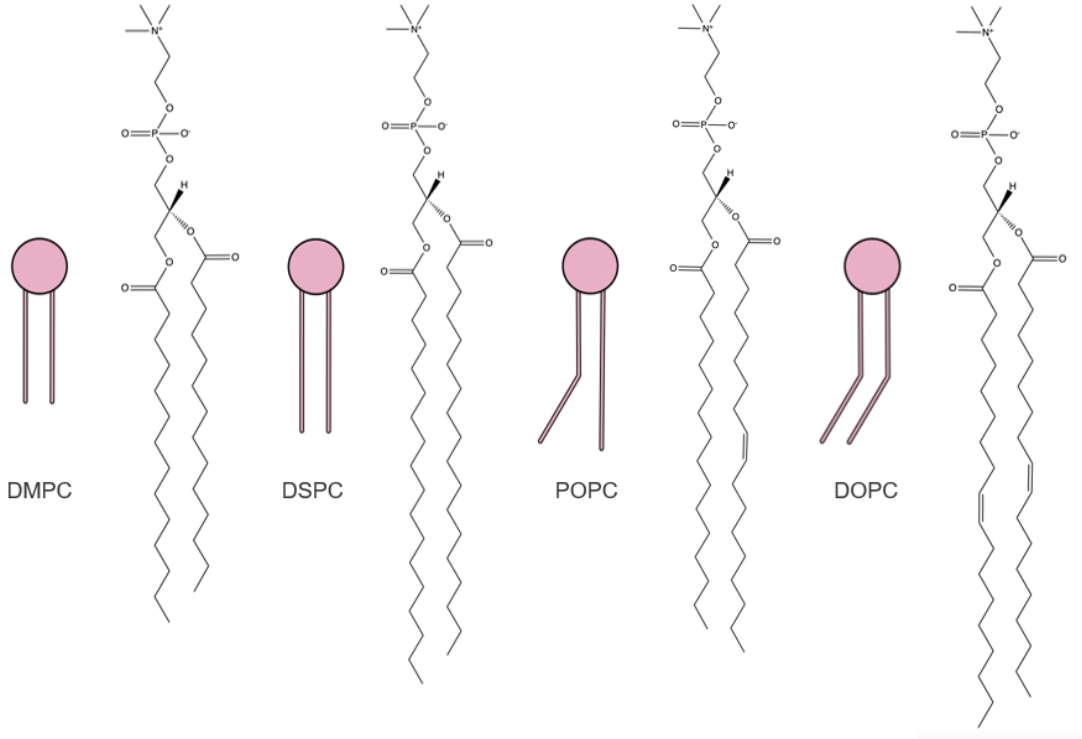

Figure 4.1: Chemical structure of the lipids used in this thesis. From left to right: DMPC (1,2-dimyristoyl-sn-glycero-3-phosphocholine), DSPC (1,2-distearoyl-sn-glycero-3-phosphocholine), POPC (1-palmitoyl-2-oleoyl-glycero-3-phosphocholine), DOPC (1,2-dioleoyl-sn-glycero-3-phosphocholine).

For the heterogeneous model systems, the lipid compositions were reproduced from the work of Heberle *et al.* [71] on rafts in model membranes. 1,2-distearoyl-sn-glycero-3-phosphocholine (DSPC) has fully saturated chains, and the unsaturated lipids used are 1-palmitoyl-2-oleoyl-sn-glycero-3-phosphocholine (POPC) which is monounsaturated, and 1,2-dioleoyl-sn-glycero-3-phosphocholine which is di-unsaturated. The selected compositions from Heberle *et al.* included one reference which should not form rafts (S1), with 34 mol % cholesterol, no DOPC and a 50 : 50 ratio between DSPC and POPC. As named in the Heberle article, the other selected compositions were D2, D4 and D6, with respectively increasing raft sizes by increasing the amount of di-unsaturated DOPC up to 13.65 mol %. A full overview of the sample compositions is given in table 4.1.

Table 4.1: Composition and naming of the phase segregating lipids. S1 is a control sample that should not phase segregate, while the following compositions D2, D4, and D6 have been shown to have an increasing raft size [71]

Lipid (molar fractions)	**S1**	**D2**	**D4**	**D6**
DSPC	0,317	0,38003	0,380	0,380
DOPC	0	0,020	0,059	0,137
POPC	0,317	0,361	0,322	0,244
Chol	0,341	0,215	0,215	0,215
DMPE-PEG	0,025	0,025	0,025	0,025
Raft-size	none	small	medium	large

These compositions were chosen to first reproduce the results obtained by Heberle *et al.* [71] and confirm the existence of rafts, and subsequently to study the impact of rafts on peptide interactions.

Because liposomes are soft self-assembled structures in a metastable state, they are expected to form multilamellar and aggregated structures over time. To obtain a maximum fraction of unilamellar stable vesicles, 2.5 mol% of 1,2-Dimyristoyl-sn-glycero-3-phosphoethanolamine with polyethylene glycol (DMPE-PEG) was added to all liposomes. PEG is a linear polyether diol with several advantages for pharmacological and research use, like biocompatibility, solubility in organic solvents and lack of toxicity [104, 105]. The hydrophilic and flexible polymer chain acts as a steric hindrance for liposomal degradation, increasing the stability and lifetime of the liposomes, based on the fact that the polymer chain occupies the space immediately adjacent to the liposome surface and tends to exclude other vesicles from this space [104]. Due to the metastable nature of the vesicles, the samples were prepared as shortly before measuring them as possible.

To reduce the liposomes' time of exposure to peptides, the mixtures were prepared from stock solutions shortly before measuring them. A waiting time of approximately half an hour ensured that all samples with added peptide had similar interaction time-spans. The stocks were prepared so that they could be mixed 50/50 to achieve the final concentrations, instead of mixing the lipids directly with a high concentration peptide solution and then diluting the sample with buffer. The mixing of equal volumes prevented the liposomes from exposure of a higher concentration of peptides than desired before diluting it to the final concentration. The same principles were followed in the preparation of samples for the SANS experiment.

4.1.2 Mixed lipid liposomes for SANS

The samples for SANS were prepared following the same protocol as described in section 4.1, but with approximately 67% of all DSPC lipids being tail deuterated (DSPC-d_{70}) and with a Tris-buffer composed of 34% D_2O. As mentioned in Section 4.3, deuterated components were added to achieve contrast matching, in order to observe phase separation. The exact theoretical compositions of the samples are shown in Table 4.2.

Table 4.2: SANS sample compositions, with d-DSPC indicating tail-deuterated DSPC (DSPC-d70).

Lipid (molar fractions)	**S1**	**D2**	**D4**	**D6**
h-DSPC	0,069	0,124	0,124	0,125
d-DSPC	0,248	0,256	0,256	0,255
DOPC	0	0,020	0,0585	0,137
POPC	0,317	0,361	0,322	0,244
Chol	0,341	0,215	0,215	0,215
DMPE-PEG	0,025	0,025	0,025	0,025
Raft-size	none	small	medium	large

4.2 Small Angle X-ray Scattering

The SAXS measurements used in this thesis were performed at the BM29 beamline for SAXS at the European Synchrotron Radiation Facility (ESRF) in Grenoble, France [87]. The instrument has an achievable q-range of $0.025 - 6$ nm^{-1}, corresponding to a maximum detectable size of 200 nm, perfect for studying bilayer systems with radii of approximately 50 nm. The sample handling system automatically injects the samples into the exposure cell (capillary). The buffer is measured both before and after each sample. The sample continuously flows through the capillary during the measurement to minimise radiation damage. The setup of the beamline is shown in figure 4.2.

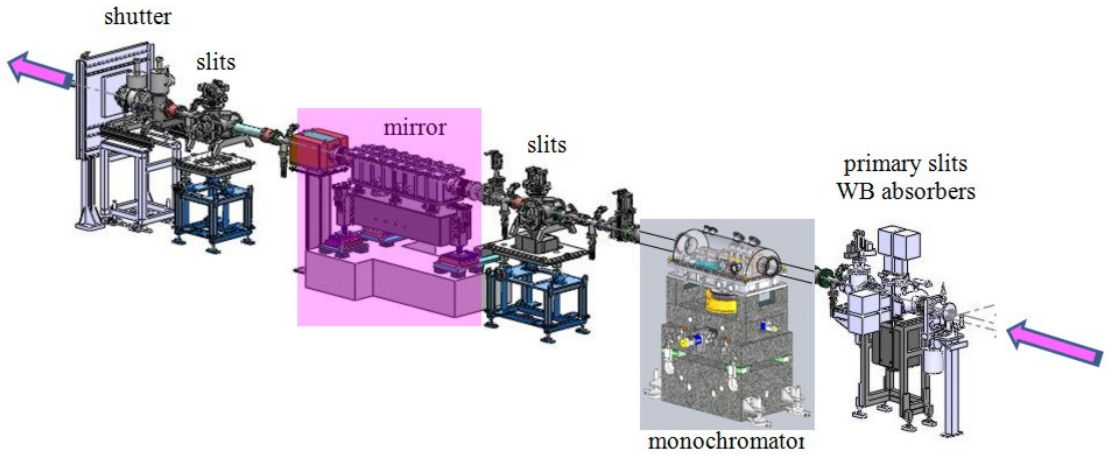

Figure 4.2: Image from the ESRF website [106], showing an overview of the optics of the BM29 SAXS beamline.

A dipole (bending magnet) bends the beam from the accelerator in the direction of the sample. After the bending magnet, the beam passes through the white beam slit defining the aperture and a water-cooled mask. White-beam absorbers reduce the low energy content of the

beam. The beam then passes through a double layer monochromator with 2.96 nm spacing. A beamstop integrated into the monochromator blocks any white beam that may escape from the first monochromator layer. A 1.1 m long cylindrical toroidal mirror is the beamline's main focusing element, which focuses the monochromatic radiation in the detector plane. A fast shutter minimises the radiation dose received by the samples.

The DMPC/Chol and POPC/Chol samples were run at 37°C, while the rest were run at 20°C.

4.3 Small Angle neutron Scattering

The SANS-I at the Paul Scherrer Institut (PSI) in Villigen, Switzerland, covers a q-range from $6 \cdot 10^{-3} nm^{-1}$ to $5.4 nm^{-1}$, and the detector can be moved laterally by $50 cm$ up to a q-range of $10.5 nm^{-1}$. The achievable q-range allows the investigation of structures from about 1 to 400 nm [107]. Figure 4.3 shows a simplified setup of the SANS-I instrument.

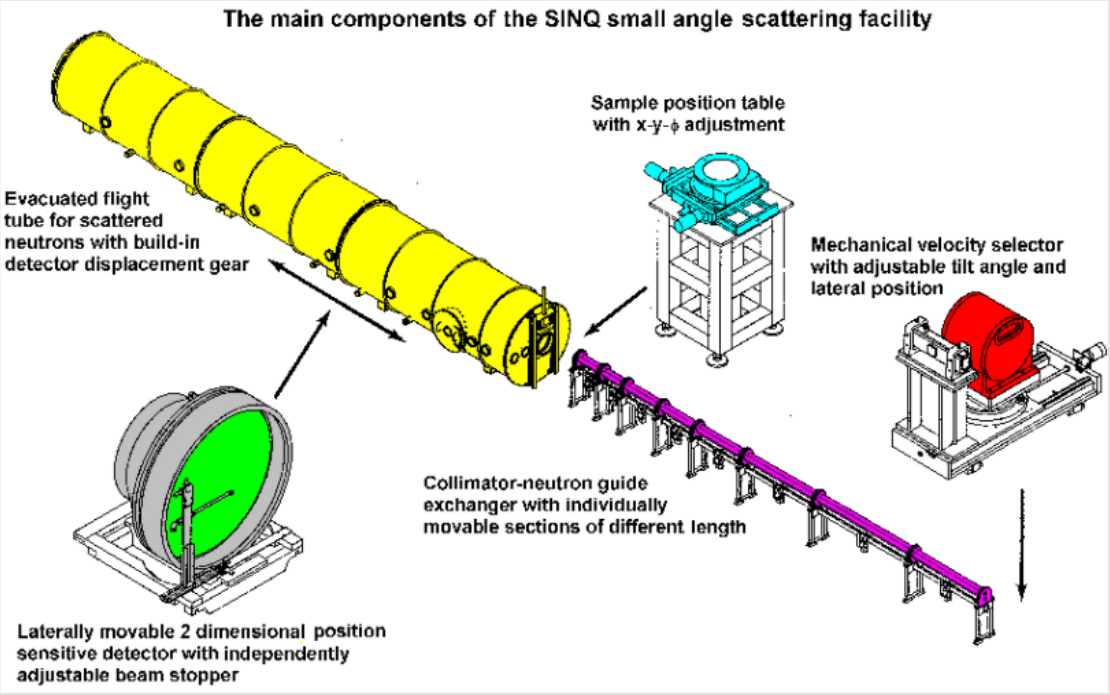

Figure 4.3: Image from the PSI website [108], shows the main components of the SANS setup with the velocity selector and neutron guide to the right and the detector and flight tube to the left of the sample table.

Neutrons are spallated from the SINQ source, and the instrument is installed at a cold neutron guide which filters out higher energy neutrons. In order to filter out neutrons with energy below the lower cut-off wavelength, the curved section is coated with isotropically enriched ^{58}Ni, ensuring that neutrons with a wavelength below 0.42 nm are absorbed. A mechanical velocity selector tailors the beam using a monochromator and a straight pinhole collimation system [107].

The collimator allows for adjustment of the distance between the two pinholes at the guide exit and the sample position. The discrete steps allowed matches the Q-resolution chosen by the sample-detector distance.

The detector can be placed from 1.5 to 20 m from the sample position, and for a further increase in the Q-range, it may be displaced laterally up to 50 cm. The maximum count rate of the detector is 20 kHz per pixel and 200 kHz for the entire detector. A beamstop is placed immediately before the detector, protecting it from the direct beam [107]. In this case, the detector was placed at 2 and 8 m, and the plots were manually merged by removing approximately the last 15 points of the data from each detector distance (the reader is referred to section 7.8 in Appendix for further detail).

The scattering data obtained were reduced using the BerSANS software from the Hahn-Meitner-Institut (HMI) in Berlin, Germany. The software is developed specifically for the reduction of neutron scattering data. After the reduction, the data acquired with a detector distance of 8 m were fitted to a simple analytical model of Ornstein-Zernike law using the non-linear least square method to observe the general trend of fluidity in the membranes. All SANS data-processing was performed by Vladimir R. Koynarev and then plotted by me using origin.

4.4 Differential Scanning Calorimetry

The DSC scans were performed with a heating/cooling rate of 2 K/min in a temperature range between 0 and 75 °C, and with 2 sweeps in each temperature direction. All DSC measurements in this thesis were performed by Bente Amalie Breiby at the Department of Pharmacy at UiO, using a Nano DSC instrument (power compensated DSC). All samples were prepared according to the protocol in Section 4.1 and scanned against Tris buffer with a pH of 7.4 as a reference. The data obtained were analysed using the NanoAnalyze software from TA instruments. In the analysis, the reference scan is subtracted from the sample scan, and the heat flow data is converted to molar heat capacity, c_p:

$$c_p = \frac{\text{heat flow}}{[\text{scan rate}] \cdot [\text{number of moles per lipid}]}. \tag{4.1}$$

Transition temperatures T_m were found by locating the peak maxima. All samples had a concentration of 0.8 or 1 mg/ml, and the results were scaled accordingly in the NanoAnalyze software.

Chapter 5

Results and discussion

The results will be presented in thematic sections and discussed consecutively. The first sections deal with pure liposome characterisation, both structural and thermal, before moving on to the interactions with the peptide. Peptide interactions are first thermally characterised using different lipid systems, after which the effect of indolicidin on raft dynamics is studied using SANS. Then, SAXS is applied to the structural characterisation of various binary lipid and cholesterol systems, followed by more complex raft-forming membranes. Finally, the effect of cholesterol content and raft presence on peptide-membrane interactions will be discussed.

5.1 Characterisation of lipid vesicles using SAXS

The backbone of this thesis is the detailed structural analysis obtained using SAXS. As almost all SAXS data analyses in the thesis apply the same model, this section presents a detailed explanation of the fitting process. Interference from structures around 10-100 nm dominates the scattering in the low-Q region, providing information on size and polydispersity. The liposome scattering in Figure 5.2 (a) includes the characteristic plateau in the low-Q region. This plateau results from oscillations in the spherical form factor, and its slope indicates the degree of polydispersity in the sample. A higher polydispersity will minimise oscillations and result in a less steep plateau, as seen in Figure 5.1, showing one fitted curve with a liposome radius of $R = 300$ and low polydispersity and one with $R = 450$ and higher polydispersity. Because of the inverse relationship between the scattering vector and the real size, larger radii move the plateau towards lower Q-values. The structure and fit in the intermediate and high Q ranges are not affected by the increase in size and polydispersity because the structure across the membrane remains the same.

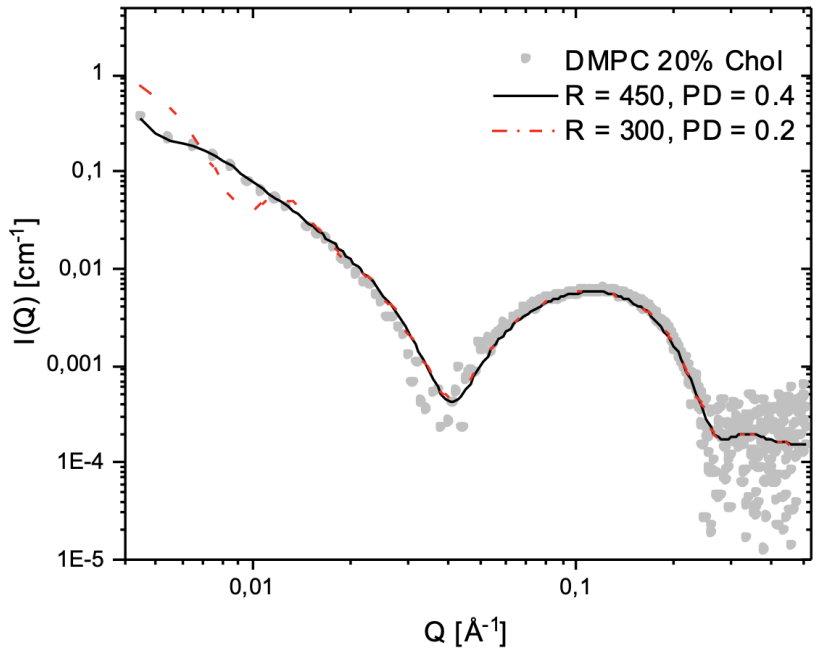

Figure 5.1: Effect of size and polydispersity. The black curve represents a liposome with a radius of 350 Å and a higher polydispersity. The red curve has a smaller liposome radius of 300 Å and a lower polydispersity.

Higher intermediate Qscattering gives information on the electron density (ED) across the bilayer. ED profiles (Figure 5.2 (b)) show the distribution of ED in the sample compared to the solvent. Z-values on the x-axis correspond to the position in the bilayer, where $z = 0$ is the centre of the bilayer. Negative z-values indicate positions in the inner leaflet, while positive values indicate positions in the outer leaflet. The minimum scattering at intermediate Q-values for liposomes is an important characteristic. From the ED profile (Figure 5.2 (b)), it is evident that the electron density of the bilayer core is lower than that of the solvent ED. This gives the hydrocarbon region a negative excess scattering length density (SLD), $\Delta\rho$. Suppose the SLD at position z is equal in absolute values, as is often approximately true for lipid bilayers. In that case, the scattering will cancel out, giving a minimum in the scattering curve. The minimum rarely goes to exactly zero since, most of the time, the SLDs in equal absolute z-values only partially cancel each other. The cause may be asymmetry in the bilayer. Even if the bilayer is symmetric, smearing from the resolution and polydispersity may lift the minimum. The minimum is highly sensitive to anything that will change the scattering properties in the bilayer. When introducing factors (for example, peptides) that may interact with the bilayer, characterisation of the minimum is essential to study its effect on the bilayer structure. Figure 5.2 (a) shows where the characteristic scattering from different length scales are found in the scattering pattern.

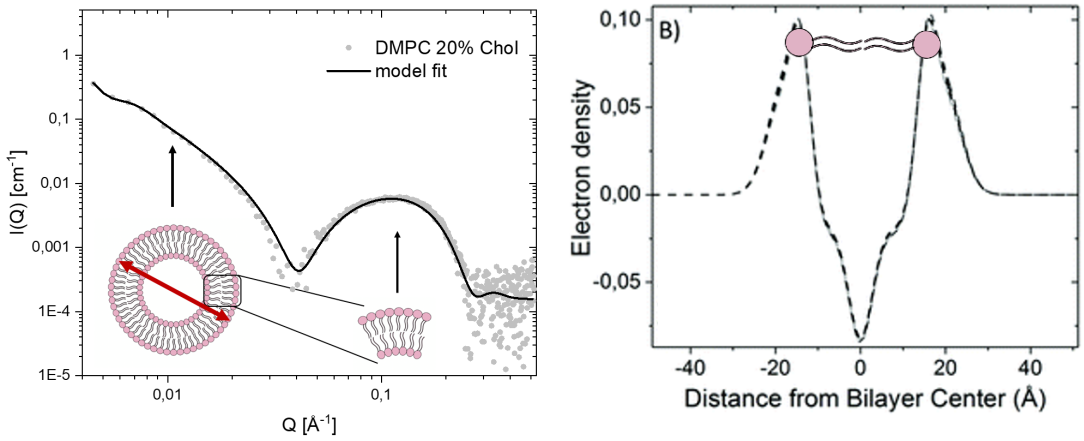

(a) **(b)**

Figure 5.2: (a) Scattering curve of DMPC with 20 mol% cholesterol with the analytical three-shell model fit shown in black, the figure also shows where the characteristic scattering of different length scales are located. (b) Electron density distribution profile, edited with permission from [20].

Using the three-shell model as described in Section 3.5.6 gives the fit indicated by the black curve in Figure 5.2 (a). The relevant structural values obtained in the fit are given in Table 5.1

Table 5.1: Relevant obtained model parameters of DMPC with 20 mol% cholesterol.

Parameter	Value	Type of parameter
Inner radius	450 ± 3	fit
Inner head group thickness	7 ± 3	fit
Outer head group thickness	5 ± 3	fit
Hydrocarbon region thickness	28 ± 1	fit
Polydispersity, hydrocarbon region	$6 \pm 0,2$	fit
Polydispersity, inner head group	5 ± 1	fit
Polydispersity, outer head group	5 ± 1	fit
Total lipid volume	1140 ± 10	fit
head group volume	330	fixed
Density of cholesterol	1.02	fixed
Fraction of cholesterol	0.2	fixed
Total radius	490 ± 3	calculated
Size polydispersity	0.370 ± 0.005	fit

DMPC/cholesterol liposomes are used as examples in Figures 5.2 (a), 5.1 and 5.3a. With its

binary composition it is one of the simplest studied systems and provide a good example of the model analysis, illustrating the need for certain modifications of the simple three-shell model.

A known concern with direct model analysis is overparameterisation, i.e. the possibility of several models fitting a given data-set equally well as long as enough parameters are introduced. In order to balance having enough parameters to provide satisfactory accuracy while keeping the number of parameters as low as possible, some parameters were restricted to avoid nonphysical results, and others were determined and fixed based on literature values. The specific volumes of cholesterol in different lipids [109], the density of the peptide in solution [20], and the lipid volumes [71] were fixed and used to calculate the scattering-length densities. Another precaution was to use only more complicated models with added parameters when simpler models could not fit the data. Because the presence of cholesterol and multiple other lipids complicates the systems, the simple three-shell model had to be altered to more accurately describe the position of cholesterol, polydispersity in the membrane thickness, and the presence of multilamellar vesicles. Since indolicidin can solubilise the membrane, it was necessary to introduce solubilised structures to the liposome model as, in some cases, they seemed to coexist.

When adding the peptide, as few parameters as possible were varied from the fit of the pure liposomes. Therefore, as far as possible, all parameters that did not involve the position or amount of peptide in the bilayer were not varied. If further changes were needed, the bilayer thickness and its smoothness value, σ_c, were fitted since indolicidin has previously been reported to cause bilayer thinning. The concentration of lipids can also vary. Although we know the initial concentration to be 2.5 mg/ml in all samples, some of the lipids may be lost during liposome preparation. However, this is rather unproblematic as concentration only affects the scaling of the scattered intensity.

Incomplete fits supported the need for more complicated models, and Figure 5.3 shows the effects of the relevant modifications made to the model. In Figure 5.3a the fit with the entire cholesterol molecule evenly distributed in the hydrocarbon region is shown by the red dotted line, and the fit with the hydroxyl group of cholesterol included in the head group region is shown by the black line. As seen in the figure, the first approximation with cholesterol placed in the hydrocarbon shell had some fitting problems in the high Q region, which was observed as a general trend for all cholesterol-containing samples. The fit with otherwise the same parameters improved substantially by including the OH-group in the head-group shells.

The presence of micelles and free peptides in the solution will raise the minimum, and decrease the bilayer scattering. Additionally, the presence of micelles will affect the scattering at low Q values. In Figure 5.3b (see Figure 7.2 in the Appendix for more details), the sample with 20% cholesterol and a peptide:lipid ratio of 1:20 was first fitted with only liposomes and a fraction of free peptides (red line) and then with some micelle formation (black line).

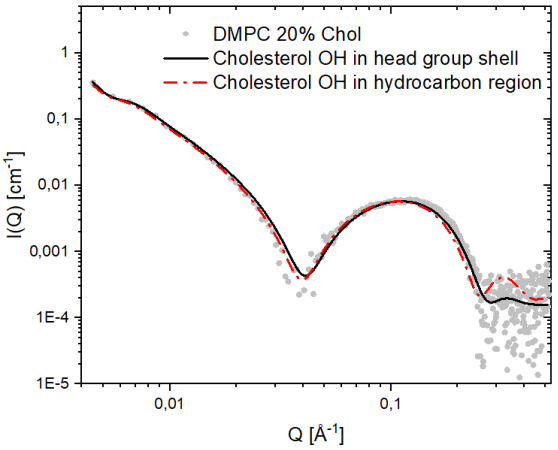

(a) Effect of the position of cholesterol. The fit with the red line places the OH group of cholesterol in the hydrocarbon region, while the black fit places it in the headgroup shells.

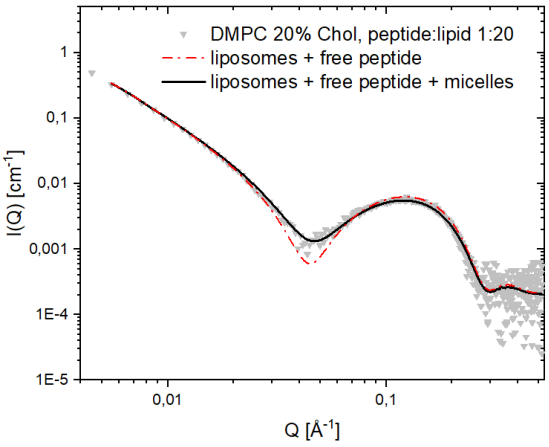

(b) Fit with and without the presence of micelles. The fit with the red line includes only liposomes and free peptides, while in the black fit 77% of the peptide not incorporated in the membrane, and 5% of the lipids were in micelles.

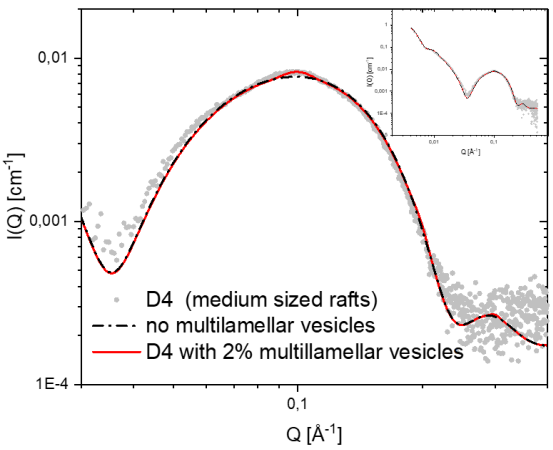

(c) Fit with and without the presence of multilamellar vesicles. The red line represents the fit with 2% multilamellar vesicles, while the fit with black line includes only unilammellar vesicles.

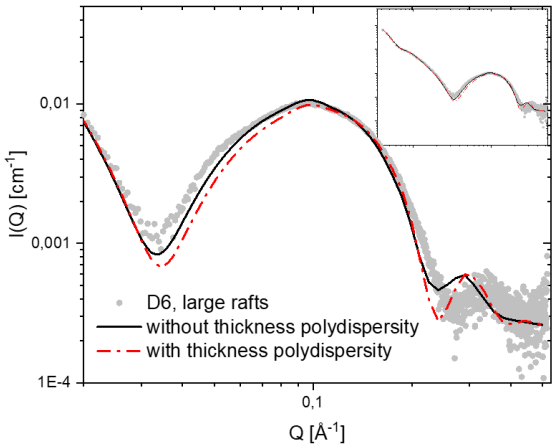

(d) Fit with and without polydispersity (PD) in the thickness as well as the size. The polydispersity parameter of the fit with the red line has a value of $\sigma_{cPD} = 0.13$.

Figure 5.3: Necessary modifications to the model. For better visualisation, figures c) and d) are zoomed in around the bilayer scattering and contains insets with the full scattering curves.

Regarding the raft forming liposomes, all D6 samples (large rafts) and the pure D4 sample (medium rafts) showed signs of multilamellarity. The presence of multilamellarity is evident in the bilayer scattering, especially in the local maxima, as it begins to show some Bragg peaks caused by the interference of waves scattered from the consecutive bilayers. From the model

analysis, the degree of multilamellarity was determined to be between 1 and 3%. Figure 5.3c shows the D4 data fitted with 2% multilamellarity and with only unilamellar liposomes. While the unilamellar fits the scattering curve quite well, it does not accurately replicate the shape of the curve at high Q-values.

In an effort to see whether the same samples could have been produced without multilamellarity, the pure D4 sample was reproduced using the same procedure as explained in Section 4.1, but with an increase in the number of extrusions from 21 to 31 times. The added extrusions seemed to eliminate multilamellarity, while the rest of the structure remained the same (Figure 7.5 in Appendix).

The final minor modification made to the model was the possibility of polydispersity in the bilayer thickness. Especially for the samples that formed phase-segregated domains, it was pretty challenging to fit the data in the high-Q region. Adding a small amount of polydispersity to the thickness increased the width of the scattering curve from the minimum to higher Q-values. This improved both the fit of the minimum and in the highest Q region (Figure 5.3d). According to Heberle *et al.* [71] raft size depends on the thickness mismatch between domains and the continuous phase. Raft-forming samples were therefore expected to have polydispersity in their bilayer thickness. The need for this modification showed that the liposomes did have a distribution of thicknesses. However, the obtained values from the fit are smaller than the error estimate for the bilayer thickness. Hence, is not possible to draw a strong conclusion regarding exact numerical values for the distribution, but for some samples we do need the distribution to get a satisfactory analytical fit. It was not necessary to include this parameter for all samples, so, when possible, it was set to 0.

When different models were applied (with modifications), all scattering curves in the thesis could be fitted quite well. Table 5.2 gives an overview over which samples required what modifications of the three-shell model.

Table 5.2: Samples in which it was necessary to include the modifications in order to procure a good fit. Ratios in parentheses indicate relevant indolicidin:lipid ratios.

Modification	Samples
Presence of micelles/bicelles	DMPC(1:10,1:5), DMPC+20% Chol (1:20,1:10,1:5), DMPC + 40% Chol (1:50, 1:20, 1:10, 1:5), DSPC(1:100, 1:50, 1:20, 1:10), DSPC+20% Chol(1:50,1:20,1:10), DSPC+40% Chol (1:10), DOPC + 40%Chol (1:10), S1 (1:50,1:10), D2 (1:50,1:10), D4 (1:10), D2 lipid ratio + 10% Chol (1:10), D2 lipid ratio + 30%Chol (1:50, 1:20, 1:10), D2 lipid ratio + 40%Chol (1:20,1:10)
Multilamellarity	POPC (0:1,1:10), POPC+20%Chol (0:1), POPC+40%Chol(0:1,1:10), D4 (0:1), D6 (0:1,1:50,1:10)
Thickness polydispersity	D2, D4, D6, D2 lipid ratio + 10%Chol, S1 lipid ratio + 30%Chol

5.2 Liposome characterisation and the verification of lipid raft domains

5.2.1 Verifying the existence of domains using SANS

In Section 4.3, the basics of contrast matching were introduced, and as mentioned, no contrast was expected for samples with randomly distributed lipids. As seen in Figure 5.4, excess scattering from the S1 standard sample was basically zero, and no peaks or increased contrast were observed. For samples D2, D4, and D6 (D2 is assumed to have the smallest domains), the scattering curves have a pronounced peak corresponding to the lateral contrast in the membranes. As mentioned in Section 4.2, scattering at low Q values corresponds to larger real-space structures. In the curves in Figure 5.4, the peaks of D2-D6 move toward lower Q values, indicating greater distances between phase-segregated domains and, therefore, larger domains. The data confirms the presence of rafts and the increase in domain size from D2 to D6 with increased DOPC fraction.

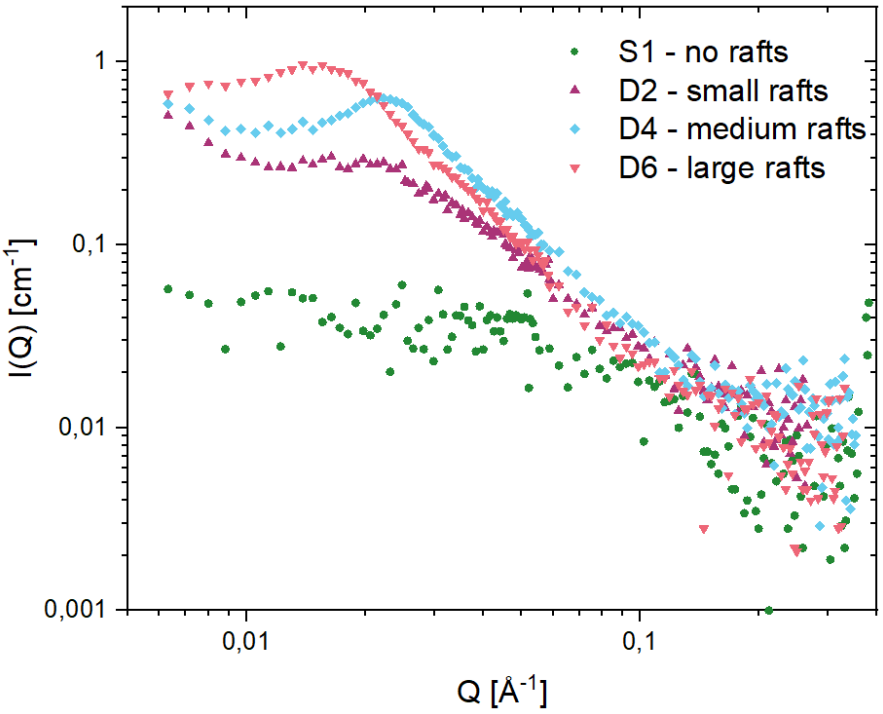

Figure 5.4: SANS scattering curves of contrast-matched raft-forming lipids (D2-D6) and the reference sample S1 with homogeneous lipid distribution. The presence of peaks confirmed the existence of lateral domains in our samples.

5.2.2 Structural characterisation of pure liposomes using SAXS

After confirming the presence of rafts, the pure liposome structures were characterised. Starting from the simplest samples of DMPC and cholesterol, this section presents the structure of the simpler binary systems of each lipid component in the raft samples with cholesterol before presenting the results of the more complex raft systems. All scattering curves were analysed using the three-shell model described in Section 3.5.6, and with the added modifications as presented in Section 5.1.

The DMPC liposomes with varying cholesterol concentrations showed an apparent increase in bilayer thickness upon the addition of cholesterol. At 37 °C, DMPC is in the l_d phase, and as mentioned in Section 2.1.3, cholesterol might have an ordering and condensing effect on the bilayer. The observed thickening of the bilayer, as seen in Figure 5.6, supports the ability of cholesterol to order the chains (condensing effect). The density of the hydrocarbon chains and cholesterol may vary when cholesterol is introduced in the liposomes. The cholesterol density was estimated from literature values [109] and kept constant to reduce the number of fitting parameters. The density of the tails decreased with increasing cholesterol content, which may be an effect of the disruption of tight phospholipid chain packing. Additionally, there is a significant increase in the hydration in the outer shell at the highest cholesterol content. Decreased density and increased hydration in the head groups points to cholesterol having an ordering effect on the

tails but increasing the distance between the individual lipids.

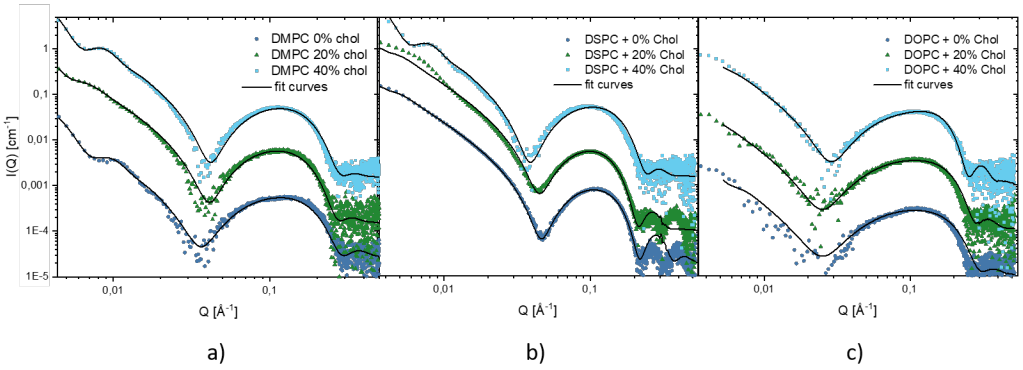

Figure 5.5: Scattering curves of pure (a) DMPC/Chol, (b) DSPC/Chol, and (c) DOPC/Chol liposomes with fitted data displaced logarithmically with factors of 10 along the y-axis for better visualisation.

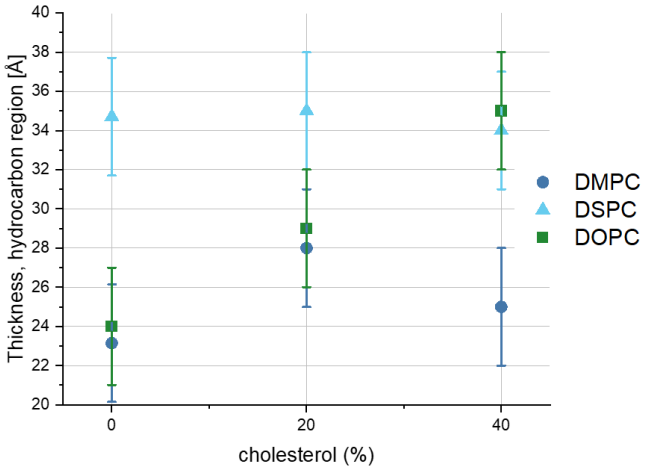

Figure 5.6: Plot of the hydrocarbon region thickness obtained for DMPC, DOPC and DSPC with increasing cholesterol content

DOPC shows a substantial increase in bilayer thickness as the concentration of cholesterol increases (see Figure 5.6 (a)), suggesting a strong condensing effect of cholesterol. The data were collected at 20 °C, far above the transition temperature of DOPC, which is below 0 °C. DSPC, on the other hand, does not show an increase in bilayer thickness (Figure 5.6 (a)). The collected measurements at 20 °C are below the transition temperature of DSPC, which means that the lipids are probably in their gel phase. As mentioned in Section 2.1.3, cholesterol has a different effect on the gel phase than the liquid phases, which may explain why no condensing effect is observed in the DSPC samples.

The raft-forming samples showed an apparent decrease in the thickness of the tail region

(Dc), see Figure 5.7 (a). The slight decrease in bilayer thickness might be attributed to the increased amount of DOPC (with two monounsaturated acyl chains) in the samples with an increasing raft size. DOPC has the same number of carbon atoms as saturated DSPC (18), which according to the literature, can decrease the membrane thickness because the cis double bond interrupts the acyl chain packing [110, 111]. The pure liposomes with the D2 DOPC/POPC ratio and varying cholesterol concentrations also shows a very slight decrease in hydrocarbon region thickness, as seen in Figure 5.7 (b). Figures 5.8 and 5.9 shows the scattering curves of the raft forming samples (S1-D6), and the scattering curves of samples with the D2 lipid composition but varying cholesterol content, respectively.

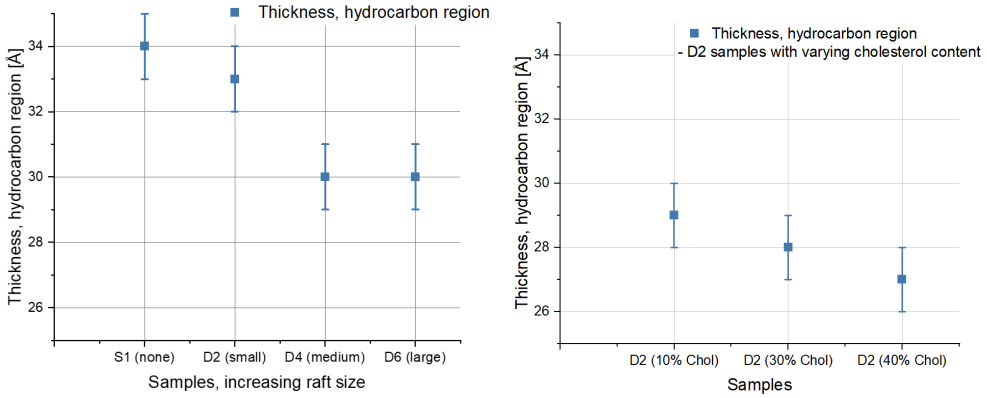

Figure 5.7: Plot of obtained average hydrocarbon region thickness for (a) the raft-forming samples and (b) the samples with a D2 POPC/DOPC ratio and varying amounts of cholesterol

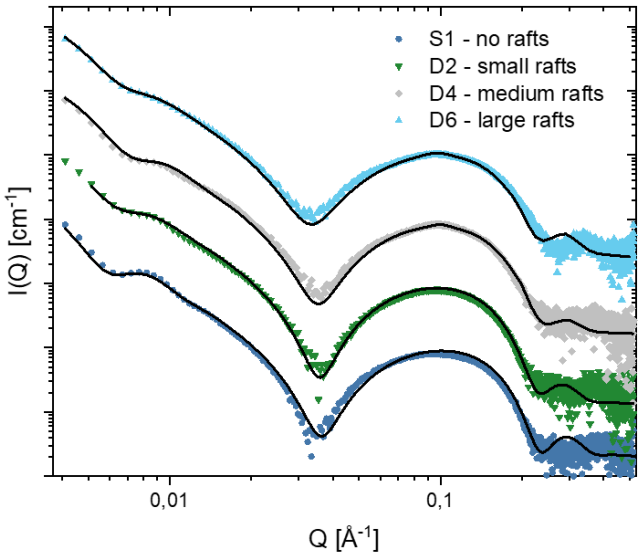

Figure 5.8: Scattering curves of pure raft forming liposomes (D2-D6) and the homogeneous S1 reference with fitted data displaced logarithmically with factors of 10 along the y-axis for better visualisation.

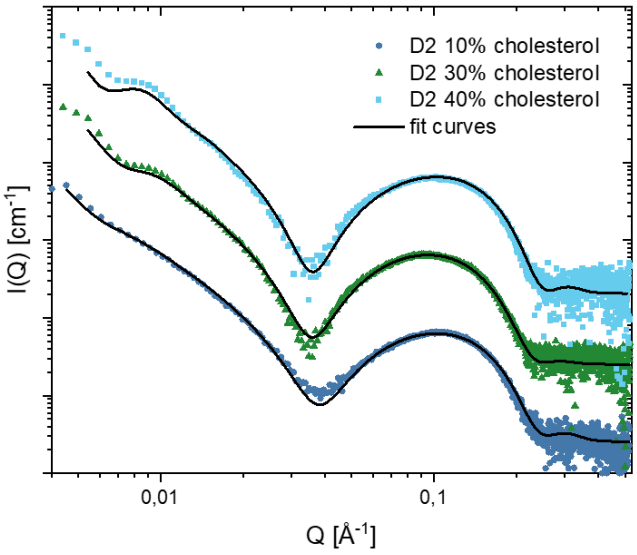

Figure 5.9: Scattering curves of pure liposomes with the D2 DOPC/POPC ratio and varying cholesterol concentrations scaled logarithmically with a factor of ten for better visualisation. Fit at low Q-values might be poor because of radiation damage (see Section 7.7 in Appendix.

Table 5.3: Melting temperatures and phase at 20°C for the different lipids.

lipids	T_m [°C]	phase at 20 °C
DSPC	55	gel
POPC	-2	l_d
DOPC	-17	l_d

5.2.3 Thermal characterisation using DSC

All peptide modes of action require some sort of membrane interaction, as peptides with an intracellular mechanism have to pass through the membrane to reach their target. When peptides interact with the membrane they will disturb or alter the packing of the lipids. Looking at the effect of peptides on the order of the lipid tails is, therefore, a good starting point to better understand peptide-membrane interactions. The main goal is to study the impact of indolicidin on the order of the lipid tails in complex raft systems. DSC is a fairly simple technique that does not probe exact structures or interactions but gives indications of the general overall order of the system. Therefore, it is of interest to first understand more about the behaviour of each lipid component in binary systems with cholesterol. Before considering the behaviour of binary mixtures of cholesterol and different lipids, the expected mixing of the lipids and the effects of increasing the amounts of unsaturation in the acyl chains is briefly discussed. Since all lipids have identical head groups, the repulsion leading to domain formation, as discussed in Section 3.1.2, is driven by a mismatch of the acyl chains. The more similar the chains are, the more the interactions promote mixing.

The three phospholipids found in the raft systems have different degrees of saturation and chain length, and will therefore have different transition temperatures (see table 5.3). DSPC is saturated with 18 carbon atoms in both chains and has a melting temperature of $T_m(DSPC) = 55°C$. POPC has a saturated chain with 16 carbon atoms and an unsaturated chain with 18 carbons. Its melting temperature is significantly lower than that of the fully saturated lipid, at $T_m(POPC) = -2°C$. Finally, DOPC has two unsaturated acyl chains, both with 18 carbons. Having two double bonds and being harder to pack tightly and order, DOPC has the lowest melting point at $T_m(DOPC) = -17°C$. At $20°C$, POPC and DOPC are probably in the liquid disordered state, while DSPC is in the gel phase together with most of the cholesterol, assuming that cholesterol has a higher affinity for saturated lipids [37, 100]. Since the exact partition of cholesterol into the different phases is unknown, this is a factor that could affect the phase transitions.

DSPC with both chains saturated and DOPC with both chains unsaturated will have the most considerable mismatch in tail length and hence have a larger tendency to form domains in order to reduce line tension. POPC has intermediate properties to both DSPC and DOPC, and is sometimes called a hybrid lipid. When all three lipids are present, it is therefore likely that POPC will be located between DOPC and DSPC areas to decrease unfavourable interactions, as illustrated in Figure 5.10. As shown in simulations by Palmieri and Safran [112], hybrid lipids such as POPC increases the presence of smaller fluctuating domains in mixtures of saturated

and unsaturated lipids. The ratio of saturated and unsaturated lipids was kept constant in the raft samples, while the proportion of unsaturated DOPC and the hybrid POPC was varied. More DOPC in the system (and hence less POPC) gives greater repulsion between domains. As the amount of POPC decreases, optimisation of the interface circumference favours the formation of larger domains. Decreasing the edge to surface ratio of the domains is favourable because it minimises the line tension.

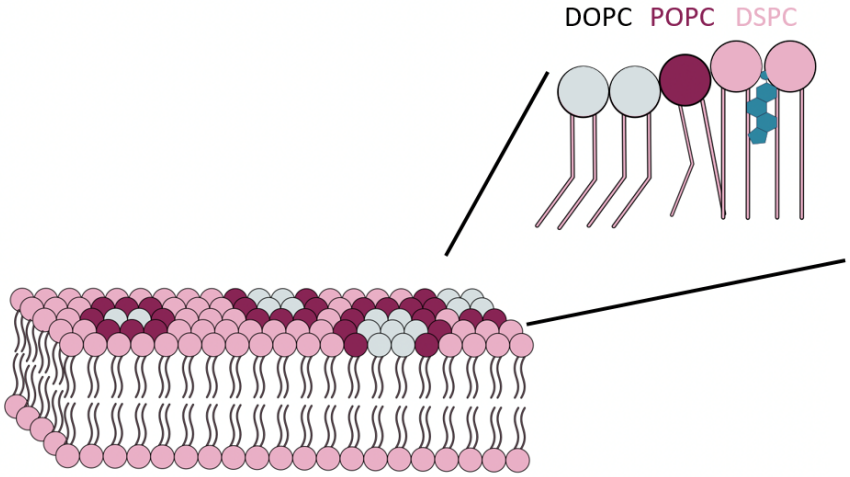

Figure 5.10: Illustration of POPC lining the domain boundaries and hence decreasing line tension.

Cholesterol interactions and phase segregation complicates the thermotropic behaviour of the system. In an effort to gradually build up the understanding of the system, the behaviour of the DSPC/cholesterol system and a short discussion on DOPC/cholesterol and POPC/cholesterol will be given before moving on to the raft-forming samples.

As seen in the cooling scans of DSPC with 0 and 20 mol% cholesterol (Figure 5.11a), the 0 mol% Chol endotherm (blue) is clearly a single peak covering a slightly smaller temperature range than the 20 mol% Chol sample (red). Upon incorporation of cholesterol, the peak consists of two components, supported by observations by McMullen *et al.* [113]. They presented evidence that the sharp component of the peak corresponds to the chain melting of cholesterol-poor domains (higher cooperativity), and the broad component corresponds to the chain melting of cholesterol-rich phospholipid domains. Figure 5.11a clearly indicates that a cholesterol content of 20 mol% Chol decreases the transition temperature. Previous studies have observed that increasing the cholesterol content in binary mixtures of DSPC/cholesterol decreases the transition temperature T_m of the broad peak relative to the sharp peak [114]. The decrease in T_m suggests a destabilisation of the gel phase, as mentioned in Section 2.1.3. It is supported by observations that cholesterol abolishes the gel-to-liquid transition, giving lipid properties closer to the l_o phase [115].

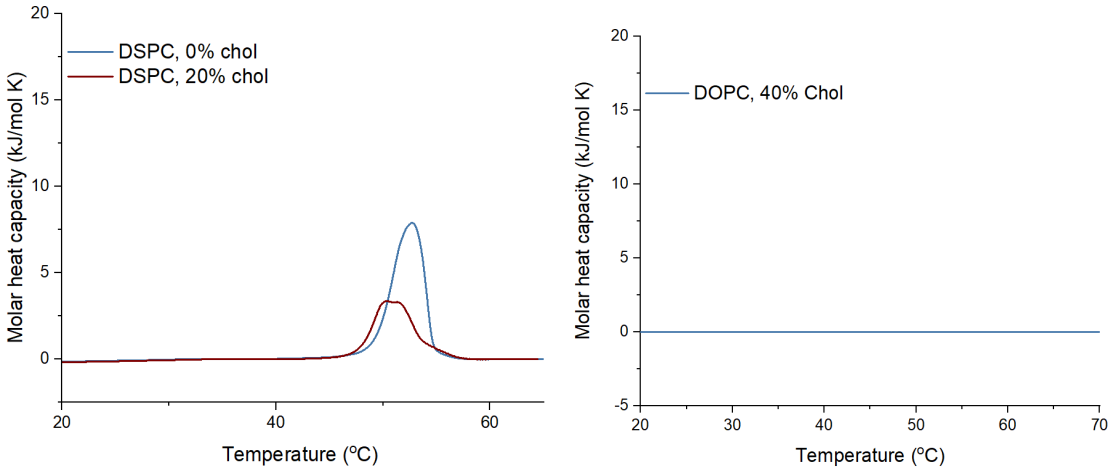

(a) **(b)**

Figure 5.11: (a) DSC cooling curve of DOPC (blue) and DOPC + 20 mol% cholesterol (red). The addition of cholesterol broadens the transition range and lowers the transition temperature. (b) DSC data of the cooling scans of pure DOPC (40% cholesterol) liposomes and mixtures of liposomes and indolicidin in a peptide:lipid ratio of 1:20. There is clearly no phase transition present in the observed temperature range.

POPC and DOPC have transition temperatures below $0°C$, making them challenging to study using DSC in the same temperature range as applied to the other samples. As seen in Figure 5.11b, there is no observed phase transition in the relevant temperature range for DOPC with 40 mol% cholesterol. Cholesterol has been observed to slightly increase the transition temperature for POPC, and DOPC can be expected to behave similarly [116]. However, other techniques than DSC (for example absorption and fluorescence measurements) had to be applied because of the low melting temperature of the lipids [44, 116]. DSC measurements of 1-stearoyl-2-oleoyl-sn-glycero-3-phosphocholine (SOPC), similar to POPC but with 18 carbons in the acyl chains giving it a higher melting temperature, have shown that cholesterol did not significantly alter the transition temperature of the lipid [77]. Based on these studies, cholesterol might increase the transition temperature of unsaturated lipids, but not significantly.

Figure 5.12 shows the DSC results of the raft-forming samples. All plotted data are cooling scans, which gives the system more time to equilibrate. Another reason for using the cooling scan was that some samples were run with a faulty setup, cooling the system in the first scan when it should have been heated. The compositions tested were those expected to form rafts and the homogeneous standard S1. As can be seen from the figure, the S1 sample is basically one broad phase transition with no pronounced peak. The other samples have multicomponent peaks, suggesting the coexistence of phases. The sharper peak probably corresponds to the l_d phase, with the lowest transition temperature. The broader peak corresponds to the l_o phase with a higher degree of order and hence a higher transition temperature. Increasing the size of the rafts (D2 being the smallest and D6 the largest) broadens the separation between sharp and broad peaks. The sharp peak moves towards lower transition temperatures with increasing raft size, while the transition temperature of the broad peak remains approximately the same, see

Table 5.4. This suggests that the disordered phase becomes less ordered with increasing raft size, which makes sense as the degree of di-unsaturated lipids increases in compositions with increasing raft size. The sharp transition also seems to broaden, indicating a lower degree of cooperativity.

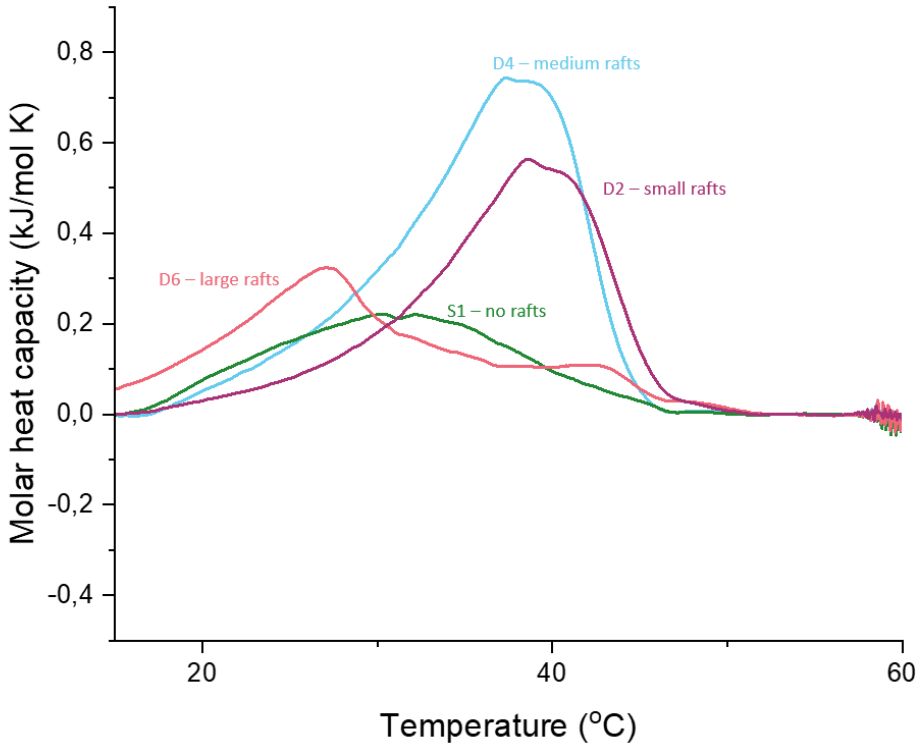

Figure 5.12: DSC cooling scans of the different raft-forming compositions with the S1 standard.

Table 5.4: Transition temperatures of the sharp and broad transitions.

lipids	T_m [°C] sharp peak	T_m [°C] broad peak	mol% Chol
S1	30 ± 1	30 ± 1	34 ± 1
D2	39 ± 1	40±1	22± 1
D4	37± 1	39± 1	22± 1
D6	27± 1	42± 1	22± 1

The amount of cholesterol and the presence of phase segregation may partially explain the sharper peaks of the raft-forming samples. S1 has a larger amount of cholesterol than the other samples, and cholesterol generally affects the PC bilayers by lowering the enthalpy of the transition and making the peak wider while not significantly affecting the transition

temperature [77, 116]. When rafts form, cholesterol-depleted domains sharpen their phase transition and have a measurably higher enthalpy [77]. The main contribution to the observed phase transitions is likely from the lipid with the highest melting temperature (DSPC) since the observed transitions at around 40 °C are close to the main transition of DSPC at 54 °C. There is a general decrease in the transition temperature with increasing raft size, suggesting a reduction of order. As seen by the DSPC/Chol DSC results in Figure 5.11a and supported by McMullen *et al.* [113], increased cholesterol content in DSPC may lower the transition temperature of the cholesterol-rich phase. Assuming that the cholesterol affinity decreases with the degree of lipid unsaturation, a possible explanation is that with increased DOPC concentration (and hence larger rafts), cholesterol would partition more into DSPC, introducing more disorder in the gel phase. The possibility of increased cholesterol content in the DSPC phase is supported by the observation that cholesterol can increase translational disorder in saturated lipids in the gel phase [117, 118]. A review by Mannock *et al.* [119] concluded that cholesterol stabilises the gel phase of saturated lipids with 16 carbons in the acyl chains or less, while it destabilises it for lipids with longer chains such as DSPC. Our results of increased disorder with higher cholesterol content, as in S1, appear to agree with their observations. Another possible contribution to the disordering with increasing raft size is the apparent effect of lipid saturation on order. DOPC is the most disordered lipid of the three in the mix, and therefore an increase in DOPC concentration will probably result in a decrease in the overall order of the system.

Wydro *et al.* [44] found that the ordering effect of cholesterol is stronger in saturated DSPC than in unsaturated phospholipids and attribute this to the existence of more favourable van der Waals interactions. While Wydro *et al.* [44] observed stronger ordering effect by cholesterol in saturated lipids, our DSC results of DSPC/Chol (Figure 5.11a) showed a decrease in order upon cholesterol addition. The seemingly contrary results might originate in the observed order from each technique. Wydro *et al.* [44] used Langmuir trough experiments to probe the orientational order of the lipids. The two-dimensional order of the lipids is assesed by measuring the surface pressure as a function of the mean molecular area. The results provide information on the monolayer's lipid packing, order, and stability [120]. It is generally accepted that the information obtained may be extrapolated to bilayer systems. However, since they are effectively only half a membrane, there might be some differences in the governing forces and morphology [115]. DSC, on the other hand, requires no deformation of the liposomes. In addition to orientation order, the lipids have translational, also called positional order. Since DSC probes the degree of freedom in the system, both the transitional and orientational order affects the curves. The probing of the system as a whole gives DSC some limitations, as it makes it difficult to pinpoint the behaviours of the different components in a mixture.

Saturated lipids in the gel phase are often tilted. A Wide Angle X-ray Scattering study by Mills *et al.* [117] on DPPC(16:0, saturated)/cholesterol at 25°C showed that upon addition of cholesterol, saturated chains are straightened and the tilt removed. More importantly, they showed that cholesterol gradually introduced disorder in the gel-phase packing of the lipids [117, 121]. For the slightly longer DSPC lipids, there is a larger difference between the lengths of the lipids and cholesterol, so other studies have reported the tilt in the chain ends to increase with cholesterol addition [122, 123]. Therefore, the observed DSC results might result from a substantial reduction in positional order and maybe some decrease in orientational order.

However, there is evidently some disagreement on the contribution of the latter.

In summary, the DSC data with two-component peaks for D2-D6 samples support raft formation, as confirmed by SANS. It is probable that the main contribution to the signal stems from DSPC. Most studies suggest that DSPC in the gel phase is disrupted by cholesterol, destabilising the gel phase and lowering the transition temperature. Destabilisation of the DSPC-rich phase might explain the significantly lower transition temperature of S1, which has a higher amount of cholesterol than the other samples.

5.3 Peptide interactions

5.3.1 Effect of indolicidin on phase transitions as seen by DSC

Before tackling complex raft systems, the interactions between indolicidin and DSPC liposomes with and without cholesterol were studied using DSC. The results are shown in Figure 5.13. Upon addition of the peptide to the pure DSPC sample, there was only a slight increase in the transition temperature but a significant increase in the sharpness of the peak. The increased sharpness indicates a higher degree of cooperativity in the solidification of the system induced by indolicidin. A possible explanation might be that indolicidin, with its many N-H bonds, may form hydrogen bonds with the oxygen in PC-head groups. The observations of peptide-lipid hydrogen binding by Hsu and Yip [14] support this hypothesis. In liposomes with 20 mol% cholesterol, there was a substantial increase in T_m and a sharpening of the peak. A possible explanation for the behaviour of the DSPC/chol system upon the addition of the peptide might be that indolicidin and cholesterol compete for the same positions in the membrane, near the tail-head group interface. Indolicidin might then push cholesterol further into the bilayer core, increasing the order of the tails here. Another possibility, or contribution, is that indolicidin may form hydrogen bonds to OH-groups of cholesterol. This hypothesis requires further investigation to confirm.

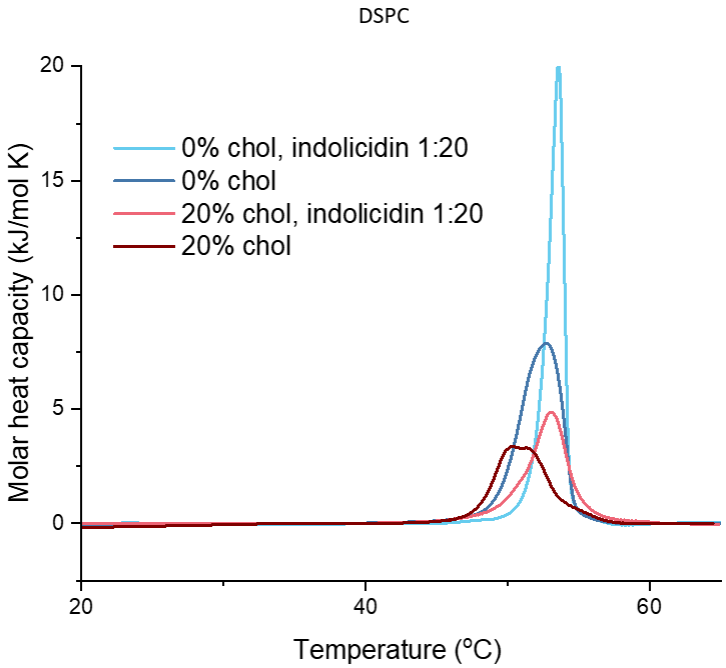

Figure 5.13: DSC cooling curves of pure DSPC with 0% and 20% cholesterol and the respective liposomes with added indolicidin in a peptide:lipid ratio of 1:20.

After probing the effect of indolicidin on the phase transitions of binary systems of lipids and cholesterol, the more complex raft forming membranes were studied. The first DSC experiment measured D4 and indolicidin in a peptide:lipid ratio of 1:10. As seen in the results in Figure 5.13, the addition of the peptide caused an increase in the transition temperature and broadened the transition peak. Note also that the molar heat capacity is much lower for raft-containing samples. The samples' amount of saturated DSPC is approximately halved, and the unsaturated DOPC and POPC has a significantly lower heat capacity.

The next natural step was to perform a DSC experiment with several peptide:lipid ratios in both a raft-forming and non-raft forming membrane to look for possible trends and distinctions. To increase complementarity between different experiments, the same compositions (S1 and D4) were studied with both SANS and DSC, and the same peptide:lipid ratios of 1:50 and 1:20 were chosen in both experiments. The results for the S1 and D4 samples are presented in Figures 5.14a and 5.14b, respectively. Table 5.5 presents the transition temperatures estimated for the given compositions.

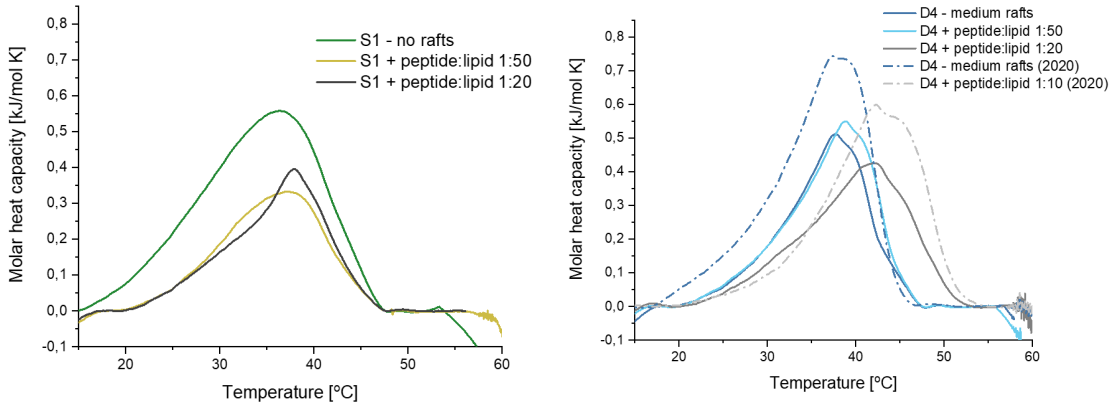

(a) S1

(b) D4

Figure 5.14: DSC cooling scans illustrating the effect of indolicidin on the thermal behaviour of (a) non-raft forming liposomes, S1, and (b) raft forming liposomes, D4. The peptide:lipid ratios are indicated in the figures.

Table 5.5: Samples with corresponding transition temperatures (for the sharp peak when multiple peaks are present) estimated from the DSC graphs.

Lipid composition	T_m (°C)	**Lipid composition**	T_m (°C)
S1	36± 1	D4	38± 1
S1 + 1:50	37± 1	D4 + 1:50	39± 1
S1 + 1:20	38± 1	D4 + 1:20	42± 1
		D4 (2020)	39± 1
		D4 + 1:10	42± 1

As seen in Figure 5.14b, adding indolicidin to raft containing membranes broadens the transition peak and increases the melting temperature T_m. The increase in the transition temperature indicates an effect of the peptide on the packing of the lipid tails and heads to a more ordered conformation. A curious result of the non-raft composition is that a more distinct peak appears at the highest peptide:lipid ratio and the transition temperature increases slightly. The sharper peak supports the possibility of indolicidin increasing lipid order. To do this, indolicidin must somehow affect the cholesterol-lipid packing to promote the formation of a more ordered phase.

Figure 5.14b also shows a difference in the height of the signal for the pure D4 liposomes between the scans performed in 2020 and 2022. There was a slight concentration difference (0.8 mg/ml and 1 mg/ml), but otherwise, the preparation of the samples was the same. The discrepancy might lie in the concentration difference or errors from dilution, but since the data were scaled according to concentration, that should not be an issue. A more probable cause

may be variations in concentration and molar ratios due to errors related to weighting out lipids and extruding them. Another possible reason might be that the buffers were from different batches, giving slightly different properties. However, as seen in Figure 7.7 in the Appendix, the differences between the buffer scans were minimal. Compared to the DSC curves of the binary or pure systems (Figure 5.13), the raft samples' molar heat capacity and transition enthalpies are quite low (Table 7.6 in Appendix) due to decreased cooperativity and order. Accordingly, even a minor variation in heat capacity will be relatively significant between different scans of the raft-forming samples. The difference of about $0,25$ kJ/molK seen in the graph in Figure 5.14b would not have been nearly as prominent in the pure or binary systems (Figure 5.13).

When comparing the DSC studies performed on the binary DSPC + 20 mol% Chol system (Figure 5.13) and the raft forming D4 samples with approximately 22 mol% cholesterol (Figure 5.14b), their behaviour are quite similar. The transition temperature is substantially lower and wider in the raft liposomes than in the DSPC/Chol system, probably a result of the addition of lipids with lower T_m. Suppose that cholesterol shows a preference for saturated lipids. In that case, it is probable that the cholesterol content in the DSPC-rich phase in D4 liposomes is just slightly lower than in the binary DSPC + 20 mol% cholesterol liposomes. Given the similar calorimetric behaviour of the two systems, it is probable that indolicidin interacts strongly with the DSPC rich l_o phase, and that it is this interaction we observe in the raft forming sample.

Without further knowledge of how indolicidin affects membrane structure and lipid organisation, the exact mechanism by which it increases lipid order remains elusive. The following sections seek to illuminate other aspects of the peptide-lipid interaction. The effect of indolicidin on rafts and the lateral organisation will be discussed before moving on to its effect on the bilayer structure.

5.3.2 Effect of indolicidin on the lateral organisation as seen by SANS

When it comes to observing changes in the raft organisation, there are specifically two things one should notice in the SANS data; the Q-position of peaks and intensity shifts. After adding indolicidin at the lowest ratio, 1:50, the peaks in the raft samples became less pronounced and moved towards lower Q-values, as seen in Figure 5.15 (a). The peaks were almost completely eliminated at the higher ratio, 1:20, seen in Figure 5.15 (b). For the S1 sample, it is evident that the low-Qscattering increases upon peptide addition. Due to an experimental error, the samples with peptide:lipid ratio 1:50 had to be diluted to 8 mg/ml (instead of 10 mg/ml). However, this should not have affected the results of the following discussion, as seen in Section 7.8 in Appendix.

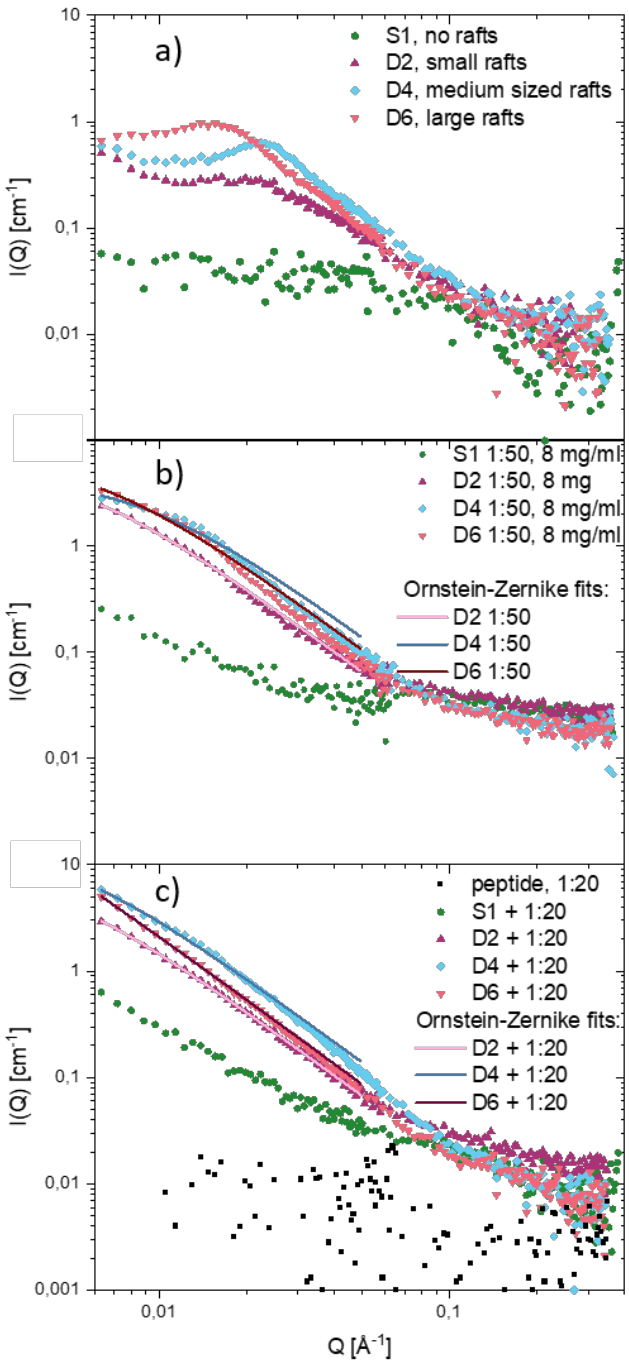

Figure 5.15: SANS data - addition of indolicidin in the peptide:lipid ratios (a) without peptide, (b) 1:50, and (c) 1:20. The fits of the Ornstein Zernike model to the data collected with a Q-range ofapproximately 0.006 to 0.06 are shown in (b) and (c) for the respective peptide:lipid ratios.

Upon peptide addition the peaks shift towards lower q-values, and the intensity increases. The peaks shifting toward lower Q values indicate increased domain sizes. The minimisation of the peaks points to less defined domains. On the other hand, the increased intensity suggests a growth of the domains. Because peptide scattering was not considered in the contrast matching, another contribution may be peptide insertion. If the protonated peptide enters the deuterated DSPC-phase, the contrast, and hence also the intensity, would be lowered. However, if it is inserted in the protonated unsaturated phase, the contrast and intensity should increase. Additionally, the SANS curve of S1 shows that peptide insertion does not increase the contrast evenly at all Q-values, which suggests an ordering effect, consistent with the DSC results.

As seen in Figure 5.15 (b), the scattering of free peptides is relatively disordered and scatters slightly above zero, meaning that although the contrast is low, it is not entirely negligible. The intensity of the liposome scattering increases with increasing peptide:lipid ratio. This intensity-shift gives important indications on the preferential partition of indolicidin in the membrane. As mentioned above, an intensity decrease would be expected if indolicidin preferred the l_o phase. If, on the other hand, indolicidin (which is protonated) is inserted in the protonated DOPC/POPC-rich l_d phase the scattering contrast should increase. The intensity increase in the SANS data points towards indolicidin having a preference for the POPC/DOPC phase, or at least no insertion in the tail region of DSPC. Other studies of indolicidin in similar, but slightly simpler systems, confirm this observation [56, 57, 124].

To further understand how indolicidin affects the rafts, the scattering data with indolicidin were fitted with the Ornstein-Zernike law. The Ornstein-Zernike law expressed as

$$I(Q) = \frac{I(0)}{1+\xi^2 Q^2}, \tag{5.1}$$

relates the forward intensity $I(0)$ and the correlation length ξ [125]. The correlation length measures the domain size. Fitting the law to scattering curves of I(Q) vs Q, it is possible to determine the corresponding correlation lengths. The fitted data are shown in Figure 5.15 (b) and (c). As may be expected, the data fit better at the highest peptide:lipid ratio as the domain peaks, which the law does not account for, are almost eradicated.

The resulting fit parameters for $I(Q)$ and ξ are shown in Table 5.6.

Table 5.6: Fitted values of I(0) and the correlation length ξ for both peptide:lipid ratios 1:50 and 1:20. SD is the standard deviation.

Sample, 1:50	$I(0) \pm SD$	$\xi \pm SD$	**Sample, 1:20**	$I(0) \pm SD$	$\xi \pm SD$
D2	5.9 ± 0.19	190 ± 4.1	D2	9.9 ± 0.23	242 ± 3.5
D4	4.5 ± 0.19	113 ± 4.2	D4	16.9 ± 0.68	220 ± 5.7
D6	7.2 ± 0.38	165 ± 6.2	D6	72 ± 8.0	580 ± 34

The results show that the correlation length ξ, and hence domain size, increases with increasing peptide concentrations for all samples. Increasing domain size and less defined peaks points towards larger and more disordered domains. The preference of indolicidin for the l_d phase and/or interface, as discussed in Section 2.2.3, might provide a possible explanation with

indolicidin acting as a *lineactant*. Lineactants are two-dimensional surfactants which reduces line tension at domain boundaries. By insertion at domain interfaces indolicidin may decrease the line tension, reducing the penalty for non-spherical domains and promoting fluctuations as the line energy is significantly reduced. This may lead to coalescence of domains into larger, more disordered domains. A study by Shaw *et al.* [57] on a similar system of DOPC/DSPC/Chol also observed domain coalescence caused by indolicidin. And, as mentioned in Section 2.2.3, preferential insertion in the interface region and reduction of line tension seems to be a general mechanism for several peptides.

A plausible mechanism describing the interaction between indolicidin and our system has to account for both domain coalescence, as seen by SANS, and the increased order observed in both DSC and SANS data. The theory of indolicidin acting as a lineactant and causing domain coalescence does not unquestionably account for the observed increase in order. It could be argued that larger correlated areas and less mismatch might facilitate regular packing and increase order, but it is, however, more likely that the order is affected by other mechanisms directly caused by indolicidin itself or indirectly through the displacement of cholesterol.

A possible mechanism by which indolicidin could increase lipid order is by locally crosslinking or otherwise reducing the degrees of freedom of the neighbouring lipids. Unpublished neutron Spin-echo data from our lab [126] suggested, as indicated by an increase in the apparent bending modulus, that indolicidin increases the membrane's stiffness, possibly by a mechanism that "glues" the lipid head groups together. This mechanism could be hydrogen-bonds crosslinking the peptide and neighbouring lipids, as supported by simulations by Hsu and Yip [14]. Indolicidin may thus introduce local areas with increased stiffness. Another membrane defect suggested to be caused by indolicidin is the induction of positive curvature defects, as suggested by Haney et al. [127]. Lipids with less translational freedom would probably be more susceptible to larger defects because the lipid reorganisation is relatively slow. The l_o phase should thus be more susceptible to solubilisation than the l_d phase.

A study done by Zhao *et al.* [58] observed augmented lipid packing and acyl chain ordering induced by indolicidin in bacterial mimicking membranes and attributed this to indolicidin adopting a trans-bilayer conformation, thereby decreasing translational movement. The observed order increased with the content of negatively charged lipids. However, this does not exclude the possibility of indolicidin having a similar effect in zwitterionic membranes. The observation might result from increased partitioning into the membrane due to the more considerable electrostatic interactions between indolicidin and the PG head groups. Nevertheless, the results of Zhao *et al.* [58] seem to agree with the DSC data that indicate that indolicidin has an ordering effect on DSPC/Chol. In summary, indolicidin may increase the order of the system, although the exact mechanism is still elusive.

Alternatively, or additionally, to ordering the system directly, indolicidin might affect the order through displacement of cholesterol. As mentioned, indolicidin appears to prefer the l_d region. However, some indolicidin molecules may still be inserted in the l_o phase at higher concentrations as the l_d phase becomes saturated (see Section 2.2.3). If indolicidin and cholesterol compete for the same positions in the membrane, indolicidin might "push" some cholesterol out of the l_o phase and force it into the l_d phase. As seen in Figure 5.6, increased cholesterol content in DOPC has a significant impact on bilayer thickness. If cholesterol is

forced into the l_d phase it may order the unsaturated chains, increasing the thickness and thereby decreasing the line tension. Additionally, cholesterol depletion of the l_o phase may help explain the observed ordering after the addition of peptide, as cholesterol has a liquefying effect on the gel phase of DSPC. The movement of cholesterol from one phase to the other will bring the properties of both phases closer to one another locally, expanding the rafts.

Both the aforementioned proposed mechanisms may explain expansion of domains, as both can lead to decreased line tension. One mechanism does not necessarily exclude the others, and based on the current data it is not possible to conclude which is more prominent. In future work it will be interesting to determine which one is the most likely mechanism by fitting the SANS data with a more complex model based on the area fraction of domains. Since there are equal amounts of saturated and unsaturated lipids, no change in domain area fraction would point towards line tension reduction being the leading mechanism.

To summarise, the following mechanisms of how indolicidin may affect the domains and order of the lipids are proposed and graphically summarised in Figure 5.16: A) Indolicidin forces the cholesterol molecules residing in the saturated domains into the unsaturated chains. In doing so, the order of the gel phase is somewhat restored. Some cholesterol is then free to further order unsaturated lipids, expanding the l_o domains; B) Indolicidin preferentially inserts itself in the interface regions, lowering line tension and promoting coalescing domains. Indolicidin itself may also order lipids according to unpublished spin echo data [126] and several other studies [14, 58]. Higher lipid order may increase the size of l_o domains and make them more dynamic.

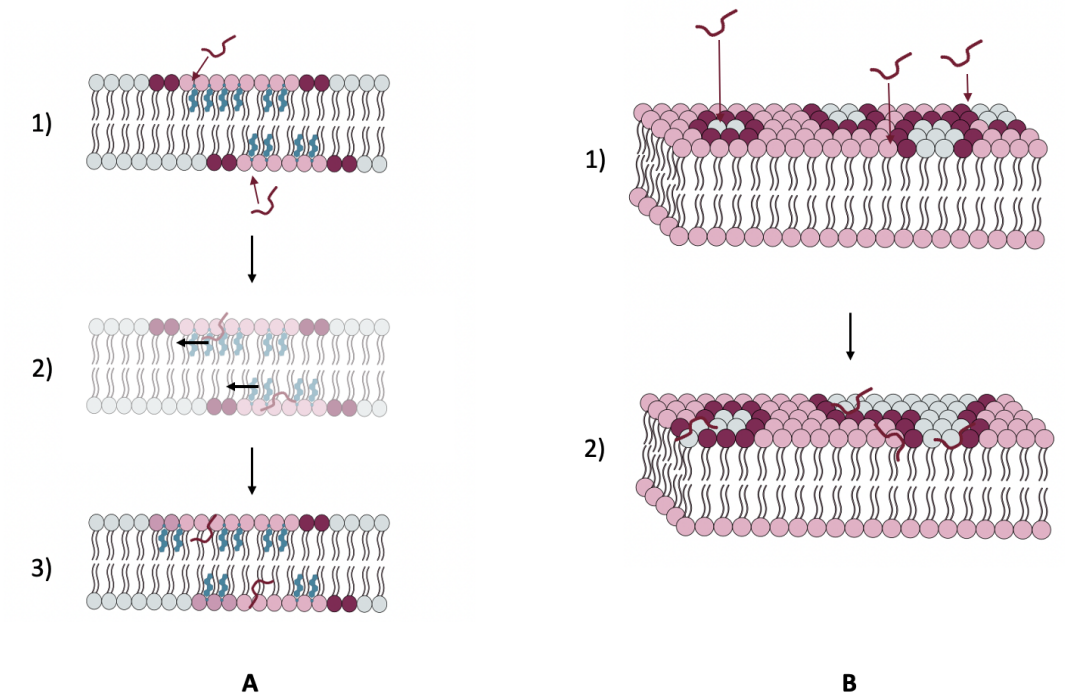

Figure 5.16: Proposed mechanisms (A) of indolicidin pushing cholesterol out of the l_o phase. 1) indolicidin is inserted into the membrane. Although all head groups are equal, saturated lipids are represented with light pink head groups, as the difference is easily visualised. 2) indolicidin and cholesterol compete for the same space, and cholesterol is pushed into the neighbouring phase. 3) Expansion of the l_o phase, visualised by the unsaturated lipids' headgroups moving from purple and blue to a light purple; (B) indolicidin acting as a lineactant, reducing line tension resulting in larger and more disorganised rafts.

Having looked at the effect of indolicidin on the lipid order, the discussion will now focus on the effect of indolicidin on the bilayer structure. As mentioned in Sections 4.2 and 3.5, SAXS is an excellent technique for studying the structural changes that occur when adding indolicidin to model membranes. The following section presents and discusses the results obtained by SAXS experiments.

5.3.3 Effect of cholesterol on membrane structure as seen by SAXS

It is usually convenient to begin with the simplest possible relevant systems to distinguish the roles of different components in complex systems. Both saturated and unsaturated lipids are commonly used as simple model systems. Therefore, it would be interesting to study the effect of cholesterol on peptide-lipid interactions with both saturated and unsaturated lipids on their own before combining them in mixed systems. The following discussion will first look at DMPC, a saturated lipid often used in model membrane systems, before building up to the raft systems by studying the binary systems of each lipid and cholesterol.

Figure 5.17 shows the scattering curves for DMPC liposomes with no, intermediate (1:20) and high (1:5) indolicidin concentration and with 0 mol%, 20 mol% and 40 mol% cholesterol. In the insets, all concentrations with corresponding fits are shown scaled logarithmically.

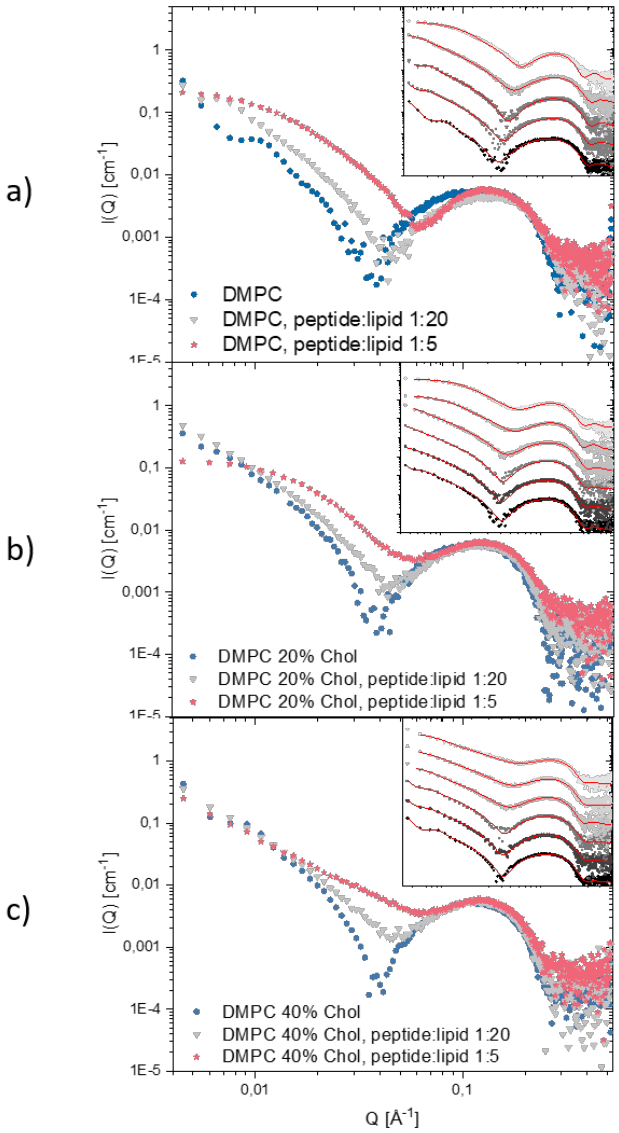

Figure 5.17: Scattering curves and respective fits for (a) pure DMPC liposomes, (b) DMPC+20 mol%Chol, and (c) DMPC+40 mol%Chol. Insets show the analytical model fits to the data, scaled logarithmically with a factor of 10 for each sample, with increasing peptide:lipid ratio from the bottom and up. The curves in the inset are displaced logarithmically with a factor of ten.

From the large changes in the Scattering curves with increasing peptide content, it is

evident that indolicidin interacts strongly with DMPC/cholesterol membranes at all cholesterol concentrations. The observed shift in minima towards intermediate Q values is attributed to the altered scattering contrast upon peptide insertion in the bilayer. The same shift in minima was observed by Nielsen *et al.* [20] upon addition of indolicidin to model membranes of DMPC/DMPG/DMPE-PEG. It is also clear from the shape of the scattering curves that some form of solubilisation has occurred. Previously, indolicidin has been reported to insert itself mainly between the outer headgroup shell and the tail region, and to cause a slight solubilisation of PE/PG membranes [13]. The scattering curve at low Q values is significantly altered and no longer displays the characteristic liposome oscillation at higher peptide:lipid ratios. Instead, the scattering displays a Guinier region, suggesting smaller structures. When comparing the curves to typical form factor curves of different geometries, as seen in Figure 3.12, it seems likely that some discs have been formed. Model analysis showed that the discs formed were bicelles in which the peptides along the rim stabilise the structures. It also suggested that indolicidin generally inserted itself into the membrane, distributing relatively evenly in the head-group and tail regions at low concentrations. At intermediate ratios, micelles began to form in addition to the liposomes, while at higher concentrations, bicelles were formed. Figure 5.18 reports the peptide:lipid ratios at which micelle and bicelle formation occurred. Bicelles appeared to form at lower peptide:lipid ratios with increasing cholesterol content.

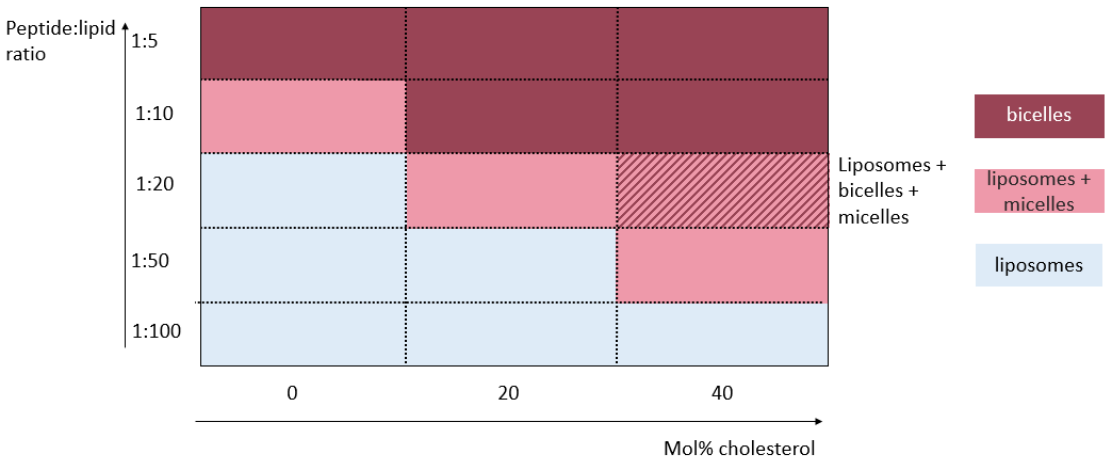

Figure 5.18: A simplified phase diagram of DMPC/cholesterol and the structures formed upon interaction with indolicidin.

The analysis shows that cholesterol does not have a protecting effect on DMPC/Chol membranes at 37 °C. Lower peptide:lipid ratios are needed to solubilise the membrane and form micelles and bicelles at higher cholesterol concentrations. These results are pretty surprising, as many studies have reported that cholesterol protects both model membranes and eukaryotic membranes from peptide solubilisation [51, 128].

According to several phase diagrams constructed for the binary mixture of DMPC and cholesterol, there is a two-phase region of l_o and l_d at $37°C$ between approximately 12 and

30 mol% cholesterol, see Figure 5.19 (a) [45, 103]. However, there is some dispute. A study by Meyer *et al.* [129] using molecular simulations found DMPC/Chol to be in a single-phase region where the l_d phase gradually approaches l_o at $37°C$. Their suggested l_o/l_d transition is found above 40 mol% cholesterol, as seen in Figure 5.19 (b).

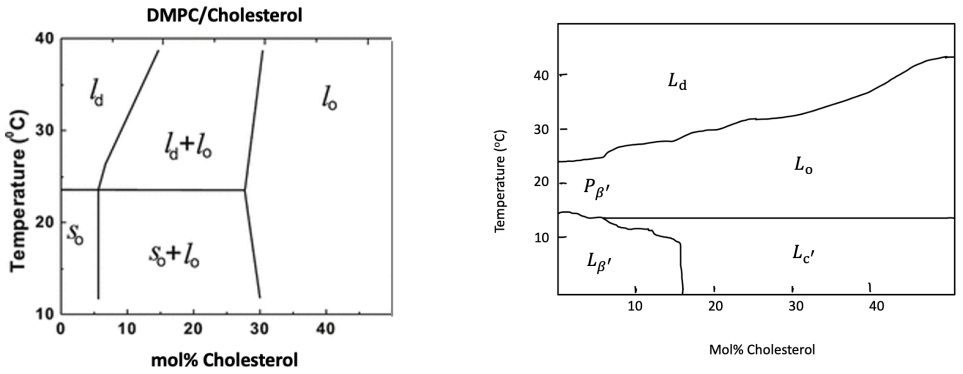

(a) **(b)**

Figure 5.19: (a) DMPC/Chol phase diagram published by Almeida *et al.* [48]. Reprinted with permission from Biochemistry. Copyright 1992 American Chemical Society. (b) DMPC/Chol phase diagram published by Meyer *et al.* [129]. Reprinted and modified with permission from the Journal of Physical Chemistry. Copyright 2010 American Chemical Society.

According to the phase diagram in Figure 5.19 (a), the 0% cholesterol samples are in the l_d phase, the 20% cholesterol samples are phase-separated in coexisting l_d and l_o phases, and the 40% cholesterol samples are in the liquid-ordered phase. The phase diagram in Figure 5.19 (b) suggests that all samples are in an l_d phase approaching the l_o phase at the highest cholesterol concentration. Fluid membranes and lipids in the l_d phase can rapidly reorganise and distribute positive curvature or other defects introduced by indolicidin. Consequently, the less fluid a membrane is, the less effectively lipids can reorganise themselves, and the membrane is less protected. The presence of l_o domains or a gradual shift towards l_o may make it harder for lipids to redistribute and make the membranes more susceptible to solubilisation. So regardless of which phase diagram is the more accurate, both cases have a l_o phase at the highest cholesterol content that may hinder the redistribution of the membrane defects causing disruption. The question of how the presence of raft may affect the peptide-lipid interaction still remains. In phase segregated systems where indolicidin prefers the l_d phase it is probable that most peptides are inserted in the l_d phase where the lipids rapidly relaxes defects, or at the domain interfaces/edges where it lowers the line tension. Hence, it is less probable that indolicidin introduces defects that might solubilise the membrane if the membrane is phase segregated.

Filippov *et al.* [130] did not observe phase separation for DOPC/Chol and POPC/Chol systems, while their DMPC/Chol system seemed to agree with the phase diagram seen in Figure 5.19 (a) with a l_o/l_d coexistence region. Another study supports the formation of domains of condensed complexes of pure cholesterol in DMPC/Chol systems with a domain size in the range of 10-20 nm at cholesterol concentrations of 40 mol% [131]. Since none of our conducted

experiments could confirm domain formation or size in the DMPC/Chol system, any attempt to conclude about the role of rafts in this specific system would be mere speculation.

The contradictory behaviour of the DMPC/Chol system to previously reported interactions presented the need to do similar studies on the different lipids in our heterogeneous system in order to understand the more complex raft systems. POPC/Chol samples with inolicidin had previously been measured by J.E. Nielsen, so we prepared liposomes of DSPC and DOPC with 0, 20 and 40 mol% cholesterol and tested them at the same beamline (BM29) with the same indolicidin:peptide molar ratios.

The scattering curves of DSPC/Chol systems with added indolicidin are shown in Figure 5.20. It might be expected that the trends observed in the DMPC/Chol systems should be quite similar for DSPC/Chol. However, the dependence of solubilisation on cholesterol concentration actually seems to be the opposite.

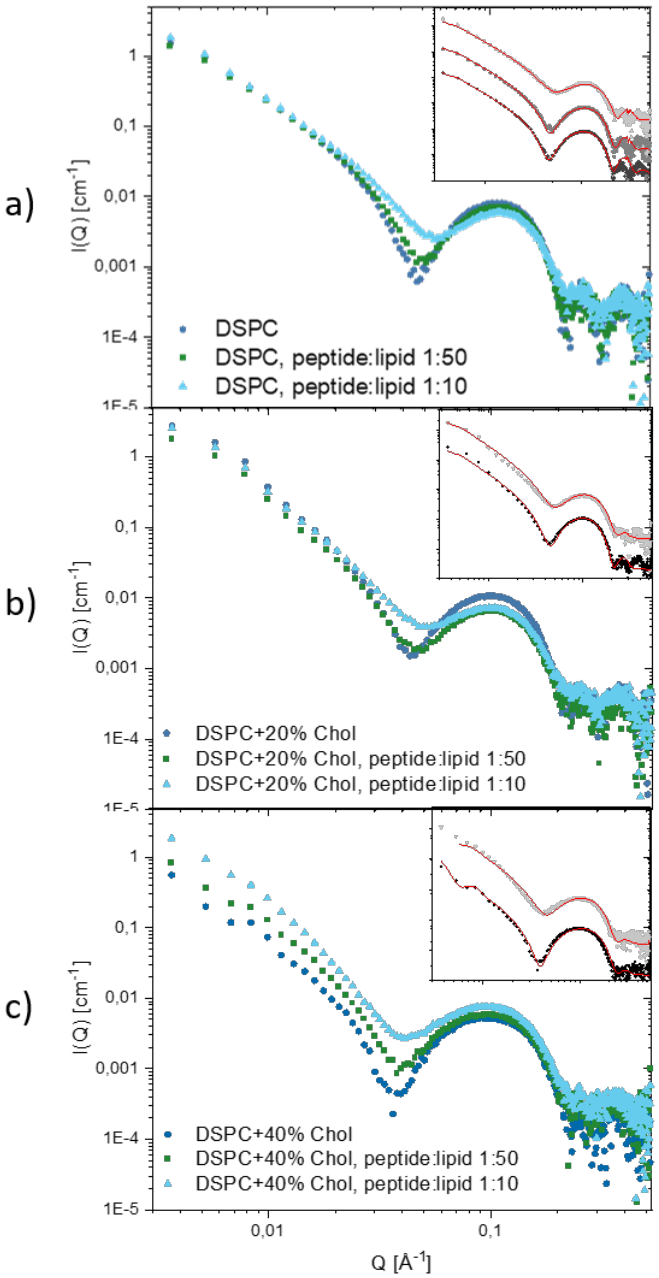

Figure 5.20: Scattering curves of DSPC with different amounts of cholesterol ((a) 0%, (b) 20%, (c) 40%) and peptide:lipid ratios of 0:1, 1:50 and 1:10 at 20 °C. Insets shows fitted curves for the pure liposomes and the lowest peptide:lipid ratios forming different solubilised structures. The curves in the inset are displaced logarithmically with a factor of ten.

From the analysis of the DSPC/Chol systems, it appears that at increasing cholesterol concentrations, a higher peptide:lipid ratio is needed to solubilise the membranes. When the membranes are solubilised, the micelles always coexist with liposomes, and only a small fraction of the lipids are included in the micelles. At 0 mol% Chol, micelles are formed at the 1:50 peptide:lipid ratio. Cholesterol may have a protective role in DSPC since at 20 and 40 mol% Chol, a higher peptide:lipid ratio of 1:20 is needed for micelle-formation. It should here be noted that to fit the scattering from DSPC liposomes with 20% cholesterol, a small amount of 0.15% of the lipids were assumed to be in micelles. Since this was lower than the assumed error of 0.2%, solubilisation was interpreted as happening when the fraction had to be significantly increased. As noted previously, increasing the cholesterol content in DSPC and other saturated lipids with more than 16 carbons in the acyl chains liquifies the gel phase, and according to the previous discussion, the membrane should become more protected from indolicidin interactions. DMPC, on the other hand, was measured at 37 °C, above its melting temperature at 24 °C, and has significantly shorter acyl chains. According to the review by Mannock [119], the l_d phase of DMPC should be strongly influenced and ordered by increasing amounts of cholesterol, which explains the different observed trends for DSPC and DMPC. Simplified phase diagrams of the binary systems of lipids and cholesterol are plotted in Figure 5.21.

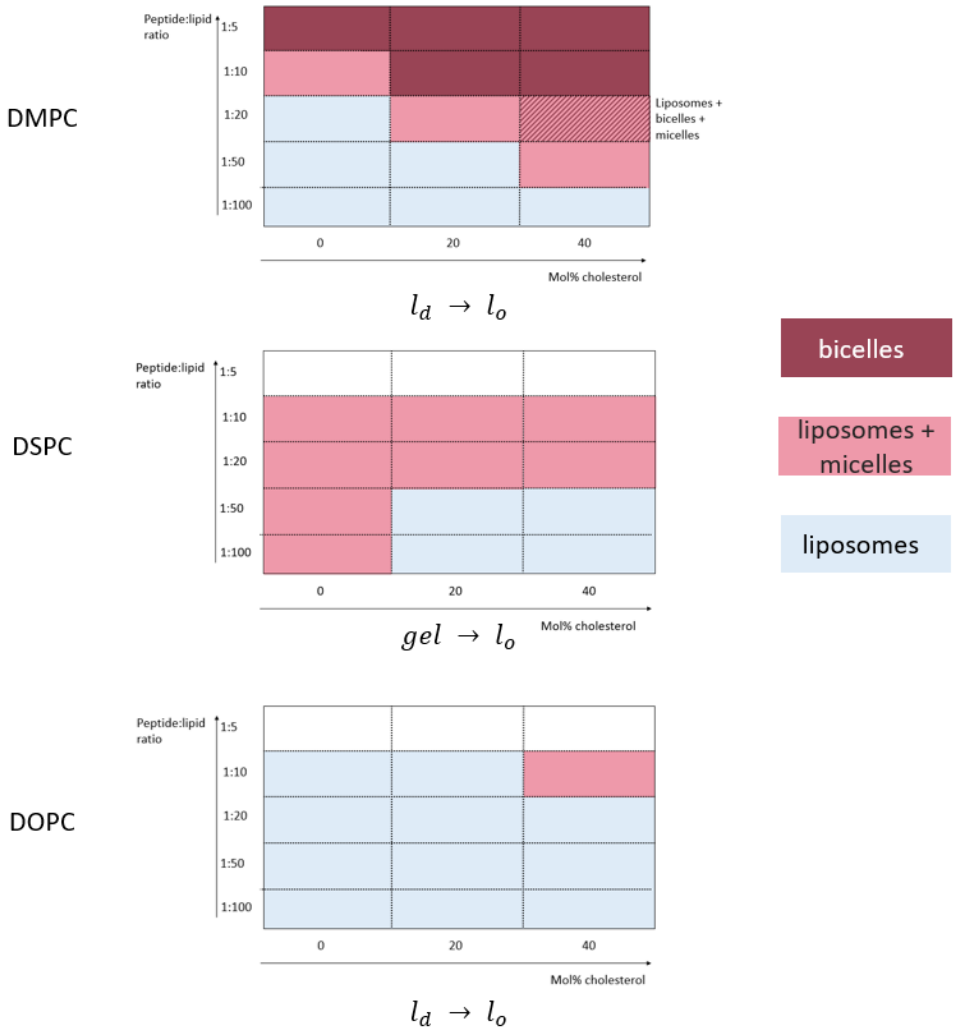

Figure 5.21: Plotted simplified phase diagrams for DMPC, DSPC and DOPC binary systems with cholesterol and their interactions with indolicidin. DMPC/Chol was measured at 37 °C, while DSPC/Chol and DOPC/Chol were measured at 20 °C.

From the phase diagrams in Figure 5.21, it is evident that the interaction of the saturated lipids/Cholesterol and indolicidin is highly dependent on the phase of the lipids. Interestingly, indolicidin does not appear to have remotely as large an effect on the unsaturated lipid/cholesterol systems.

The analyses of the POPC+cholesterol samples (Figure 5.22) showed that no solubilisation occured at any peptide:lipid ratios. Indolicidin merely inserted itself in the membrane. The insets in Figure 5.22 a) and b) show the fitting curves of the pure liposomes and those with added peptide in the 1:5 ratio. In Figure 5.22 c) the peptide:lipid ratio in the inset is 1:10. This

is due to the scattering curve of the 1:5 ratio being quite disordered, and hence challenging to satisfactory fit with the analytical model.

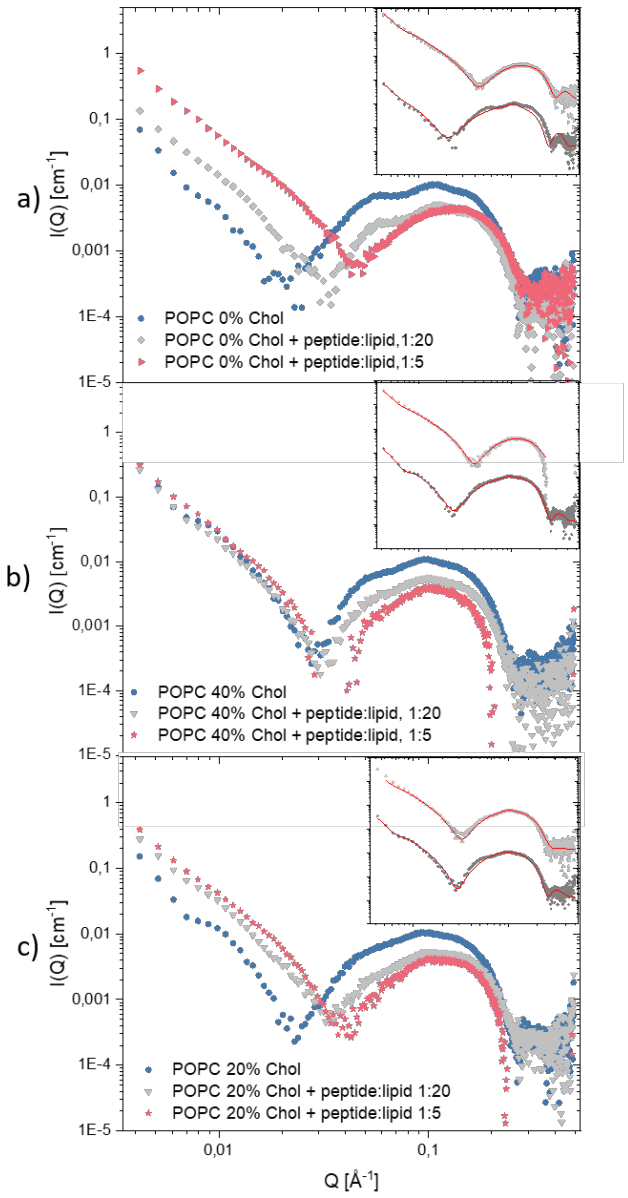

Figure 5.22: Scattering curves of POPC with different amounts of cholesterol ((a) 0%, (b) 20%, (c) 40%) and peptide:lipid ratios of 0:1, 1:20 and 1:5 at 37 °C. Insets shows fitted curves for the pure liposomes and the lowest peptide:lipid ratios forming different solubilised structures. The curves in the inset are displaced logarithmically with a factor of ten.

The observed behaviour of the POPC systems appear, as expected, to be similar to the DOPC systems. Both lipids are unsaturated and have transition temperatures relatively close to one another. The important differences are that the POPC samples were measured at 37°C, while DOPC samples were measured at 20°C. It is probable that the disorder in the liquid state of POPC is higher than it would have been at 20°C. Additionally, the POPC samples showed clear signs of multilamillarity which the DOPC samples did not. Therefore, the exact ratios at which solubilisation occurs cannot be compared directly, but their general behaviour seem to be in agreement with each other. In future work it would be beneficial to repeat the POPC/Chol samples at 20 °C.

Based on the general shape of the DOPC scattering curves in Figure 5.23, it does not appear that the curve is significantly altered but instead shifted in intensity with increasing peptide concentration. The intensity shift may imply insertion of the peptide into the membrane without any significant reorganisation of the bilayer structure. To confirm this more explicitly, model analyses were performed.

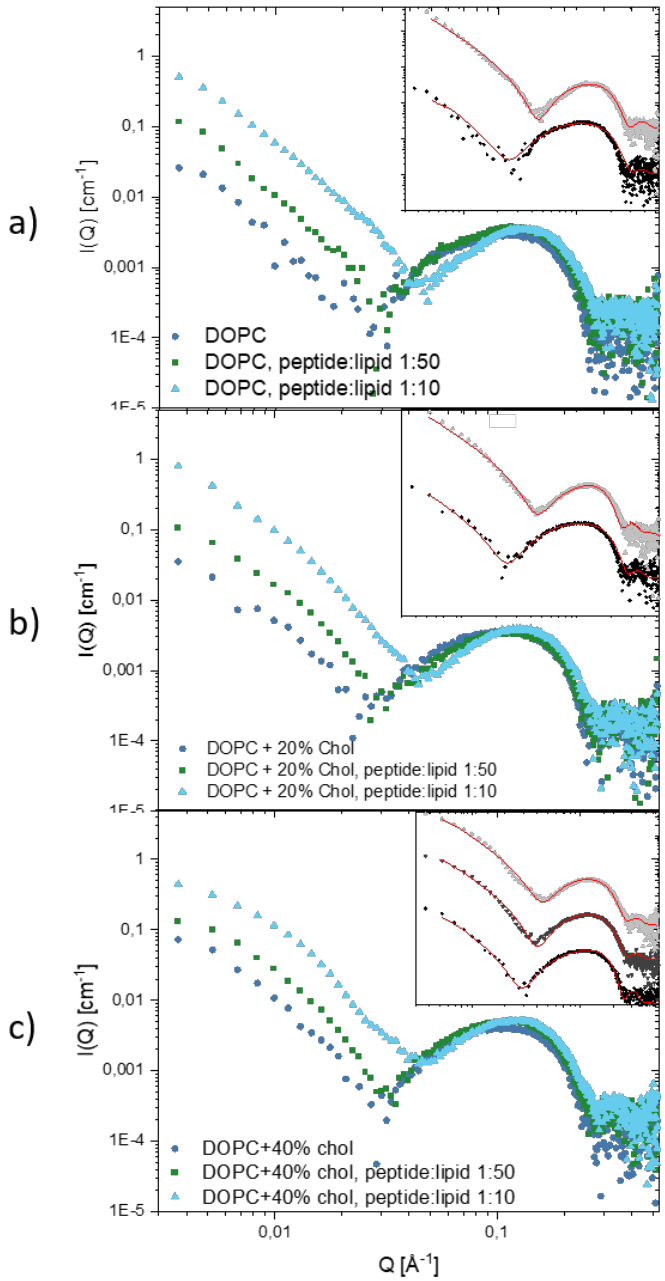

Figure 5.23: Scattering curves of DOPC with different amounts of cholesterol ((a) 0%, (b) 20%, (c) 40%) and peptide:lipid ratios of 0:1, 1:50 and 1:10. Insets show fitted curves for the pure liposomes and the lowest peptide:lipid ratios forming different solubilised structures. The curves in the inset are displaced logarithmically with a factor of ten.

By doing model analysis on the pure liposomes and the liposomes with the highest peptide:lipid ratio, it can be shown that at 0 and 20 mol% cholesterol, the peptide is merely inserted in the membrane but does not cause any noticeable membrane reorganisation. On the other hand, at 40 mol% cholesterol, the highest peptide concentration solubilised structures are formed. According to McHenry *et al.* [61], DOPC/Chol systems should not phase segregate and are all in an l_o phase at cholesterol concentrations above 20 mol% cholesterol. In summary, it seems to be more challenging for indolicidin to solubilise the DOPC membranes below 20 mol% cholesterol, which are in the l_d state, while DOPC + 40% cholesterol probably is in the l_o state and thus solubilised more easily. This supports the theory that more liquid biayers are more protected as they can reorganise themselves faster than defects can cause solubilisation.

5.4 Effect of rafts on peptide interactions as seen by SAXS

After examining the binary systems of saturated and unsaturated PC lipids with cholesterol, SAXS was used to study the effect of indolicidin on the more complex systems of DSPC/POPC/DOPC/Chol. Figure 5.24 presents the scattering curves of the raft forming samples, and the insets again show all concentrations together with the fitted analytical curves, scaled logarithmically. Before applying model-analysis, it can be noticed that indolicidin seems to have the largest effect on S1 (no rafts), seen in Figure 5.24 (a). The scattering curves of the samples with larger rafts appear to be less affected by indolicidin, as seen in Figures 5.24 (c) and (d).

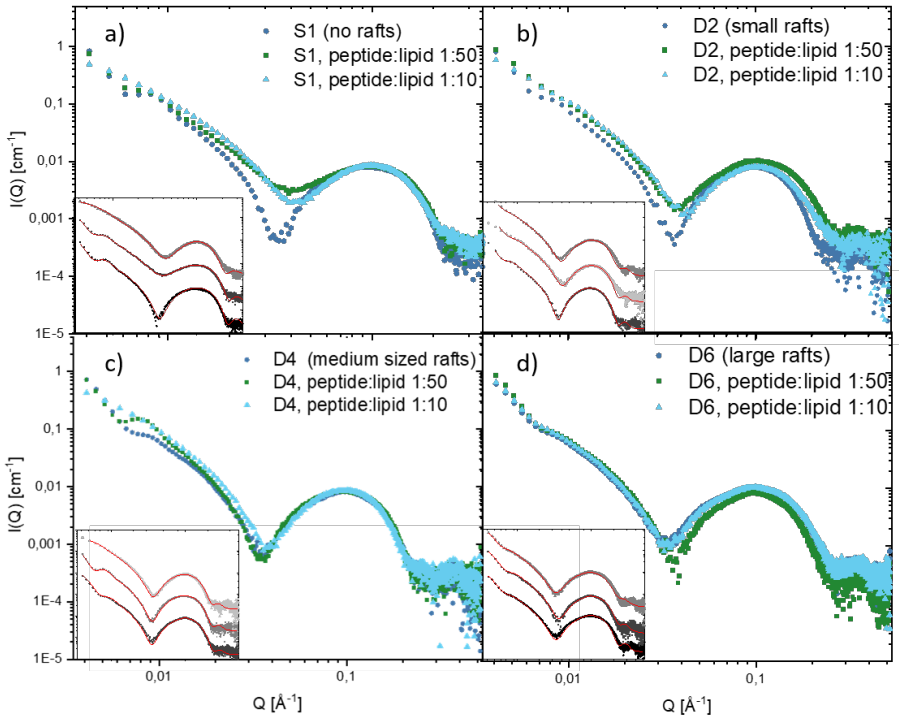

Figure 5.24: Scattering curves of (a) S1, no expected rafts, (b) D2 with small rafts, (c) D4 with medium rafts, and (d) D6 with large rafts, all with peptide:lipid ratios of 0:1, 1:50 and 1:10. Insets show fitted curves from lowest to highest peptide:lipid ratio, where the curves are displaced logarithmically with a factor of ten.

The results obtained from the model analyses are summarised in a simplified phase diagram in Figure 5.25.

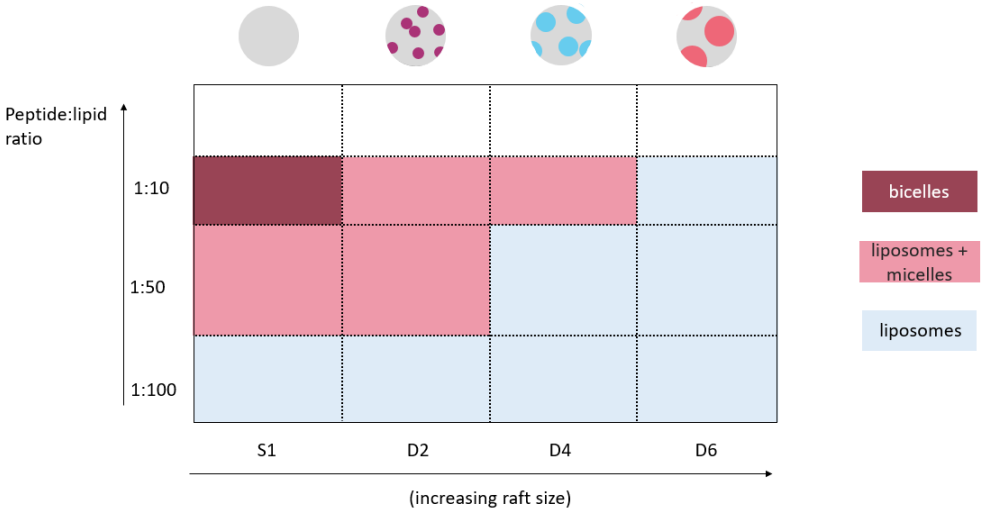

Figure 5.25: Simplified phase diagram for the raft forming systems and their interaction with indolicidin. The samples were measured at 20 °C.

Based on these results, larger rafts seem to have a protective effect against solubilisation by indolicidin as there is no observed solubilisation of the D6 samples. The observation of raft size decreasing the peptide-induced solubilisation is quite surprising, as several studies have reported phase segregation to nullify the assumed protective effects of cholesterol against other small AMPs [61, 132]. Losada-Pérez *et al.* [132] studied the effect of Melittin on DPPC/DOPC/Chol systems. They observed that cholesterol acted as a stronger protecting agent in homogeneous membranes than in heterogeneous membranes, also supported by [55]. Unlike indolicidin, melittin has a potent haemolytic activity. Considering the greater presence of rafts in eukaryotic membranes, it might be reasonable that melittin has a mode of action that is not affected or might even be increased by the presence of rafts.

As mentioned in Section 2.2.3, McHenry *et al.* [61] found that cholesterol acts protectively in homogeneous liposomes of DOPC and DPPC but not in heterogeneous liposomes with DPPC:DOPC ratios of 1:1 and 2:1. It is interesting to note that their results might not be as oppositional to ours as first assumed. First, the technique in [61] of dye-release cannot be said to exclusively observe solubilisation, as increased lipid dynamics may also facilitate dye release. Therefore, the observed phenomena are not necessarily the same. Additionally, our data say a lot about structure and solubilisation, while it is not possible to conclude anything regarding the permeability of the membrane. The observed reorganisation of the domains by SANS and the lack of solubilisation at larger domain sizes does not necessarily exclude the possibility of membrane leakage. Secondly, the much lower peptide:lipid ratio of 1:1000, and no cholesterol in their system, makes the results hard to compare directly. However, the study by McHenry *et al.* [61] does support the observation of a preferential partitioning into the l_d phase.

After studying the effect of cholesterol and rafts on their own, an attempt was made to combine the two effects and study the effect of cholesterol content in membranes with compositions known to form rafts.

5.4.1 Combining rafts and cholesterol variations

In an effort to combine the two effects, the D2 lipid ratios of DSPC/DOPC/POPC were held constant, but the cholesterol concentrations varied. The chosen cholesterol amounts of 10, 30 and 40 mol% were within the range typically found in biological eukaryotic membranes. 20 mol% Chol was excluded as it would basically be the same as D2 (with 21.45 mol% Chol). Some apparent drawbacks to this experiment are that it was impossible to determine if phase segregation into domains occurred in all samples and how the raft size eventually varied as they were not studied using SANS. Again, the results are presented with no, intermediate, and high concentrations of indolicidin in the main figure and an inset with all ratios and fitted curves scaled logarithmically. Figure 5.26 (a) shows the data for the sample with 10% cholesterol. Immediately it is evident that there is no drastic change in the liposome structure. The shape of the scattering curve of the 1:10 ratio at low Q values seems to have flattened a little, indicating the presence of micelles. The model analysis confirmed this.

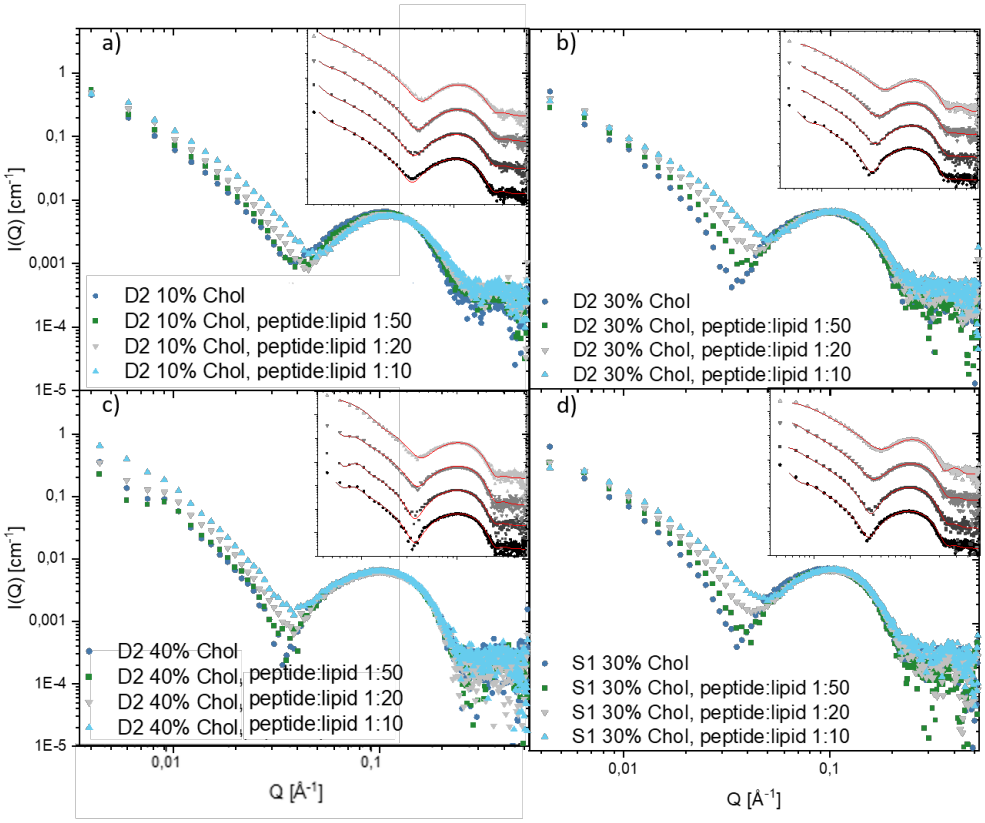

Figure 5.26: Scattering curves of liposomes of D2 lipid ratios with (a) 10 mol% Chol, (b) 30 mol% Chol, (c) 40 mol% Chol, and (d) S1 lipid ratios with approximately 30 mol% Chol. The peptide:lipid ratios were 0:1, 1:50, and 1:10. Insets show fitted curves from lowest to highest peptide:lipid ratio, where the curves are displaced logarithmically with a factor of ten.

At 30% cholesterol, there was a more drastic structural change, as seen in Figure 5.26 (b). The highest peptide:lipid ratio (1:10) caused the formation of bicelles, as previously seen in the DMPC/chol samples with 20 and 40% cholesterol, and the original S1 sample. As seen when comparing Figure 5.26 (b) with (d), the effect of indolicidin on S1 with 34% cholesterol and D2 with 30% cholesterol is quite similar. When looking more closely at the compositions of these samples, it becomes evident why. They are almost identical, except that the D2 30% cholesterol sample has a tiny amount of DOPC, which S1 does not have.

The effect of indolicidin on the sample with the highest cholesterol content (40%) is shown in Figure 5.26 (c). Just from the scattering curves, it seems like the structural effects are less dramatic here than in the sample with 30% cholesterol. The expected relatively rigid membrane without l_o domains should make the membrane more susceptible to solubilisation. Figure 5.27 summarises the results obtained from the model analyses. The results also include the original D2 sample with 21.5 mol% cholesterol to highlight possible trends.

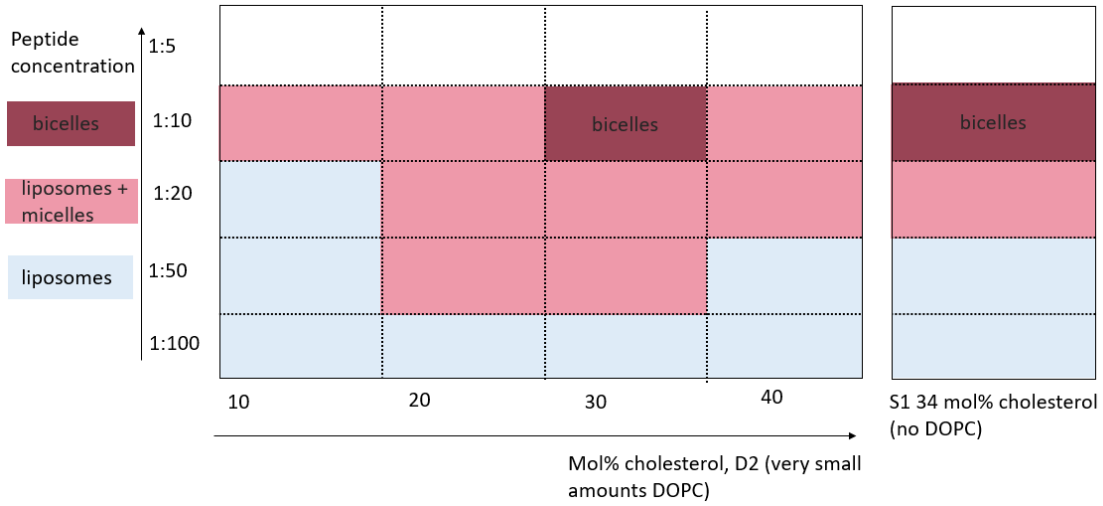

Figure 5.27: Simplified phase diagram of liposomes with the D2 lipid ratios and varying cholesterol content, and their interaction with indolicidin.

To understand what is going on, it might be helpful to look at the phase diagrams for the system published by Heberle *et al.* [71] and Konyakhina *et al.* [133] for the DOPC/POPC/DSPC/Chol system at 23 °C, in Figures 5.28 and 5.29 respectively:

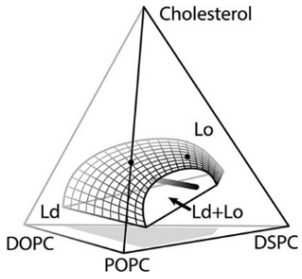

Figure 5.28: Phase diagram published by Heberle *et al.* [71]. Republished with permission from the Journal of the American Chemical Society. Copyright American Chemical Society 2013.

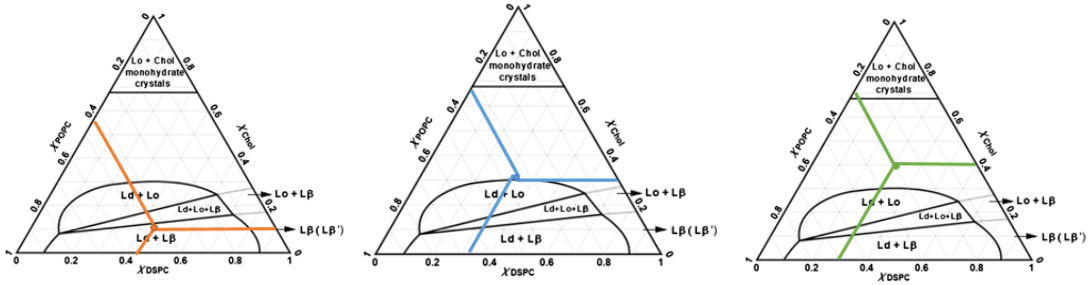

(a) D2 10% cholesterol **(b)** D2 30% cholesterol **(c)** D2 40% cholesterol

Figure 5.29: Phase diagrams published by Konyakhina *et al.* [133], where the points indicate relevant compositions for a) D2 lipid ratio with 10 mol% cholesterol, b)D2 lipid ratio with 30 mol% cholesterol and c)D2 lipid ratio with 40 mol% cholesterol. Reprinted and adapted with permission from Biochimica et Biophysica Acta (BBA) - Biomembranes. Copyright Elsevier 2013.

S1 and D2 are very close in their fractions of DSPC/POPC/DOPC (S1 has no DOPC while D2 has a little DOPC). As confirmed by our SANS experiments regarding the presence of domains, S1 probably resides right outside the $l_d + l_o$ region, while D2 is just inside it. We know that rafts form at $\sim 20\%$ cholesterol for this lipid ratio. Based on the phase diagram in Figure 5.28, the 10% cholesterol sample likely resides within a two-phase region, while the 40% cholesterol is in the l_o region. Since S1 has no DOPC and D2 has a very low mol% DOPC, it is natural to look more closely at the DSP/POPC/Chol side, where the fraction of DOPC is 0. The compositions of D2 10, 30 and 40 mol% cholesterol are shown in Figures 5.29a, 5.29b and 5.29c, respectively, at the intersections of the coloured lines.

Based on the phase diagrams, D2 with 10% cholesterol is likely in a phase segregated region, which may explain the protected nature given the data obtained by SAXS for the samples with increasing raft size. The samples with a D2 lipid ratio and 30% and 40% cholesterol are probably in a single-phase l_o region. Based on the SAXS results of the binary lipid/Chol samples and the assumption that the D2 $30-40\%$ cholesterol samples are both in the l_o phase, a higher cholesterol content may increase the membrane's fluidity and thus decrease the effect of indolicidin on the membranes. However, it is not certain whether this is the actual effect of

cholesterol on the single-phase region. At 30 mol% cholesterol, the model analysis places the peptide in the outer leaflet of the membrane, also when solubilisation occurs. The fit data for 40 mol% cholesterol, on the other hand, suggest that when solubilisation occurs, the peptide penetrates deeper into the membrane. Furthermore, the estimated amount of free peptide is significantly higher in liposomes with 30 mol% than 40 mol% Chol. Together with the results of the previous systems, this points towards cholesterol liquefying the l_o phase, thereby facilitating incorporation of peptides and protecting the membrane from solubilisation. However, there are uncertainties connected to the last results, given what phase the composition is in and whether they are homogeneous or not.

In hindsight, this experiment could have been designed better by using, for example, the phase diagram published by Konyakhina *et al.* [133] to choose compositions within a two-phase region with different cholesterol concentrations. Alternatively, SANS could have been used to confirm the presence and size of rafts. The important results to take away from this section are that phase, and phase separation, play important roles in membrane interactions, and that cholesterol *might* have a protective effect in the l_o phase.

5.4.2 Discussion on the role of rafts in indolicidin's mode of action

As presented in Section 5.3.2, there are several possible mechanisms by which indolicidin might interact with the membrane. In one of the proposed mechanisms indolicidin reduces the line tension between domains, and it may therefore be said to act as a lineactant. If the line tension is sufficiently high, the lineactants may cluster in the interface areas. For heterogeneous lipid membranes the line tension is small enough for lineactants to distribute more homogeneously in liquid domains [134]. If indolicidin does act as a lineactant the size of domains could affect the interactions. Larger rafts have a smaller domain edge to area ratio (equivalent to surface to volume ratio in 3D). If the mode of action relies on insertion in the interface region, there would be statistically fewer interactions for larger domains, as the interface is smaller. However, in our case, the larger domains have a larger amount of DOPC which lowers the transition temperatures. The more fluid nature of the unsaturated lipid phase could counteract the effect of the size of the interface itself. As mentioned in Sections 5.3.2 and 5.3.1 indolicidin seems to show a preference for the l_d phase. Larger domains probably have larger continuous phases, and it might be plausible that larger continuous l_d phases facilitates the lipids reorganisation and hence the relaxation of defects that otherwise could have led to solubilisation.

Indolicidin is generally thought to reside mainly just below the head groups, as the bulky and hydrophobic tryptophan side groups prefer the interface area between the tail and head groups [20]. The model analyses places indolicidin in the hydrophobic core to a large degree (Section 5.4). For the S1 membranes solubilised by indolicidin, its position seems to be just at the interface, with an approximate 50/50 distribution in the outer head group shell and the hydrocarbon region. For the raft containing liposomes more peptides resided in the inner head group shell with increasing concentration. When it comes to the binary samples of DMPC and cholesterol, indolicidin in the pure DMPC samples resided in the outer head group shell and the tail region of the membrane. When cholesterol was added, the position of indolicidin was estimated to be in the inner shell to a greater extent. These results may point to indolicidin having a deeper position in the membrane when it causes solubilisation versus when it is merely

inserted. It may also be a consequence of cholesterol taking up space in the preferred region, forcing the peptide to reside deeper in the membrane. However, the errors and uncertainties of the fits, and the lack of a clear trend makes it challenging to make a definitive conclusion. Tables 5.7 and 5.8 show the distribution of the peptide in the different regions of the bilayer for the homogeneous DMPC membranes and the raft-forming membranes, respectively.

Table 5.7: DMPC, position of peptide. Head group is denoted by h.g., and the ratios indicates peptide:lipid ratios. All values have an uncertainty of 20%.

Lipid composition DMPC/Chol + indo / Partition in bilayer	0% Chol, 1:50	0% Chol, 1:10	20% Chol, 1:50	20% Chol, 1:20	40% Chol, 1:50	40% Chol, 1:20
outer h.g. shell	0.3 ± 0.2	0.2± 0.2	0.5± 0.2%	0.3± 0.2	0.5± 0.2	0.3± 0.2
tail region	0.7± 0.2	0.8± 0.2	0.5± 0.2	0.7± 0.2	0.0± 0.2	0.2± 0.2
inner h.g. shell	0.0± 0.2	0.0± 0.2	0.0± 0.2	0.0± 0.2	0.5± 0.2	0.5± 0.2
Solubilisation	no	yes	no	yes	yes	yes

Table 5.8: Raft samples, position of peptide. Head group is denoted by h.g., and the ratios indicates peptide:lipid ratios. All values have an uncertainty of 20%

Composition / Partition in bilayer	S1, 1:50	D2, 1:50	D2, 1:10	D4, 1:50	D4, 1:10	D6, 1:50	D6, 1:10
outer h.g. shell	0.5± 0.2	25 %	0.1± 0.2	0.5± 0.2	0.5± 0.2	0.5± 0.2	0.2± 0.2
tail region	0.5± 0.2	75%	0.4± 0.2	0.5± 0.2	0.3± 0.2	0.5± 0.2	0.3± 0.2
inner h.g. shell	0.0± 0.2	0.0± 0.2	0.5± 0.2	0.0± 0.2	0.2± 0.2	0.0± 0.2	0.5± 0.2
Solubilisation	yes	yes	yes	no	yes	no	no

In the cases where indolicidin solubilised the membrane, spherical micelles were formed at lower concentrations and bicelles at higher concentrations. Oreopoulos *et al.* [56] did not observe solubilisation of the eukaryotic mimicking membrane but propose that some DOPC were pushed out of the DPPC/DOPC/Chol bilayer as a result of indolicidin induced rearrangement of the bilayer. Their indolicidin concentration was lower than those used in this thesis, but this could indicate that the heightening of the membrane, which pushes out lipids, is a preliminary step before solubilisation [56]. On the other hand, Shaw *et al.* [57] reported that

indolicidin, when interacting with supported DOPC/DSPC/Chol bilayers, initiates a reduction in the height of the gel phase domains at high concentrations. Reduction in bilayer thickness in gel phase domains does contradict the observations of Oreopoulos *et al.* [56], but it might be difficult to conclude if one phase was elevated or the other lowered, and the compositional differences in their systems might also affect the observations. The observed variations in membrane thickness in our samples were almost negligible and within the error range, but it did seem like there was a general trend of some membrane thinning. What Shaw *et al.* [57] and Oreopulos *et al.* [56] can agree on is that the change in membrane thickness can be explained by lipid loss in the presence of high concentrations of indolicidin. Indolicidin has previously been reported to insert itself into the outer head group region, destabilising the membrane and facilitating significant removal of lipids in liposomes containing anionic and zwitterionic head groups [21]. The strong interaction observed between indolicidin and DSPC in our DSC data and solubilisation based on our SAXS data imply that the same might hold for purely zwitterionic membranes. The observed micelle-formation may be explained by lipid removal following membrane insertion of indolicidin and defect/curvature induction.

Based on the obtained results, the following interaction mechanism between indolicidin and model membrane systems is proposed. At lower concentrations, indolicidin inserts itself into the membrane at the interface between the head and tail groups, preferentially in l_d phases. Solubilisation may occur due to defects (for example, curvature defects), which facilitates lipid removal. At higher peptide concentrations bicelles are formed. What drives the formation of exactly bicelles is a complicated question. Bicelles allow the lipids to maintain their optimal packing, while AMPs stabilises the rim. Bicelles might, therefore, be a more energetically favourable packing for the lipids than micelles, but in order to confirm this molecular dynamics simulations are needed. Unsaturated lipids pack in a more disordered fashion, and may thus tolerate a larger curvature than saturated lipids. Consequently, saturated lipids should have a stronger tendency to form bicelles/discs. Liquid phases have a protective nature because the lipids may rapidly reorganise themselves and distribute peptide-induced defects. In membranes containing domains, indolicidin might work as a lineactant, reducing the line tension, causing the domains to become more dynamic and fuse together. The required concentrations to reach each solubilisation step appear to depend on the amount of cholesterol, domain presence/size and the lipids' phase.

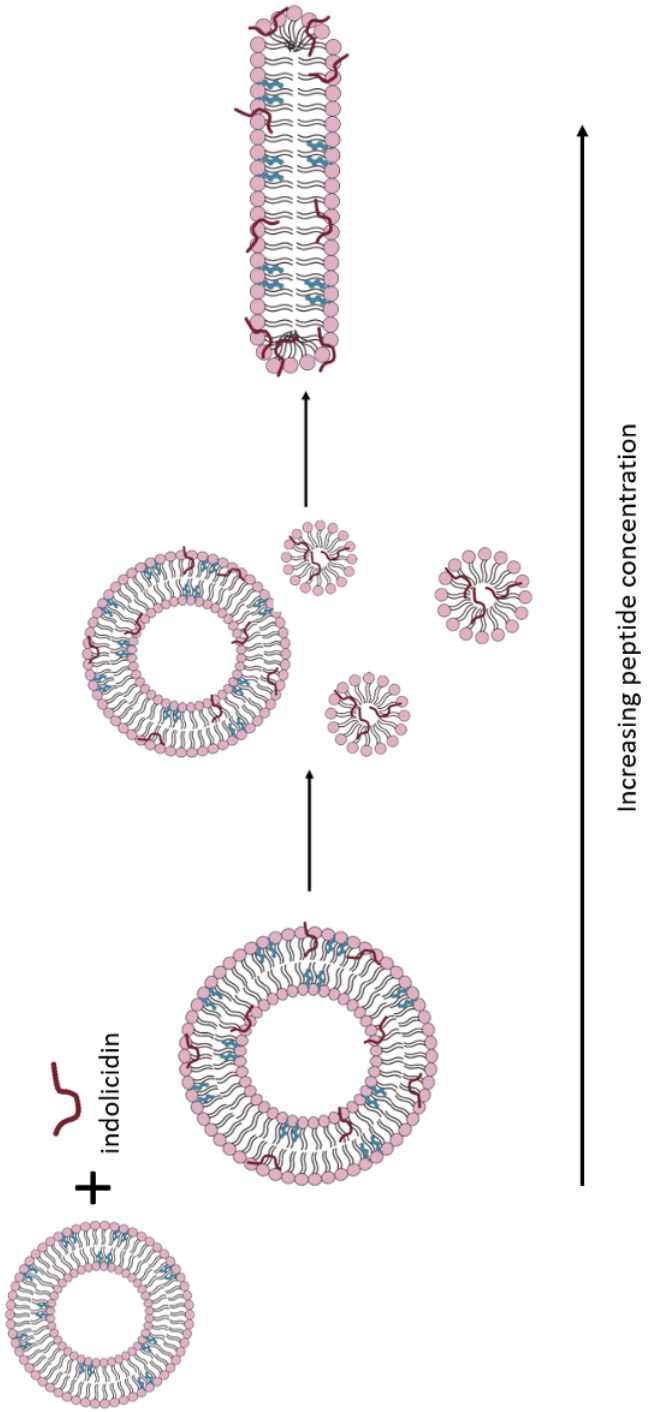

Figure 5.30: Proposed concentration dependent mechanism of Indolicidin solubilising model membranes, forming micelles and bicelles at increasing peptide concentrations.

Chapter 6

Conclusion and outlook

One of the challenges facing the world today is the rising antibiotic resistance. Without new alternatives, diseases now considered trivial or eradicated may become life-threatening again. Antimicrobial peptides (AMPs) are considered one of the more promising alternatives to traditional antibiotics. However, to use AMPs in drug design, it is essential to fully understand the mechanisms by which they act on bacteria.

The main goal of this thesis was to further the understanding of what protects eukaryotic membranes from membrane disruption by AMPs. This was done by investigating the structure of and order in model membrane systems mimicking eukaryotic membranes. We studied two groups of model membranes. First, binary systems with different lipid species and increasing cholesterol content, and secondly, heterogeneous model membrane systems confirmed to form rafts. The membrane effects of indolicidin were determined by determining the membrane structure at different peptide:lipid ratios. Scattering techniques (SAXS/SANS) were applied to resolve the structure of the membranes, supplemented with calorimetry (DSC) probing lipid order.

Using DSC for thermal analysis, we found that indolicidin has an ordering effect on lipids in homogeneous and heterogeneous membranes. The observed ordering effect was supported by other studies showing that indolicidin can bind neighbouring lipids and that the membrane becomes stiffer in the vicinity of the peptide.

The lateral organisation of lipids in the raft model membranes was probed using SANS. The results confirmed that the compositions did form rafts that increased in size with an increasing amount of DOPC compared to POPC. Domain size depends on differences in bilayer thickness mismatch and hence the line tension between domains. Upon adding indolicidin, the rafts grew and became more disordered. It was also confirmed that indolicidin prefers the l_d region. These results point towards indolicidin acting as a lineactant in the presence of membrane domains, reducing line tension and thus promoting the reorganisation of lipids.

All model membranes were structurally characterised using SAXS with different analytical models. From the analyses of the homogeneous membranes (Section 5.4), increasing cholesterol content appeared to protect membranes in the gel phase from solubilisation upon the addition of cholesterol. In contrast, it had the opposite effect on membranes in the liquid phase. When put in context with the results from the heterogeneous models, the more fluid the membrane is,

and the larger continuous areas of the liquid phase are present, the more protected the membrane appears to be from solubilisation by indolicidin.

Based on the results, it is safe to conclude that, in model membrane systems, cholesterol itself does not generally act protectively. Instead, it seems to be the ability of cholesterol to modulate the physical properties of the membrane that determines the protective ability of cholesterol. The more liquid the membrane lipids are, the more protected it seems to be from solubilisation by cholesterol. Therefore, it may be questioned whether or not previous observations of cholesterol's protective abilities in erythrocytes have been a consequence of cholesterol's effect on membrane mechanical properties or the need for cholesterol in raft formation.

Given the low minimal inhibitory concentration of indolicidin (at μg/ml concentrations) and its proposed inter-cellular mode of action, the observation that larger rafts protect membranes from solubilisation is probably only part of the protection of eukaryotic cells from indolicidin. Hopefully, this thesis has contributed to confirming previous observations regarding the mode of action and preferences of indolicidin and supported it with some new insight (the protective effect of rafts). Several pieces have been puzzled together to form a larger picture, but several unanswered questions remain.

The effect and role of cholesterol in membranes remain controversial. In order to give the results presented in this thesis even more strength and certainty, it would be interesting to try and locate the exact positions of cholesterol in the raft-forming membranes. Another uncertainty in the literature that may have affected the interpretation of certain results in this thesis is whether or not there were two co-existing phases in the DMPC/cholesterol systems. SANS and contrast variation would be an invaluable tool to confirm where cholesterol resides in domains and whether or not cholesterol-rich domains form in different binary systems.

Biological membranes are incredibly complicated structures, and even our relatively complex raft-forming system is just a crude model of reality. It would therefore be interesting to gradually converge the composition of the model towards membranes having more biologically relevant compositions. More accurate models could be prepared by, for example, adding sphingomyelins (another large lipid group found in eukaryotic membranes) or eventually including membrane proteins.

The conclusion may be summarised as follows: indolicidin seems to have a membrane mode of action that can classify it as a lineactant, where insertion in the membrane decreases line tension and introduces defects, leading to solubilisation. The solubilisation ability of indolicidin is significantly impacted by lipid phase and domain size in model membranes mimicking eukaryotic cells. The role of cholesterol as a protective agent has neither been completely denied nor confirmed, as it has been shown to depend on the phase of the lipids.

Bibliography

[1] Kyriacos C Nicolaou and Stephan Rigol. 'A brief history of antibiotics and select advances in their synthesis'. In: *J Antibiot* 71.2 (2018), pp. 153–184.

[2] Simon J Howard et al. 'Antibiotic resistance: global response needed'. In: *Lancet Infect Dis* 13.12 (2013), pp. 1001–1003.

[3] WHO. *Antibiotic resistance*. 2020. URL: https://www.who.int/news-room/fact-sheets/detail/antibiotic-resistance (visited on 22/02/2022).

[4] Christopher JL Murray et al. 'Global burden of bacterial antimicrobial resistance in 2019: a systematic analysis'. In: *Lancet* 399.10325 (2022), pp. 629–655.

[5] Cruz L Matos de Opitz and Peter Sass. 'Tackling antimicrobial resistance by exploring new mechanisms of antibiotic action'. In: *Future Microbiol* 15.9 (2020), pp. 703–708.

[6] Christopher D Fjell et al. 'Designing antimicrobial peptides: form follows function'. In: *Nat Rev Drug Discov* 11.1 (2012), pp. 37–51.

[7] Vitor Teixeira, Maria J. Feio and Margarida Bastos. 'Role of lipids in the interaction of antimicrobial peptides with membranes'. In: *Prog Lipid Res* 51.2 (2012), pp. 149–177.

[8] KVR Reddy, RD Yedery and C Aranha. 'Antimicrobial peptides: premises and promises'. In: *Int J Antimicrob Agents* 24.6 (2004), pp. 536–547.

[9] Maria Magana et al. 'The value of antimicrobial peptides in the age of resistance'. In: *Lancet Infect Dis* 20.9 (2020), e216–e230.

[10] Thomas Kruse and Hans-Henrik Kristensen. 'Using antimicrobial host defense peptides as anti-infective and immunomodulatory agents'. In: *Expert review of anti-infective therapy* 6.6 (2008), pp. 887–895.

[11] Chilukuri Subbalakshmi and Narasimhaiah Sitaram. 'Mechanism of antimicrobial action of indolicidin'. In: *FEMS microbiology letters* 160.1 (1998), pp. 91–96.

[12] Jess Vergis et al. 'Antimicrobial efficacy of indolicidin against multi-drug resistant enteroaggregative Escherichia coli in a Galleria mellonella model'. In: *Front Microbiol* (2019), p. 2723.

[13] Josefine Eilsø Nielsen et al. 'Impact of antimicrobial peptides on E. coli-mimicking lipid model membranes: correlating structural and dynamic effects using scattering methods'. In: *Faraday Discuss* 232 (2021), pp. 203–217.

[14] Jenny CY Hsu and Christopher M Yip. 'Molecular dynamics simulations of indolicidin association with model lipid bilayers'. In: *Biophys J* 92.12 (2007), pp. L100–L102.

[15] Licui Chen et al. 'Theoretical insight into the relationship between the structures of antimicrobial peptides and their actions on bacterial membranes'. In: *J Phys Chem B* 119.3 (2015), pp. 850–860.

[16] Deseree J Reid et al. 'Investigating Antimicrobial Peptide–Membrane Interactions Using Fast Photochemical Oxidation of Peptides in Nanodiscs'. In: *J Am Soc Mass Spectrom* 33.1 (2021), pp. 62–67.

[17] J Michael Henderson et al. 'Antimicrobial peptides share a common interaction driven by membrane line tension reduction'. In: *Biophys J* 111.10 (2016), pp. 2176–2189.

[18] Timothy J Falla, D Nedra Karunaratne and Robert EW Hancock. 'Mode of action of the antimicrobial peptide indolicidin'. In: *J Biol Chem* 271.32 (1996), pp. 19298–19303.

[19] Chun-Hua Hsu et al. 'Structural and DNA-binding studies on the bovine antimicrobial peptide, indolicidin: evidence for multiple conformations involved in binding to membranes and DNA'. In: *Nucleic Acids Res* 33.13 (2005), pp. 4053–4064.

[20] Josefine Eilsø Nielsen, Victoria Ariel Bjørnestad and Reidar Lund. 'Resolving the structural interactions between antimicrobial peptides and lipid membranes using small-angle scattering methods: the case of indolicidin'. In: *Soft Matter* 14.43 (2018), pp. 8750–8763.

[21] Josefine Eilsø Nielsen et al. 'A biophysical study of the interactions between the antimicrobial peptide indolicidin and lipid model systems'. In: *Biochim Biophys Acta Biomembr* 1861.7 (2019), pp. 1355–1364.

[22] Josefine Eilsø Nielsen et al. 'Beyond structural models for the mode of action: How natural antimicrobial peptides affect lipid transport'. In: *J Colloid Interface Sci* 582 (2021), pp. 793–802.

[23] Josefine Eilso Nielsen and Reidar Lund. 'Understanding the Mechanism of Antimicrobial Peptides using Small-Angle X-ray and Neutron Scattering Techniques'. In: *Biophys J* 118.3 (2020), 384a.

[24] Mikhail Bogdanov and William Dowhan. 'Functional roles of lipids in biological membranes'. In: *Biochemistry of Lipids, Lipoproteins and Membranes*. Elsevier, 2021. Chap. 1, pp. 1–51. URL: https://www.sciencedirect.com/science/article/pii/B9780128240489000201 (visited on 01/2022).

[25] Ilya Levental, Kandice R. Levental and Frederick A. Heberle. 'Lipid Rafts: Controversies Resolved, Mysteries Remain'. In: *Trends Cell Biol* 30.5 (2020), pp. 341–353.

[26] Sean Munro. 'Lipid rafts: elusive or illusive?' In: *Cell* 115.4 (2003), pp. 377–388.

[27] Ken Jacobson, Ole G Mouritsen and Richard GW Anderson. 'Lipid rafts: at a crossroad between cell biology and physics'. In: *Nat Cell Biol* 9.1 (2007), pp. 7–14.

[28] Thomas J Silhavy, Daniel Kahne and Suzanne Walker. 'The bacterial cell envelope'. In: *Cold Spring Harb Perspect Biol* 2.5 (2010), a000414.

[29] Rosaleen Anderson et al. 'Microorganisms'. In: *Antibacterial agents: chemistry, mode of action, mechanisms of resistance and clinical applications*. John Wiley & Sons, 2012, pp. 1–33. URL: https://onlinelibrary.wiley.com/doi/book/10.1002/9781118325421 (visited on 02/2022).

[30] Michael R. Yeaman and Nannette Y. Yount. 'Mechanisms of Antimicrobial Peptide Action and Resistance'. In: *Pharmacol Rev* 55.1 (2003), pp. 27–55.

[31] Raquel F. Epand Richard M. Epand. 'Lipid domains in bacterial membranes and the action of antimicrobial agents'. In: *Biochim Biophys Acta Biomembr* (2009).

[32] Donald Voet and Judith G Voet. 'Lipids, Bilayer and Membranes'. In: *Biochemistry*. 4th. ed. John Wiley & Sons, 2010. Chap. 9, pp. 241–287.

[33] 'Sterols'. In: *Encyclopedia of Genetics, Genomics, Proteomics and Informatics*. Springer Netherlands, 2008, p. 1884. DOI: 10.1007/978-1-4020-6754-9_16188. URL: https://doi.org/10.1007/978-1-4020-6754-9_16188.

[34] J. Volkman. 'Sterols in microorganisms'. In: *Appl Microbiol Biotechnol* 60.5 (2003), pp. 495–506.

[35] J Henriksen et al. 'Universal behavior of membranes with sterols'. In: *Biophys J* 90.5 (2006), pp. 1639–1649.

[36] Ole G Mouritsen and Luis A Bagatolli. 'The More We Are Together'. In: *LIFE-AS A MATTER OF FAT*. Springer, 2016, pp. 95–110. URL: https://link.springer.com/book/10.1007/b138577 (visited on 20/01/2022).

[37] Norbert Kučerka et al. 'Cholesterol in Bilayers with PUFA Chains: Doping with DMPC or POPC Results in Sterol Reorientation and Membrane-Domain Formation'. In: *Biochemistry* 49.35 (2010), pp. 7485–7493.

[38] Drew Marquardt et al. 'Cholesterol's location in lipid bilayers'. In: *Chem Phys Lipids* 199 (2016), pp. 17–25.

[39] Juyang Huang and Gerald W Feigenson. 'A microscopic interaction model of maximum solubility of cholesterol in lipid bilayers'. In: *Biophys J* 76.4 (1999), pp. 2142–2157.

[40] Maikel C Rheinstädter and Ole G Mouritsen. 'Small-scale structure in fluid cholesterol–lipid bilayers'. In: *Curr Opin Colloid Interface Sci* 18.5 (2013), pp. 440–447.

[41] Paulo FF Almeida. 'Thermodynamics of lipid interactions in complex bilayers'. In: *Biochim Biophys Acta Biomembr* 1788.1 (2009), pp. 72–85.

[42] Keith J Fritzsching, Jihyun Kim and Gregory P Holland. 'Probing lipid–cholesterol interactions in DOPC/eSM/Chol and DOPC/DPPC/Chol model lipid rafts with DSC and 13C solid-state NMR'. In: *Biochim Biophys Acta Biomembr* 1828.8 (2013), pp. 1889–1898.

[43] Frédérick de Meyer and Berend Smit. 'Effect of cholesterol on the structure of a phospholipid bilayer'. In: *Proc Natl Acad Sci* 106.10 (2009), pp. 3654–3658.

[44] Paweł Wydro, Sabina Knapczyk and Marta Łapczyńska. 'Variations in the condensing effect of cholesterol on saturated versus unsaturated phosphatidylcholines at low and high sterol concentration'. In: *Langmuir* 27.9 (2011), pp. 5433–5444.

[45] Paulo FF Almeida, Antje Pokorny and Anne Hinderliter. 'Thermodynamics of membrane domains'. In: *Biochim Biophys Acta Biomembr* 1720.1-2 (2005), pp. 1–13.

[46] C Dietrich et al. 'Lipid rafts reconstituted in model membranes'. In: *Biophys J* 80.3 (2001), pp. 1417–1428.

[47] Kai Simons and Winchil LC Vaz. 'Model systems, lipid rafts, and cell membranes'. In: *Annu Rev Biophys Biomol Struct* 33 (2004), pp. 269–295.

[48] Paulo FF Almeida, Winchil LC Vaz and TE Thompson. 'Lateral diffusion in the liquid phases of dimyristoylphosphatidylcholine/cholesterol lipid bilayers: a free volume analysis'. In: *Biochemistry* 31.29 (1992), pp. 6739–6747.

[49] Omar Bakht, Priyadarshini Pathak and Erwin London. 'Effect of the structure of lipids favoring disordered domain formation on the stability of cholesterol-containing ordered domains (lipid rafts): identification of multiple raft-stabilization mechanisms'. In: *Biophys J* 93.12 (2007), pp. 4307–4318.

[50] Richard M Epand and Raquel F Epand. 'Bacterial membrane lipids in the action of antimicrobial agents'. In: *J Pept Sci* 17.5 (2011), pp. 298–305.

[51] Katsumi Matsuzaki et al. 'Molecular basis for membrane selectivity of an antimicrobial peptide, magainin 2'. In: *Biochemistry* 34.10 (1995), pp. 3423–3429.

[52] Seema Joshi et al. 'Interaction studies of novel cell selective antimicrobial peptides with model membranes and E. coli ATCC 11775'. In: *Biochim Biophys Acta Biomembr* 1798.10 (2010), pp. 1864–1875.

[53] Yanyu Zhu, Sonisilpa Mohapatra and James C Weisshaar. 'Rigidification of the Escherichia coli cytoplasm by the human antimicrobial peptide LL-37 revealed by superresolution fluorescence microscopy'. In: *Proc Natl Acad Sci* 116.3 (2019), pp. 1017–1026.

[54] Georg Pabst et al. 'Membrane thickening by the antimicrobial peptide PGLa'. In: *Biophys J* 95.12 (2008), pp. 5779–5788.

[55] H Raghuraman and Amitabha Chattopadhyay. 'Interaction of melittin with membrane cholesterol: a fluorescence approach'. In: *Biophys J* 87.4 (2004), pp. 2419–2432.

[56] John Oreopoulos and Christopher M Yip. 'Combinatorial microscopy for the study of protein–membrane interactions in supported lipid bilayers: Order parameter measurements by combined polarized TIRFM/AFM'. In: *J Struct Biol* 168.1 (2009), pp. 21–36.

[57] James E Shaw et al. 'Mechanisms of antimicrobial peptide action: studies of indolicidin assembly at model membrane interfaces by in situ atomic force microscopy'. In: *J Struct Biol* 154.1 (2006), pp. 42–58.

[58] Hongxia Zhao et al. 'Comparison of the membrane association of two antimicrobial peptides, magainin 2 and indolicidin'. In: *Biophys J* 81.5 (2001), pp. 2979–2991.

[59] Tatyana I Rokitskaya et al. 'Indolicidin action on membrane permeability: carrier mechanism versus pore formation'. In: *Biochim Biophys Acta Biomembr* 1808.1 (2011), pp. 91–97.

[60] Durba Sengupta et al. 'Toroidal pores formed by antimicrobial peptides show significant disorder'. In: *Biochim Biophys Acta Biomembr* 1778.10 (2008), pp. 2308–2317.

[61] Austin J. McHenry et al. 'Does cholesterol suppress the antimicrobial peptide induced disruption of lipid raft containing membranes?' In: *Biochim Biophys Acta Biomembr* 1818.12 (Dec. 2012), pp. 3019–3024.

[62] Antje Pokorny and Paulo FF Almeida. 'Permeabilization of raft-containing lipid vesicles by δ-lysin: a mechanism for cell sensitivity to cytotoxic peptides'. In: *Biochemistry* 44.27 (2005), pp. 9538–9544.

[63] Juanjuan Su, Siewert J Marrink and Manuel N Melo. 'Localization preference of antimicrobial peptides on liquid-disordered membrane domains'. In: *Frontiers in cell and developmental biology* 8 (2020), p. 350.

[64] Peter Atkins, Peter William Atkins and Julio de Paula. *Atkins' physical chemistry*. Oxford university press, 2014.

[65] JN Israelachvili. *Intermolecular and Surface Forces*. 3rd. ed. Elsevier, 2011. URL: https://www.sciencedirect.com/book/9780123751829/intermolecular-and-surface-forces?via=ihub= (visited on 02/2022).

[66] Ken A Dill, Sarina Bromberg and Dirk Stigter. *Molecular driving forces: statistical thermodynamics in biology, chemistry, physics, and nanoscience, 2. edition*. Garland Science, 2011.

[67] Mariana Ruiz Villarreal. *Phospholipids aqueous solution structures.svg*. 2007. URL: https://commons.wikimedia.org/w/index.php?curid=3032610 (visited on 25/03/2022).

[68] Charles Tanford. *The hydrophobic effect: formation of micelles and biological membranes. 2nd. ed*. J. Wiley., 1980.

[69] Yogita P Patil and Sameer Jadhav. 'Novel methods for liposome preparation'. In: *Chem Phys Lipids* 177 (2014), pp. 8–18.

[70] Jacob Israelachvili. 'Self-assembly in two dimensions: surface micelles and domain formation in monolayers'. In: *Langmuir* 10.10 (1994), pp. 3774–3781.

[71] Frederick A Heberle et al. 'Bilayer thickness mismatch controls domain size in model membranes'. In: *J Am Chem Soc* 135.18 (2013), pp. 6853–6859.

[72] Ole G Mouritsen and Luis A Bagatolli. *Life-as a matter of fat: lipids in a membrane biophysics perspective*. Springer, 2015. URL: https://link.springer.com/book/10.1007/b138577 (visited on 20/01/2022).

[73] Garth L Nicolson. 'The Fluid—Mosaic Model of Membrane Structure: Still relevant to understanding the structure, function and dynamics of biological membranes after more than 40 years'. In: *Biochim Biophys Acta Biomembr* 1838.6 (2014), pp. 1451–1466.

[74] Ole G Mouritsen and Luis A Bagatolli. 'Biological Membranes—Models and Fashion'. In: *LIFE-AS A MATTER OF FAT*. Springer, 2016, pp. 75–81. URL: https://link.springer.com/book/10.1007/b138577 (visited on 20/01/2022).

[75] Ole G Mouritsen and Luis A Bagatolli. 'Lipids in Bilayers—A Stress-Full and Busy Life'. In: *LIFE-AS A MATTER OF FAT*. Springer, 2016, pp. 85–93. URL: https://link.springer.com/book/10.1007/b138577 (visited on 20/01/2022).

[76] Avanti Polar Lipids. *What Is The Transition Temperature Of The Lipid*. URL: https://avantilipids.com/tech-support/faqs/transition-temperature (visited on 22/02/2022).

[77] Richard M Epand. 'Detecting the presence of membrane domains using DSC'. In: *Biophys Chem* 126.1-3 (2007), pp. 197–200.

[78] D. Lombardo M.A. Kiselev. 'Structural characterization in mixed lipid membrane systems by neutron and X-ray scattering'. In: *Biochim Biophys Acta* (2017).

[79] P Lindner and Th Zemb. 'Chapter 1. Introduction to Scattering Experiments'. In: *Neutrons, X-rays and light: scattering methods applied to soft condensed matter*. 2002.

[80] D.S. Sivia. *Elementary Scattering Theory: For X-ray and Neutron users*. Oxford University Press, Jan. 2011. DOI: 10.1093/acprof:oso/9780199228676.001.0001. URL: https://doi.org/10.1093/acprof:oso/9780199228676.001.0001.

[81] Andrew J Jackson. 'Introduction to Small-Angle Neutron Scattering and Neutron Reflectometry'. In: 2008.

[82] P Lindner and Th Zemb. 'Chapter 2. Scattering Experiments'. In: *Neutrons, X-rays and light: scattering methods applied to soft condensed matter*. 2002.

[83] JS Pedersen. 'Small-angle scattering from surfactants and block copolymer micelles'. In: *Soft Matter Characterization* 1 (2008), p. 191.

[84] Dan A Neumann. 'Neutron scattering and hydrogenous materials'. In: *Mater Today* 9.1-2 (2006), pp. 34–41.

[85] P Lindner and Th Zemb. 'Chapter 16. Modelling of Small-Angle Scattering Data'. In: *Neutrons, X-rays and light: scattering methods applied to soft condensed matter*. 2002.

[86] J Skov Pedersen, Dorthe Posselt and Kell Mortensen. 'Analytical treatment of the resolution function for small-angle scattering'. In: *J Appl Crystallogr* 23.4 (1990), pp. 321–333.

[87] Petra Pernot et al. 'Upgraded ESRF BM29 beamline for SAXS on macromolecules in solution'. In: *J Synchrotron Radiat* 20.4 (2013), pp. 660–664.

[88] Martha Elisabeth Brennich et al. 'Online data analysis at the ESRF bioSAXS beamline, BM29'. In: *J Appl Crystallogr* 49.1 (2016), pp. 203–212.

[89] Lixin Fan et al. 'The absolute calibration of a small-angle scattering instrument with a laboratory X-ray source'. In: *J Phys Conf Ser*. Vol. 247. 1. IOP Publishing. 2010, p. 012005.

[90] author unknown. *BioXTAS Raw*. date unknown. URL: https://bioxtas-raw.readthedocs.io/en/latest/ (visited on 02/05/2022).

[91] V Pipich. *QtiKWS: user-friendly program for reduction, visualization, analysis and fit of SA (N) S data*. 2012.

[92] U Keiderling. 'The new 'BerSANS-PC'software for reduction and treatment of small angle neutron scattering data'. In: *Appl Phys A* 74.1 (2002), s1455–s1457.

[93] Yang Leng. 'Thermal Analysis'. In: *Materials characterization: introduction to microscopic and spectroscopic methods*. 2nd ed. John Wiley & Sons, 2009. Chap. 10, pp. 333–364.

[94] Muhammad Sajid Hamid Akash and Kanwal Rehman. 'Differential scanning calorimetry'. In: *Essentials of pharmaceutical analysis*. Springer, 2020, pp. 199–206. URL: https://link.springer.com/chapter/10.1007/978-981-15-1547-7_17 (visited on 03/2022).

[95] Marie-Lise Jobin and Isabel D Alves. 'The contribution of differential scanning calorimetry for the study of peptide/lipid interactions'. In: *Microcalorimetry of Biological Molecules*. Springer, 2019, pp. 3–15. URL: https://link.springer.com/protocol/10.1007/978-1-4939-9179-2_1 (visited on 03/2022).

[96] John Mackenzie Grant Cowie and Valeria Arrighi. 'Polymercharacterization - Molar Masses'. In: *Polymers: chemistry and physics of modern materials*. 3rd ed. CRC press, 2007. Chap. 9, pp. 229–252.

[97] Natalia Molchanova et al. 'Halogenation as a tool to tune antimicrobial activity of peptoids'. In: *Sci Rep* 10.1 (2020), pp. 1–10.

[98] Victoria Ariel Bjørnestad, Marcella Orwick-Rydmark and Reidar Lund. 'Understanding the Structural Pathways for Lipid Nanodisc Formation: How Styrene Maleic Acid Copolymers Induce Membrane Fracture and Disc Formation'. In: *Langmuir* 37.20 (2021), pp. 6178–6188.

[99] Lize Arleth and Charlotte Vermehren. 'An analytical model for the small-angle scattering of polyethylene glycol-modified liposomes'. In: *J Appl Crystallogr* 43.5 (2010), pp. 1084–1091.

[100] Drew Marquardt et al. 'Cholesterol's location in lipid bilayers'. In: *Chem Phys Lipids* 199 (2016), pp. 17–25.

[101] Joachim Kohlbrecher. *User guide for the SASfit software package*. 2022. URL: https://docs.sasfit.org (visited on 25/04/2022).

[102] Dr. Stephen Burgess. *Liposome Preparation - Avanti® Polar Lipids*. URL: https://www.sigmaaldrich.com/NO/en/technical-documents/protocol/cell-culture-and-cell-culture-analysis/transfection-and-gene-editing/liposome-preparation (visited on 25/03/2022).

[103] Witold K Subczynski et al. 'High cholesterol/low cholesterol: effects in biological membranes: a review'. In: *Cell Biochem Biophys* 75.3 (2017), pp. 369–385.

[104] Maria Laura Immordino, Franco Dosio and Luigi Cattel. 'Stealth liposomes: review of the basic science, rationale, and clinical applications, existing and potential'. In: *Int J Nanomedicine* 1.3 (2006), p. 297.

[105] Jung Soo Suk et al. ‘PEGylation as a strategy for improving nanoparticle-based drug and gene delivery’. In: *Adv Drug Deliv Rev* 99 (2016), pp. 28–51.

[106] the European Synchrotron ESRF. *Beam Delivery*. URL: https://www.esrf.fr/home/UsersAndScience/Experiments/MX/About_our_beamlines/bm29/beamline-setup/beam-delivery.html (visited on 25/03/2022).

[107] Joachim Kohlbrecher and Werner Wagner. ‘The new SANS instrument at the Swiss spallation source SINQ’. In: *J Appl Crystallogr* 33.3 (2000), pp. 804–806.

[108] Paul Scherrer Institut PSI. *Instrument Description*. URL: https://www.psi.ch/en/sinq/sansi/components (visited on 25/03/2022).

[109] Alexander I Greenwood, Stephanie Tristram-Nagle and John F Nagle. ‘Partial molecular volumes of lipids and cholesterol’. In: *Chem Phys Lipids* 143.1-2 (2006), pp. 1–10.

[110] Barbara A Lewis and Donald M Engelman. ‘Lipid bilayer thickness varies linearly with acyl chain length in fluid phosphatidylcholine vesicles’. In: *J Mol Biol* 166.2 (1983), pp. 211–217.

[111] Norbert Kučerka, Mu-Ping Nieh and John Katsaras. ‘Fluid phase lipid areas and bilayer thicknesses of commonly used phosphatidylcholines as a function of temperature’. In: *Biochim Biophys Acta Biomembr* 1808.11 (2011), pp. 2761–2771.

[112] Benoit Palmieri and Samuel A Safran. ‘Hybrid lipids increase the probability of fluctuating nanodomains in mixed membranes’. In: *Langmuir* 29.17 (2013), pp. 5246–5261.

[113] Todd PW McMullen and Ronald N McElhaney. ‘Differential scanning calorimetric studies of the interaction of cholesterol with distearoyl and dielaidoyl molecular species of phosphatidylcholine, phosphatidylethanolamine, and phosphatidylserine’. In: *Biochemistry* 36.16 (1997), pp. 4979–4986.

[114] Todd PW McMullen and Ronald N McElhaney. ‘New aspects of the interaction of cholesterol with dipalmitoylphosphatidylcholine bilayers as revealed by high-sensitivity differential scanning calorimetry’. In: *Biochim Biophys Acta Biomembr* 1234.1 (1995), pp. 90–98.

[115] Behfar Moghaddam et al. ‘The application of monolayer studies in the understanding of liposomal formulations’. In: *Int J Pharm* 417.1-2 (2011), pp. 235–244.

[116] Rodrigo FM De Almeida, Aleksandre Fedorov and Manuel Prieto. ‘Sphingomyelin/phosphatidylcholine/cholesterol phase diagram: boundaries and composition of lipid rafts’. In: *Biophys J* 85.4 (2003), pp. 2406–2416.

[117] Thalia T Mills et al. ‘Effects of cholesterol and unsaturated DOPC lipid on chain packing of saturated gel-phase DPPC bilayers’. In: *Gen Physiol Biophys* 28.2 (2009), p. 126.

[118] J Hjort Ipsen et al. ‘Phase equilibria in the phosphatidylcholine-cholesterol system’. In: *Biochim Biophys Acta Biomembr* 905.1 (1987), pp. 162–172.

[119] David A Mannock et al. ‘The effect of variations in phospholipid and sterol structure on the nature of lipid–sterol interactions in lipid bilayer model membranes’. In: *Chem Phys Lipids* 163.6 (2010), pp. 403–448.

[120] Ana Casadó et al. ‘Langmuir monolayers and Differential Scanning Calorimetry for the study of the interactions between camptothecin drugs and biomembrane models’. In: *Biochim Biophys Acta Biomembr* 1858.2 (2016), pp. 422–433.

[121] Thalia T Mills et al. ‘Order parameters and areas in fluid-phase oriented lipid membranes using wide angle X-ray scattering’. In: *Biophys J* 95.2 (2008), pp. 669–681.

[122] TH Huang et al. ‘A carbon-13 and deuterium nuclear magnetic resonance study of phosphatidylcholine/cholesterol interactions: Characterization of liquid-gel phases’. In: *Biochemistry* 32.48 (1993), pp. 13277–13287.

[123] Thomas J McIntosh. ‘The effect of cholesterol on the structure of phosphatidylcholine bilayers’. In: *Biochim Biophys Acta Biomembr* 513.1 (1978), pp. 43–58.

[124] Hans Jakob Askou, Rasmus Neergaard Jakobsen and Peter Fojan. ‘An atomic force microscopy study of the interactions between indolicidin and supported planar bilayers’. In: *J Nanosci Nanotechnol* 8.9 (2008), pp. 4360–4369.

[125] Chiara Nicolini, Pappannan Thiyagarajan and Roland Winter. ‘Small-scale composition fluctuations and microdomain formation in lipid raft models as revealed by small-angle neutron scattering’. In: *Phys Chem Chem Phys* 6.24 (2004), pp. 5531–5534.

[126] Josefine E. Nielsen and Vladimir R. Koynarev. 2022.

[127] Evan F Haney et al. ‘Induction of non-lamellar lipid phases by antimicrobial peptides: a potential link to mode of action’. In: *Chem Phys lipids* 163.1 (2010), pp. 82–93.

[128] Rohit Sood and Paavo KJ Kinnunen. ‘Cholesterol, lanosterol, and ergosterol attenuate the membrane association of LL-37 (W27F) and temporin L’. In: *Biochim Biophys Acta Biomembr* 1778.6 (2008), pp. 1460–1466.

[129] Frédérick J-M de Meyer et al. ‘Molecular simulation of the DMPC-cholesterol phase diagram’. In: *J Phys Chem B* 114.32 (2010), pp. 10451–10461.

[130] Andrey Filippov, Greger Orädd and Göran Lindblom. ‘The effect of cholesterol on the lateral diffusion of phospholipids in oriented bilayers’. In: *Biophys J* 84.5 (2003), pp. 3079–3086.

[131] Gregory M Troup et al. ‘Detection and characterization of laterally phase separated cholesterol domains in model lipid membranes’. In: *Colloids Surf B Biointerfaces* 29.2-3 (2003), pp. 217–231.

[132] Patricia Losada-Pérez et al. ‘Melittin disruption of raft and non-raft-forming biomimetic membranes: a study by quartz crystal microbalance with dissipation monitoring’. In: *Colloids Surf B Biointerfaces* 123 (2014), pp. 938–944.

[133] Tatyana M Konyakhina et al. ‘Control of a nanoscopic-to-macroscopic transition: modulated phases in four-component DSPC/DOPC/POPC/Chol giant unilamellar vesicles’. In: *Biophys J* 101.2 (2011), pp. L8–L10.

[134] Nelli Erwin et al. ‘Lipoprotein insertion into membranes of various complexity: lipid sorting, interfacial adsorption and protein clustering’. In: *Phys Chem Chem Phys* 18.13 (2016), pp. 8954–8962.

[135] Peter Boesecke. ‘Reduction of two-dimensional small-and wide-angle X-ray scattering data’. In: *J Appl Crystallogr* 40.s1 (2007), s423–s427.

Chapter 7

Appendix

7.1 Estimation of errors

The errors obtained for the fit parameters in the QtiSAS software are defined as

$$Err(i) = \frac{\chi}{\sqrt{DoF} \cdot covar(\chi_i \cdot \chi_i)}. \tag{7.1}$$

where χ is a vector of the statistical variables of the experiment (in 2D scattering patterns this is the pixels). DoF are the degrees of freedom (DoF = number of points in the experimental curve - number of fit parameters) and $covar(\chi_i \cdot \chi_i)$ is a covariant matrix of two statistical variables [135]. After reaching a satisfactory fit all fitted parameters were fitted again simultaneously to obtain the fitting errors. Some parameters that were highly dependent on other parameters were adjusted manually and held constant while varying other parameters held constant. in order to define the limits where the fit no longer was acceptable. These parameters were: the lipid density. lipid and peptide concentrations. fraction of free peptide. fraction of peptide and lipids in micelles. the number of stacked bilayers. the paracrystalline disorder factor and the distance between stacked bilayers.

For the error in the transition temperatures and estimated from the DSC data. the standard deviation for the pure D4 samples were found. Standard deviation is found by

$$S_x = \sqrt{\frac{\sum_{i=1}^{n} (x_i - \bar{x})^2}{n-1}} \tag{7.2}$$

The error was assumed to be representative for all estimated transition temperatures.

7.2 Figures corresponding to results in section 5.1

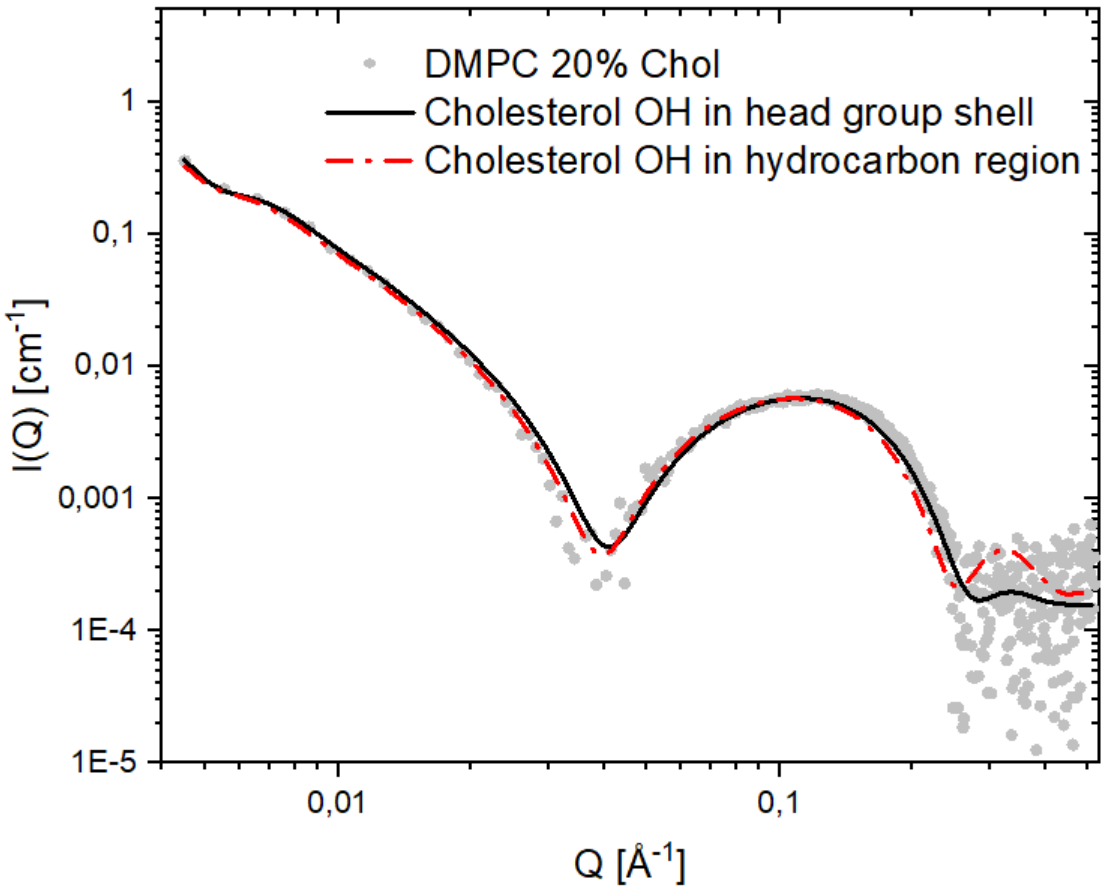

Figure 7.1: Effect of the position of cholesterol. The fit with the red line places the OH group of cholesterol in the hydrocarbon region, while the black fit places it in the headgroup shells.

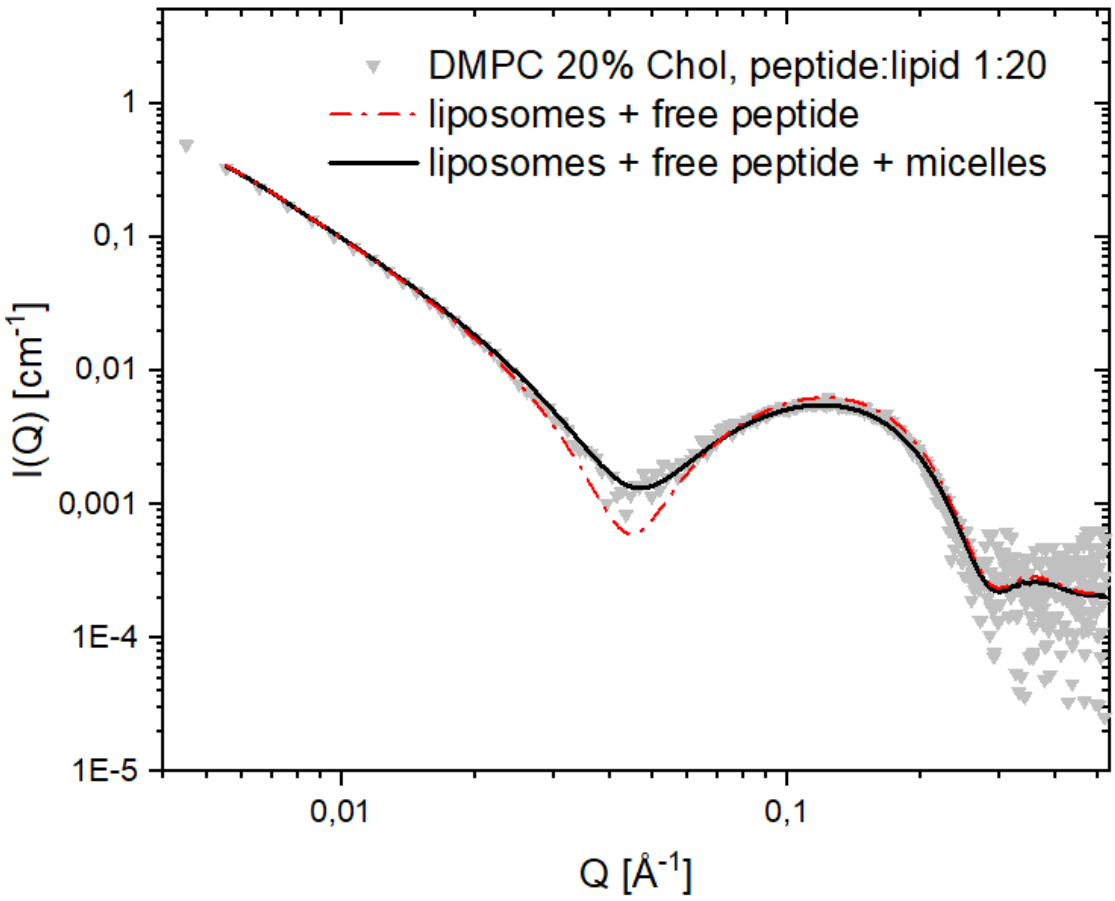

Figure 7.2: Fit with and without the presence of micelles. The fit with the red line includes only liposomes and free peptides, while in the black fit 77% of the peptide not incorporated in the membrane, and 5% of the lipids were in micelles.

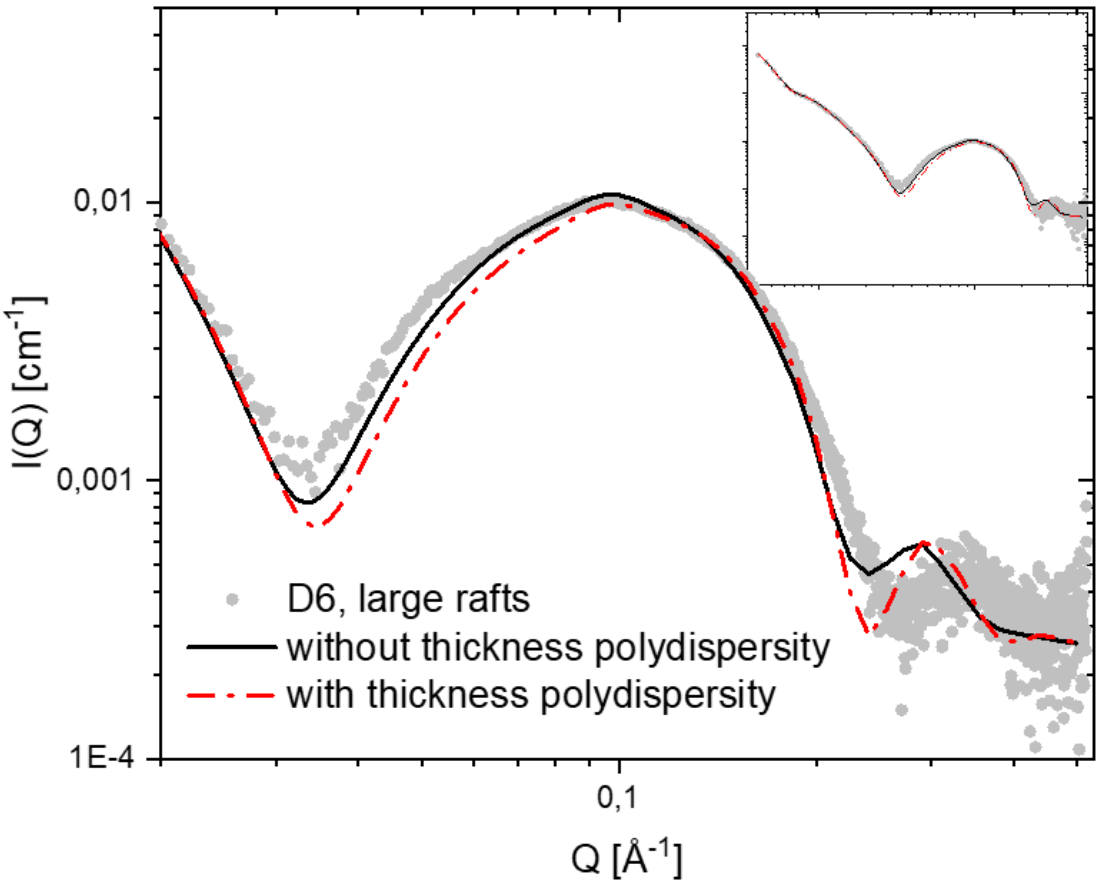

Figure 7.3: Fit with and without polydispersity (PD) in the thickness as well as the size. The polydispersity parameter of the fit with the red line has a value of $\sigma_{cPD} = 0.13$.

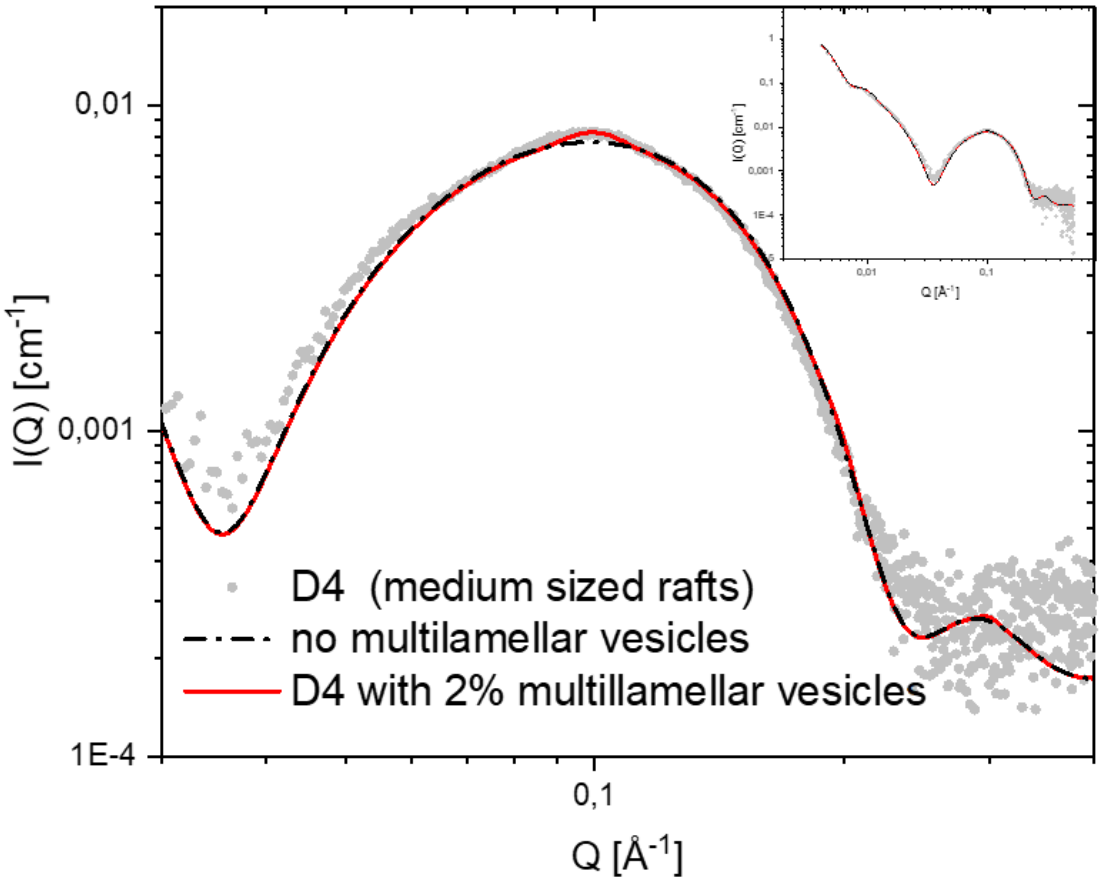

Figure 7.4: Fit with and without the presence of multilamellar vesicles. The red line represents the fit with 2% multilamellar vesicles, while the fit with black line includes only unilammellar vesicles

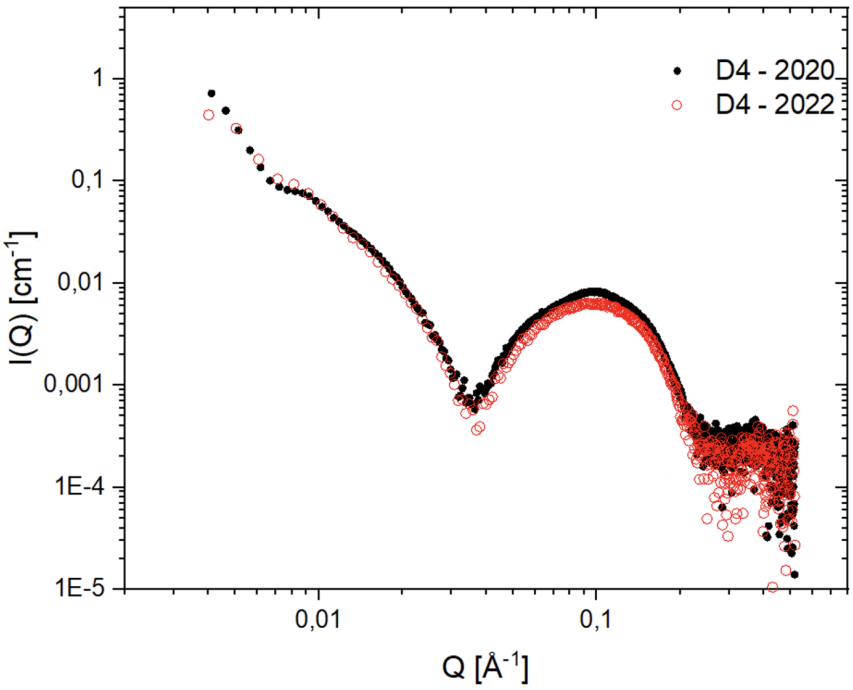

Figure 7.5: The scattering curves of pure D4 liposomes (medium sized rafts). The sample from extruded 21 times (black. 2020) clearly shows signs of multilamillarity. while the sample extruded 31 times (red. 2022) does not.

7.3 Tables corresponding to results in section 5.4

Table 7.1: Fitted bilayer thickness and thickness polydispersity for DMPC/Chol samples.

DMPC	thickness. hydrocarbon region [Å]	thickness polydispersity	fraction of water. outer shell
0 % Chol	23 ± 1	0 ± 0.03	0.21 ± 0.08
20 % Chol	28 ± 1	0 ± 0.03	0.12 ± 0.08
40 % Chol	25 ± 1	0 ± 0.03	0.56 ± 0.08

Table 7.2: Fitted bilayer thickness and thickness polydispersity for DOPC/Chol samples.

DOPC	thickness. hydrocarbon region [Å]	thickness polydispersity
0 % Chol	24± 1	0 ± 0.03
20 % Chol	29± 1	0± 0.03
40 % Chol	35± 1	0± 0.03

Table 7.3: Fitted bilayer thickness and thickness polydispersity for DSPC/Chol samples.

DSPC	thickness. hydrocarbon region [Å]	thickness polydispersity
0 % Chol	35 ± 1	0± 0.03
20 % Chol	35 ± 1	0± 0.03
40 % Chol	34± 1	0± 0.03

Table 7.4: Fitted bilayer thickness and thickness polydispersity for raft-forming samples.

Sample	Hydrocarbon region thickness [Å]	thickness polydispersity	ρ
S1	34 ± 1	0 ± 0.03	0
D2	33 ± 1	0.07 ± 0.03	5
D4	30 ± 1	0.09 ± 0.03	17
D6	30± 1	0.13 ± 0.03	35

Table 7.5: Fitted bilayer thickness and thickness polydispersity for liposomes with the D2 DOPC/POPC ratio and varying cholesterol concentrations.

Sample	Hydrocarbon region thickness [Å]	thickness polydispersity
D2 10% chol	29 ± 1	0.1 ± 0.03
D2 30% chol	28 ± 1	0 ± 0.03
D2 40% chol	27 ± 1	0 ± 0.03
S1 30% chol	31 ± 1	0.1± 0.03

7.4 DSC baseline subtraction

For all samples there was a substantial decrease in the heat capacity of the baseline from scan 1 to the rest of the scans. as seen for the D4 and indolicidin 1:50 sample in figure 7.6a. This change in heat capacity may be attributed to slightly different heating rates or the system not being fully calibrated. To compensate for this the baseline was fitted with a sigmoidal curve and subtracted from all scans. as seen in figure 7.6b. Figure 7.6b also shows that the main transition is not completely reversible. as the heating and cooling scans do not overlap or have the same shape.

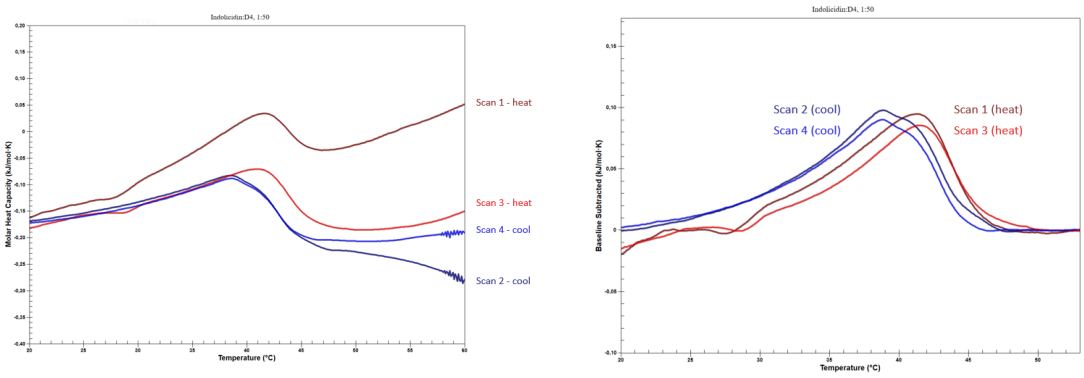

(a) Not subtracted baseline

(b) Subtracted baseline

Figure 7.6: All scans of D4 1:50. shows the importance of baseline subtraction

7.5 DSC - buffer data

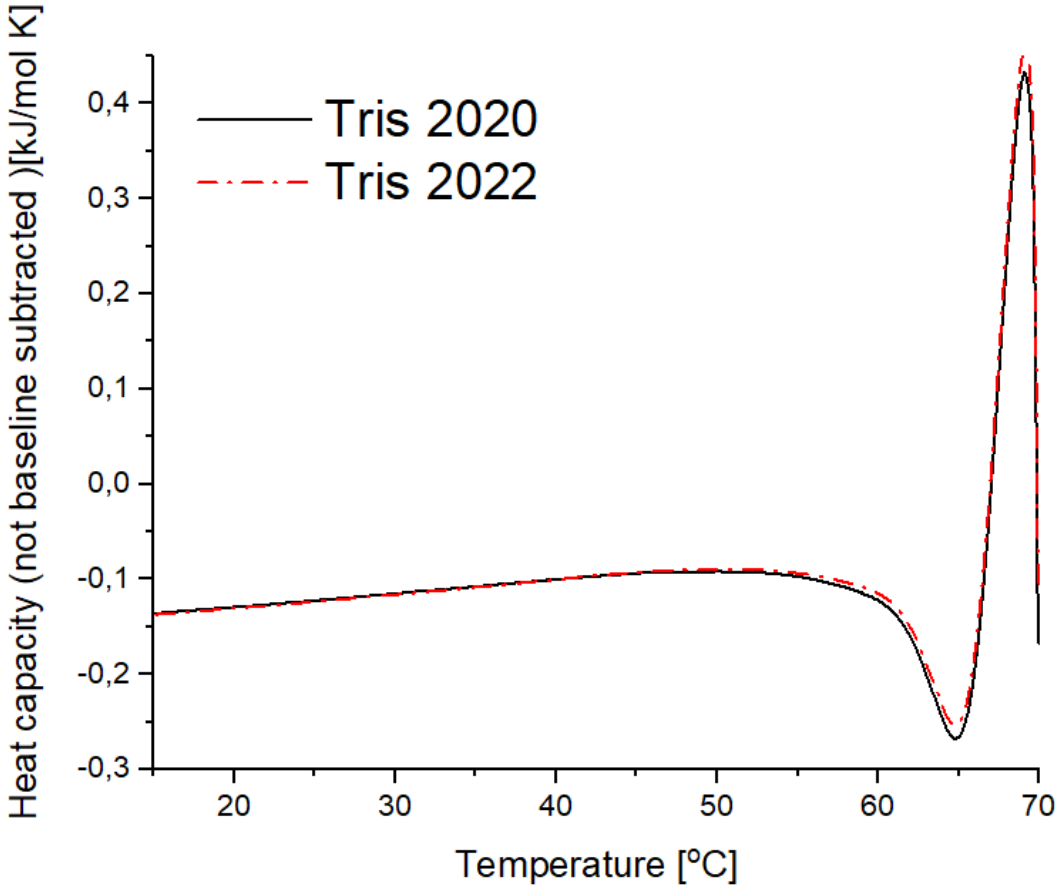

Figure 7.7: Molar heat capacity. tris buffer. Not baseline subtracted.

7.6 Transition enthalpies as found by DSC

Transition enthalpies were estimated using the NanoAnalyze software.

Table 7.6: Transition enthalpies estimated using NanoAnalyze software

	S1	S1 (2022)	D2	D4	D4 (2022)	D6	DSPC	DSPC (20% Chol)
ΔH (kJ/mol)	4	7	7.3	9.3	5.5	5	30.2	16.7
ΔH (kJ/mol). peptide:lipid 1:50	-	4.5	-	-	6.2	-	-	-
ΔH (kJ/mol). peptide:lipid 1:20	-	4.5	-	-	6	-	30.3	18.5
ΔH (kJ/mol). peptide:lipid 1:10	-	-	-	8	-	-	-	-

7.7 Radiation damage

Some of the data collected in September 2021 showed weak signs of radiation damage. possibly aggregation and/or fragmentation. This was evident in the scattering curves as the intensity at low-q values increased or decreased with each run (figure 7.8). The samples were the intensity increased had an increase in molar mass. indicating aggregation. The opposite is true for a decrease in intensity indicating fragmentation. This is a known issue that may arise in bioSAXS [**hopkins2016quantifying**]. The deviation was. however. quite small. The data subtraction was therefore performed manually with only those runs that did not deviate significantly from the first runs. The error at low q-values was probably larger in these data than in the other. which may have affected the fit of the data at low q-values.

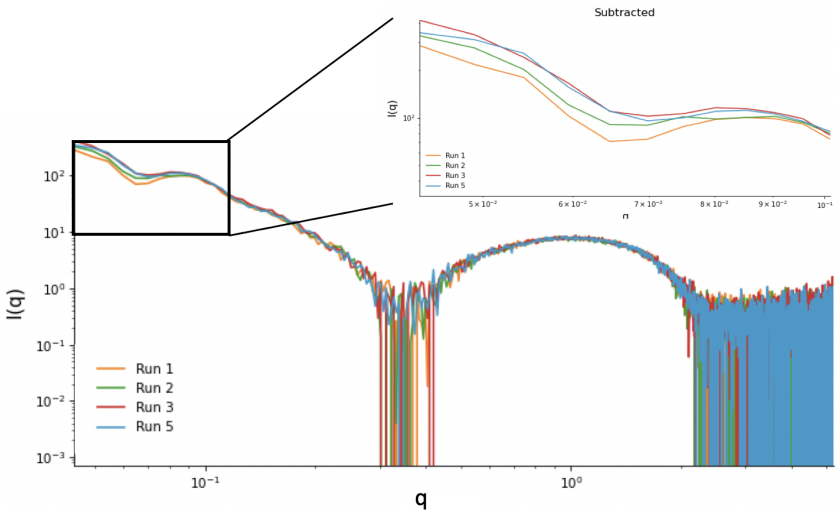

Figure 7.8: Raw scattering data (pre-subtraction) of the D2 DOPC/POPC ratio sample with 40% Cholesterol showing radiation damage. The two most outlying scans were the two last runs. Amongst the other there is a steady small decrease in intensity at low q-values. indicating fragmentation.

7.8 SANS

7.8.1 Merging of data-points

Since the data were acquired at two detector distances (2 and 8 m). the data-points were merged to form continuous plots. By removing approximately the last 15 points in each data set. the curves overlapped nicely. as seen in figure 7.9.

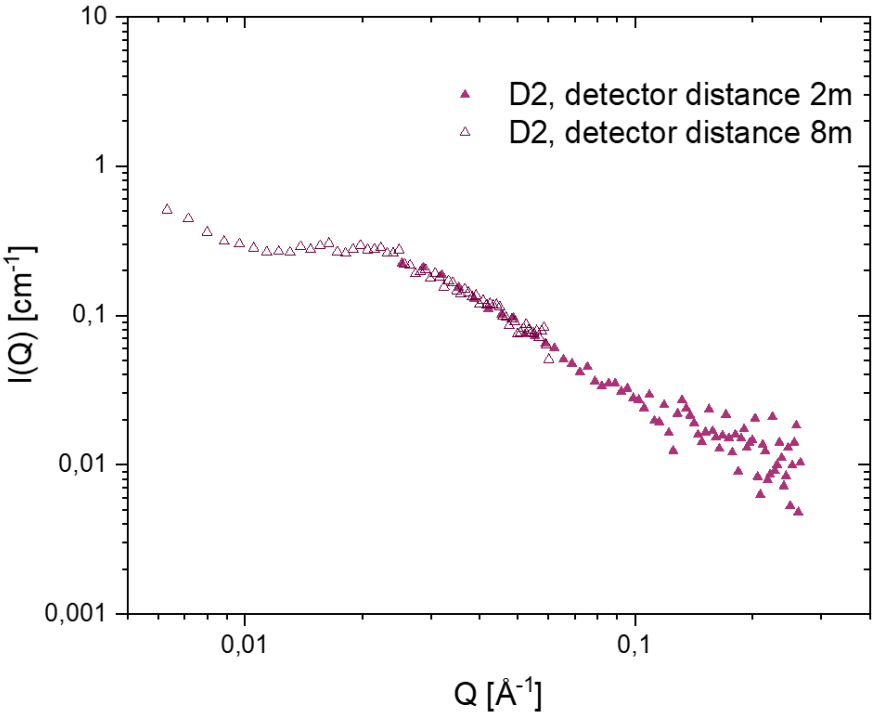

Figure 7.9: Overlap of data measured at detector distances of 2 and 8 m.

7.8.2 Dilution

Due to an experimental error the samples with peptide:lipid ratio 1:50 were diluted to 8 mg/ml (from 10 mg/ml). The small decrease in intensity. however. has no implications on the general observed trends or the discussion presented in section 5.3.2. The only quantitative parameter it might have an impact on is the forward intensity as found in the Ornstein-Zernike function. But. as seen in figure 7.10. there is very little difference in the low-q scattering.

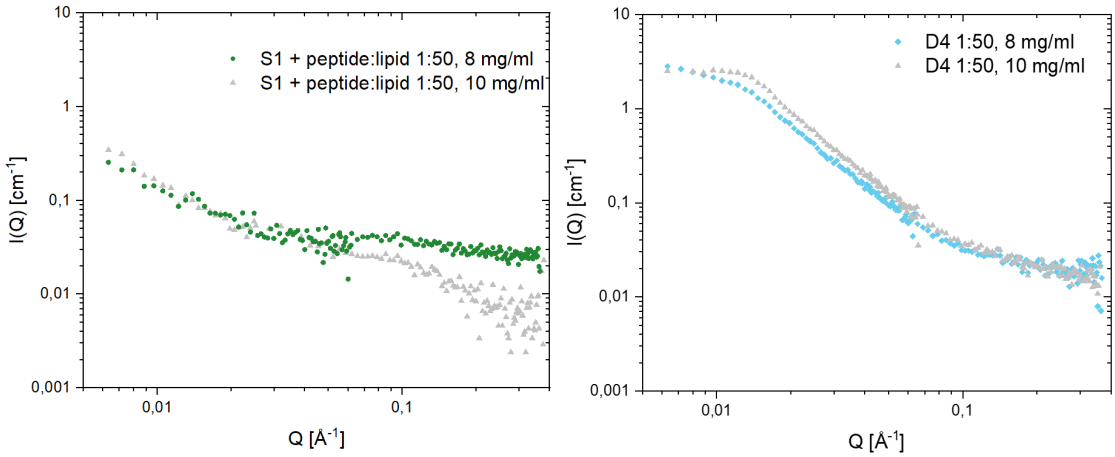

(a) **(b)**

Figure 7.10: (a) S1 samples measured at concentrations of 8 and 10 mg/ml. (b) D4 samples measured at concentrations of 8 and 10 mg/ml

Figure 7.10a shows that the overall expected increase in intensity with increased concentration does not described the observed behaviour at high q-values. However. the intensity in this area is quite low. and the errors large (figure 7.11). so it is difficult to pinpoint a cause for this behaviour. A possible explanation is a manual mix-up while inserting the samples in the sample holder at the instrument. The only way to confirm or deny this would be to re-test the data at the same SANS beam-line.

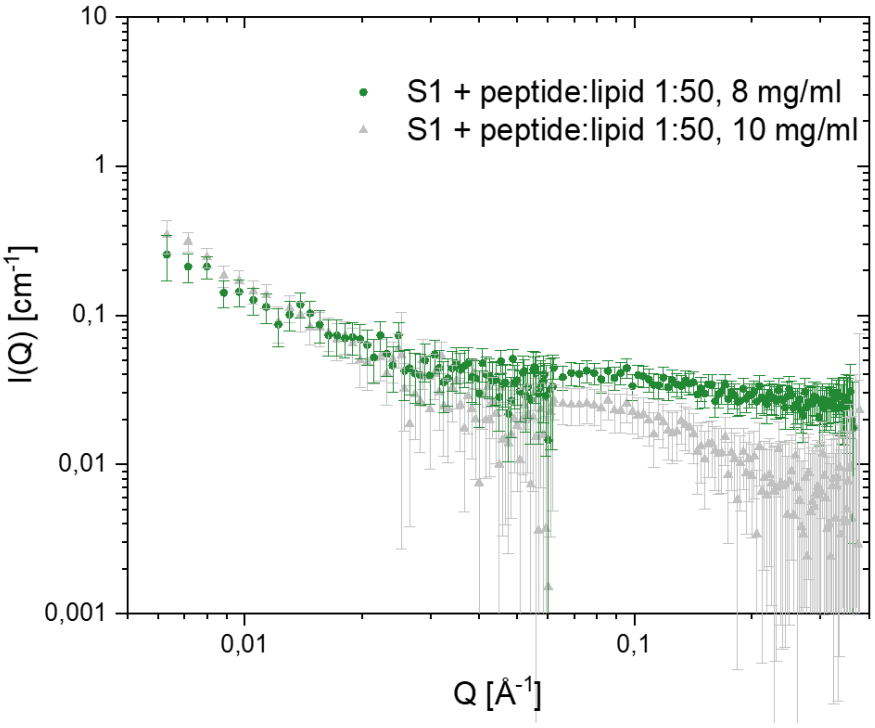

Figure 7.11: S1 measured at concentrations of 8 and 10 mg/ml with error-bars.

7.9 Other

As a consequence of the Covid19 pandemic it was not possible to go in person to Grenoble. France. and perform SAXS experiments. so some of the samples were sent to Grenoble and tested by he staff there. When analysing the samples sent in December 2020 it became evident that there had been a mix-up either on our or their account regarding the labels of the samples. The samples marked with peptide:lipid ratios of 1:10 seemed more plausible to have a ratio of 1:50. and reversed. In order to confirm these suspicions the D4 samples with both peptide:lipid ratios were re-tested in February 2022. As seen in figure 7.12 the mix-up was confirmed.

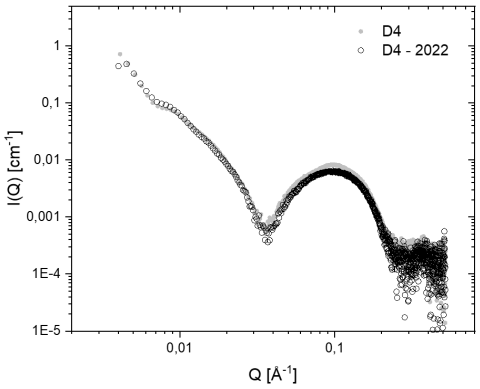

(a) D4 2022

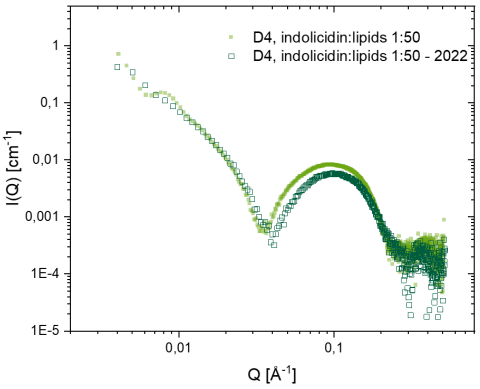

(b) D4 1:50 2022

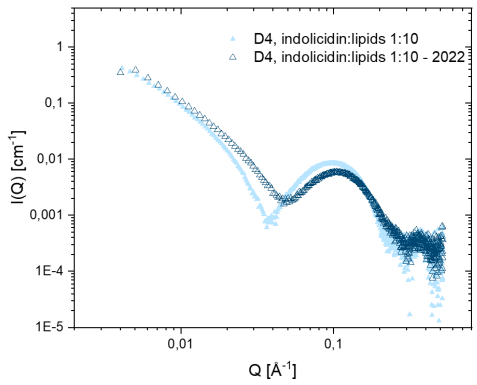

(c) D4 1:10 2022

Figure 7.12: SAXS data comparing the scattering obtained at BM29 for the D4 samples in 2020 and 2022 to confirm that the labels of the samples returned in 2020 were indeed switched.

7.10 Fitting data

Explanations of parameter names are given in table 7.7.

Table 7.7: Model parameters and full names.

Parameter	Full name	Parameter	Full name
Ri	inner radius	Rsc	bicelle radius
ti	thickness. inner headgroup shell	L	length of bicelle
to	thickness. outer headgroup shell	dL	thickness of face micellar shell
Dc	thickness. hydrocarbon region	dRsc	thickness of side micellar shell
sigma_c	disorder parameter. hydrocarbon region	fp_tail	fraction of peptide inside tail region
sigma_ti	disorder parameter. inner headgroup shell	Vtot_lipid_b	total volume of lipid
sigma_to	disorder parameter. outer headgroup shell	fw_dL	fraction of water in dL
fwi	fraction of water in inner shell	fw_dR	fraction of water in dRsc
fwo	fraction of water in outer shell	f_surf_dR	fraction of peptide in dRsc
conc_lip	concentration of lipids. mg/ml	dEqual	if =1 the ratio of lipids and peptides in dRsc is the same
conc_pep	concentration of peptide. mg/ml	f_lipid_dR	fraction of lipids in dRsc
ratioPL	calculated peptide:lipid ratio	bhead_lipid	number of electrons. lipid head
Rgp	radius of gyration. peptide	btail_lipid	number of electrons. lipid tail
Mwp	molecular weight peptide. g/ml	sigma_shell	disorder parameter. bicelle shell
dp	peptide density	sigma_core	disorder parameter. bicelle core
f_free	fraction of free peptide	f_uni	fraction of unilamellar liposomes
VtotL	lipid total volume	Nu	diffuse background
VheadL	volume of lipid headgroup	N	number of consecutive bilayers
d_tailL	density of lipid tail	sigma_d	variance
M_tail	average lipid tail molecular weight	d	distance between consecutive layers
Ml	average lipid total molecular weight	Delta	stacking disorder parameter
Zhead	number of electrons. lipid head		
Ztail	number of electrons. lipid tail		
RhoSolvent	SLD solvent		
dens_sol	density of solvent. g/cm3		
Z_chol	number of electrons. cholesterol		
d_chol	density. cholesterol		
f_chol	fraction of cholesterol		
bcg	background		
Rtot	total radius (calculated)		
P_lip	Aggregation number		
fp_OS	fraction of peptide in outer shell		
fp_HC	fraction of peptide in hydrocarbon region		
fp_IS	fraction of peptide in inner shell		
RhoP0	SLD peptide		
fPEG	fraction PEG		
sigma_cPD	polydispersity parameter. bilayer thickness		
MPEG	molecular weight. DMPE-PEG		
Rg	radius of gyration PEG		
f_inner	fraction PEG in inner leaflet		
RhoPEG	SLD-PEG		
f_linM	fraction of lipids in micelles		
f_pinM	fraction peptide in micelles		
R_mic	radius of micelles		
r_R_Rsc	ratio (radius of liposomes):(radius of bicelles)		

7.10.1 DMPC/Cholesterol

The following tables are raw-data of the analytical model fits. Parameters marked with "literature values" were estimated based on the following articles: [20, 71, 109].

Table 7.8: DMPC 0 % cholesterol liposomes

Parameters	**0:1**	**1:50**	**1:20**	**1:10**	**Fitted?**
Ri [Å]	360 ± 3	451 ± 3	490 ± 3	500 ± 3	yes
ti [Å]	6 ± 3	6 ± 3	6 ± 3	6 ± 3	yes
to [Å]	6 ± 3	6 ± 3	6 ± 3	6 ± 3	yes
Dc [Å]	23 ± 1	22 ± 1	21 ± 1	21 ± 1	yes
sigma_c	2.5 ± 0.2	2.0 ± 0.2	1.5 ± 0.2	1.0 ± 0.2	yes
sigma_ti	5± 1	4 ± 1	5± 1	5 ± 1	yes
sigma_to	5 ± 1	5± 1	5± 1	5± 1	yes
fwi	0.16 ± 0.08	0.21± 0.08	0.24± 0.08	0.25± 0.08	calculated
fwo	0.21± 0.08	0.24± 0.08	0.26± 0.08	0.27± 0.08	calculated
conc_lip [mg/ml]	2.5 ± 0.1	2.6 ± 0.1	2.5± 0.1	2.5± 0.1	yes
conc_pep [mg/ml]	0	0.13 ± 0.03	0.33 ± 0.03	0.65 ± 0.03	yes
ratioPL	0	0.02	0.04	0.08	yes
Rgp [Å]	12	12	18	12	literature value
Mwp [g/mol]	1906	1906	1906	1906	no
dp [g/cm3]	1.35	1.35	1.35	1.35	no
f_free	0	0 ± 0.1	0± 0.1	0± 0.1	yes
VtotL [Å3]	1100.21	1100.20	1100.20	1100.20	calculated
VheadL [Å3]	330	330	330	330	literature value
d_tailL [g/cm3]	0.79 ± 0.02	0.79± 0.02	0.79± 0.02	0.79± 0.02	yes
M_tail [g/mol]	366.7	366.7	366.7	366.7	no
Ml [g/mol]	677.9	677.9	677.9	677.9	no
ZHead	164	164	164	164	no
ZTail	210	210	210	210	no
RhoSolvent [cm-2]	9.43E10	9.43E10	9.43E10	9.43E10	no
dens_sol	1	1	1	1	no
Z_chol	215	215	215	215	no
d_chol [g/cm3]	1.02	1.02	1.02	1.02	literature values
f_chol	0	0	0	0	no
bcg	2.7E-4	2.7E-4	2E-4	2.7E-4	yes
Rtot [Å]	395 ± 3	485 ± 3	523 ± 3	533 ± 3	calculated
P_lip	53921	78634	89573	91491	calculated
fp_OS	0.50 ± 0.2	0.25 ± 0.2	0.09 ± 0.2	0.18 ± 0.2	yes
fp_HC	0.00 ± 0.2	0.75 ± 0.2	0.91 ± 0.2	0.82 ± 0.2	yes
fp_IS	0.50 ± 0.2	0.00 ± 0.2	0.00 ± 0.2	0.00± 0.2	yes
RhoP0 [cm-2]	1.22E11	1.22E11	1.22E11	1.22E11	literature values
fPEG	0.025	0.025	0.025	0.025	no
sigma_cPD	0	0	0	0.05	yes
MPEG [g/mol]	2693.32	2693.32	2693.32	2693.32	no
Rg [Å]	15	15	15	15	no
f_inner	0.5	0.5	0.5	0.5	yes
RhoPEG [cm-2]	1.11E11	1.11E11	1.11E11	1.11E11	no
f_linM	0	0	0	0.01 ± 0.002	yes
f_pinM	0	0	0	0.045 ± 0.006	yes
R_mic [Å]	30	30	30	25 ± 8	yes
Sigma_Gauss_SD	0.27	0.34	0.27	0.4	yes

Table 7.9: DMPC 20 % cholesterol liposomes

Parameters	**0:1**	**1:100**	**1:50**	**1:20**	**Fitted?**
Ri [Å]	450 ± 3	450 ± 3	450 ± 3	500 ± 3	yes
ti [Å]	7 ± 3	7 ± 3	7 ± 3	7 ± 3	yes
to [Å]	5 ± 3	5± 3	5± 3	5± 3	yes
Dc [Å]	28 ± 1	26± 1	26 ± 1	24± 1	yes
sigma_c	6± 0.2	5.3± 0.2	5.3± 0.2	3.9± 0.2	yes
sigma_ti	5± 1	5± 1	5± 1	5 ± 1	yes
sigma_to	5 ± 1	5± 1	5± 1	5± 1	yes
fwi	0.28 ± 0.08	0.33 ± 0.08	0.33 ± 0.08	0.33± 0.08	calculated
fwo	0.13± 0.08	0.19± 0.08	0.19± 0.08	0.25± 0.08	calculated
conc_lip [mg/ml]	2.5 ± 0.1	2.5 ± 0.1	2.5± 0.1	2.5± 0.1	yes
conc_pep [mg/ml]	0	0.07± 0.03	0.13± 0.03	0.33± 0.03	yes
ratioPL	0	0.009	0.013	0.044	yes
Rgp [Å]	12	12	12	12	literature value
Mwp [g/mol]	1906	1906	1906	1906	no
dp [g/cm3]	1.35	1.35	1.35	1.35	no
f_free	0	0	0.3	0	yes
VtotL [Å3]	1144.2	1144.2	1144.2	1144.2	calculated
VheadL [Å3]	330	330	330	330	literature value
d_tailL [g/cm3]	0.71 ± 0.02	0.71 ± 0.02	0.71± 0.02	0.71± 0.02	yes
M_tail [g/mol]	366.7	366.7	366.7	366.7	no
Ml [g/mol]	677.9	677.9	677.9	677.9	no
ZHead	164	164	164	164	no
ZTail	210	210	210	210	no
RhoSolvent [cm-2]	9.43E10	9.43E10	9.43E10	9.43E10	no
dens_sol	1	1	1	1	no
Z_chol	216	216	216	216	no
d_chol [g/cm3]	1.02	1.02	1.02	1.02	literature values
f_chol	0.2	0.2	0.2	0.2	no
bcg	1.5E-4	2E-4	2E-4	2E-4	yes
Rtot [Å]	490 ± 3	488± 3	488± 3	536± 3	calculated
P_lip	95724	88503	88503	99627	caluclated
fp_OS	0.50 ± 0.2	0.50± 0.2	0.50± 0.2	0.25± 0.2	yes
fp_HC	0.00 ± 0.2	0.00± 0.2	0.50± 0.2	0.75± 0.2	yes
fp_IS	0.50± 0.2	0.50± 0.2	0.00± 0.2	0.00± 0.2	yes
RhoP0 [cm-2]	1.22E11	1.22E11	1.22E11	1.22E11	literature values
fPEG	0.025	0.025	0.025	0.025	no
sigma_cPD	0	0	0	0	yes
MPEG [g/mol]	2693.32	2693.32	2693.32	2693.32	no
Rg [Å]	15	15	15	15	no
f_inner	0.5	0.5	0.5	0.5	yes
f_linM	0	0	0	0.054± 0.002	yes
f_pinM	0	0	0	0.770± 0.006	yes
R_mic [Å]	24 ± 8	24 ± 8	24 ± 8	22 ± 8	yes
Sigma_Gauss	0.37 ± 0.05	0.50± 0.05	0.76± 0.05	0.50± 0.05	yes

Table 7.10: DMPC 40 % cholesterol liposomes

Parameters	**0:1**	**1:100**	**1:50**	**Fitted?**
Ri [Å]	420 ± 3	420 ± 3	420± 3	yes
ti [Å]	7± 3	7± 3	7± 3	yes
to [Å]	7± 3	7± 3	7± 3	yes
Dc [Å]	25± 1	25±1	25±1	yes
sigma_c	5.5 ± 0.2	5.7 ± 0.2	5.5 ± 0.2	yes
sigma_ti	5 ± 1	5± 1	5± 1	yes
sigma_to	5 ± 1	5 ± 1	5± 1	yes
fwi	0.53 ± 0.08	0.53± 0.08	0.53± 0.08	calculated
fwo	0.57± 0.08	0.57± 0.08	0.57± 0.08	calculated
conc_lip [mg/ml]	2.3 ± 0.1	2.6 ± 0.1	2.5± 0.1	yes
conc_pep [mg/ml]	0	0.07± 0.03	0.13± 0.03	yes
ratioPL	0	0.00529	0.00529	calculated
Rgp [Å]	12	12	12	literature value
Mwp [g/mol]	1906	1906	1906	no
dp [g/cm3]	1.35	1.35	1.35	no
f_free	0	0.4 ± 0.1	0.4± 0.1	yes
VtotL [Å3]	1169.6	1169.6	1169.6	calculated
VheadL [Å3]	330	330	330	literature value
d_tailL [g/cm3]	0.62± 0.02	0.62± 0.02	0.62± 0.02	yes
M_tail [g/mol]	366.7	366.7	366.7	no
Ml [g/mol]	677.9	677.9	677.9	no
ZHead	164	164	164	no
ZTail	210	210	210	no
RhoSolvent [cm-2]	9.43E10	9.43E10	9.43E10	no
dens_sol	1	1	1	no
Z_chol	216	216	216	no
d_chol [g/cm3]	1.02	1.02	1.02	literature values
f_chol	0.4	0.4	0.4	no
bcg	1.5E-4	2E-4	2E-4	yes
Rtot [Å]	458	458	458	calculated
P_lip	72134.0317	72134.4715	72134.4715	caluclated
fp_OS	nd	0.50± 0.2	0.33± 0.2	yes
fp_HC	nd	0.00± 0.2	0.67± 0.2	yes
fp_IS	nd	0.50± 0.2	0.000± 0.2	yes
RhoP0 [cm-2]	1.22E11	1.22E11	1.22E11	literature values
fPEG	0.025	0.025	0.025	no
sigma_cPD	0	0	0	yes
MPEG [g/mol]	2693.32	2693.32	2693.32	no
Rg [Å]	15	15	15	no
f_inner	0.5	0.5	0.5	yes
RhoPEG [cm-2]	1.11E11	1.11E11	1.11E11	no
f_linM	0	0	0.0004 ± 0.002	yes
f_pinM	0	0	0.001 ± 0.006	yes
R_mic [Å]	nd	nd	25±8	yes
Sigma_Gauss_SD	0.25 ± 0.05	0.37± 0.05	0.35 ± 0.05	yes

Table 7.11: DMPC 40 % cholesterol liposomes with bicelle and micelle formation

Parameters	**1:20**	**Fitted?**	**Parameters**	**1:20**	**Fitted?**
Ri [Å]	416 ± 3	yes	r_R_Rsc	0.45	yes
ti [Å]	6 ± 3	yes	L [Å]	25 ± 1	yes
to [Å]	7 ± 3	yes	dL	7.8± 0.6	yes
Dc [Å]	24 ± 1	yes	dRsc	6.1± 0.3	yes
sigma_c	5 ± 0.2	yes	fp_tail	0.8 ± 0.2	yes
sigma_ti	5± 1	yes	Vtot_lipid_b	1103 ± 3	yes
sigma_to	5± 1	yes	fw_dL	0.46 ± 0.008	calculated
fwi	0.48± 0.08	calculated	fw_dR	0.46 ± 0.008	calculated
fwo	0.58± 0.08	calculated	f_pep_dR	0.15	calculated
conc_lip [mg/ml]	2.5± 0.1	yes	sigma_shell	4 ± 1	yes
conc_pep [mg/ml]	0.33 ± 0.03	yes	sigma_core	2± 1	yes
ratioPL	0.026	calculated	RhoTail	8.14138E10	calculated
Rgp [Å]	12	literature value	RhoHead_dR	1.39295E11	calculated
Mwp [g/mol]	1906	no	P	3135	calculated
dp [g/cm3]	1.35	no	r_pep_lipid	0.038	calculated
f_free	0.4 ± 0.1	yes	dEqual	1	yes
VtotL [Å3]	1169.6	calculated	f_lipid_dR	0.15	calculated
VheadL [Å3]	330	literature value	RhoHead_dL	1.39295E11	calculated
d_tailL [g/cm3]	0.62 ± 0.02	yes	Rsc	187.57	calculated
M_tail [g/mol]	366.7	no	f_bic	0.87	yes
Ml [g/mol]	677.9	no	bhead_lipid	164	no
ZHead	164	no	btail_lipid (with chol)	212.4	no
ZTail	210	no	Sigma_Gauss_SD	0.450 ± 0.05	yes
RhoSolvent [cm-2]	9.43E10	no			
dens_sol	1	no			
Z_chol	216	no			
d_chol [g/cm3]	1.02	literature values			
f_chol	0.4	no			
bcg	1.98143E-4	yes			
Rtot [Å]	453 ± 3	calculated			
P_lip	67851	caluclated			
fp_OS	0.29 ± 0.2	yes			
fp_HC	0.21 ± 0.2	yes			
fp_IS	0.50 ± 0.2	yes			
RhoP0 [cm-2]	1.22E11	literature values			
fPEG	0.025	no			
sigma_cPD	0.076	yes			
MPEG [g/mol]	2693.32	no			
Rg [Å]	15	no			
f_inner	0.5	yes			
RhoPEG [cm-2]	1.11E11	no			
f_linM	0.012 ± 0.002	yes			
f_pinM	0.246 ± 0.006	yes			
R_mic [Å]	27 ± 8	yes			

Table 7.12: Bicelle fitting values. DMPC and cholesterol samples

Parameter	**0 chol. 1:5**	**20 chol. 1:10**	**20 chol. 1:5**	**40 chol. 1:10**	**40 chol. 1:5**	**Fitted?**
Rsc [Å]	103 ± 10	113 ± 10	54 ± 10	120 ± 10	110 ± 10	yes
L [Å]	25± 1	25± 1	25± 1	23± 1	26± 1	yes
dL [Å]	10.5 ± 0.6	9.7 ± 0.6	7.9 ± 0.6	6.3± 0.6	8.4± 0.6	yes
dRsc [Å]	6.0 ± 0.3	11.3± 0.3	11.7± 0.3	5.5± 0.3	5.5± 0.3	yes
conc_pep [mg/ml]	1.30 ± 0.1	0.65± 0.1	1.30 ± 0.1	0.65± 0.1	1.30± 0.1	yes
conc_lip [mg/ml]	2.5± 0.1	2.5± 0.1	2.5± 0.1	2.5± 0.1	2.5± 0.1	yes
dens_pep [g/cm3]	1.35	1.35	1.35	1.35	1.35	no
fp_tail	0.6 ± 0.2	0.5± 0.2	0.4± 0.2	0.4± 0.2	0.4± 0.2	yes
Vhead_lipid [Å3]	330	330	330	330	330	literature values
Vtot_lipid [Å3]	1150.6	1108.8	1138.6	1124.6	1174.9	yes
Vhead_dL [Å3]	437.8	347.5	428.9	380.9	466.1	calculated
bcg	0.00038	2.5E-4	3.5E-4	2E-4	2.8E-4	yes
fw_dL	0.510±0.008	0.490±0.008	0.290±0.008	0.187±0.008	0.268±0.008	calculated
fw_dR	0.663±0.008	0.750±0.008	0.806±0.008	0.472±0.008	0.412±0.008	calculated
f_peptide_dR	0.16 ± 0.2	0.16± 0.2	0.16± 0.2	0.16± 0.2	0.16± 0.2	calculated
Mw_lip [g/mol]	677.93	677.95	677.95	677.9	677.9	no
Mw_pep [g/mol]	1906	1906	1906	1906	1906	no
b_peptide	1018	1018	1018	1018	1018	no
Vhead_dR [Å3]	78.97	81.63	146.70	65.66	97.32	calculated
btail_lipid	210	211.2	211.2	212.4	212.4	no
bhead_lipid	164	164	164	164	164	no
RhoSolvent [cm-2]	9.43E+10	9.43E10	9.43E10	9.43E10	9.43E10	no
sigma_shell	1 ± 1	3 ± 1	4± 1	4± 1	2± 1	yes
sigma_core	1 ± 1	1± 1	2± 1	3± 1	4± 1	yes
Vtail [Å3]	1068 ± 3	878± 3	959± 3	858± 3	971± 3	yes
Mchol [g/mol]	386.65	386.65	386.65	386.65	386.65	no
f_chol	0	0.2	0.2	0.4	0.4	no
IntegralRel	1E-07	1E-7	1E-7	1E-7	1E-7	
P	786	1144	235	1213	1007	calculated
r_peptide_lipid	0.185	0.085	0.169	0.077	0.153	calculated
dEqual	0	0	0	0	0	
f_lipid_dR	0.15	0.2	0.327	0.14	0.183	yes
Sigma_Gauss_SD	0.300± 0.05	0.300± 0.05	0.613± 0.05	0.667± 0.05	0.614± 0.05	yes

7.10.2 DSPC/Cholesterol

Table 7.13: DSPC with 0% cholesterol fitting values

Parameter	DSPC	DSPC. 1:100	DSPC. 1:50	DSPC. 1:10	Fitted?
Ri	600±3	600±3	600±3	600±3	yes
ti	7±3	7±3	7 ±3	7±3	yes
to	6±3	6±3	6±3	6±3	yes
Dc	34±1	31 ±1	31±1	30±1	yes
sigma_c	2.1±0.2	2.1±0.2	2.1±0.2	2.4±0.2	yes
sigma_ti	3±1	5±1	5±1	4±1	yes
sigma_to	5±1	5±1	5±1	5±1	yes
fwi	0.12 ±0.08	0.17±0.08	0.17±0.08	0.20±0.08	yes
fwo	0.04 ±0.08	0.10±0.08	0.10±0.08	0.13±0.08	yes
conc_lip	2.5 ±0.1	2.5±0.1	2.5±0.1	2.5±0.1	yes
conc_pep	0	0.06±0.13	0.11±0.13	0.57±0.3	yes
ratioPL	0	0.00936	0.01254	0.06045	calculated
Rgp	12	12	12	12	literature values
Mwp	1906	1906	1906	1906	no
dp	1.35	1.35	1.35	1.35	literature values
f_free	0	0.5 ±0.1	0.3 ±0.1	0.3 ±0.1	yes
VtotL	1243.65	1243.65	1243.65	1243.65	calculated
VheadL	330	330	330	330	literature values
d_tailL	0.571±0.02	0.57±0.02	0.57±0.02	0.57±0.02	yes
M_tail	311.25	311.25	311.25	311.25	no
Ml	790.15	790.15	790.15	790.15	no
ZHead	164	164	164	164	no
ZTail	274	274	274	274	no
RhoSolvent	9.43E10	9.43E10	9.43E10	9.43E10	calculates
dens_sol	1	1	1	1	no
Z_chol	216	216	216	216	no
d_chol	1.05	1.05	1.05	1.05	no
f_chol	0	0	0	0	no
bcg	2E-4	2E-4	1.5E-4	2E-4	yes
Rtot	645±3	644±3	644±3	641±3	calculated
P_lip	184735	165257	165257	164525	calculated
fp_OS	0.0±0.2	0.5±0.2	0.0±0.2	0.0±0.2	yes
fp_HC	0.5 ±0.2	0.0±0.2	0.5±0.2	0.5±0.2	yes
fp_IS	0.5±0.2	0.5±0.2	0.5±0.2	0.5±0.2	yes
RhoP0	1.22E11	1.22E11	1.22E11	1.22E11	calculated
fPEG	0.025	0.025	0.025	0.025	no
MPEG	2693.32	2693.32	2693.32	2693.32	no
Rg	15	15	15	15	no
f_inner	0.5	0.5	0.5	0.5	no
RhoPEG	1.11E11	1.11E11	1.11E11	1.11E11	literature values
f_linM	0	0.005±0.002	0.003±0.002	0.048±0.002	yes
f_pinM	0	0.500±0.006	0.05±0.006	0.525±0.006	yes
R_mic	nd	20±8	31 ±8	31±8	yes
Sigma_Gauss_SD	0.40±0.05	0.40±0.05	0.40±0.05	0.40±0.05	yes

Table 7.14: DSPC with 20% cholesterol fitting values

Parameter	DSPC 20% Chol	DSPC, 1:50	DSPC, 1:20	DSPC, 1:10	Fitted?
Ri	598±3	598±3	598±3	300±3	yes
ti	7±3	7±3	7±3	7±3	yes
to	11±3	11±3	11±3	11±3	yes
Dc	35±1	35±1	33±1	33±1	yes
sigma_c	5.1±0.2	7.6±0.2	7.1±0.2	7.1±0.2	yes
sigma_ti	4±1	6 ±1	4±1	5±1	yes
sigma_to	5±1	6±1	5±1	5 ±1	yes
fwi	0.21±0.08	0.21±0.08	0.24±0.08	0.23±0.08	yes
fwo	0.54±0.08	0.54±0.08	0.56±0.08	0.59±0.08	yes
conc_lip	2.5 ±0.1	2.5±0.1	2.5±0.1	2.6±0.1	yes
conc_pep	0	0.13±0.03	0.32±0.03	0.65±0.03	yes
ratioPL	0	0.0211	0.03023	0.04695	calculated
Rgp	12	12	12	12	literature values
Mwp	1906	1906	1906	1906	no
dp	1.35	1.35	1.35	1.35	literature values
f_free	0	0 ±0.1	0.4±0.1	0.5±0.1	yes
VtotL	1258.08	1258.08	1258.08	1258.08	calculated
VheadL	330	330	330	330	literature values
d_tailL	0.51 ±0.02	0.51±0.02	0.51±0.02	0.51±0.02	yes
M_tail	311.25	311.25	311.25	311.25	no
Ml	790.15	790.15	790.15	790.15	no
ZHead	164	164	164	164	no
ZTail	274	274	274	274	no
RhoSolvent	9.43E10	9.43E10	9.43E10	9.43E10	calculates
dens_sol	1	1	1	1	no
Z_chol	216	216	216	216	no
d_chol	1.12	1.12	1.12	1.12	no
f_chol	0.2	0.2	0.2	0.2	no
bcg	2E-4	2E-4	2E-4	2E-4	yes
Rtot	650±3	650±3	649±3	350±3	calculated
P_lip	183482	183482	177951	46679	calculated
fp_OS	0.0±0.2	0.5±0.2	0.5±0.2	0.5±0.2	yes
fp_HC	0.5±0.2	0.0±0.2	0.0±0.2	0.0±0.2	yes
fp_IS	0.5±0.2	0.5±0.2	0.5±0.2	0.5±0.2	yes
RhoP0	1.22E11	1.22E11	1.22E11	1.22E11	calculated
fPEG	0.025	0.025	0.025	0.025	no
MPEG	2693.32	2693.32	2693.32	2693.32	no
Rg	15	15	15	15	no
f_inner	0.5	0.5	0.5	0.5	yes
RhoPEG	1.11E11	1.11E11	1.11E11	1.11E11	literature values
f_linM	0.002 ±0.002	0.002 ±0.002	0.015±0.002	0.01±0.002	yes
f_pinM	0	0±0.006	0.180±0.006	0.400±0.006	yes
R_mic	30±8	30±8	24±8	24±8	yes
Sigma_Gauss_SD	0.40±0.05	0.40±0.05	0.40±0.05	0.80±0.05	yes

Table 7.15: DSPC with 40% cholesterol fitting values

Parameter	DSPC 40% Chol	peptide:lipid 1:50	peptide:lipid 1:20	Fitted?
Ri	455 ±3	440±3	431±3	yes
ti	5 ±3	9±3	9±3	yes
to	8±3	5 ±3	7±3	yes
Dc	35±1	34±1	32±1	yes
sigma_c	8.0±0.2	7.7±0.2	7.7±0.2	yes
sigma_ti	5±1	5±1	5±1	yes
sigma_to	5±1	5±1	5 ±1	yes
fwi	0.28±0.08	0.61±0.08	0.64±0.08	yes
fwo	0.56±0.08	0.36±0.08	0.55±0.08	yes
conc_lip	2.5 ±0.1	2.7 ±0.1	2.4±0.1	yes
conc_pep	0	0.13±0.03	0.325 ±0.03	yes
ratioPL	0	0.0137	0.04198	calculated
Rgp	12	12	12	literature values
Mwp	1906	1906	1906	no
dp	1.35	1.35	1.35	literature values
f_free	0	0.3 ±0.1	0.2±0.1	yes
VtotL	1336.09	1336.09	1336.09	calculated
VheadL	330	330	330	literature values
d_tailL	0.40±0.02	0.40±0.0	0.40±0.0	yes
M_tail	311.25	311.25	311.25	no
Ml	790.15	790.15	790.15	no
ZHead	164	164	164	no
ZTail	274	274	274	no
RhoSolvent	9.43E10	9.43E10	9.43E10	calculates
dens_sol	1	1	1	no
Z_chol	216	216	216	no
d_chol	1.12	1.12	1.12	no
f_chol	0.4	0.4	0.4	no
bcg	1.5E-4	1.5E-4	1.5E-4	yes
Rtot	502±3	488±3	479±3	calculated
P_lip	99618	92261	83021	calculated
fp_OS	0.5 ±0.2	0.0±0.2	0.0±0.2	yes
fp_HC	0.0±0.2	1.0±0.2	1.0±0.2	yes
fp_IS	0.5±0.2	0.0±0.2	0.0±0.2	yes
RhoP0	1.22E11	1.22E11	1.22E11	calculated
fPEG	0.025	0.025	0.025	no
MPEG	2693.32	2693.32	2693.32	no
Rg	15	15	15	no
f_inner	0.5	0.5	0.5	yes
RhoPEG	1.11E11	1.11E11	1.11E11	literature values
f_linM	0	0	0.011 ±0.002	yes
f_pinM	0	0	0.180±0.006	yes
R_mic	nd	nd	30 ±8	yes
Sigma_Gauss_SD	0.250±0.005	0.300±0.005	0.350±0.005	yes

7.10.3 DOPC/Cholesterol

Table 7.16: DOPC with 0% cholesterol fitting values

Parameter	DOPC 0% Chol	peptide:lipid 1:10	Fitted?
Ri	406±3	407±3	yes
ti	6 ±3	6±3	yes
to	6±3	6±3	yes
Dc	24±1	24 ±1	yes
sigma_c	5.0±0.2	2.8±0.2	yes
sigma_ti	3±1	3±1	yes
sigma_to	5±1	5±1	yes
fwi	0.29±0.08	0.29±0.08	yes
fwo	0.35±0.08	0.35±0.08	yes
conc_lip	2.5±0.1	2.5 ±0.	yes
conc_pep	0	0.57 ±0.1	yes
ratioPL	0	0.08595	calculated
Rgp	12	12	literature values
Mwp	1906	1906	no
dp	1.35	1.35	literature values
f_free	0	0±0.1	yes
VtotL	1299.65	1299.65	calculated
VheadL	330	330	literature values
d_tailL	0.53±0.02	0.53±0.02	yes
M_tail	311.25	311.25	no
Ml	786.11	786.11	no
ZHead	164	164	no
ZTail	270	270	no
RhoSolvent	9.43E10	9.43E10	calculates
dens_sol	1	1	no
Z_chol	216	216	no
d_chol	1.01	1.01	no
f_chol	0	0	no
bcg	1E-4	2E-4	yes
Rtot	442±3	443±3	calculated
P_lip	55821	56284	calculated
fp_OS	nd	0.1	yes
fp_HC	nd	0.9±0.2	yes
fp_IS	nd	0.00±0.2	yes
RhoP0	1.22E11	1.22E11	calculated
fPEG	0.025	0.025	no
MPEG	2693.32	2693.32	no
Rg	15	15	no
f_inner	0.5	0.5	yes
RhoPEG	1.11E11	1.11E11	literature values
Sigma_Gauss_SD	0.40 ±0.05	0.8	yes

Table 7.17: DOPC with 20% cholesterol fitting values

Parameter	DOPC 20% Chol	peptide:lipid 1:10	Fitted?
Ri	406±3	405±3	yes
ti	6 ±3	6±3	yes
to	6±3	6±3	yes
Dc	29±1	35±1	yes
sigma_c	7.3 ±0.2	8.8±0.2	yes
sigma_ti	3±1	3±1	yes
sigma_to	5±1	5±1	yes
fwi	0.33±0.08	0.18±0.08	yes
fwo	0.39±0.08	0.27±0.08	yes
conc_lip	2.5±0.1	2.5±0.1	yes
conc_pep	0	0.63±0.03	yes
ratioPL	0	0.0659	calculated
Rgp	12	12	literature values
Mwp	1906	1906	no
dp	1.35	1.35	literature values
f_free	0	0.3±0.1	yes
VtotL	1327.84	1327.84	calculated
VheadL	330	330	literature values
d_tailL	0.48±0.02	0.48±0.02	yes
M_tail	311.25	311.25	no
Ml	786.11	786.11	no
ZHead	164	164	no
ZTail	270	270	no
RhoSolvent	9.43E10	9.43E10	calculates
dens_sol	1	1	no
Z_chol	216	216	no
d_chol	1.01	1.01	no
f_chol	0.2	0.2	no
bcg	1E-4	1.5E-4	yes
Rtot	447±3	452±3	calculated
P_lip	66423	80780	calculated
fp_OS	0.0±0.2	0.0±0.2	yes
fp_HC	0.9±0.2	1.0±0.2	yes
fp_IS	0.1±0.2	0.0±0.2	yes
RhoP0	1.22E11	1.22E11	calculated
fPEG	0.025	0.025	no
MPEG	2693.32	2693.32	no
Rg	15	15	no
f_inner	0.5	0.5	yes
RhoPEG	1.11E11	1.11E11	literature values
Sigma_Gauss_SD	0.80 ±0.05	0.80±0.50	yes

Table 7.18: DOPC with 40% cholesterol fitting values

Parameter	DOPC 40% Chol	peptide:lipid 1:20	peptide:lipid 1:10	Fitted?
Ri	405±3	300±3	405±3	yes
ti	6 ±3	6±3	6±3	yes
to	6 ±3	6±3	6±3	yes
Dc	35 ±1	30±1	30±1	yes
sigma_c	8.8 ±0.2	6.8±0.2	6.2±0.2	yes
sigma_ti	3±1	3±1	3±1	yes
sigma_to	5±1	5±1	5±1	yes
fwi	0.39 ±0.08	0.45±0.08	0.48±0.08	yes
fwo	0.45±0.08	0.52±0.08	0.53±0.08	yes
conc_lip	2.5 ±0.1	2.5±0.1	2.5±0.1	yes
conc_pep	0	0.35±0.03	0.71±0.03	yes
ratioPL	0	0.03821	0.0734	calculated
Rgp	12	12	12	literature values
Mwp	1906	1906	1906	no
dp	1.35	1.35	1.35	literature values
f_free	nd	0.3±0.1	0.3±0.1	yes
VtotL	1325.31	1317.61	1325.31	calculated
VheadL	330	330	330	literature values
d_tailL	0.419 ±0.02	0.42±0.02	0.42±0.02	yes
M_tail	311.25	311.25	311.25	no
Ml	786.11	786.11	786.11	no
ZHead	164	164	164	no
ZTail	270	270	270	no
RhoSolvent	9.43E10	9.43E10	9.43E10	calculates
dens_sol	1	1	1	no
Z_chol	216	216	216	no
d_chol	1.01	1.01	1.01	no
f_chol	0.4	0.4	0.4	no
bcg	1E-4	2E-4	2E-4	yes
Rtot	451±3	342±3	447±3	calculated
P_lip	80985	39969	68597	calculated
fp_OS	0.0±0.2	0.0±0.2	0.0±0.2	yes
fp_HC	1.0±0.2	1.0±0.2	1.0±0.2	yes
fp_IS	0.0±0.2	0.0 ±0.2	0.0±0.2	yes
RhoP0	1.22E11	1.22E11	1.22E11	calculated
fPEG	0.025	0.025	0.025	no
MPEG	2693.32	2693.32	2693.32	no
Rg	15	15	15	no
f_inner	0.5	0.5	0.5	yes
RhoPEG	1.11E11	1.11E11	1.11E11	literature values
f_linM	0	0	0.001 ±0.002	yes
f_pinM	0	0	0.001 ±0.006	yes
R_mic	nd	nd	30±8	yes
Sigma_Gauss_SD	0.5	0.7835	0.5	yes

POPC + Cholesterol

Table 7.19: Fitting values. POPC with 0% cholesterol

Parameter	POPC	POPC. peptide:lipid 1:5	Fitted?
Ri	267± 3	267±3	yes
ti	10±3	10±39	yes
to	10±3	10±3	yes
Dc	27±1	21±1	yes
sigma_c	2±0.2	1±0.2	yes
sigma_ti	1±1	1± 1	yes
sigma_to	1± 1	1±1	yes
fwi	0.48± 0.08	0.60±0.08	yes
fwo	0.56±0.08	0.66± 0.08	yes
conc_lip	2.5± 0.1	2.5± 0.1	yes
conc_pep	0	1.3± 0.03	yes
ratioPL	0	0.1678	calculated
Rgp	12	12	literature values
Mwp	1906	1906	no
dp	1.35	1.35	literature values
f_free	0	0.05± 0.1	yes
VtotL	1256.88	1256.88	calculated
VheadL	330	330	literature values
d_tailL	0.85± 0.02	0.85± 0.02	yes
M_tail	475	475	no
Ml	786	786	no
ZHead	164	164	no
ZTail	256	256	no
RhoSolvent	9.43E10	9.43E10	calculates
dens_sol	1	1	no
Z_chol	216	216	no
d_chol	1.03	1.03	no
f_chol	0	0	no
bcg	1.5E-4	1.5E-4	yes
Rtot	315± 3	309±3	calculated
P_lip	30980	23805	calculated
fp_OS	0.50± 0.2	0.44±0.2	yes
fp_HC	0.46±0.2	0.56±0.2	yes
fp_IS	0.04±0.2	0±0.2	yes
RhoP0	1.22E11	1.22E11	calculated
fPEG	0.025	0.025	no
MPEG	2693.32	2693.32	no
Rg	15	15	no
f_inner	0.5	0.5	no
RhoPEG	1.11E11	1.11E11	literature values
f_uni	0.92± 0.03	0.97± 0.03	yes
Nu	1± 5	1± 5	yes
N	4± 1	4±1	yes
sigma_d	1± 5	1±5	yes
d	59± 2	59± 2	yes
Delta	5±3	5±3	yes
Sigma_Gauss_SD	0.6± 0.05	0.6± 0.05	yes

Table 7.20: Fitting values. POPC with 20% cholesterol

Parameter	POPC 20% Chol	POPC 40% Chol. peptide:lipid 1:5	Fitted?
Ri	348± 3	263± 3	yes
ti	7±3	7±3	yes
to	7± 3	7±3	yes
Dc	28±1	20 28±1	yes
sigma_c	4.7±0.2	4.4±0.2	yes
sigma_ti	4 28±1	6 28±1	yes
sigma_to	4 28±1	728±1	yes
fwi	0.42±0.08	0.58±0.08	calculated
fwo	0.48±0.08	0.63±0.08	calculated
conc_lip	2.5±0.1	2.5±0.1	yes
conc_pep	0	1.30±0.03	yes
ratioPL	0	0.17657	calculated
Rgp	12	12	literature values
Mwp	1906	1906	no
dp	1.35	1.35	literature values
f_free	0	0± 0.1	yes
VtotL	1290.49	1290.57	calculated
VheadL	330	330	literature values
d_tailL	0.76± 0.02	0.76±0.02	yes
M_tail	475	475	no
Ml	786	786	no
ZHead	164	164	no
ZTail	256	256	no
RhoSolvent	9.43E10	9.43E10	calculates
dens_sol	1	1	no
Z_chol	216	216	no
d_chol	1.03	1.03	no
f_chol	0.2	0.2	no
bcg	1.3E-4	1.3E-4	yes
Rtot	390± 3	297±3	calculated
P_lip	49796	20455	calculated
fp_OS	0.50± 0.2	0.50±0.2	yes
fp_HC	0.28± 0.2	0.46± 0.2	yes
fp_IS	0.22± 0.2	0.04±0.2	yes
RhoP0	1.22E11	1.22E11	calculated
fPEG	0.025	0.025	no
MPEG	2693.32	2693.32	no
Rg	15	15	no
f_inner	0.5	0.5	no
RhoPEG	1.11E11	1.11E11	literature values
f_uni	0.95± 0.03	1.00± 0.03	yes
Nu	15± 5	15±5	yes
N	3± 1	3±1	yes
sigma_d	1± 5	1±5	yes
d	65± 3	65± 3	yes
Delta	0± 3	0± 3	yes
Sigma_Gauss_SD	0.320±0.007	0.630±0.007	yes

Table 7.21: Fitting values. POPC with 40% cholesterol

Parameter	POPC 40% Chol	POPC 40% Chol. peptide:lipid 1:10	Fitted?
Ri	320± 3	250±3	yes
ti	6± 3	6± 3	yes
to	8±3	8±3	yes
Dc	27±1	23±1	yes
sigma_c	3.5±0.2	5.0±0.2	yes
sigma_ti	6±1	6± 1	yes
sigma_to	6±1	6±1	yes
fwi	0.515±0.08	0.58±0.08	calculated
fwo	0.66±0.08	0.71±0.08	yes
conc_lip	2.4± 0.1	2.6± 0.1	yes
conc_pep	0	0.65± 0.03	yes
ratioPL	0	0.09346	calculated
Rgp	12	12	literature values
Mwp	1906	1906	no
dp	1.35	1.35	literature values
f_free	0	0± 0.1	yes
VtotL	1285.71	1285.71	calculated
VheadL	330	330	literature values
d_tailL	0.67± 0.02	0.67± 0.02	yes
M_tail	475	475	no
Ml	786	786	no
ZHead	164	164	no
ZTail	256	256	no
RhoSolvent	9.43E10	9.43E10	calculates
dens_sol	1	1	no
Z_chol	216	216	no
d_chol	1.03	1.03	no
f_chol	0.4	0.4	no
bcg	1.3E-4	1.3E-4	yes
Rtot	360 ± 3	286 ± 3	calculated
P_lip	40122.7008	21624.8389	calculated
fp_OS	0.50 ± 0.2	0.50± 0.2	yes
fp_HC	0.28 ± 0.2	0.28 ± 0.2	yes
fp_IS	0.22 ± 0.2	0.22 ± 0.2	yes
RhoP0	1.22E11	1.22E11	calculated
fPEG	0.025	0.025	no
MPEG	2693.32	2693.32	no
Rg	15	15	no
f_inner	0.5	0.5	no
RhoPEG	1.11E11	1.11E11	literature values
f_uni	0.96 ± 0.03	0.95± 0.03	yes
Nu	6± 5	6± 5	yes
N	2 ± 1	3± 1	yes
sigma_d	1± 5	1± 5	yes
d	63 ± 2	63± 2	yes
Delta	0 ± 3	0 ± 3	yes
Sigma_Gauss_SD	0.450± 0.05	0.800 ± 0.05	yes

7.10.4 Raft forming lipids. December 2020

Table 7.22: S1 liposomes and indolicidin

Parameters	S1 2022 0:1	1:50	Fitted?
Ri [Å]	440 ±3	430±3	yes
ti [Å]	6 ±3	6±3	yes
to [Å]	7±3	7±3	yes
Dc [Å]	34±1	33±1	yes
sigma_c	6 ±0.2	6 ±0.2	yes
sigma_ti	5 ±1	5±1	yes
sigma_to	3 ±1	3±1	yes
fwi	0.32 ±0.08	0.36 ±0.08	calculated
fwo	0.47±0.08	0.49±0.08	calculated
conc_lip [mg/ml]	2.5 ±0.1	2.5±0.1	yes
conc_pep [mg/ml]	0	0.13±0.03	yes
ratioPL	0	0.021	yes
Rgp [Å]	12	12	literature value
Mwp [g/mol]	1906	1906	no
dp [g/cm3]	1.35	1.35	no
f_free	0	0 ±0.1	yes
VtotL [Å3]	1292.8	1292.8	calculated
VheadL [Å3]	330	330	literature value
d_tailL [g/cm3]	0.67 ±0.02	0.67±0.02	yes
M_tail [g/mol]	463.88	463.88	no
Ml [g/mol]	775.12	775.12	no
ZHead	164	164	no
ZTail	265	265	no
RhoSolvent [cm-2]	9.43E10	9.43E10	no
dens_sol	1	1	no
Z_chol	216	216	no
d_chol [g/cm3]	1.07	1.07	literature values
f_chol	0.34	0.34	no
bcg	2E-4	2E-4	yes
Rtot [Å]	488 ±3	476 ±3	calculated
P_lip	96674	88227	calculated
fp_OS	0.50 ±0.2	0.50±0.2	yes
fp_HC	0.50±0.2	0.50±0.2	yes
fp_IS	0.00±0.2	0.00±0.2	yes
RhoP0 [cm-2]	1.22E11	1.22E11	literature values
fPEG	0.025	0.025	no
sigma_cPD	0	0	yes
MPEG [g/mol]	2693.32	2693.32	no
Rg [Å]	15	15	no
f_inner	0.5	0.5	yes
RhoPEG [cm-2]	1.11E11	1.11E11	no
f_linM	nd	0.007 ±0.002	yes
f_pinM	nd	0.030 ±0.006	yes
R_mic [Å]	25 ±8	25±8	yes
Sigma_Gauss	0.260 ±0.007	0.300±0.007	yes

Table 7.23: Bicelle fitting values. S1

Parameter	**S1. 1:10**	**Fitted?**
Rsc [Å]	240 ±10	yes
L [Å]	30±1	yes
dL [Å]	9±0.6	yes
dRsc [Å]	5±0.3	yes
conc_peptide [mg/ml]	0.65±0.03	yes
conc_lipid [mg/ml]	2.5 ± 0.1	yes
dens_peptide [g/cm3]	1.35	no
fp_tail	0.5 ± 0.3	yes
Vhead_lipid [Å3]	330	literature values
Vtot_lipid [Å3]	1232 ±3	yes
Vhead_dL [Å3]	395.9	calculated
bcg	3.5E-4	yes
fw_dL	0.35±0.01	calculated
fw_dR	0.35±0.01	calculated
f_peptide_dR	0.1 ±0.1	calculated
Mw_lipid [g/mol]	690.3	no
Mw_peptide [g/mol]	1906	no
b_peptide	1018	no
Vhead_dR [Å3]	44.4	calculated
btail_lipid	248.3	no
bhead_lipid	164	no
RhoSolvent [cm-2]	9.43E10	no
sigma_shell	5±1	yes
sigma_core	3±1	yes
Vtail [Å3]	1010 ±3	yes
Mchol [g/mol]	5	no
f_chol	0.34	no
IntegralRel	1E-7	
P	5373	calculated
r_peptide_lipid	0.094	calculated
dEqual	1	
f_lipid_dR	0.101 ±0.02	yes
Sigma_Gauss_SD	0.291±0.007	yes

Table 7.24: D2 liposomes and indolicidin

Parameters	**D2 0:1**	**1:50**	**1:10**	**Fitted?**
Ri [Å]	365 ± 3	280 ± 3	280± 3	yes
ti [Å]	6± 3	6± 3	6± 3	yes
to [Å]	9 ± 3	9± 3	9± 3	yes
Dc [Å]	33± 1	33± 1	29± 1	yes
sigma_c	6.3 ± 0.2	6.3 ± 0.2	3.3± 0.2	yes
sigma_ti	5± 1	4 ± 1	4± 1	yes
sigma_to	4± 1	4 ± 1	4 ± 1	yes
fwi	0.21± 0.08	0.20± 0.08	0.29± 0.08	calculated
fwo	0.53± 0.08	0.54± 0.08	0.60± 0.08	calculated
conc_lip [mg/ml]	2.5± 0.1	2.5± 0.1	2.5± 0.1	yes
conc_pep [mg/ml]	0	0.13± 0.03	0.65± 0.03	yes
ratioPL	0	0.02	0.07	calculated
Rgp [Å]	12	12	12	literature value
Mwp [g/mol]	1906	1906	1906	no
dp [g/cm3]	1.35	1.35	1.35	no
f_free	nd	0.1 ± 0.1	0.3± 0.1	yes
VtotL [Å3]	1282.3	1282.3	1282.3	calculated
VheadL [Å3]	330	330	330	literature value
d_tailL [g/cm3]	0.74 ± 0.02	0.74± 0.02	0.74± 0.02	yes
M_tail [g/mol]	463.2	463.2	463.2	no
Ml [g/mol]	774.45	774.45	774.45	no
ZHead	164	164	164	no
ZTail	265.36	265.36	265.36	no
RhoSolvent [cm-2]	9.43E10	9.43E10	9.43E10	no
dens_sol	1	1	1	no
Z_chol	216	216	216	no
d_chol [g/cm3]	1.06	1.06	1.06	literature values
f_chol	0.2145	0.2145	0.2145	no
bcg	1.3E-4	2E-4	2.5E-4	yes
Rtot [Å]	413 ± 3	328± 3	324± 3	calculated
P_lip	65426	39475	34582	caluclated
fp_OS	0.50 ± 0.2	0.25± 0.2	0.11± 0.2	yes
fp_HC	0.50± 0.2	0.75± 0.2	0.39± 0.2	yes
fp_IS	0.00± 0.2	0.0± 0.2	0.50± 0.2	yes
RhoP0 [cm-2]	1.22E11	1.22E11	1.22E11	literature values
fPEG	0.025	0.025	0.025	no
sigma_cPD	0.07 ± 0.03	0.095± 0.03	0.16 ± 0.03	yes
MPEG [g/mol]	2693.32	2693.32	2693.32	no
Rg [Å]	15	15	15	no
f_inner	0.5	0.5	0.5	yes
RhoPEG [cm-2]	1.11E11	1.11E11	1.11E11	no
f_linM	0	0.000 ± 0.002	0.004± 0.002	yes
f_pinM	0	0.014± 0.006	0.045± 0.006	yes
R_mic [Å]	50 ± 8	74± 8	77± 8	yes
Sigma_Gauss_SD	0.350± 0.05	0.450± 0.05	0.550± 0.05	yes

Table 7.25: D4 liposomes and indolicidin

Parameters	**D4 0:1**	**1:50**	**1:10**	**Fitted?**
Ri [Å]	340 ± 3	450 ± 3	450± 3	yes
ti [Å]	8± 3	8 ± 3	8 ± 3	yes
to [Å]	9± 3	9± 3	9± 3	yes
Dc [Å]	30± 1	32± 1	32± 1	yes
sigma_c	6.0± 0.2	6.1± 0.2	6.1± 0.2	yes
sigma_ti	6± 1	5± 1	5± 1	yes
sigma_to	3± 1	3± 1	3± 1	yes
fwi	0.46 ± 0.08	0.43± 0.08	0.43± 0.08	calculated
fwo	0.55± 0.08	0.52± 0.08	0.52± 0.08	calculated
conc_lip [mg/ml]	2.5 ± 0.1	2.5± 0.1	2.5± 0.1	yes
conc_pep [mg/ml]	0	0.13± 0.03	0.65± 0.03	yes
ratioPL	0	0.021	0.10	calculated
Rgp [Å]	18	18	18	literature value
Mwp [g/mol]	1906	1906	1906	no
dp [g/cm3]	1.35	1.35	1.35	no
f_free	0	0	0	yes
VtotL [Å3]	1288.6	1288.6	1288.6	calculated
VheadL [Å3]	330	330	330	literature value
d_tailL [g/cm3]	0.73 ± 0.02	0.73± 0.02	0.73± 0.02	yes
M_tail [g/mol]	461.88	461.88	461.88	no
Ml [g/mol]	773.11	773.11	773.11	no
ZHead	164	164	164	no
ZTail	266.07	266.07	266.07	no
RhoSolvent [cm-2]	9.43E10	9.43E10	9.43E10	no
dens_sol	1	1	1	no
Z_chol	216	216	216	no
d_chol [g/cm3]	1.06	1.06	1.06	literature values
f_chol	0.2145	0.2145	0.2145	no
bcg	1.6E-4	2E-4	2E-4	yes
Rtot [Å]	387 ± 3	498± 3	498± 3	calculated
P_lip	51851	93623	93623	calculated
fp_OS	0.50 ± 0.2	0.50± 0.2	0.50± 0.2	yes
fp_HC	0.00± 0.2	0.50± 0.2	0.32± 0.2	yes
fp_IS	0.50± 0.2	0.00± 0.2	0.18± 0.2	yes
RhoP0 [cm-2]	1.22E11	1.22E11	1.22E11	literature values
fPEG	0.025	0.025	0.025	no
sigma_cPD	0.09 ± 0.03	0.10± 0.03	0.12± 0.03	yes
MPEG [g/mol]	2693.32	2693.32	2693.32	no
Rg [Å]	15	15	15	no
f_inner	0.5	0.5	0.5	yes
RhoPEG [cm-2]	1.11E11	1.11E11	1.11E11	no
f_linM	0	0	0.015 ± 0.002	yes
f_pinM	0	0	0.139± 0.006	yes
R_mic [Å]	nd	nd	30 ± 0.03	yes
f_uni	0.98 ± 0.03	1± 0.03	1± 0.03	yes
Nu	0	nd	nd	yes
N	4 ± 1	nd	nd	yes
sigma_d	0.1 ± 5	nd	nd	yes
d	63 ± 2	nd	nd	yes
Delta	0	nd	nd	yes
Sigma_Gauss_SD	0.320 ± 0.05	0.240± 0.05	0.450± 0.05	yes

Table 7.26: D4 liposomes and indolicidin. SAXS experiment 2022

Parameters	**D4 2022 0:1**	**1:50**	**1:10**	**Fitted?**
Ri [Å]	345 ± 3	300 ± 3	300± 3	yes
ti [Å]	8 ± 3	8± 3	8 ± 3	yes
to [Å]	9± 3	9± 3	9± 3	yes
Dc [Å]	31± 1	30 ± 1	30± 1	yes
sigma_c	7.4 ± 0.2	7.4± 0.2	6.8± 0.2	yes
sigma_ti	7± 1	5± 1	5± 1	yes
sigma_to	4± 1	4± 1	4± 1	yes
fwi	0.44 ± 0.08	0.45± 0.08	0.45± 0.08	calculated
fwo	0.54± 0.08	0.56± 0.08	0.56± 0.08	calculated
conc_lip [mg/ml]	2.5	2.5	2.5	yes
conc_pep [mg/ml]	0	0.13	0.65	yes
ratioPL	0	0.021	0.076	yes
Rgp [Å]	12	12	12	literature value
Mwp [g/mol]	1906	1906	1906	no
dp [g/cm3]	1.35	1.35	1.35	no
f_free	nd	0 ± 0.1	0.2± 0.1	yes
VtotL [Å3]	1288.6	1288.6	1288.6	calculated
VheadL [Å3]	330	330	330	literature value
d_tailL [g/cm3]	0.73 ± 0.02	0.73± 0.02	0.73± 0.02	yes
M_tail [g/mol]	461.88	461.88	461.88	no
Ml [g/mol]	773.11	773.11	773.11	no
ZHead	164	164	164	no
ZTail	266.07	266.07	266.07	no
RhoSolvent [cm-2]	9.43E10	9.43E10	9.43E10	no
dens_sol	1	1	1	no
Z_chol	216	216	216	no
d_chol [g/cm3]	1.06	1.06	1.06	literature values
f_chol	0.2145	0.2145	0.2145	no
bcg	1E-4	1.5E-4	2E-4	yes
Rtot [Å]	392.5	346.5	346.5	calculated
P_lip	55214	41058	41058	calculated
fp_OS	0.00 ± 0.2	0.50± 0.2	0.00± 0.2	yes
fp_HC	0.50± 0.2	0.50± 0.2	0.50± 0.2	yes
fp_IS	0.50± 0.2	0.00± 0.2	0.50± 0.2	yes
RhoP0 [cm-2]	1.22E11	1.22E11	1.22E11	literature values
fPEG	0.025	0.025	0.025	no
sigma_cPD	0.05 ± 0.03	0.10± 0.03	0.10± 0.03	yes
MPEG [g/mol]	2693.32	2693.32	2693.32	no
Rg [Å]	15	15	15	no
f_inner	0.5	0.5	0.5	yes
RhoPEG [cm-2]	1.11E11	1.11E11	1.11E11	no
f_linM	0	0± 0.002	0.037± 0.002	yes
f_pinM	nd	0± 0.006	0.426± 0.006	yes
R_mic [Å]	72 ± 10	72 ± 10	72 ± 10	yes
Sigma_Gauss_SD	0.400 ± 0.05	0.350 ± 0.05	0.450 ± 0.05	yes

Table 7.27: D6 liposomes and indolicidin

Parameters	**D6 0:1**	**1:50**	**1:10**	**Fitted?**
Ri [Å]	330 ± 3	330± 3	330± 3	yes
ti [Å]	10 ± 3	9± 3	9 ± 3	yes
to [Å]	9 ± 3	9± 3	9± 3	yes
Dc [Å]	30± 1	30 ± 1	29 ± 1	yes
sigma_c	5.3± 0.2	6.6± 0.2	5.3± 0.2	yes
sigma_ti	2 ± 1	2± 1	2 ± 1	yes
sigma_to	2± 1	2± 1	2± 1	yes
fwi	0.57± 0.08	0.52 ± 0.08	0.53 ± 0.08	calculated
fwo	0.58± 0.08	0.58± 0.08	0.59± 0.08	calculated
conc_lip [mg/ml]	2.5 ± 0.1	2.5± 0.1	2.5± 0.1	yes
conc_pep [mg/ml]	nd	0.13 ± 0.03	0.65± 0.03	yes
ratioPL	0	0.021	0.067	yes
Rgp [Å]	18	18	18	literature value
Mwp [g/mol]	1906	1906	1906	no
dp [g/cm3]	1.35	1.35	1.35	no
f_free	nd	0 ± 0.1	0.3 ± 0.1	yes
VtotL [Å3]	1293.1	1293.1	1293.1	calculated
VheadL [Å3]	330	330	330	literature value
d_tailL [g/cm3]	0.72 ± 0.02	0.72 ± 0.02	0.72 ± 0.02	yes
M_tail [g/mol]	459.2	459.2	459.2	no
Ml [g/mol]	770.45	770.45	770.45	no
ZHead	164	164	164	no
ZTail	267.51	267.51	267.51	no
RhoSolvent [cm-2]	9.43E10	9.43E10	9.43E10	no
dens_sol	1	1	1	no
Z_chol	216	216	216	no
d_chol [g/cm3]	1.05	1.05	1.05	literature values
f_chol	0.2145	0.2145	0.2145	no
bcg	2E-4	1.5E-4	2.4E-4	yes
Rtot [Å]	379 ± 3	378 ± 3	377 ± 3	calculated
P_lip	49361	49084	47312	calculated
fp_OS	0.50 ± 0.2	0.50± 0.2	0.27± 0.2	yes
fp_HC	0.00± 0.2	0.50± 0.2	0.25± 0.2	yes
fp_IS	0.50± 0.2	0.00± 0.2	0.48± 0.2	yes
RhoP0 [cm-2]	1.22E11	1.22E11	1.22E11	literature values
fPEG	0.025	0.025	0.025	no
sigma_cPD	0.13± 0.03	0.17± 0.03	0.224 ± 0.03	yes
MPEG [g/mol]	2693.32	2693.32	2693.32	no
Rg [Å]	15	15	15	no
f_inner	0.6	0.6	0.6	yes
RhoPEG [cm-2]	1.11E11	1.11E11	1.11E11	no
f_uni	0.970 ± 0.03	0.980± 0.03	0.980 ± 0.03	yes
Nu	0	0	0	yes
N	2 ± 1	3± 1	3± 1	yes
sigma_d	0.05	0.05	0.05	yes
d	65 ± 2	65 ± 2	65± 2	yes
Sigma_Gauss_SD	0.400 ± 0.05	0.350 ± 0.05	0.450 ± 0.05	yes

7.10.5 POPC/DOPC/DSPC/Chol liposomes with D2 peptide:lipid ratio

Table 7.28: D2 10% chol liposomes and indolicidin

Parameters	**D2 10% chol 0:1**	**1:50**	**1:20**	**1:10**	**Fitted?**
Ri [Å]	145 0 ± 3	300 ± 3	402 ± 3	402± 3	yes
ti [Å]	9± 3	9± 3	9± 3	9± 3	yes
to [Å]	6± 3	6± 3	6± 3	6± 3	yes
Dc [Å]	29± 1	28± 1	26 ± 1	26± 1	yes
sigma_c	4.5 ± 0.2	5± 0.2	4.8 ± 0.2	4.2 ± 0.2	yes
sigma_ti	5± 1	5 ± 1	5 ± 1	5 ± 1	yes
sigma_to	5± 1	5 ± 1	5 ± 1	5 ± 1	yes
fwi	0.41 ± 0.08	0.48± 0.08	0.52± 0.08	0.52± 0.08	calculated
fwo	0.31± 0.08	0.32± 0.08	0.35± 0.08	0.35± 0.08	calculated
conc_lip [mg/ml]	2.5± 0.1	2.5± 0.1	2.7± 0.1	2.7± 0.1	yes
conc_pep [mg/ml]	0	0.13 ± 0.03	0.33± 0.03	0.65 ± 0.03	yes
ratioPL	0	0.007	0.023	0.050	yes
Rgp [Å]	12	12	12	12	literature value
Mwp [g/mol]	1906	1906	1906	1906	no
dp [g/cm3]	1.35	1.35	1.35	1.35	no
f_free	nd	0.6± 0.1	0.5± 0.1	0.4± 0.1	yes
VtotL [Å3]	1263.6	1270.2	1270.2	1270.2	calculated
VheadL [Å3]	330	330	330	330	literature value
d_tailL [g/cm3]	0.79 ± 0.02	0.79± 0.02	0.79± 0.02	0.79± 0.02	yes
M_tail [g/mol]	463.22	463.22	463.22	463.22	no
Ml [g/mol]	774.45	774.45	774.45	774.45	no
ZHead	164	164	164	164	no
ZTail	265.36	265.4	265.4	265.4	no
RhoSolvent [cm-2]	9.43E10	9.43E10	9.43E10	9.43E10	no
dens_sol	1	1	1	1	no
Z_chol	216	216	216	216	no
d_chol [g/cm3]	1.06	1.06	1.06	1.06	literature values
f_chol	0.1	0.1	0.1	0.1	no
bcg	2.5E-4	2.5E-4	3E-4	3E-4	yes
Rtot [Å]	189 ± 3	343± 3	443± 3	443± 3	calculated
P_lip	11118	38323	62456	62456	calculated
fp_OS	0.00 ± 0.2	0.25 ± 0.2	0.03± 0.2	0.03± 0.2	yes
fp_HC	1.00± 0.2	0.75± 0.2	0.97± 0.2	0.97 ± 0.2	yes
fp_IS	0.00± 0.2	0.00± 0.2	0.00± 0.2	0.00± 0.2	yes
RhoP0 [cm-2]	1.22E11	1.22E11	1.22E11	1.22E11	literature values
fPEG	0.025	0.025	0.025	0.025	no
sigma_cPD	0.10 ± 0.03	0.10 ± 0.03	0.10 ± 0.03	0.10 ± 0.03	yes
MPEG [g/mol]	2693.32	2693.32	2693.32	2693.32	no
Rg [Å]	15	15	15	15	no
f_inner	0.65	0.65	0.6	0.6	yes
RhoPEG [cm-2]	1.11E11	1.11E11	1.11E11	1.11E11	no
f_linM	0	0	0	0.012± 0.002	yes
f_pinM	0	0	0	0.300 ± 0.006	yes
R_mic [Å]	nd	nd	nd	25 ± 8	yes
Sigma_Gauss_SD	0.600 ± 0.05	0.600 ± 0.05	0.480 ± 0.05	0.480 ± 0.05	yes

Table 7.29: D2 30% chol liposomes and indolicidin

Parameters	**D2 30% chol 0:1**	**1:50**	**1:20**	**Fitted?**
Ri [Å]	330 ± 3	550± 3	250± 3	yes
ti [Å]	11± 3	11± 3	11± 3	yes
to [Å]	9± 3	9± 3	9± 3	yes
Dc [Å]	28 ± 1	26± 1	26± 1	yes
sigma_c	7.5 ± 0.2	6.5± 0.2	6.5 ± 0.2	yes
sigma_ti	6 ± 1	6± 1	6 ± 1	yes
sigma_to	6 ± 1	6 ± 1	6 ± 1	yes
fwi	0.66 ± 0.08	0.69± 0.08	0.67± 0.08	calculated
fwo	0.65± 0.08	0.67± 0.08	0.68± 0.08	calculated
conc_lip [mg/ml]	2.5 ± 0.1	2.5± 0.1	2.5 ± 0.1	yes
conc_pep [mg/ml]	0	0.13± 0.03	0.33 ± 0.03	yes
ratioPL	0	0.017	0.038	yes
Rgp [Å]	12	12	12	literature value
Mwp [g/mol]	1906	1906	1906	no
dp [g/cm3]	1.35	1.35	1.35	no
f_free	0.7± 0.1	0.2 ± 0.1	0.2± 0.1	yes
VtotL [Å3]	1292.1	1292.1	1292.1	calculated
VheadL [Å3]	330	330	330	literature value
d_tailL [g/cm3]	0.69 ± 0.02	0.69± 0.02	0.69± 0.02	yes
M_tail [g/mol]	463.22	463.22	463.2	no
Ml [g/mol]	774.45	774.45	774.4	no
ZHead	164	164	164	no
ZTail	265.36	265.36	265.36	no
RhoSolvent [cm-2]	9.43E10	9.43E10	9.43E10	no
dens_sol	1	1	1	no
Z_chol	216	216	216	no
d_chol [g/cm3]	1.06	1.06	1.06	literature values
f_chol	0.3	0.3	0.3	no
bcg	2.44996E-4	2.44996E-4	2.44996E-4	yes
Rtot [Å]	390 ± 3	596± 3	296± 3	calculated
P_lip	49276	111707	25415	calculated
fp_OS	0.50 ± 0.2	0.00± 0.2	0.15± 0.2	yes
fp_HC	0.50 ± 0.2	0.10± 0.2	0.85± 0.2	yes
fp_IS	0.00± 0.2	0.00± 0.2	0.00± 0.2	yes
RhoP0 [cm-2]	1.22E11	1.22E11	1.22E11	literature values
fPEG	0.025	0.025	0.025	no
sigma_cPD	0	0	0	yes
MPEG [g/mol]	2693.32	2693.32	2693.32	no
Rg [Å]	15	15	15	no
f_inner	0.5	0.5	0.5	yes
RhoPEG [cm-2]	1.11E11	1.11E11	1.11E11	no
f_linM	0	0.002 ± 0.002	0.006± 0.002	yes
f_pinM	0	0.022 ± 0.006	0.0404± 0.006	yes
R_mic [Å]	23 ± 8	23± 8	23± 8	yes
Sigma_Gauss_SD	0.350 ± 0.05	0.320± 0.05	0.650± 0.05	yes

Table 7.30: D2 40% chol liposomes and indolicidin

Parameters	**D2 40% chol 0:1**	**1:50**	**1:20**	**1:10**	**Fitted?**
Ri [Å]	415 ± 3	420 ± 3	390± 3	96± 3	yes
ti [Å]	7± 3	7± 3	7± 3	7± 3	yes
to [Å]	11± 3	11± 3	11± 3	11± 3	yes
Dc [Å]	27± 1	27± 1	27± 1	26± 1	yes
sigma_c	6.3± 0.2	6.2 ± 0.2	6.2± 0.2	5.1± 0.2	yes
sigma_ti	5± 1	5± 1	5± 1	6± 1	yes
sigma_to	5 ± 1	5 ± 1	5± 1	6± 1	yes
fwi	0.58 ± 0.08	0.58± 0.08	0.58± 0.08	0.53± 0.08	calculated
fwo	0.76± 0.08	0.76± 0.08	0.76± 0.08	0.80± 0.08	calculated
conc_lip [mg/ml]	2.7 ± 0.1	2.5 ± 0.1	2.7± 0.1	2.6± 0.1	yes
conc_pep [mg/ml]	0	0.13± 0.03	0.33± 0.03	0.65± 0.03	yes
ratioPL	0	0.021	0.047	0.092	yes
Rgp [Å]	12	12	12	12	literature value
Mwp [g/mol]	1906	1906	1906	1906	no
dp [g/cm3]	1.35	1.35	1.35	1.35	no
f_free	0	0 ± 0.1	0.1± 0.1	0 ± 0.1	yes
VtotL [Å3]	1296.8	1296.8	1296.8	1296.8	calculated
VheadL [Å3]	330	330	330	330	literature value
d_tailL [g/cm3]	0.64 ± 0.02	0.64 ± 0.02	0.64 ± 0.02	0.64 ± 0.02	yes
M_tail [g/mol]	463.2	463.2	463.2	463.22	no
Ml [g/mol]	774.4	774.4	774.4	774.45	no
ZHead	164	164	164	164	no
ZTail	265.36	265.36	265.36	265.36	no
RhoSolvent [cm-2]	9.43E10	9.43E10	9.43E10	9.43E10	no
dens_sol	1	1	1	1	no
Z_chol	216	216	216	216	no
d_chol [g/cm3]	1.06	1.06	1.06	1.06	literature values
f_chol	0.4	0.4	0.4	0.4	no
bcg	2E-4	2E-4	1.5E-4	2E-4	yes
Rtot [Å]	460 ± 3	465± 3	435± 3	139± 3	calculated
P_lip	66547	68083	59126	4520	calculated
fp_OS	0.50 ± 0.2	0.50± 0.2	0.00± 0.2	0.00± 0.2	yes
fp_HC	0.50± 0.2	0.28± 0.2	0.52± 0.2	0.58± 0.2	yes
fp_IS	0.00± 0.2	0.22± 0.2	0.48± 0.2	0.42± 0.2	yes
RhoP0 [cm-2]	1.22E11	1.22E11	1.22E11	1.22E11	literature values
fPEG	0.025	0.025	0.025	0.025	no
sigma_cPD	0 ± 0.03	0.08± 0.03	0.08± 0.03	0.08± 0.03	yes
MPEG [g/mol]	2693.32	2693.32	2693.32	2693.32	no
Rg [Å]	15	15	15	15	no
f_inner	0.5	0.5	0.5	0.5	yes
RhoPEG [cm-2]	1.11E11	1.11E11	1.11E11	1.11E11	no
f_linM	0	0	0.002 ± 0.002	0.03± 0.002	yes
f_pinM	0	0	0.020± 0.006	0.247± 0.006	yes
R_mic [Å]	nd	nd	30 ± 8	30± 8	yes
Sigma_Gauss_SD	0.260± 0.05	0.210± 0.05	0.300± 0.05	0.600± 0.05	yes

Table 7.31: S1 30% chol liposomes and indolicidin

Parameters	**S1 30% chol 0:1**	**1:50**	**1:20**	**Fitted?**
Ri [Å]	329 ± 3	560 ± 3	560± 3	yes
ti [Å]	7± 3	7 ± 3	7 ± 3	yes
to [Å]	6± 3	6± 3	6± 3	yes
Dc [Å]	31± 1	31± 1	29± 1	yes
sigma_c	6.4 ± 0.2	6.4± 0.2	5.3± 0.2	yes
sigma_ti	6 ± 1	6 ± 1	6± 1	yes
sigma_to	5 ± 1	5± 1	5± 1	yes
fwi	0.43 ± 0.08	0.44± 0.08	0.49± 0.08	calculated
fwo	0.42± 0.08	0.40± 0.08	0.44± 0.08	calculated
conc_lip [mg/ml]	2.5 ± 0.1	2.5± 0.1	2.5± 0.1	yes
conc_pep [mg/ml]	0	0.13 ± 0.03	0.33± 0.03	yes
ratioPL	0	0.01357	0.04993	yes
Rgp [Å]	12	12	12	literature value
Mwp [g/mol]	1906	1906	1906	no
dp [g/cm3]	1.35	1.35	1.35	no
f_free	nd	0.4 ± 0.1	0± 0.1	yes
VtotL [Å3]	1295.4	1284.0	1295.4	calculated
VheadL [Å3]	330	330	330	literature value
d_tailL [g/cm3]	0.68 ± 0.02	0.68± 0.02	0.68± 0.02	yes
M_tail [g/mol]	459.2	459.2	459.2	no
Ml [g/mol]	770.45	770.45	770.45	no
ZHead	164	164	164	no
ZTail	267.59	267.51	267.51	no
RhoSolvent [cm-2]	9.43E10	9.43E10	9.43E10	no
dens_sol	1	1	1	no
Z_chol	216	216	216	no
d_chol [g/cm3]	1.06	1.06	1.06	literature values
f_chol	0.3	0.3	0.3	no
bcg	2E-4	1.3E-4	2E-4	yes
Rtot [Å]	373 ± 8	604± 8	602 ± 8	calculated
P_lip	49960	138590	127675	calculated
fp_OS	0.50± 0.2	0.00± 0.2	0.00± 0.2	yes
fp_HC	0.50± 0.2	1.00± 0.2	0.70± 0.2	yes
fp_IS	0.00± 0.2	0.00± 0.2	0.30± 0.2	yes
RhoP0 [cm-2]	1.22E11	1.22E11	1.22E11	literature values
fPEG	0.025	0.025	0.025	no
sigma_cPD	0.10 ± 0.03	0.10± 0.03	0.10± 0.03	yes
MPEG [g/mol]	2693.32	2693.32	2693.32	no
Rg [Å]	15	15	15	no
f_inner	0.5	0.5	0.5	yes
RhoPEG [cm-2]	1.11E11	1.11E11	1.11E11	no
f_linM	0	0	0.033 ± 0.002	yes
f_pinM	0	0	0.500± 0.006	yes
R_mic [Å]	nd	nd	24 ± 8	yes
Sigma_Gauss_SD	0.380 ± 0.05	0.350± 0.05	0.304± 0.05	yes

Table 7.32: Bicelle fitting values. S1 and D2 with 30% chol

Parameter	D2 30% chol. 1:10	S1 30% chol. 1:10	Fitted?
Rsc [Å]	120 ± 10	101± 10	yes
L [Å]	26± 1	30± 1	yes
dL [Å]	5.2 ± 0.6	6.0 ± 0.6	yes
dRsc [Å]	7.8± 0.3	8.2± 0.3	yes
conc_peptide [mg/ml]	0.65 ± 0.03	0.65 ± 0.03	yes
conc_lipid [mg/ml]	2.5 ± 0.1	2.5 ± 0.1	yes
dens_peptide [g/cm3]	1.35	1.35	no
fp_tail	0.9± 0.2	0.7± 0.2	yes
Vhead_lipid [Å3]	330	330	literature values
Vtot_lipid [Å3]	1224 ± 3	1224± 3	yes
Vhead_dL [Å3]	284	313	calculated
bcg	2.8E-4	2.5E-4	yes
fw_dL	0.35 ± 0.01	0.25± 0.01	calculated
fw_dR	0.67± 0.01	0.69± 0.01	calculated
f_peptide_dR	0.272	0.296	calculated
Mw_lipid [g/mol]	774.45	770.45	no
Mw_peptide [g/mol]	1906	1906	no
b_peptide	1018	1018	no
Vhead_dR [Å3]	67.00898	77.10577	calculated
btail_lipid	250.55	250.3	no
bhead_lipid	164	164	no
RhoSolvent [cm-2]	9.43E10	9.43E10	no
sigma_shell	6 ± 1	5 ± 1	yes
sigma_core	1 ± 1	1 ± 1	yes
Vtail [Å3]	1084± 3	1039± 3	yes
Mchol [g/mol]	386.65	386.65	no
f_chol	0.34	0.34	no
P	1100	934	calculated
r_peptide_lipid	0.08977	0.0873	calculated
f_lipid_dR	0.19 ± 0.02	0.18± 0.02	yes
Sigma_Gauss_SD	0.794 ± 0.05	0.700± 0.05	yes

7.11 For the interested.creative reader

During my work on making a figure of the bilayer for this thesis I was once asked if I was looking at a knitting chart. It then hit me as a marvellous idea to actually make a lipid bilayer pattern. Therefore. I made a draft for a bilayer knitting pattern. as seen in figure 7.13. Disclaimer: the pattern has not yet been tested. as the author has been otherwise occupied writing a thesis.

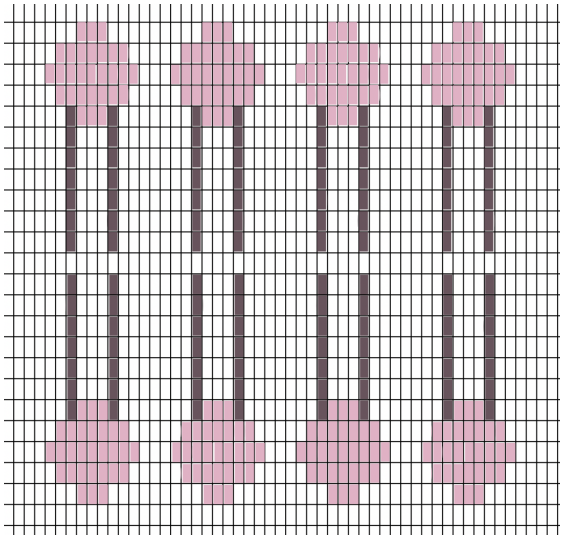

Figure 7.13: Lipid bilayer knitting pattern